JOURNAL OF RESEARCH

OF THE U.S. GEOLOGICAL SURVEY

MAY–JUNE 1975
VOLUME 3, NUMBER 3

Scientific notes and summaries of investigations in geology, hydrology, and related fields

U.S. DEPARTMENT OF THE INTERIOR

UNITED STATES DEPARTMENT OF THE INTERIOR
ROGERS C. B. MORTON, Secretary
GEOLOGICAL SURVEY
V. E. McKelvey, Director

For sale by the Superintendent of Documents, U.S. Government Printing Office, Washington, DC 20402. Order by SD Catalog No. JRGS. Annual subscription rate $18.90 (plus $4.75 for foreign mailing). Single copy $3.15. Make checks or money orders payable to the Superintendent of Documents.

Send all subscription inquiries and address changes to the Superintendent of Documents at the above address.

Purchase orders should not be sent to the U.S. Geological Survey library.

Library of Congress Catalog-card No. 72-600241.

The Journal of Research is published every 2 months by the U.S. Geological Survey. It contains papers by members of the Geological Survey and their professional colleagues on geologic, hydrologic, topographic, and other scientific and technical subjects.

Correspondence and inquiries concerning the Journal (other than subscription inquiries and address changes) should be directed to the Journal of Research, Publications Division, U.S. Geological Survey, National Center 321, Reston, VA 22092.

Papers for the Journal should be submitted through regular Division publication channels.

The Secretary of the Interior has determined that the publication of this periodical is necessary in the transaction of the public business required by law of this Department. Use of funds for printing this periodical has been approved by the Director of the Office of Management and Budget through June 30, 1980.

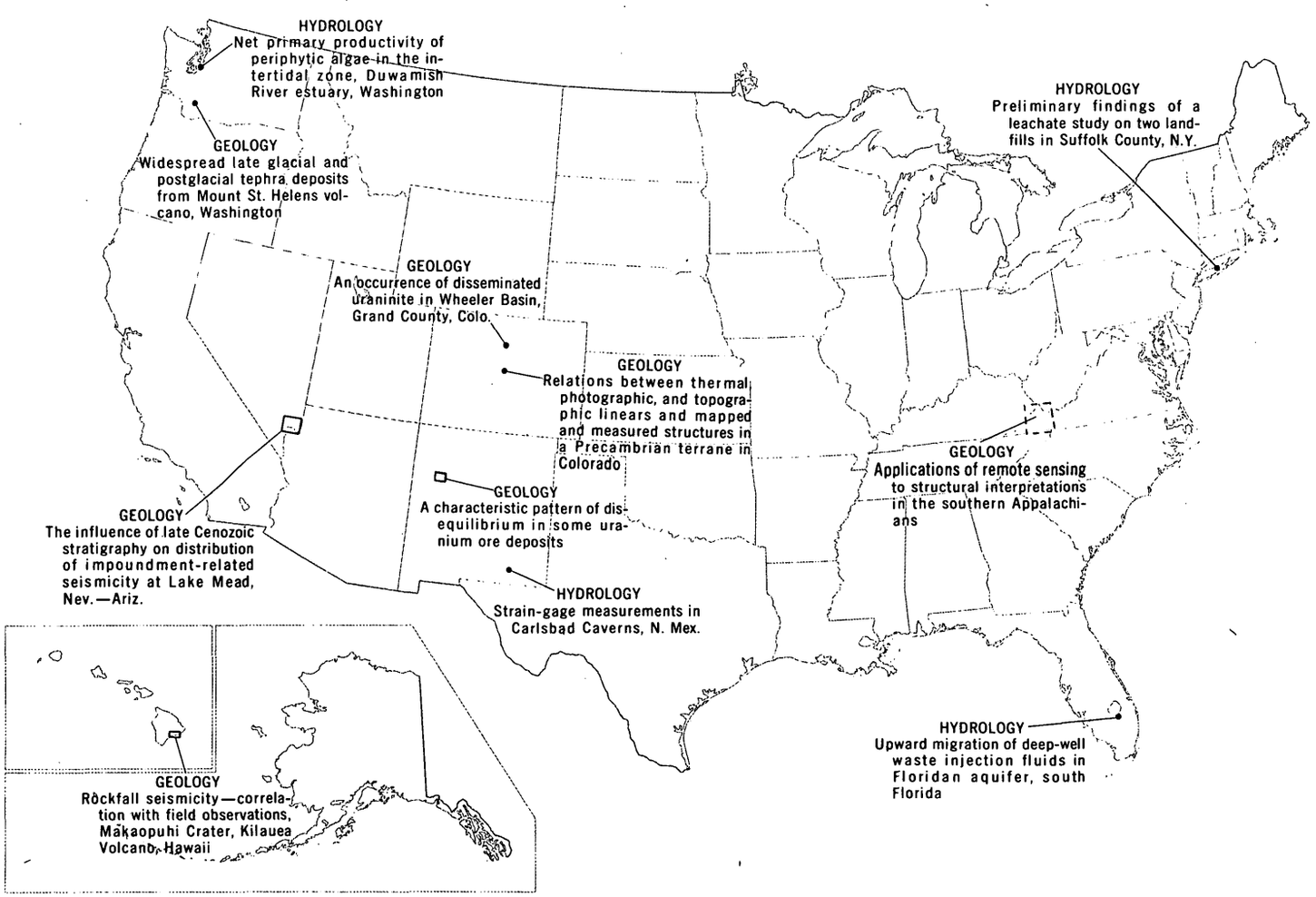

GEOGRAPHIC INDEX TO ARTICLES

See "Contents" for articles concerning areas outside the United States and articles without geographic orientation.

JOURNAL OF RESEARCH

of the

U.S. Geological Survey

Vol. 3 No. 3 May–June 1975

CONTENTS

ABBREVIATIONS

A ---------angstrom
a_0 ---------unit cell edge
alt --------altitude
avg -------average
B.P. ------before present
b.y. -------billion years
cal -------calorie
calc -------calculated
COD ------chemical oxygen demand
concd -----concentrated
cP --------centipoise
c/s -------counts per second; cycles per second
D --------debye unit
d ---------day
dB -------decibel
d.f. -------degree of freedom
diam -----diameter
DO -------dissolved oxygen
Eh --------oxidation-reduction potential
eq --------equation
EROS ----Earth Resources Observation Systems
ERTS ----Earth Resources Technology Satellite (now Landsat)
eU --------equivalent uranium
ft-c -------foot-candle
h ---------hour
J ---------joule
K --------kelvin
kV -------kilovolt
kWh ------kilowatt-hour
lat --------latitude
LDMW ---locally derived meteoric water
lm --------lumen
log -------logarithm (common)
long ------longitude
M --------molarity; molar (concentration)
m --------molality; molal (concentration)
mA -------milliampere
MBAS ----methylene blue active substance
meq ------milliequivalent
MeV ------megaelectronvolt
mg -------milligram
mGal -----milligal
MIBK ----methyl isobutyl ketone
min -------minute
Ml -------million litres
ml --------millilitre
mo -------month
mol -------mole
mV -------millivolt
m.y. ------million years
μcal ------microcalorie
μg --------microgram
μm -------micrometre
μmho -----micromho
N ---------normality
n ---------neutron
NASA ----National Aeronautics and Space Administration
nm -------nanometre
NOAA ----National Oceanic and Atmospheric Administration
P.d.t. -----Pacific daylight time
pH -------measure of hydrogen ion activity
ppb -------part per billion
ppm ------part per million
r/min ----revolutions per minute
s ---------second
(s) -------solid
SI --------Système International (International System)
SMOW ----standard mean ocean water
std -------standard
σ ---------population standard deviation
U.S.P. ----United States Pharmacopeia
W --------watt
w/v ------weight per volume
yd --------yard
yr --------year

Jour. Research U.S. Geol. Survey
Vol. 3, No. 3, May–June 1975, p. 253–259

NET PRIMARY PRODUCTIVITY OF PERIPHYTIC ALGAE IN THE INTERTIDAL ZONE, DUWAMISH RIVER ESTUARY, WASHINGTON

By LARRY J. TILLEY and WILLIAM L. HAUSHILD,
Menlo Park, Calif., Tacoma, Wash.

Prepared in cooperation with the Municipality of Metropolitan Seattle (METRO)

Abstract.—Net primary productivity of periphyton in the intertidal zone of an economically important estuary in south Seattle, Wash., was determined. This productivity, measured as chlorophyll *a* concentration in the periphyton on fixed glass substrates, was 0.11 mg/m^2 per week. The low productivity of attached algae on the substrates was attributed to out-of-water desiccation, and part of the variability in accumulation of periphytic algae was attributed to the time out-of-water exposure, which varied greatly from week to week owing to the irregularity of tides in the estuary.

In a comprehensive study of the Duwamish River estuary, Seattle, Wash. investigations of the amount of algal biomass produced or deposited in the estuary included an estimation of the rate of growth of attached algae. A program of the U.S. Geological Survey in cooperation with the Municipality of Metropolitan Seattle (Metro) includes determining the causes and effects of low DO (dissolved oxygen) concentrations in the estuary and predicting results on future DO concentrations of greater releases of sewage effluent from Metro's secondary sewage-treatment plant near Renton, Wash., river kilometre 20.4. Welch (1969) and Welch, Emery, Matsuda, and Dawson (1972) estimated growth rates for the phytoplankton and periphyton accumulated on floating substrates, respectively, and related these rates to phytoplankton blooms and environmental influences.

Periphyton is a biotic community composed of organisms attached to submerged objects in water; algae normally represent a significant fraction of this community. In this study, periphyton was collected on glass microscope slides because they are a standard, bare, uniform substrate for periphyton attachment and chlorophyll *a* was used to estimate algal productivity.

Because the banks and bed of the estuary have much more surface area than do floating objects within the estuary, they have a high potential to produce more algal biomass. The growth of algae on floating substrates reflects more closely the phytoplankton than the periphyton growth rates and, as a result, estimates of attached algal growth on the banks of the estuary are too high.

Algal growth on fixed substrates in the intertidal zone is strongly influenced by alternate wetting and drying, and this effect upon growth rates may be dominant regardless of quality of water in the estuary.

THE ESTUARY

The Duwamish River estuary, like many estuaries in urban areas, is undergoing changes in waste-water input and in its riverbanks. Historically, the junction of the Black and Green Rivers (river kilometre 19.1) is considered the beginning of the Duwamish River (fig. 1, this report; Richardson and others, 1968). Elliott Bay, an arm of Puget Sound, is between the river estuary and the sound, which is considered the Duwamish's free connection with the Pacific Ocean.

The estuary (fig. 1) is narrow in proportion to length, and for the greater part its banks are fairly straight and nearly parallel; only a few shallow side channels remain from old meanders. It is maintained as a navigational channel by dredging upstream to river kilometre 10.0 The bed of the estuary is composed of mixtures of sand, silt, clay, and organic detritus. The composition increases in sand during periods of high freshwater inflow and in silt, clay, and organic detritus during periods of low freshwater inflow.

The extent of saltwater excursion upstream depends on the river discharge and tides. During low river discharges, tides affect the flow and stage in the Green River to about river kilometre 25.1. Whether saltwater intrudes to at least river kilometre 12.4 for discharges between 17.7 and 28.3 m^3/s depends on tidal height.

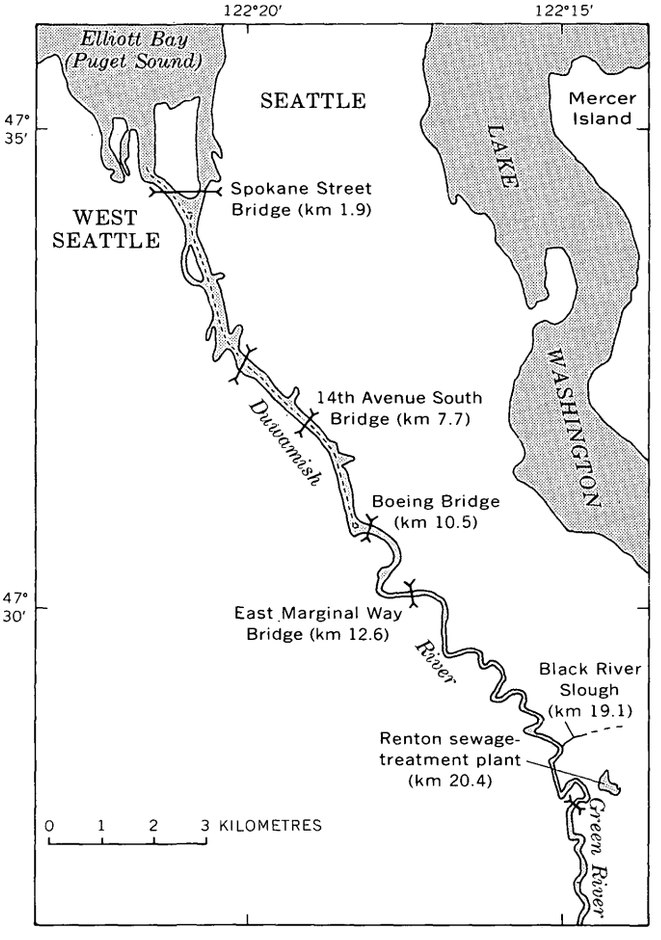

FIGURE 1.—Bridge locations used as sampling points, Duwamish River estuary, Seattle, Wash.

Stoner (1967) showed that saltwater intrudes to river kilometre 12.4 for river discharges less than 17.7 m^3/s and never intrudes to river kilometre 12.4 for discharges more than 28.3m^3/s. For all river discharges, the water moving into the estuary from Puget Sound forms a saltwater wedge. In saltwater-wedge estuaries —as defined by Pritchard (1955)—net movement of water in the wedge is landward because the water moving seaward in an overlying layer entrains saltwater from the wedge. Therefore, the salinity of water in the overlying layer increases in the seaward direction.

The freshwater inflow varies from sporadic peak flows of 333 m^3/s to a minimum of 5–6.7 m^3/s in dry weather. High flows occur in the winter and spring months, especially when heavy rains follow closely a period of heavy snowfall in the Cascade Range. Warm temperatures coupled with the heavy rains can cause unseasonable melting of snow. From mid-July through September, low flows are predominant and are much less than 16.7 m^3/s.

Semidiurnal tides in the Duwamish River estuary are as much as 4 m. A complete tidal cycle takes about 25 h, and a cycle usually has two high waters and two low waters. High water is the maximum height reached by each rising tide and low water is the minimum height reached by each falling tide. Heights of successive low waters and successive high waters usually are unequal. The largest inequalities generally are those for the low waters, although large differences between heights of successive high waters frequently occur. Dawson and Tilley (1972) further describe the general circulation patterns within the Duwamish River estuary.

WATER QUALITY

Inflowing freshwater is a calcium bicarbonate type water and has small amounts of total dissolved solids, 33 to 71 mg/l (Santos and Stoner, 1972). However, the water that reaches the estuary has large amounts of plant nutrients (Welch, 1969; Santos and Stoner, 1972). DO concentration prior to 1968 never was less than 4.0 mg/l. at a water-quality monitoring station established in 1965 at East Marginal Way Bridge, river kilometre 12.6 (Santos and Stoner, 1972).

Saltwater enters the estuary in the lower layer and has nearly the same salinity and temperature as the water in Elliot Bay, an arm of Puget Sound. DO concentration near the bottom is always greater at river kilometre 1.9 than at river kilometre 7.7 (Dawson and Tilley, 1972).

DO concentrations as low as 2.0 mg/l were observed at river kilometre 7.7 prior to 1971 (Welch, 1969; Welch and others, 1972). Santos and Stoner (1972), prior to 1968, measured DO concentrations less than 1.0 mg/l and suggested that phytoplankton respiration and decomposition after death contributed to the low DO levels. Tilley and Dawson (1971) demonstrated how plant nutrients are trapped by the estuary, primarily in the area of river kilometre 7.7 where the lowest DO levels were found.

Because excess algal growths can contribute to low DO levels in water, it was necessary to account for all the algae that was potentially available to the Duwamish River estuary. Algal biomass in the form of phytoplankton, incoming river phytoplankton, in situ periphyton, and periphyton attached to floating objects was estimated in other studies by Welch and Isaac (1967), Welch (1969), Santos and Stoner (1972), Welch, Emery, Matsuda, and Dawson (1972), and Tilley and Hauschild (written commun., 1974). A remaining source of algae would be the attached algae in the periphyton of the intertidal zone which this study estimates.

SAMPLING STATIONS

Three vertical staffs with substrates distributed over the tidal range were placed at bridges in the estuary. Two staffs were at two of three drawbridges in the dredged part of the estuary: one staff at river kilometre 1.9, the farthest downstream drawbridge, and one staff at river kilometre 7.7, the farthest upstream drawbridge. The third staff was at the first bridge upstream from the dredged part of the estuary, river kilometre 10.5. Table 1 summarizes the station features and characteristics.

TABLE 1.—*Some sampling station features and characteristics, Duwamish River estuary, southern Seattle, Wash.*

River kilometre	Sampling station	Streambank features and characteristics
10.5	Boeing Bridge ------	High mudbanks of intertidal stream.Grass and weeds in areas not covered by asphalt parking lots on both sides of stream.
7.7	14th Avenue South Bridge, a drawbridge.	No vegetation. Factory on east bank, mobile home park and marina on west bank.
1.9	Spokane Street Bridge, a drawbridge.	No vegetation. Flour mill and marina on east bank, steel mill on west bank.

METHODS

Water levels in the intertidal zone of the estuary vary as much as 4 m during some tidal cycles, and much of the bank is alternately above and below water. To estimate growth of algae that undergo alternate wetting and drying, periphyton accumulation on substrates attached to removable vertical staffs that were placed on bridge piers and fenders was observed during the summer and fall of 1970.

Glass microscope slides, 25 by 75 mm, bearing identification numbers etched by a glass-marking pencil, were used in this study as artificial substrates for sampling periphyton. Advantages of using glass slides were documented by Sládečková (1962). The slides were positioned flat against the vertical staff and only the periphyton that accumulated on the exposed side of each slide was analyzed for chlorophyll *a*. Before scraping the exposed side of the substrate, the edges and back side of the slide facing the staff were cleared of all accumulations. The exposed side of a slide was scraped with the edge of a clean glass slide, using a solution of 90 percent acetone as the scraping and rinsing medium. Disruption of cells and extraction of pigments were done simultaneously during scraping. The acetone mixture was transferred to a 10-ml centrifuge tube, capped, shaken vigorously, and refrigerated overnight. Tilley (1972) used the scraping procedure and reported an average recovery of 99.8 percent of the accumulated periphyton. Chlorophyll *a* was determined by using a spectrophotometer and the techniques described by Strickland and Parsons (1968, p. 185–192).

Seven glass substrates were placed 0.6 m apart along the length of each staff which, in turn, was so positioned that the uppermost substrate was just under water at the higher high tides (approx 3.6 m above mean lower low water) and the lowermost substrate was just above water at the lower low tides (approx 0.3 m below mean lower low water). Three substrates were exposed for each periphyton sample collected to obtain better representation and, if necessary, to allow for losses. Substrates were retrieved and replaced weekly in a manner allowing for the determination of the periphyton growth for totals of 1, 2, 3, and 4 weeks. Each 4-week-long exposure series did not overlap. The three series of exposure were during the low freshwater flows of July, August, and September 1970.

RESULTS AND STATISTICAL ANALYSIS

The results from the three series of exposure of glass substrates are contained in table 2. The glass substrates were out of water or under water to a degree that depended on their elevation (height relative to mean lower low water). The gross effect of the intermittency of time under water of periphyton biomass is indicated by the observation that the chlorophyll *a* concentrations in periphyton accumulated on continuously wet substrates in the estuary during the summer and fall of 1969 (Tilley and Haushild, written commun., 1974) was much greater (tenfold) than the concentrations on intermittently wet substrates during summer and early fall of 1970.

An analysis of covariance indicated that differences in chlorophyll *a* concentrations among the three exposure series are no greater than would be expected by chance alone (95-percent confidence level). Therefore, the three 1-month series of data were averaged. Results shown in figure 2 suggest that (1) chlorophyll *a* concentration in periphyton accumulations in the intertidal zone increases with exposure time and, (2) chlorophyll *a* concentration at river kilometre 7.7 may be somewhat greater than that at river kilometres 1.9 and 10.5. However, the differences between concentrations at the stations were not significant because variability in chlorophyll *a* concentration was as great as the differences.

A multiple-regression analysis was used to relate periphyton biomass, Y, on substrates in the intertidal zone to length of exposure time, T, and substrate elevation, E. The resulting equation for the regression model is

TABLE 2.—*Chlorophyll a concentration, in milligram per square metre, in periphyton accumulations on glass substrates in the intertidal zone of the Duwamish River estuary during summer and fall 1970*

[1, 2, 3, and 4 are exposure times in weeks for indicated monthly series]

Substrate elevation[1] (metres)	July				August				September			
	1	2	3	4	1	2	3	4	1	2	3	4
At Boeing Bridge, river kilometre 10.5												
3.45	0.2	<0.1	<0.1	0.2	<0.1	<0.1	0.5	.04	<0.1	<0.1	0.5	0.3
2.85	.2	<.1	.5	.4	.4	<.1	.8	.7	.3	<.1	.4	.5
2.25	.5	<.1	.5	.2	1.0	<.1	1.3	.8	.4	<.1	.9	.2
1.65	.9	<.1	1.1	.3	.4	<.1	1.8	1.1	.4	.2	.4	.4
1.05	[2]3.7	<.1	.7	.2	.8	----	1.1	1.1	.3	.2	.5	.2
.45	1.8	.3	1.6	.2	2.1	<.1	3.5	2.6	.4	1.4	.3	.3
−.15	1.6	1.0	[2]8.2	1.4	.5	----	2.8	[2]7.7	.4	.7	1.3	2.0
At 14th Avenue South Bridge, river kilometre 7.7												
3.45	<0.1	0.2	0.3	<0.1	<0.1	<0.1	<0.1	0.3	<0.1	<0.1	0.2	0.2
2.85	<.1	.6	<.1	.3	<.1	<.1	<.1	.2	1.2	<.1	.5	.8
2.25	.2	1.0	.3	1.9	<.1	.4	.3	--	2.1	.4	2.0	2.7
1.65	<.1	1.1	.3	2.2	<.1	.5	.2	.7	.4	.4	.9	[2]2.6
1.05	<.1	.7	.5	1.9	<.1	1.1	.4	.8	1.3	1.6	2.0	[2]4.7
.45	.5	1.7	.5	3.6	<.1	1.0	.7	5.5	.6	1.5	1.7	5.6
−.15	.5	2.3	.7	3.5	<.1	1.9	1.4	2.2	1.5	.5	.8	2.0
At Spokane Street Bridge, river kilometre 1.9												
3.45	<0.1	<0.1	<0.1	<0.1	<0.1	<0.1	0.2	<0.1	<0.1	<0.1	<0.1	<0.1
2.85	<.1	.2	<.1	.3	<.1	<.1	.3	<.1	<.1	<.1	.4	.2
2.25	<.1	1.1	<.1	.7	<.1	<.1	.7	.5	.3	<.1	.4	.3
1.65	<.1	.5	.2	.8	<.1	<.1	.5	1.1	.2	.2	.2	.2
1.05	<.1	2.1	<.1	1.0	<.1	<.1	.5	1.4	.3	<.1	.3	.6
.45	<.1	1.1	<.1	1.3	<.1	<.1	1.8	2.2	.4	<.1	<.1	.2
−.15	.2	1.8	<.1	1.8	<.1	<.1	2.1	3.1	<.1	<.1	.3	<.1

[1] Zero elevation of substrate equals elevation of mean lower low water.
[2] Values found to be outliers resulting from application of the Dixon-criterion (Natrella, 1963, p. 17–3).

$$Y = 0.90 + 0.11T - 0.30E, \qquad (1)$$

where Y is expressed in milligrams of chlorophyll a per square metre, T is in weeks, and E is in metres.

The model is restricted to the values of T and E and to estuary locations given in table 2 or figure 2. Although the relation expressed by equation 1, was significant at the 95-percent confidence level, the standard error of estimate is 0.8 mg/m² which reflects the great variability within the chlorophyll a data.

Use of a weighted percentage of the time a substrate was out of water instead of substrate elevation as an independent variable did not improve the determination of periphyton biomass. However, a model using percentage of out-of-water time for substrates is in a form more directly comparable with results of studies in other estuaries, so its development is presented here. Tide stage was recorded every 15 min at river kilometre 5.5, and from that data cumulative frequency distributions of the high and low waters during July through September 1970 were determined (fig. 3). The few low and high extremes in the tidal-stage data were not used in computing the cumulative frequency distribution for each high or low water; the occasional times substrates were under water during extreme high waters probably did not aid periphyton growth on substrates at high elevations nor was growth on substrates at low elevations deterred much by an occasional brief exposure to air.

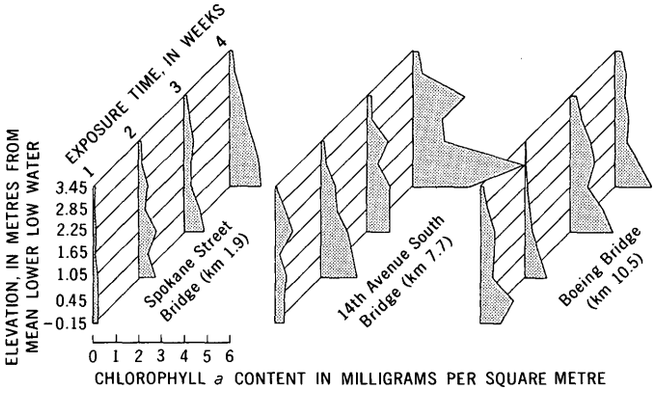

FIGURE 2.—Variations in average chlorophyll a concentration in periphyton samples with exposure time and elevation of periphyton samples from three locations in the Duwamish River estuary during summer and fall 1970.

The relation of periphyton biomass (as is indicated by chlorophyll a concentration, Y) to exposure time, T, and the weighted percentage of days that substrates were out of water, P, were determined from a regression analysis. First, the cumulative frequency of out-of-water time for each substrate location was determined for each high and low water from the data in figure 3. The weighted frequencies resulting from these determinations are listed in table 3.

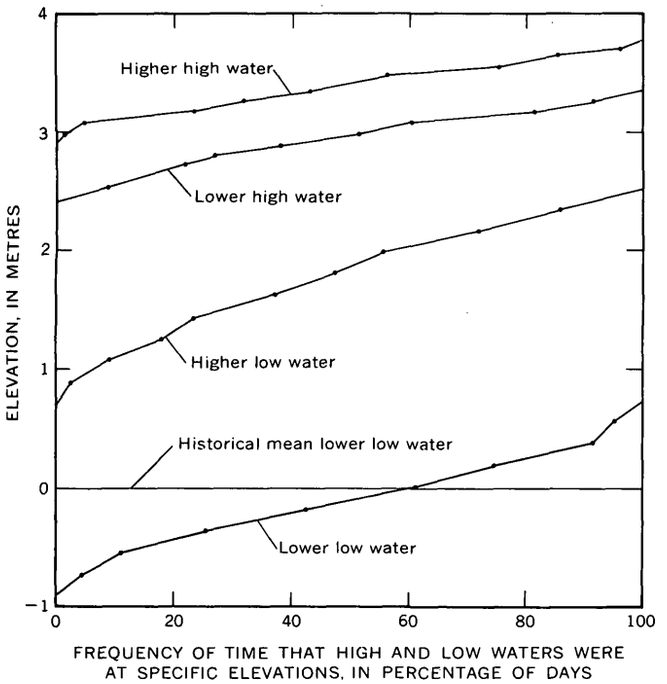

FIGURE 3.—Distribution of frequency of occurrence for high and low water in the Duwamish River estuary during summer and early fall 1970. The five highest and five lowest waters were not included in the analysis for each high and low water.

TABLE 3.—*Weighted percentage of days substrates were out of water*

Substrate elevation (metres)	Low tide		High tide		Total
	Lower	Higher	Lower	Higher	
3.45	100	100	100	54	585
2.85	100	100	35	0	320
2.25	100	79	0	0	218
1.65	100	39	0	0	158
1.05	100	8	0	0	112
0.45	93	0	0	0	93
−0.15	45	0	0	0	45
Weighting factor --	1.0	1.5	2.0	2.5	--

Weighting of the frequencies was based on the reasoning that periphyton accumulation on substrates under water only during high waters would be much less than that on substrates out of water only during low waters. Multipliers of 2.5, 2.0, 1.5, and 1.0, rather than other combinations of multipliers, were applied to the frequency percentages for higher high, lower high, higher low, and lower low waters, respectively (see table 3), because computed concentrations agreed most closely with observed concentrations. The equation for the regression model expressing the relationship among Y, T, and P is

$$Y = 0.81 + 0.11T - 0.002P, \quad (2)$$

where Y is expressed in milligrams of chlorophyll a per square metre, T is time in weeks (Y and T are the same as in equation 1), and P is the accumulated weighted frequency in percent, at an elevation in the intertidal zone.

The standard error of estimate for equation 2 is 0.8 mg/m^2. The restrictions on variable values for equation 1 also apply to equation 2.

Equations for models 1 and 2 express periphyton biomass in terms of exposure time and substrate elevation—or its substitute, the percentage of time a substrate is out of water. Because of the large variability within the observed data and the relatively low amounts of chlorophyll a found growing on the substrates after the 4-week-long exposure series, productivity can only be poorly estimated by using either equation 1 or 2. For the 4-week-long exposure series, the fit of observed chlorophyll a concentrations to computed chlorophyll a concentrations is shown in table 4. The end points of the ranges in water-surface elevations are the elevations (within the range sampled) that are exceeded by high and low waters on 5 and 95 percent of the days during the study period. The data in table 4 indicate a general increase in periphyton biomass that correlates with a decrease in the frequency substrates underwent desiccation.

DISCUSSION

Observed chlorophyll a concentrations in the periphyton of the Duwamish River estuary were highly variable. Tilley and Haushild (written commun., 1974) show that for 21 replicate observations of chlorophyll a concentration in accumulated periphyton the standard deviations averaged 20 percent of the mean concentration.

Although differences in periphyton accumulation among the three sampling locations in the estuary seemed possible, they were not determinable from the observed data. The large temporal and spatial variability in chlorophyll a concentration means that there were relatively large errors in estimating the concentration from models using time-dependent and space-dependent variables.

In similar studies along the Oregon coast, Castenholz (1961) found that grazers (zooplankton) at Yoakin Point effectively kept bare areas free of marine littoral diatom populations during three summers. Castenholz (1963) later speculated that desiccation was the primary reason for slow repopulation of marine littoral diatoms on bare areas at Gregory Point. In the intertidal zone of the Duwamish River estuary, desiccation of substrates during out-of-water periods seriously affected periphyton accumulation, but the degree of any effect attributable to grazing on the periphyton population is unknown.

TABLE 4.—*Means and ranges of 4-week chlorophyll a concentrations, in milligrams per square metre, in periphyton accumulations on glass substrates during summer and early fall 1970 for various ranges of water-surface elevation in the intertidal zone of the Duwamish River estuary*

Range in water-surface elevation[1] (metres)	4-week chlorophyll *a* concentration				Remarks
	Observed		Computed range		
	Mean	Range	Equation 1	Equation 2	
≥3.79	0.2	———	0–0.1	0	Higher high water, was higher than elevation 3.79 m on 5 percent of the days during the study period.
3.35–3.79	.2	<0.1–0.5	0.2–0.3	0–0.3	Lower high water was higher than elevation 3.35 m on 5 percent of the days during the study period.
2.46–3.35	.4	<0.1–0.8	0.3–0.6	0.3–0.7	The 2.46 m elevation was below lower high water and above higher low water on about 95 and 5 percent of the days, respectively, during the study period.
0.72–2.46	.7	<0.1–2.0	0.6–1.1	0.7–1.0	The 0.72 m elevation was below higher low water and above lower low water on about 95 and 5 percent of the days, respectively during the study period.
−0.15–0.72	1.2	<0.1–3.5	1.1–1.4	1.0–1.3	The −0.15 m elevation, the lowest observed, was under water 95 percent of the days during the study period.

[1] Zero elevation of water surface equals elevation of mean lower low water.

Periphyton accumulation in the estuary varied with the exposure time and the frequency that substrates were out of water. Models for estimating variability of chlorophyll *a* concentration in periphyton accumulations were determined from regression of chlorophyll *a* concentration against two sets of independent variables and had about equal standard errors of estimates. Concentrations determined from the model using substrate elevation agreed somewhat closer with observed concentrations, whereas models using the frequency that substrates are out of water may be more suitable for comparison with the results of studies of other estuarine environments.

Periphyton both use and contribute to the oxygen supply in stream water through photosynthesis, respiration, and decomposition during their life cycle. The models that provide a means of estimating biomass and growth rate of periphyton are an aid to evaluating the effect of periphyton on dissolved oxygen levels in the Duwamish River estuary.

As determined by this study, the net primary productivity of the periphyton in the intertidal zone of the Duwamish River estuary is too low to be a major factor in decreasing DO levels in the estuary. The data suggest that the amount of periphyton that can be produced in excess of the capacity of the estuary to rid itself of that algae is negligible. The net primary productivity of chlorophyll *a* as determined by both mathematical models is about 0.1 mg/m² per week. Welch, Emery, Matsuda, and Dawson (1972) estimated net primary productivity rates as much as 100 mg/m² per week for algae in periphyton accumulated on floating substrates and as much as 70 mg/l chlorophyll *a* for phytoplankton in the Duwamish estuary. Wetzel (1965) suggested that growth rates for periphyton collected on floating substrates in a lake are probably a measure of the potential rate of growth of phytoplankton algae. However, both estimates of net primary productivity rates in the Duwamish estuary by Welch, Emery, Matsuda, and Dawson (1972) are much greater than the estimate for attached algae in the intertidal zone determined in this study. Therefore, it is the phytoplankton, rather than periphytic algae, that affect DO concentrations in the estuary through their photosynthesis, respiration, and decomposition.

REFERENCES CITED

Castenholz, R. W., 1961, The effect of grazing on marine littoral diatom populations: Ecology, v. 42, no. 4, p. 783–794.

——— 1963, An experimental study of the vertical distribution of littoral marine diatoms: Limnology and Oceanography, v. 8, no. 4, p. 450–462.

Dawson, W. A., and Tilley, L. J., 1972, Measurement of salt-wedge excursion distance in the Duwamish River estuary, Seattle, Washington, by means of the dissolved-oxygen gradient: U.S. Geol. Survey Water-Supply Paper 1873–D, 27 p.

Natrella, M. G., 1963, Experimental statistics: U.S. Dept. Commerce, Natl. Bur. Statistics Handb. 91 chap. 17, p. 17-3; reprinted in 1966 with corrections.

Pritchard, D. W., 1955, Estuarine circulation patterns: Am. Soc. Civil Engineers Proc., v. 81, separate 717, 11 p.

Richardson, Donald, Bingham, J. W., and Madison R. J., 1968, Water resources of King County, Washington, *with a section on* Sediment in streams, by R. C. Williams: U.S. Geol. Survey Water-Supply Paper 1852, 74 p.

Santos, J. F., and Stoner, J. D., 1972, Physical chemical and biological aspects of the Duwamish River estuary, King County Washington, 1963–67: U.S. Geol. Survey Water-Supply Paper 1873–C, 74 p.

Sládečková, Alena, 1962, Limnological investigation methods for the periphyton (aufwuchs) community: Bot. Rev., v. 28, no. 2, p. 286–350.

Stoner, J. D., 1967, Prediction of salt-water intrusion in the Duwamish River estuary, King County, Washington, *in* Geological Survey research 1967: U.S. Geol. Survey Prof. Paper 575–D, p. D253–D255.

Strickland, J. D. H., and Parsons, T. R., 1968, A practical handbook of seawater analysis: Fisheries Research Board Canada Bull. 167, 311 p.

Tilley, L. J., 1972, A method for rapid and reliable scraping of periphyton slides, *in* Geological Survey research 1972: U.S. Geol. Survey Prof. Paper 800–D, p. D221–D222.

Tilley, L. J., and Dawson, W. A., 1971,, Plant nutrients and the estuary mechanism in the Duwamish River estuary, Seattle, Washington, *in* Geological Survey research 1971: U.S. Geol. Survey Prof. Paper 750–C, p. C185–C191.

Welch, E. B., 1969, Factors initiating phytoplankton blooms and resulting effects on dissolved oxygen in Duwamish River estuary Seattle, Washington: U.S. Geol. Survey Water-Supply Paper 1873–A, 62 p.

Welch, E. B., Emery, R. M., Matsuda, R. I., and Dawson, W. A., 1972, The relation of periphytic and planktonic algal growth in an estuary to hydrographic factors: Limnology and Oceanography, v. 17, no. 5, p. 731–737.

Welch, E. B., and Isaac, G. W., 1967, Chlorophyll variation with tide and with plankton productivity in an estuary: Water Pollution Control Federation Jour. v. 39, no. 3, p. 360–366.

Wetzel, R. G., 1965, Techniques and problems of primary productivity measurements in higher aquatic plants and periphyton, *in* Goldman, C. R., ed., Primary productivity in aquatic environments: Ist. Italiano Idrobiologia Mem., supp. 18, p. 249–267; printed [1966] by California Univ. Press, Berkeley, Calif.

Jour. Research U.S. Geol. Survey
Vol. 3, No. 3, May–June 1975, p. 261–271

UPWARD MIGRATION OF DEEP-WELL WASTE INJECTION FLUIDS IN FLORIDAN AQUIFER, SOUTH FLORIDA

By M. I. KAUFMAN and D. J. McKENZIE, Tallahassee and Miami, Fla.

Abstract—Geochemical data from an industrial deep-well waste injection system southeast of Lake Okeechobee indicate a decrease in sulfate concentration concomitant with an increase in hydrogen sulfide concentration, a result of oxidation of injected organic waste by anaerobic bacteria. Subtle decreases in the sulfate-chloride ratio suggest that the waste migrated upward to a shallow monitor well about 27 mo after waste injection began and again within 15 mo of the resumption of waste injection after the injection well was deepened. The possibility of a hydraulic connection between the injection zone and overlying monitoring zone is implied. The decrease in the sulfate-chloride ratio appears to be a sensitive indicator of waste migration. Potential conflicts exist in the use of the Floridan aquifer for waste disposal and subsequent use as a natural resource.

Hydraulic and geochemical data were collected at an industrial deep-well waste injection system southeast of Lake Okeechobee near Belle Glade, Fla. (fig. 1), during 1971–73 as part of the U.S. Geological Survey's research program to evaluate the effects of underground waste disposal on the Nation's subsurface environment (Kaufman, 1973).

The objectives of this investigation were to understand more comprehensively subsurface geochemical interactions of injected liquid waste and to determine the movement and the ultimate fate of these wastes in a highly permeable saline carbonate aquifer.

During the investigation, anaerobic decomposition and sulfate reduction were found to result in increased hydrogen sulfide concentration (Kaufman, 1973; Kaufman, Goolsby, and Faulkner, 1973). The decrease in sulfate concentration and concomitant increase in hydrogen sulfide are attributed to oxidation of the injected organic waste by anaerobic bacteria. The principal source of sulfide is the reduction of sulfate in the native ground water, the sulfate serving as the oxygen supply for the bacteria. Since chloride is a conservative parameter, sulfate reduction is best expressed in terms of sulfate-chloride ratios.

In discussing the upward migration of the waste, Kaufman, Goolsby, and Faulkner (1973, p. 532) noted that "* * * a slight decrease in the sulfate-to-chloride ratio suggest[s] that the waste front arrived at the shallow monitor well in February–March 1969, about 27 months after waste injection began." Upward migration of the waste was first detected by the operators several months later, during the fall of 1969.

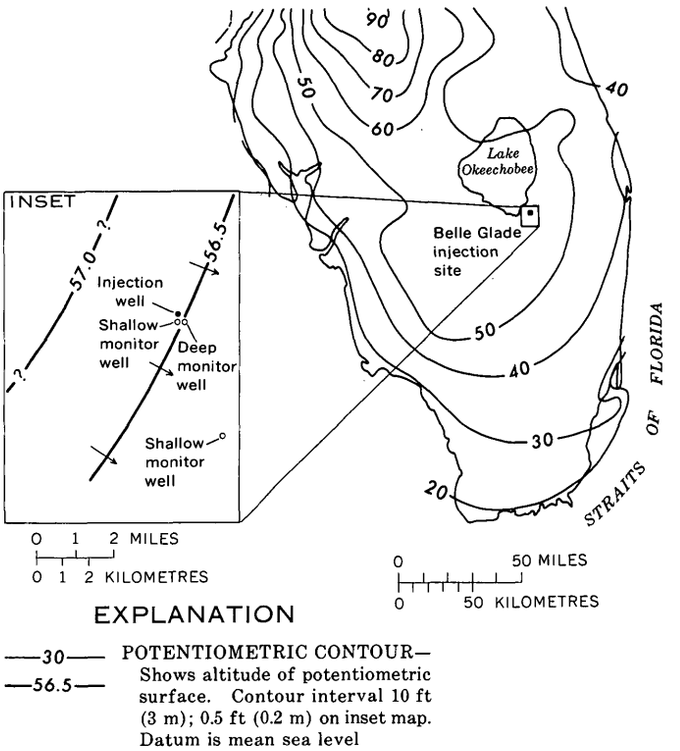

FIGURE 1.—Belle Glade area and potentiometric surface map of Floridan aquifer in south Florida (modified from Healy, 1962). Arrows show direction of ground-water movement.

The purpose of this paper is (1) to evaluate subsurface geochemical interactions of injected liquid wastes, (2) to explore the concept that changes in sulfate-chloride ratios are a sensitive indicator of the migration of these organic wastes, and (3) to evaluate the movement and position of the waste front.

In this report values are given in both English and metric units of measurement. The following table lists the factors used for conversion of the English units to the metric International System (SI) units:

Conversion table

English units	*Multiply by*	*To obtain metric units*
Inches (in)	2.54	Centimetres (cm).
Feet (ft)	.3048	Metres (m).
Miles (mi)	1.609	Kilometres (km).
Gallons	3.785×10^{-3}	Cubic metres (m^3).
Million gallons (10^6 gal).	3,785	Cubic metres (m^3).
Gallons per minute (gal/min).	6.309×10^{-5}	Cubic metres per second (m^3/s).
Million gallons per day (Mgal/d).	.04381	Cubic metres per second (m^3/s).
Square feet per day (ft^2/d).	.0929	Square metres per day (m^2/d).
Feet per day (ft/d)	.305	Metres per day (m/d).

Acknowledgments.—The authors thank Robert Pease, R. F. LaRovere, and Fred Rumagosa of the Quaker Oats Co., for their cooperation and assistance during sampling, and J. I. Garcia-Bengochea and Ross Sproul of Black, Crow, and Eidsness, Inc., for furnishing data and engineering reports on the deep-well injection system.

HYDROGEOLOGIC SETTING AND DESCRIPTION OF INJECTION SYSTEM

Early Tertiary age carbonate rocks that include several highly permeable cavernous zones filled with saline water and separated from one another by dense, relatively impermeable carbonate or evaporite beds underlie southern Florida at depths from about 1,000 to 3,500 ft (305–1,070 m). The upper 1,000 ft (305 m) of this thick carbonate section is a part of the principal artesian aquifer of the southeastern United States, commonly called the Floridan aquifer in Florida (Stringfield, 1966).

The Floridan aquifer, as defined by Parker, Ferguson, Love, and others (1955, p. 188–189), consists mostly of limestone and dolomite of middle Eocene to middle Miocene age. The permeability of the aquifer and of those Tertiary carbonate rocks underlying it is variable; in many places the rocks in the intervals between zones of relatively impermeable limestone and dolomite are extremely cavernous. Figure 2 shows the general sequence of permeable and impermeable beds in a subsurface section from Belle Glade to the Straits of Florida.

From December 1966 through 1971, hot acid liquid waste was injected into the lower part of the Floridan aquifer at the Belle Glade site between depths of about 1,500 and 1,900 ft (460 and 580 m). The injection zone is separated from the overlying upper part of the Floridan aquifer by 150 ft (46 m) of dense carbonate rocks. The confining beds above and below the injection zone and the beds in the aquifer are subject to attack by the acid waste injected.

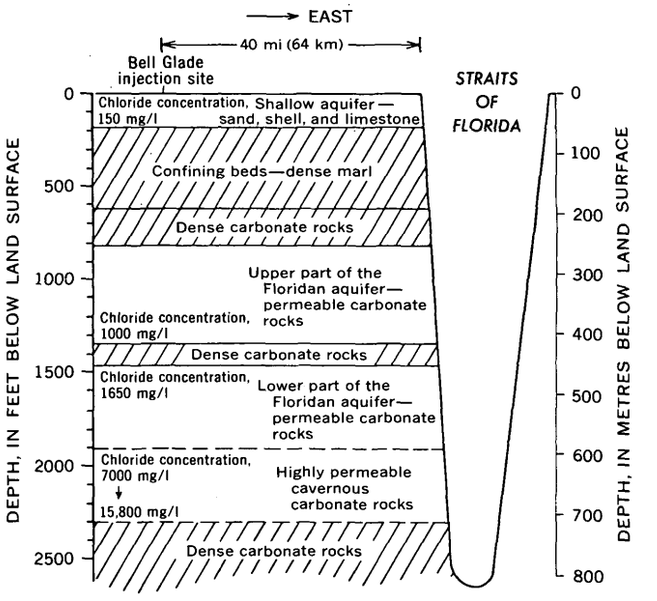

FIGURE 2.—Generalized hydrogeologic section between Belle Glade and the Straits of Florida (partial data sources include Garcia-Bengochea and Vernon, 1970, and Kaufman, 1973).

The Belle Glade injection system consists of one injection well, one shallow monitor well, and one deep monitor well which is also used as a standby injection well (fig. 3). The two monitor wells are used to assess the effects of waste injection on the aquifer.

The injection well was originally cased to a depth of 1,495 ft (465 m) with 12-in (30-cm) casing and was completed as an open hole to a depth of 1,939 ft (591 m) in the lower part of the Floridan aquifer. Injection was through an 8-in (20-cm) stainless steel liner run to the bottom of the casing and set with a packer.

The shallow monitor well is 75 ft (23 m) south of the injection well. The well is cased to a depth of 648 ft (198 m) and is completed as an open hole to a depth of 1,400 ft (427 m) in the upper part of the Floridan aquifer. The well monitors hydraulic and geochemical effects within the upper part of the Floridan aquifer above the confining beds and within the upper 50 ft (15 m) of the confining beds.

The deep monitor well is 1,000 ft (305 m) southeast of the injection well and is used to assess effects within the injection zone. It is cased to 1,490 ft (454 m) with 12-in (30-cm) casing and is completed as an open hole to 2,067 ft (630 m) in the lower part of the Floridan aquifer. This well also has an 8-in (20-cm) stainless steel liner run to the bottom of the casing and set with a packer.

The injected waste fluids include the effluent from a furfural plant and from an adjacent sugar mill. Fur-

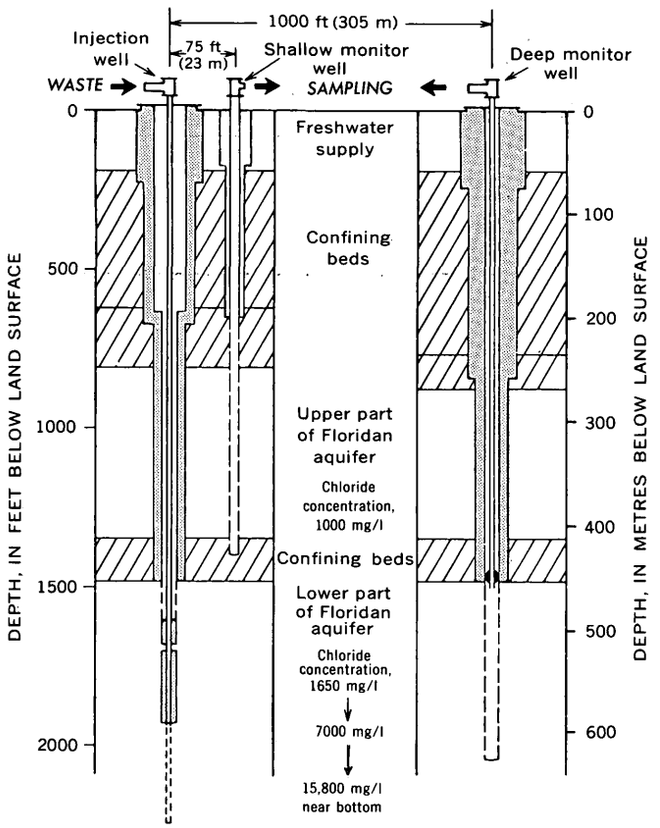

FIGURE 3.—Industrial waste injection and monitoring system, as of January 1972 after deepening injection well. Before deepening, the casing depth was 1,495 ft and the open-hole depth was 1,939 ft. (Modified from Garcia-Bengochea and Vernon, 1970.) Chloride concentrations at a given depth were the same after deepening the well as they were before.

fural is an aldehyde processed from sugarcane bagasse. The effluent is hot and acidic (≈1 percent acetic acid) and has a large content of organic material.

When injection began late in 1966, it was seasonal; by 1973 it had become more or less continuous. During 1966–73 more than 1.1 billion gallons (4.16×10^6 m^3) of waste were injected. Dissolution of the carbonate rocks is indicated by comparing a borehole caliper log of the 100-ft (30-m) section of the injection well just below the casing made in June 1966 with one made in August 1971 (Kaufman, 1973). The logs show considerable enlargement of the borehole and localized channels in the carbonate rocks. The injection index (injection rate divided by the difference between bottom-hole pressure and preinjection pressure) has increased indicating that the permeability near the well bore has increased locally.

As indicated by traces of acetate ion, the liquid waste was detected at the deep monitor well in 1967 shortly after operations started, according to Vernon and Garcia-Bengochea (1967) and Garcia-Bengochea and Vernon (1970).

An increase in COD and a decrease in pH were detected by the company in the shallow monitor well in the fall of 1969, at the start of the fourth operating season, and indicated upward migration of the injected waste.

Native ground water near the base of the upper part of the Floridan aquifer contains about 1,000 mg/l chloride. A permit for the injection system, issued by the Florida State Board of Health, limited waste injection into zones of native ground water containing more than 1,500 mg/l chloride.

In an effort to confine the waste to the lower part of the Floridan aquifer, the well was modified. In the fall of 1971, the well was deepened to 2,242 ft (683 m), and the liner (inner casing) was extended and cemented to 1,938 ft (591 m) (fig. 3).

During the modification phase, October 1971 through January 1972, the deep monitor well was used for waste injection. More than 75 million gal (2.84×10^5 m^3) of waste was injected. Injection of liquid waste into the deepened injection well was resumed in mid-January 1972.

METHODS OF STUDY

Injected waste, native Floridan aquifer water, and fluids from the injection zone were periodically sampled for comprehensive chemical analyses and for determination of dissolved gases and microbe concentration (Kaufman and others, 1973).

To detect and estimate the concentration of anaerobic sulfate-reducing bacteria, a procedure of serial inoculation of water from the monitor wells and the waste into a series of 9-ml sterile vials containing Bacto-sulfate API Broth (code 0500, Difco Laboratories) was utilized in March 1972. The procedure was carried out in accordance with the recommended practice given by the American Petroleum Institute (1959).

Dissolved gas samples were collected from the shallow monitor well and deep monitor well in October 1971 and March 1972, respectively. The samples were collected by use of a Hamilton gastight syringe and were analyzed by use of gas chromatography.

Comprehensive chemical analyses of the water samples included such determinations as hydrogen sulfide, pH, alkalinity, acidity, sulfate, chloride, organic carbon, turbidity, COD, and specific gravity. Correlations of specific chemical data were made between the injected fluid and the fluids in the shallow and deep monitor wells. The movement and position of the waste front were calculated on the basis of an assumed porosity and permeability distribution, and chloride distribution within the upper part of the Floridan aquifer was assessed.

Changes in sulfate-chloride ratios in the monitor well fluids were evaluated and compared with operational changes in the injection system. Emphasis was placed on interpreting observed changes in this ratio with respect to waste migration. By use of a ratio rather than absolute concentration, it is relatively simple to discriminate between changes due to sulfate reduction associated with waste migration and changes due to dilution and or mixing of various waters. The extent of mixing with underlying more saline waters having a lower sulfate to chloride ratio may be ascertained from the chloride concentration.

RESULTS AND DISCUSSION

Injected waste

The injected waste is hot (≈75°–93°C), acidic (pH≈2.6–4.5), and high in organic and nitrogen and phosphorus concentrations. The organic carbon concentration exceeds 5,000 mg/l and suspended solids exceed 1,800 mg/l. The chloride concentration of approximately 100 mg/l is more than an order of magnitude lower than that of the native ground water in the injection zone. The sulfate concentration ranges from 80 to 190 mg/l. Owing to the higher temperature and relatively low salinity at which the waste is injected, the waste is less dense than the native ground water (Kaufman, and others, 1973).

Backflow of injected waste (from deep monitor well)

The deep monitor well was used for waste injection from October 8, 1971, to January 12, 1972. After cessation of waste injection the injected wastes were allowed to backflow continuously at about 2 to 3 gal/min (12–80×10^{-5} m^3/s. The fluid was sampled to provide information on subsurface geochemical interactions, anaerobic degradation, and the ultimate fate of organic wastes with residence time.

Evaluation of the chemical data for the backflushed fluid indicates that the fluid was partly neutralized and decomposed. The waste was partly neutralized to a pH of 5.5 within the carbonate environment almost immediately (January 1972), after which the pH gradually increased until at about a pH of 6.5 equilibrium between carbonate and waste was established.

In native ground water, the relation between chloride concentration and that of several other constituents present is constant. Therefore, the concentration of various constituents of native ground water may be accurately estimated if the chloride concentration is known, chloride behaving as a conservative parameter. Table 1 shows the composition of native ground water with concentrations of constituents "normalized" to ground water having a chloride concentration of 1,300 mg/l, as compared to the actual composition of injection zone fluids backflushed from the deep monitor well and having an equivalent chloride concentration. Significant changes from the "normalized" composition indicate subsurface geochemical interactions.

TABLE 1.—*Changes in injection zone fluid 75 days after waste emplacement*

	Normalized composition[1]	Actual composition[2] (mg/l)	Percent change
Chloride	1,300	1,300	0
Alkalinity (as $CaCO_3$)	100	3,920	+3,820
Calcium	120	1,100	+817
Magnesium	125	700	+460
Silica	18	58	+220
Sulfate	420	228	−45
SO_4:Cl ratio	0.32	0.18	−44
H_2S	4	68	+1,600

[1] Composition of native ground water with concentrations of constituents normalized to ground water having a chloride concentration of 1,300 mg/l.
[2] Composition of injection zone fluids backflushed from deep monitor well 75 days after emplacement of wastes.

Alkalinity increased substantially (probably because of weak acids in the injected waste), as did hydrogen sulfide, the latter increase due to sulfate reduction by anaerobic bacteria. Increases in calcium, magnesium, and silica are attributed to dissolution of carbonate and minor amounts of quartz within the injection zone.

Sulfate reduction with time in the backflushed fluid, accompanied by an increase in hydrogen sulfide, is indicated in figure 4. The sulfate-chloride ratio decreased from 0.38 to 0.005, the sulfate concentration decreased from 365 to 4 mg/l, and the hydrogen sulfide concentration increased from 3.4 to 87 mg/l. The increase in chloride concentration during 1972 reflects mixing with underlying, more saline, native ground water.

A gas sample collected from the deep monitor well on March 27, 1972, contained about 75 percent carbon dioxide, 23 percent methane, and 2 percent nitrogen. Additionally, the presence of sulfate-reducing bacteria in the backflushed fluid was confirmed. Hydrogen sulfide concentration was 68 mg/l.

Thus, oxidation of the organic waste by anaerobic bacteria is taking place within the saline subsurface environment. The principal source of hydrogen sulfide is the reduction of sulfate which serves as an oxygen source for the bacteria.

Also, in the process of methane fermentation (reduction of CO_2 to CH_4), dissolved carbon dioxide could

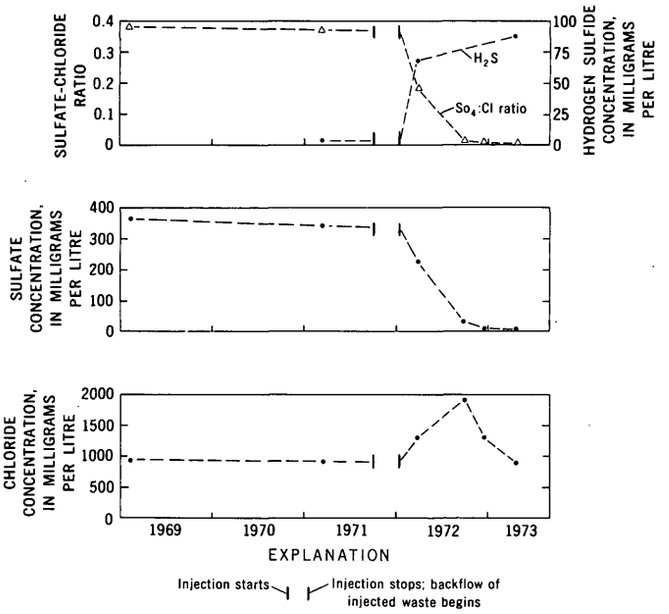

FIGURE 4.—Sulfate reduction and changes in chloride concentration with time in fluid from the deep monitor well.

serve as an oxygen source for the anaerobic oxidation of organic matter in the waste, methane gas being one of the byproducts of bacterial use of the waste. Both sulfate reduction and methane fermentation are apparently occurring.

In this system the decreased sulfate concentrations can be quantitatively accounted for by the increased hydrogen sulfide concentration, which is attributed to sulfate reduction. However, in other systems some loss of sulfate might be accounted for by sulfate precipitation as calcium sulfate (gypsum) (D. A. Goolsby, U.S. Geol. Survey, written commun., Mar. 29, 1974). This probability is suggested because of the decreasing solubility of gypsum with increasing temperature, coupled with increased calcium concentration due to dissolution of carbonate.

Geochemical effects (shallow monitor well fluids)

Upward migration of the acidic waste to the shallow monitor well is indicated by analyses of water from that well (table 2). The effects by March 1971 include increase in calcium and organic carbon contents, COD, color, and alkalinity; decrease in pH, sulfate content, and sulfate-chloride ratios; and generation of a considerable quantity of hydrogen sulfide.

The reduction of sulfate with time (indicated by changes in sulfate-chloride ratios) in fluid from the shallow monitor well is shown in figure 5. Changes in the sulfate-chloride ratios are compared with operational changes in the injection system and with presumed arrival of the organic-rich waste at the shallow monitor well. During 1969–70 and the first half of 1973, the reduction of sulfate with time is similar to that shown in figure 4 after the commencement of backflow of injected waste from the deep monitor well. Native water from the upper part of the Floridan aquifer at the injection site has a sulfate-chloride ratio greater than 0.40 (table 2) and a hydrogen sulfide concentration of about 4 mg/l.

Subtle chemical changes in water from the shallow monitor well, as indicated by slight increases in calcium and chloride concentration and in alkalinity, and by a decrease in the sulfate-chloride ratio from 0.41 to 0.35 (fig. 5), suggest that the waste migrated upward to the shallow monitor well in February or March 1969, about 27 mo after waste injection began. The operators reported upward leakage of waste at the shallow monitor well in November 1969. The sulfate-chloride ratio declined to 0.22 by March 1971. The sulfate concentration decreased from 350 mg/l in February 1969 to 186 mg/l in March 1971.

Analyses of the three samples collected from March 1971 through March 1972 suggest that the water from the shallow monitor had stabilized (table 2), probably owing, in part, to the temporary cessation of injection of wastes and the deepening of the injection well.

TABLE 2.—*Partial chemical analyses—shallow monitor well, Belle Glade, Fla.*

[Analyses in milligrams per litre, except as indicated. Jtu, Jackson turbidity units. Color, platinum—cobalt units]

	3–14–66 [1]	2–5–69 [1]	3–4–69 [1]	3–18–71	10–20–71	3–28–72	9–28–72	12–15–72	4–19–73	7–6–73
Alkalinity (as $CaCO_3$)	118	132	157	902	898	902	845	853	902	925
pH	7.4	7.85	8.00	6.61	6.61	6.47	-----	6.5	6.6	6.4
Calcium	99	105	118	258	252	250	270	260	280	240
COD	-----	20	-----	[1] 698	[1] 461	[1] 486	[1] 529	1,100	1,100	[1] 410
								[2] (311)	[1] (726)	
Organic carbon	-----	-----	-----	475	480	365	280	334	274	237
Color (units)	1	0	8	50	60	20	40	120	40	60
Turbidity (Jtu)	-----	-----	-----	-----	20	20	30	110	100	120
Sulfate	364	350	363	186	218	210	310	380	240	170
Chloride	855	845	1,025	830	870	940	860	900	900	860
H_2S	-----	-----	-----	85	98	83	-----	-------	72	-----
SO_4:Cl ratio	0.48	0.41	0.35	0.22	0.25	0.22	0.36	0.42	0.27	0.20

[1] Furnished by courtesy of Black, Crow, and Eidsness, Inc., Gainesville, Fla. Analysis on or within 1 day of date shown.
[2] Analysis 12–12–72. Furnished by courtesy of Black, Crow, and Eidsness, Inc.

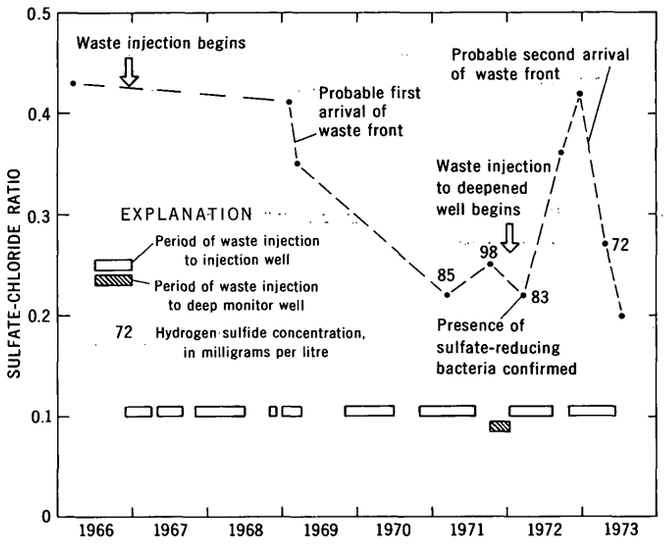

FIGURE 5.—Sulfate reduction with time in fluid from the shallow monitor well.

Hydrogen sulfide concentrations ranged from 83 to 98 mg/l during that same period. Methane, nitrogen, and carbon dioxide were present in March 1971, and the presence of anaerobic sulfate-reducing bacteria was confirmed in March 1972.

The slight increase in the sulfate-chloride ratio just prior to October 1971 is correlated with a plant shutdown. Waste injection into the deepened injection well began in January 1972. Subsequently, in March 1972, the sulfate-chloride ratio in the shallow monitor well fluid decreased slightly.

From March to September 1972 the ratio increased from 0.22 to 0.36. Beyond September 1972 it continued to rise and reached a value of 0.42 by December 1972. This increase is correlated with a plant shutdown and cessation of waste injection from early August through the end of October 1972. An anomaly (perhaps owing to residual effects of the previous waste presence) is the relatively high organic carbon, color, turbidity, and COD (U.S. Geol. Survey analysis) of the fluid sampled in December 1972, occurring simultaneously with an apparent cessation of anaerobic bacterial activity.

Waste injection resumed in November 1972, after which the sulfate-chloride ratio decreased from 0.42 in December 1972 to 0.27 in April and to 0.20 in July 1973. The sulfate concentration decreased from 380 mg/l in December 1972 to 170 mg/l in July 1973 while the chloride concentration remained almost constant. Acidity increased slightly from 1.0 meq/l of hydrogen ions in December 1972 to 3.9 meq/l in April 1973.

The decrease in ratio suggests a return of the nutrient-rich, organic-rich waste, a return contributing to increased anaerobic bacterial metabolic activity. The decrease in the ratio is significant in that it suggests that the waste migrated upward again to the shallow monitor well during or before April 1973, within 15 mo of the resumption of waste injection into the deepened injection well in January 1972. Further, if the resumption of waste injection in November 1972 is used as the base of reference, then a response to injection was detected within 6 mo in the shallow monitor well. In June 1973 the injection well was shut down by the operators, and the injection of waste was again shifted to the deep monitor well.

The upward migration of the waste after resumption of waste injection, in part due to solution of the carbonate rocks, may also be attributed to increased effective transmissivity resulting from the higher temperature and hence the comparatively lower viscosity of the waste fluid with respect to formation fluid. As discussed in detail later, the apparent hydraulic conductivity of the aquifer at the injection site could increase about 2.5 times because of temperature difference alone.

Percentage changes in certain parameters in shallow monitor well fluids from March 1966 to March 1971 and from December 1972 to July 1973 are given in table 3. Chloride serves as a conservative parameter for comparison. Calcium concentration increased markedly from 1966 to 1971, attributed to dissolution of carbonate rock. Alkalinity also increased, probably associated with the presence of weak acids in the injected waste. Sulfate concentration and the sulfate-chloride ratio decreased because of sulfate reduction associated with anaerobic decomposition of the waste.

TABLE 3.—*Changes in shallow monitor well fluids*

Parameter	Percentage changes	
	Mar. 1966 to Mar. 1971	*Dec. 1972 to July 1973*
Chloride	−3	−4
Calcium	+160	−8
Alkalinity	+665	+8
Sulfate	−49	−55
SO_4:Cl ratio	−49	−52

From December 1972 to July 1973 calcium and alkalinity changed very little, reflecting the residual effects of the previous waste presence; however, sulfate concentration and the sulfate-chloride ratio changed considerably, apparently reflecting the greater sensitivity of these parameters to renewed waste migration with consequent increased bacterial action.

The quick response and apparent sensitivity of the sulfate-chloride ratio to operational changes in the injection system implies the possibility of a hydraulic connection between the injection zone and the overlying upper part of the Floridan aquifer. This possibility

is supported by a comparison of pH data for samples from the shallow and deep monitor wells collected June 1972 through May 1973 (fig. 6) and by a comparison of COD data for samples collected January 1972 through February 1973 fig. 7).

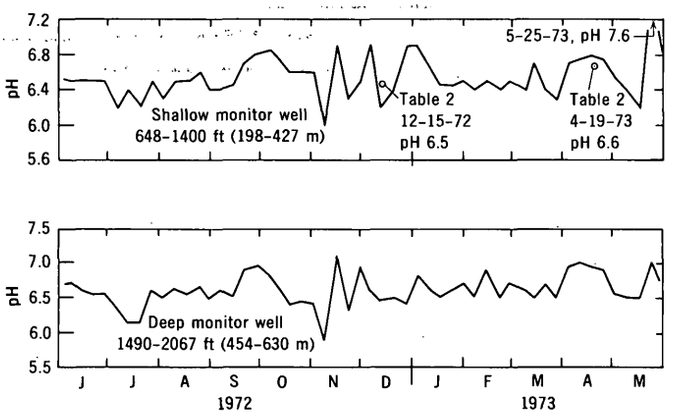

FIGURE 6.—Comparison of pH data for the shallow and deep monitor wells. (Data furnished by courtesy of Quaker Oats Co.)

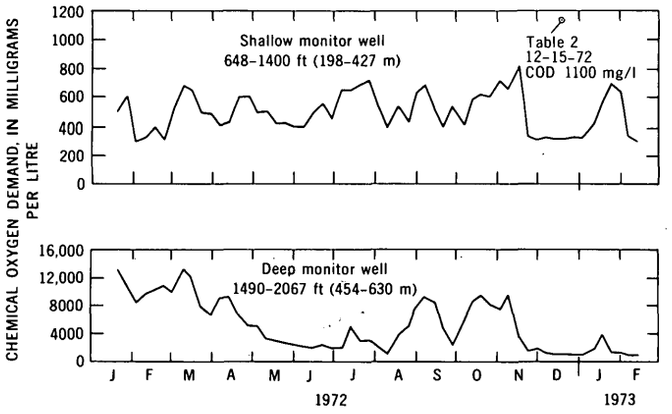

FIGURE 7.—Comparison of COD data for the shallow and deep moniter wells. (Data furnished by courtesy of Quaker Oats Co.)

Weekly data furnished by the company were used for consistency in comparison during the above time periods.

Movement and position of the waste front

An increase in COD of the fluid from the deep monitor well from August to November 1972 might be attributed to the arrival of a new waste front from the injection well, where waste injection recommenced on January 13, 1972.

To explore this possibility, the COD of the injected waste was plotted for the period January 19 through August 9, 1972, and compared with a COD plot for the fluid from the deep monitor well (fig. 8). Some similarities are evident. The fluctuations in COD of the fluid from the deep monitor well appear to be a somewhat drawn out and diluted version of the fluctuations in COD of the injected waste. The fluid from the deep monitor well appears to reflect, with a 2–3 mo lag, the chemistry of the injected effluent to be expected after the waste is mixed and diluted with native fluids as it moves the 1,000 ft (305 m) to the deep monitor well. Further, the presence of new waste in the fluid from the deep monitor well is indicated by an increase in acidity, from 4 meq/l of hydrogen ions in December 1972 to 23 meq/l in April 1973.

If waste injected in June and July 1972 (about 50×10^6 gal or 1.89×10^5 m^3) was detected in the deep monitor well during August through November 1972 (fig. 8), the implication is that the waste moved predominantly through a relatively thin part of the injection zone (discussed below), probably a cavernous zone. As noted earlier, effects of waste injection were detected at the deep monitor well in 1967 (Vernon and Garcia-Bengochea, 1967; Garcia-Bengochea and Vernon, 1970). This also indicates that the waste moved through a relatively thin section of the injection zone, considering the volume of waste injected by that time (about 40×10^6 gal or 1.51×10^5 m^3).

The thickness of the injection zone (h) through which the waste is moving and the position of the waste front (r) can be estimated by the following equations:[1]

$$h=\frac{V}{7.48\pi r^2\phi}, \qquad (1)$$

and

$$r=\sqrt{\frac{V}{7.48\pi h\phi}}, \qquad (2)$$

or in metric units

$$h=\frac{V}{\pi r^2\phi}, \qquad (1)$$

and

$$r=\sqrt{\frac{V}{\pi h\phi}}, \qquad (2)$$

where V is pore volume in gallons (cubic metres), r is radius of storage area (that is, position of waste front) in feet (metres), h is thickness of injection zone in feet (metres), and ϕ is porosity in percent.

A porosity of 33 to 35 percent in chalky limestone indicated by Puri and Winston (1974) is based on their geologic framework studies in south Florida. They also note a 10 to 20 percent porosity in dolomite and a dominance of horizontal permeability over vertical permeability. Thus, assumed porosities of 15 per-

[1] Does not take into account the possible effects of (1) drift downgradient with the native ground water flow and (2) temperature on the viscosity of the waste fluid and hence on the hydraulic conductivity of the aquifer, to be discussed later in this report.

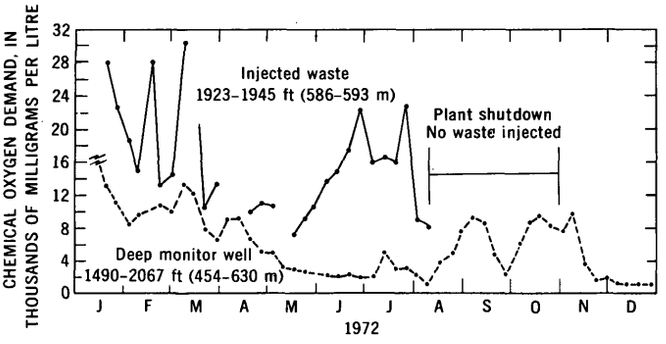

FIGURE 8.—Comparison of COD data for the injected waste and for the fluid from the deep monitor well. (Data furnished by courtesy of Quaker Oats Co.)

cent and 35 percent are used to establish reasonable limits to subsequent calculations and interpretations.

On the basis of the observations of times of travel, previously noted for 1967 and 1972, which are in agreement with the volume of waste injected, and assuming radial movement of waste from the injection well, we estimated the waste was moving predominantly through a 10-ft (3-m)-thick section.

If the potential occurrence of upward leakage is recognized, the position of the waste front would be a maximum when calculated on the basis of the previous assumptions. If a porosity of 15 percent is assumed and if all the waste injected through July 1973 moved radially outward through a section that is 10 ft (3 m) thick, the probable position of the waste front in September 1973 would be about 1 mi (1.6 km) from the center of the injection well system. If a porosity of 35 percent is assumed, the probable position of the waste front would be about 0.6 mi (1 km) from the assumed point of injection. Curves reflecting these computations and showing the estimated position of the waste front versus time are given by curves 1 and 2 in fig. 9.

Caliper logs run prior to deepening the injection well indicate that the waste initially seemed to be moving through a 100-ft (30-m)-thick section. Computations using h equals 100 ft (30 m) are presented as curves 3 and 4 in figure 9.

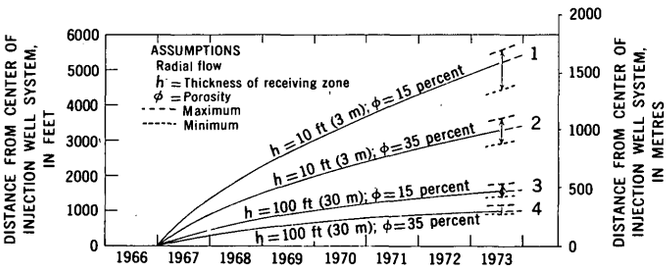

FIGURE 9.—Estimated position of the waste front, Belle Glade system.

From January 1972 through June 1973, 400×10^6 gal (1.51×10^6 m^3) of waste were injected into a deeper horizon below 1,900 ft (580 m) (fig. 3). Two assumptions are made: (1) All waste migrates to initial injection zone (below 1,500 ft; 457 m), or (2) no waste migrates to initial injection zone. These establish maximum and minimum extremes for the position of the waste front as shown in figure 9. Given the known lithology and nature of the waste, there is no reason to expect that the waste will remain below 1,900 ft (580 m).

Of the four curves presented in figure 9, those assuming a receiving zone 100 ft (30 m) thick (curves 3 and 4) are not consistent with data on the time of travel to the deep monitor well. The most probable position of the waste front lies somewhere between 0.6 and 1 mi (1 and 1.6 km) from the center of the injection well system in September 1973, as defined by curves 1 and 2. Verification of the above estimates would require a deep monitor well positioned about 1 mi (1.6 km) downgradient.

Where permeability of the limestone is high and cavernous zones occur, uniform radial movement is unlikely. Rather, it would seem that waste movement is controlled by preferential zones of circulation such as solution channels.

The concept of drift of the waste cone downgradient —in the direction of natural ground-water flow—is not considered in the foregoing calculations of the position of the waste front. However, the rate of such drift can be evaluated by the following equation:

$$V=\frac{365\,KI}{\phi}, \qquad (3)$$

where V is velocity, K is hydraulic conductivity, I is hydraulic gradient (dimensionless), and ϕ is porosity in percent.

The hydraulic gradient (fig. 1) is relatively low, ranging from about 3.16×10^{-5} to 9.47×10^{-5} ft/ft (m/m). Assumed porosities of 15 percent and 35 percent may be used as in an earlier discussion. Hydraulic conductivity values for the aquifer at the injection site are not available and are virtually nonexistent for the aquifer anywhere in southeast Florida. However, data obtained from an aquifer test of a well tapping the Floridan aquifer within the depth range from 1,100 to 1,400 ft (335–427 m) about 100 mi (161 km) south of the injection site (Porter Knowles of Dames and Moore, oral commun., July 16, 1974) indicate a transmissivity of about 33,500 ft^2/d (3,100 m^2/d) and a hydraulic conductivity of about 110 ft/d (34 m/d). At the injection site—assuming that hydraulic conductivity does not change significantly through

this 100-mi (161-km) reach and a 300-ft (91-m) thickness of aquifer is representative—drift is computed from equation 3. For the two assumed porosity values, drift would be about 3.7 to 8.6 ft/yr (1.1–2.6 m/yr) under a hydraulic gradient of 3.16×10^{-5} and about 11 to 26 ft/yr (3.4–7.9 m/yr) under a hydraulic gradient of 9.47×10^{-5}. These rates are considered minor; however, they do not take into account the effects of temperature.

Because viscosity changes with temperature, the relatively high temperature (75°–93°C) at which the waste fluid is injected results in an increase in effective transmissivity and, hence, the hydraulic conductivity of the aquifer. A comparison of the hydraulic conductivities of the aquifer containing native fluids at about 26.5°C (K_1) with that of the aquifer containing liquid wastes at about 85° C (K_2) can be approximated by the following equation (Lohman and others, 1972):

$$K_2=\frac{\nu_1 K_1}{\nu_2}, \qquad (4)$$

where ν_1/ν_2 is the dimensionless ratio of the kinematic viscosities of the native fluid and the liquid waste, respectively.

Solving equation 4 for the specified temperatures yields

$$K_2=\frac{0.87}{0.35}K_1=2.5\ K_1.$$

Thus, the hydraulic conductivity in the immediate vicinity of the injection well (and consequently the rate of waste movement) due to temperature alone can be increased 2.5 times over that of the native ground water. Enhanced upward migration of the waste at the injection site may be related in part to this temperature effect as mentioned earlier.

Dissipation of the heat with time and distance as the waste moves through the aquifer is anticipated. A sample of injected waste, backflushed from the deep monitor well after 75 d of residence time in the aquifer, had a temperature of 40°C. Owing to the increased temperature, the rate of drift of the waste cone is expected to be somewhat greater than that of the native ground water and could be as much as 2.5 times greater.

Chloride distributions

Natural chloride distributions within the Floridan aquifer are of significance with respect to the migration and ultimate fate of the waste fluids.

Stringfield (1933), in studying the chemistry of water from the experiment station well 3 mi (4.8 km) south-southeast of the injection site, noted that a sample of water from a depth between 300 and 900 ft (91 and 274 m) was more mineralized (chloride 2,250 mg/l) than a sample from a depth between 957 and 1,332 ft (292 and 406 m) (chloride 1,650 mg/l).

A similar observation was made by Garcia-Bengochea and Vernon (1970) during test-well drilling at the Belle Glade site. They reported an anomalous vertical distribution of chloride; at a depth of 1,100 ft (335 m) the chloride concentration was 1,200 mg/l, whereas at a depth of 1,320 ft (402 m) the chloride concentration was 620 mg/l.

The above observations are plotted on a northwest-southeast cross-section along with isochlors reflecting an interpretation of the chloride distribution within the Floridan aquifer (fig. 10).

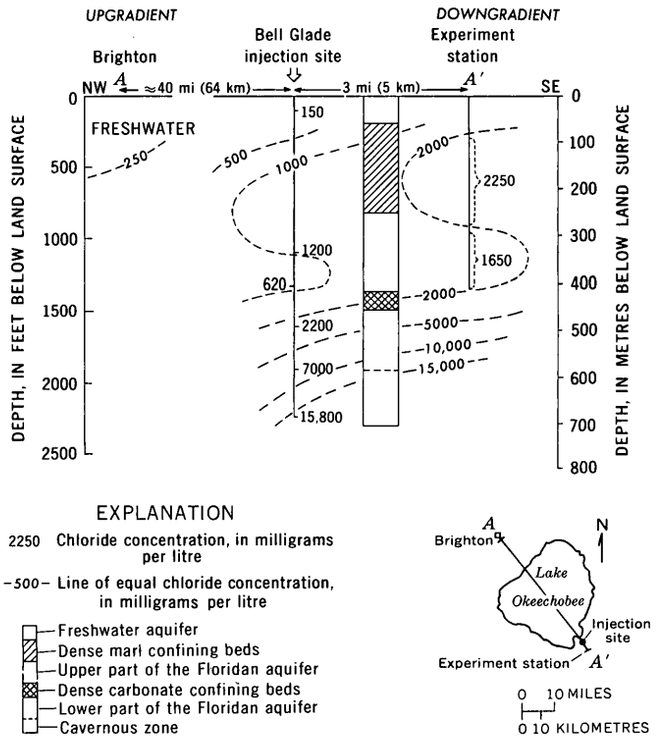

FIGURE 10.—Diagrammatic section showing chloride distributions within the artesian aquifer system, Belle Glade area.

The chloride distribution suggests good groundwater circulation and permeability near the base of the upper part of the Floridan aquifer. This, in turn, indicates a preferred avenue for waste migration should the waste leak upward from the injection zone and an increased potential for lateral movement of the upward leaking waste within this particular zone, a zone for which other uses are contemplated. These include freshwater storage and potential desalinization in coastal areas, less than 40 mi (64 km) to the east.

Further, as noted by Klein (1971), the upper part of the Floridan aquifer (fig. 10) contains potable water about 40 mi (64 km) to the northwest upgradient from Belle Glade. Thus, the potential for conflicting uses of the aquifer should be recognized, especially in regard to the future development and use of the subsurface environment as a natural resource.

A detailed vertical profile showing chloride distributions at the Belle Glade site in March 1966 (Black, Crow, and Eidsness, Inc., 1965) is given in figure 11 (left). The profile indicates that two zones of relatively high permeability are present as follows: First, a narrow zone from about 950 to 1,050 ft (290–320 m), and second, a somewhat broader one from about 1,200 to 1,400 ft (366–427 m).

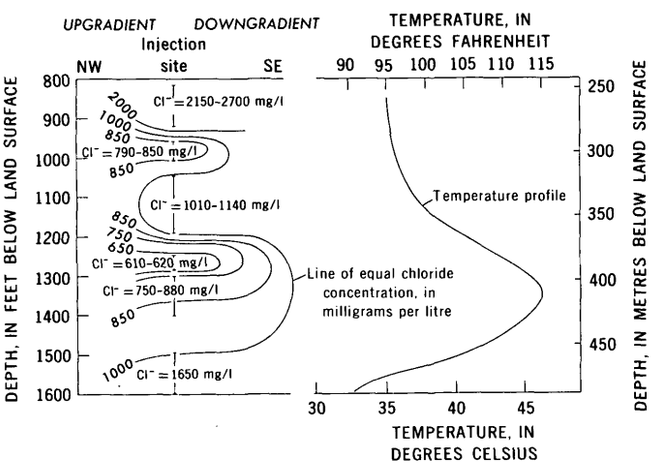

FIGURE 11.—Chloride distribution within the upper Floridan aquifer, March 1966, and temperature profile, January 1972, after 5 yr. (1966–71) of waste injection below the base of the casing at 1,495 ft. Chloride data are from Black, Crow, and Eidsness, Inc. (1965). Temperature log of injection well, January 6, 1972, after deepening and cementing casing to 1,938 ft. in fall 1971, is from the Florida Bureau of Geology (unpub. data, 1972).

On January 6, 1972, after 5 yr of waste injection, a vertical temperature profile was run by the Florida Bureau of Geology. The profile confirms that the waste has migrated upward and that the waste is positioned for the most part between 1,250 and 1,450 ft (381 and 442 m) (fig. 11, right).

Comparison of the chloride and temperature data suggests that the position of the upward leaking waste may be clearly correlated with the zone of high permeability between 1,200 and 1,400 ft (366 and 427 m). Should waste continue to leak upward, a preferred avenue for lateral waste migration within this zone seems likely to exist.

With respect to the long-term future of the waste injection system, several management alternatives based on answers to the following questions may be warranted:

1. Would surface pretreatment of the waste itself prior to injection, such as cooling, neutralization, and increasing its density, be useful in reducing or eliminating upward movement?
2. Would significant deepening of the injection system to several thousand feet be useful?
3. Should the deep-well injection system be discontinued and surface treatment be substituted?

SUMMARY

The utilization of sulfate as an oxygen source by anaerobic bacteria, apparently stimulated by the arrival of the nutrient-rich, organic-rich waste injected into the subsurface environment, results in marked reductions in sulfate-chloride ratios of the aquifer waters. Decreases in the ratio suggest that the waste migrated upward into the upper part of the Floridan aquifer about 27 mo after waste injection began and again within 15 mo after the injection well was deepened and waste injection resumed. Changes in the sulfate-chloride ratio imply a hydraulic connection between the injection zone and overlying monitoring zone and may be a sensitive indicator of subsurface waste migration where organic wastes are injected into a typical saline, high sulfate subsurface environment.

Injected waste fluid has probably migrated within the injection zone radially 0.6 to 1.0 mi (1–1.6 km) from the injection site. The waste was estimated to be moving through a 10-ft(3-m)-thick section. Chloride distributions indicate good ground-water circulation and permeability near the base of the upper part of the Floridan aquifer. Thus, a preferred avenue for waste migration and lateral movement of the upward leaking waste within this particular zone is indicated, a zone for which other uses are contemplated.

The confining beds above and below the injection zone are subject to attack by the acid waste injected; the question that remains is whether the relatively hot acid wastes can be restricted to the injection zone or whether upward movement will continue to take place. A potential for conflicting uses of the aquifer should be recognized.

REFERENCES CITED

American Petroleum Institute, 1959, Recommended practice for biological analysis of water-flood injection waters: Am. Petroleum Inst. RP 38, 6 p., issued by Am. Petroleum Inst., Div. Production, Dallas, Tex.

Black, Crow, and Eidsness, Inc., 1965, Engineering report on the drilling and testing of waste disposal well No. 1, Furfural Plant, Sugar Cane Growers Cooperative of Florida, Belle Glade, Florida: Gainesville, Fla., Black, Crow, and Eidsness, Inc., 10 p., app.

Garcia-Bengochea, J. I., and Vernon, R. O., 1970, Deep-well disposal of waste waters in saline aquifers of south Florida: Water Resources Research, v. 6, no. 5, p. 1464–70.

Healy, H. G., 1962, Piezometric surface and areas of artesian flow of the Floridan aquifer in Florida, July 6–17, 1961: Florida Geol. Survey Map Ser. 4.

Kaufman, M. I., 1973, Subsurface wastewater injection, Florida: Am. Soc. Civil Engineers Proc., Jour. Irrigation and Drainage Div., v. 99, no. I R1, p. 53–70.

Kaufman, M. I., Goolsby, D. A., and Faulkner, G. L., 1973, Injection of acidic industrial waste into a saline carbonate aquifer—geochemical aspects, *in* Braunstein, J., ed., Underground waste management and artificial recharge: Internat. Symposium, 2d. New Orleans, La., Sept. 26–30, 1973, Preprints, v. 1, p. 526–551.

Klein, Howard, 1971, Depth to base of potable water in Floridan aquifer: Florida Bur. Geology Map Ser. 42.

Lohman, S. W., and others, 1972, Definitions of selected groundwater terms—revisions and conceptual refinements: U.S. Geol. Survey Water-Supply Paper 1988, 21 p.

Parker, G. G., Ferguson, G. E., Love, S. K., and others, 1955, Water resources of southeastern Florida: U.S. Geol. Survey Water-Supply Paper 1255, 956 p.

Puri, H. S., and Winston, G. O., 1974, Geologic framework of the high transmissivity zones in south Florida: Florida Bur. Geology Spec. Pub. 20, 101 p.

Stringfield, V. T., 1933, Groundwater in the Lake Okeechobee area, Florida: Florida Geol. Survey Rept. Inv. 2, 31 p.

———1966, Artesian water in Tertiary limestone in the southeastern United States: U.S. Geol. Survey Prof. Paper 517, 226 p.

Vernon, R. O., and Garcia-Bengochea, J. I., 1967, Deep-well injection of industrial wastes in south Florida: Am. Water Works Assoc., Florida Pollution Control Assoc., joint mtg., Miami, Fla., Nov. 1, 1967, 25 p.

Jour. Research U.S. Geol. Survey
Vol. 3, No. 3, May–June 1975, p. 273–280

PRELIMINARY FINDINGS OF A LEACHATE STUDY ON TWO LANDFILLS IN SUFFOLK COUNTY, NEW YORK

By GRANT E. KIMMEL and OLIN C. BRAIDS, Mineola, N.Y.

Work done in cooperation with the Suffolk County Department of Environmental Control

Abstract.—Plumes of leachate-enriched ground water extend 10,600 and 5,000 ft (3,200 and 1,500 m) downgradient from landfills in the towns of Babylon and Islip, respectively, and extend vertically beneath the landfills to the base of the upper glacial aquifer, whose thickness ranges from 71 to 77 ft (22–24 m) at the Babylon site and is 170 ft (52 m) at the Islip site. The Babylon and Islip landfills were started in 1947 and 1933, respectively. The quantities of ground water in the plumes are 2×10^9 gal (8×10^6 m^3) at Babylon and 1×10^9 gal (4×10^6 m^3) at Islip. Differences in quantity of water in the plumes and length of the plumes may result partly from a slower rate of refuse accumulation at Islip than at Babylon; however, the rate of travel for the front of the Islip plume is considerably less than the prevailing ground-water velocity would indicate. Distance traveled by the front of the Islip plume was roughly one-third the distance indicated by the calculated minimum ground-water velocity and may result from greater vertical travel distance in the upper glacial aquifer at Islip. Concentrations of HCO_3^-, Cl^-, and SO_4^{-2} in the leachate-enriched ground water are higher than those in ambient ground water. Concentrations of Fe and Mn in the plumes are as much as 400,000 μg/l and 200,000 μg/l, but concentrations of other metals, including Zn (220 μg/l), do not exceed the U.S. Public Health Service drinking-water standards. The concentration of NH_4^+, the predominant nitrogen species in plume water, is usually more than 10 percent of the total cations in plume water and is greater than NH_4^+ concentrations in ambient ground water; concentrations of NO_3^- in plume water are less than those in ambient ground water at Babylon and at some locations in Islip.

Leachate from solid waste is a factor in the contamination of ground water (Zanoni, 1972), but, until recently, little regard was given to ground-water contamination near solid-waste disposal sites. At present (1975), the movement of leachate from waste materials is of considerable interest, but, in general, data on how such leachate affects ground-water quality have been sparse. Location, shape, and chemical characteristics of two leachate plumes near landfills in southwestern and south-central Suffolk County, N.Y., in the towns of Babylon and Islip (fig. 1) are described in this report.

METHODS OF STUDY

Quality of the ground water was determined by analysis of water samples collected from observation wells. The wells, installed by the U.S. Geological Survey for this study, consist of either 2-in(5-cm)-diam standard black iron pipe fitted with 1.25 by 36-in(3.2 by 90-cm)-long, 0.018-in(0.045-cm)-slot, wire-wrapped, stainless-steel well points, or 2-in(5-cm)-diam, PVC (polyvinyl chloride) pipe fitted with 48-in (122-cm)-long, 0.016-in(0.041-cm)-slot PVC screens. Holes for iron-pipe wells were augered to the desired depth. After the auger was removed, pipe and well point were pushed into the hole with the hydraulic table of the drilling rig. PVC-pipe wells were set with a hollow-stem auger.

The water-sampling procedure for this study was predicated on the assumption that removing as much

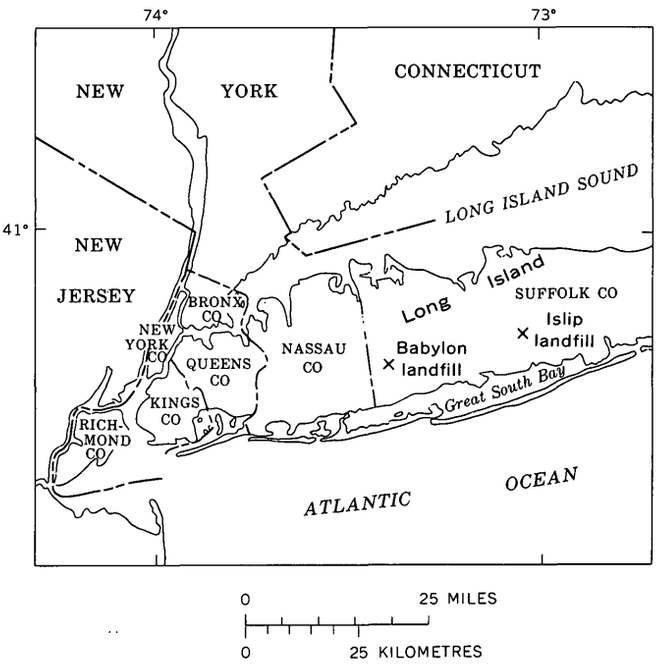

FIGURE 1.—Locations of Babylon and Islip landfills.

water as possible in as short a time as practical would flush the well bore, pump, and hoses and, thus, would minimize contamination. Yields of as much as 60 gal/min (4 l/s) were attained. Withdrawals for some samples were large enough that water may have come from as much as 10 ft (3 m) from the well screen. Given the high hydraulic conductivity and uniformity of the aquifers involved, withdrawals of this magnitude should not significantly distort the shape of the leachate plume as measured in this study. Specific conductance and pH were measured in the field, and NH_4^+ and NO_3^- were measured with specific-ion electrodes in the office. Complete chemical analyses were made on the samples at the U.S. Geological Survey laboratory in Albany, N.Y.

HYDROGEOLOGY

Long Island is underlain by coastal-plain sediments of Cretaceous age that dip gently southeast and are overlain by deposits of Pleistocene age, which are primarily of glacial origin. Over most of the northern half of the island, the Pleistocene deposits contain much morainal material; over most of the southern half, they consist of outwash. In some places in the towns of Babylon and Islip, the outwash is separated from the Cretaceous sediments by beds of clay, silt, sand, and shells. Jensen and Soren (1971) have correlated these beds with the Gardiners Clay.

The major hydrogeologic units on Long Island have been described by Cohen, Franke, and Foxworthy (1968, p. 18). The uppermost unit is the upper glacial aquifer. This aquifer overlies the Gardiners Clay in the Babylon area and the Magothy aquifer in the Islip area. The upper glacial aquifer, the saturated part of the outwash deposits, consists mostly of medium to coarse sand but contains some gravel. On the basis of the specific capacity of public supply wells in the area, the hydraulic conductivity of the upper glacial aquifer is estimated to range from 130 to 400 ft/d (40–120 m/d) at both the Babylon and the Islip sites.

Recharge to the ground-water reservoir occurs from precipitation. A regional ground-water flow system heads near the middle part of the island and flows outward toward the surrounding bodies of saltwater. In addition to the regional system, ground-water bodies are recharged locally by infiltration of precipitation to the water table. Cohen, Franke, and Foxworthy (1968) have estimated that about one-half the precipitation infiltrates. Annual precipitation at the Babylon site is 47 in (1,190 mm) and at the Islip site is 43 in (1,090 mm) (Miller and Frederick, 1969, pl. 1). Infiltration is probably greater in these landfills than in the surrounding area because of the loose, coarse sand and lack of vegetation on them, but the increased amount is unknown.

The two landfill sites are on an outwash plain that slopes toward Great South Bay, 4.6 mi (7.3 km) from the Babylon site and 3.9 mi (6.2 km) from the Islip site (fig. 1). Both sites are 60 ft (18 m) above sea level. The water table is about 15 ft (4.6 m) and 20 ft (6 m) below land surface at the Babylon and Islip sites, respectively.

The movement of contaminants in the ground-water system depends on rate and direction of flow of the water. In the area of the study sites, regional flow in the upper glacial aquifer is primarily parallel to the water table and along the hydraulic gradient, which is south toward discharge areas along streams and the Great South Bay. The velocity of ground-water movement can be computed from the hydraulic conductivity, the hydraulic gradient, which is assumed to be the slope of the water table, and the effective porosity, which is somewhat less than the actual porosity. On the basis of a range in estimated hydraulic conductivity from 130 to 400 ft/d (40–120 m/d), gradients of $0.0020 \pm .0001$ at Babylon and $0.0016 \pm .0001$ at Islip, and an effective porosity of 25 percent, the ground-water velocity ranges from 1 to 3 ft/d (0.3–1.0 m/d), or roughly 400 to 1,000 ft/yr (120–300 m/yr) at the two sites.

GENERAL WATER-QUALITY CONDITIONS

The dissolved-solids concentration of uncontaminated ground water in the upper glacial aquifer is generally less than 50 mg/l (Cohen and others, 1968, p. 80), and the specific conductance is usually less than 100 μmho/cm at 25°C. Ca^{+2} and Na^+ in concentrations ranging from 2 to 4 mg/l are commonly the most abundant of the principal cations, which are Ca^{+2}, Mg^{+2}, Na^+, and K^+. Concentrations of the principal anions, which are HCO_3^-, SO_4^{-2}, and Cl^-, range from 4 to 8 mg/l. Concentration of SiO_2 commonly ranges from 5 to 8 mg/l, and concentration of NO_3^- is less than 1 mg/l. The pH of the water ranges from 4 to 6. Concentrations of Fe and Mn vary widely in ground water on Long Island. At some places in the upper glacial aquifer the concentrations of these metals exceed the drinking-water standards of 0.3 and 0.05 mg/l, respectively, set by the U.S. Public Health Service (1962). Concentrations of other heavy metals occur in trace amounts (less than 100 μg/l).

Changes in ground-water quality throughout many parts of long Island have resulted from urbanization and other activities of man. Septic tank and cesspool wastes and possibly products from agriculture, once common in the area, have modified the ground-water

quality by increasing the concentrations of HCO_3^-, SO_4^{-2}, Cl^-, Na^+, MBAS (methylene blue active substances), the number of species of N in the water, and the degree of hardness of water. In those parts of the study area where man contributes wastes, specific conductance may be as much as 400 μmho/cm at 25°C in the upper part of the upper glacial aquifer. Water in the lower part of the upper glacial aquifer may be either uncontaminated or, at most, slightly contaminated. Because of the similarity of regionally contaminated water and plume water, the solute concentration of ambient water limits the extent to which leachate-enriched water can be traced. For example, SO_4^{-2} must exceed 50 mg/l in Babylon or 20 mg/l in Islip to differentiate ambient from leachate-enriched water. The relatively high concentrations of SO_4^{-2} in Babylon, compared with those in Islip, reflect the larger contribution from cesspools and septic tanks in Babylon.

BABYLON SITE

The Babylon landfill site, which consists of a complex of facilities and landfills in a 1,650 by 2,260 ft (505 by 689 m) rectangle, was established in 1947. About one-third of the area is covered by rubbish in three more-or-less discrete piles (fig. 2). Pile 1 was used from 1947 to 1965. Pile 2, probably begun in the 1950's was completed in 1968. Pile 3 was started in 1968 and is now (1975) the major area of waste disposal. Collectively, the refuse piles cover about 25 acres (10 ha). Excavation of sand and gravel preceded rubbish deposition in all piles and continues on about one-third of the site. Scavenger-waste disposal pits and settling basins for chlorinated scavenger-waste effluent occupy the northwest quarter of the area.

Solid waste is disposed of by incineration and direct dumping. Scavenger waste is discharged into underground tanks and surface basins. Incineration of refuse at the Babylon site was begun in 1947 and was continued to 1975. All combustible refuse is incinerated, except when occasional breakdowns and overloads require its deposition directly to the landfill. From 1968 to 1972 incinerated rubbish amounted to 368 tons (334 t) per day, and demolition waste, compostables, and noncombustibles amounted to 602 yd^3 (461 m^3) per day. Scavenger waste amounted to 40,000 gal (150,000 l) per day in 1972. Although the amount of scavenger waste handled previously at the Babylon site is unknown, this type of waste has been deposited there since 1966. Scavenger waste has been discharged over rubbish piles 1 and 2.

Because of sand and gravel removal, refuse deposits at piles 2 and 3 extend from 15 ft (5 m) below to 45

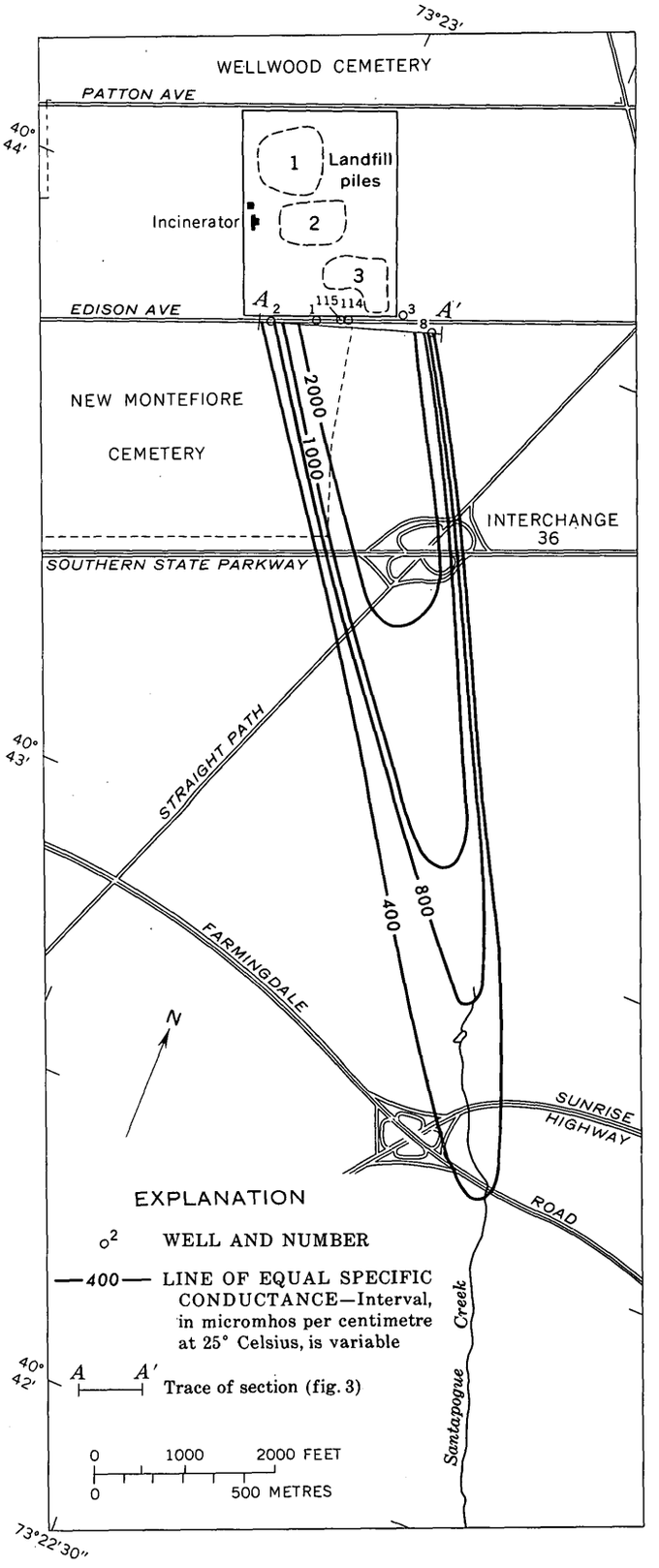

FIGURE 2.—Specific conductance of leachate-enriched ground water in the upper glacial aquifer south of the Babylon landfill in 1973.

ft (14 m) above land surface. Refuse in pile 1 has been partly removed. The volume of piles 1, 2, and 3 was estimated to be 2.3×10^6 yd^3 (1.7×10^6 m^3) in 1973.

The areas adjacent to the landfill on the east and west sides are industrialized. Typical businesses include scrap dealers, machinery sales, and wholesale-distribution centers, each of which has its own sanitary disposal facility. Beyond the industrial zones and on the north and south sides of the landfills are large cemeteries. Ground-water contamination from these other sources is probably slight.

The upper glacial aquifer at Babylon is underlain by the Gardiners Clay, a uniform layer of dense, tough, silty clay that extends throughout the area. This formation extends at least as far north as the northern limits of the solid-waste disposal area and south beyond the end of the leachate plume. In the locality of the solid-waste site, thickness of the formation is 10 to 12 ft (3–4 m), and the downward head differential across the clay is 3 ft (1 m). Although some water from the upper glacial aquifer may penetrate the clay, most of the ground water flowing under the landfill remains in the upper glacial aquifer. Below the clay are beds of fine, silty sand. The hydrology of these silty beds was not determined, but the beds yield little water to wells.

Thickness of the upper glacial aquifer at the Babylon landfill site ranges from 71 ft (22 m) at the north side of the landfill to 79 ft (24 m) near the south end of the leachate plume, a distance of 2.0 mi (3.2 km). The land surface is planar and has a greater slope than the water table, which intersects the land surface at the head of Santapogue Creek 1.4 mi (2.2 km) south of the landfill.

Conductance of leachate-enriched ground water south of the landfill at Babylon is shown in figures 2 and 3, where the farthest extent of the plume is indicated by the 400-μmho/cm specific conductance line. This conductance is the limit for differentiation of plume water from ambient ground water. At times, conductance of plume water at the south side of the landfill has been at least 4,000 μmho/cm. This corresponds to a dissolved-solids concentration of 2,200 mg/l.

On the basis of the 400-μmho/cm specific conductance line, the plume of leachate at Babylon extends downgradient (southward) 10,600 ft (3,200 m) from the center of pile 1. The tongue-shaped plume, 2,000 ft (610 m) wide at the landfill, tapers toward the south end. Thickness of the plume is 70 ft (21 m); so, assuming a porosity of 30 percent, the quantity of the leachate-contaminated water in the plume is estimated to be 2×10^9 gal (8×10^6 m^3).

ISLIP SITE

The Islip landfill site (fig. 4) was established in 1933 in a sand and gravel pit. The refuse pile extends from the pit floor, which was probably near the water table 30 ft (9 m) below land surface in 1933, to 16 ft (5 m) above land surface. The landfill has a maximum thickness of 46 ft (14 m) and its sides slope gradually to the prevailing land surface. In 1973, refuse covered 17 acres (7 ha).

Incineration facilities have been available since landfilling was started and are still used for all combustibles. A daily average of 151 tons (137 t) of rubbish was incinerated from 1970 through 1972, and a total of 6,200 tons (5,600 t) of demolition and noncombustible waste was deposited directly on the landfill during that period. Since the landfill was started 40 yr ago, 8.3×10^5 yd^3 (6.3×10^5 m^3) of material, about one-half that at Babylon, has accumulated.

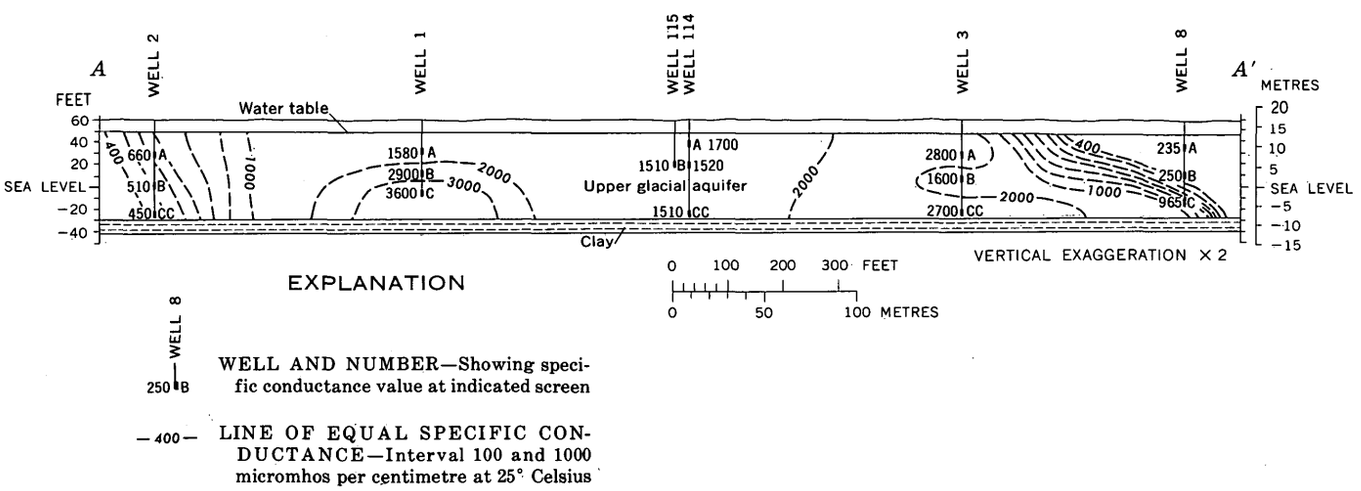

FIGURE 3.—Specific conductance of water in the upper glacial aquifer at the south side of the Babylon landfill in December 1973.

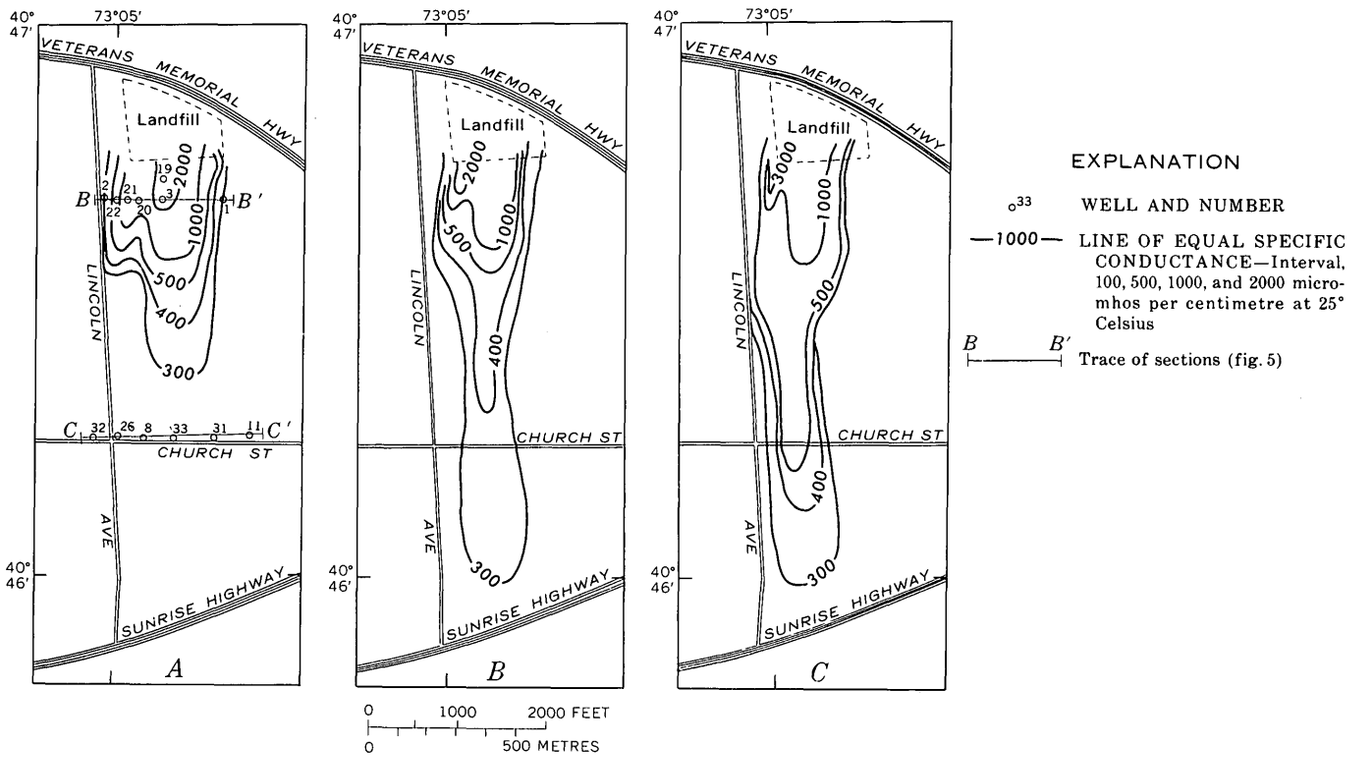

FIGURE 4.—Specific conductance of leachate-enriched ground water in the upper glacial aquifer south of the Islip landfill in 1973 at the following depths below the water table: *A*, 23 to 43 ft (7–13 m); *B*, 65 to 87 ft (20–26 m); and *C*, 90 to 120 ft (27–37 m).

A residential area has been developed southward from the landfill-property line. Undeveloped woodland and scattered industrial and residential developments surround the remainder of the property. About 50 percent of the land area in the vicinity of the Islip landfill is developed, whereas 90 percent or more of the area around the Babylon site is developed.

At the Islip site, the upper glacial aquifer is 170 ft (52 m) thick or more than twice its thickness at Babylon. The lithology of the upper glacial aquifer at Islip is similar to that at Babylon; however, below 170 ft (52 m) are beds of silty fine sand that are probably Pleistocene in age and are genetically related to the outwash deposits (H. M. Jensen, oral commun., 1973). Only one well is screened in the silty fine sand, 190 ft (58 m) below land surface. Contaminants were not detected in an analysis of water from this well, which suggests that the silty sand is a hydrologic boundary that retards downward flow of ground water and prevents contamination of underlying ground water by leachate-enriched water. This fine-grained phase of the outwash deposit is probably the base of the upper glacial aquifer in the Islip area. The Gardiners Clay is probably absent at this site.

The Magothy aquifer consists mostly of fine sand, silt, and clay, and some beds of coarse-grained material, and it underlies the upper glacial aquifer. In the Islip area, the Magothy aquifer extends downward for hundreds of feet. The hydraulic conductivity of the Magothy aquifer is estimated to be 50 ft/d (16 m/d) (McClymonds and Franke, 1972, pl. 2), or one-fifth that of the upper glacial aquifer.

At the Islip site, plume water, whose specific conductance exceeds 300 μmho/cm, can generally be differentiated from ambient ground water. Because the conductance of ambient ground water ranges from 80 to 180 μmho/cm in the vicinity of section *C–C′* (fig. 5), ambient and plume ground water can be differentiated where the specific conductance of plume water exceeds 200 μmho/cm. Ground water is virtually uncontaminated in places near the leachate plume (fig. 5).

The length of the plume emanating from the Islip landfill is 5,000 ft (1,500 m), but its shape is more complex than the one emanating from Babylon. Changes in shape with depth are shown on figure 4*A*, *B*, and *C*. At section *B–B′*, the plume is 1,300 ft (400 m) wide and 170 ft (52 m) thick (fig. 5*A*). At section *C–C′*, it is 660 ft (200 m) wide and 100 ft (30 m) thick (fig. 5*B*). Quantity of water in the Islip plume is estimated to be 1×10^9 gal (4×10^6 m^3), which is one-half that in the Babylon plume.

Distribution of solute in the Islip plume follows

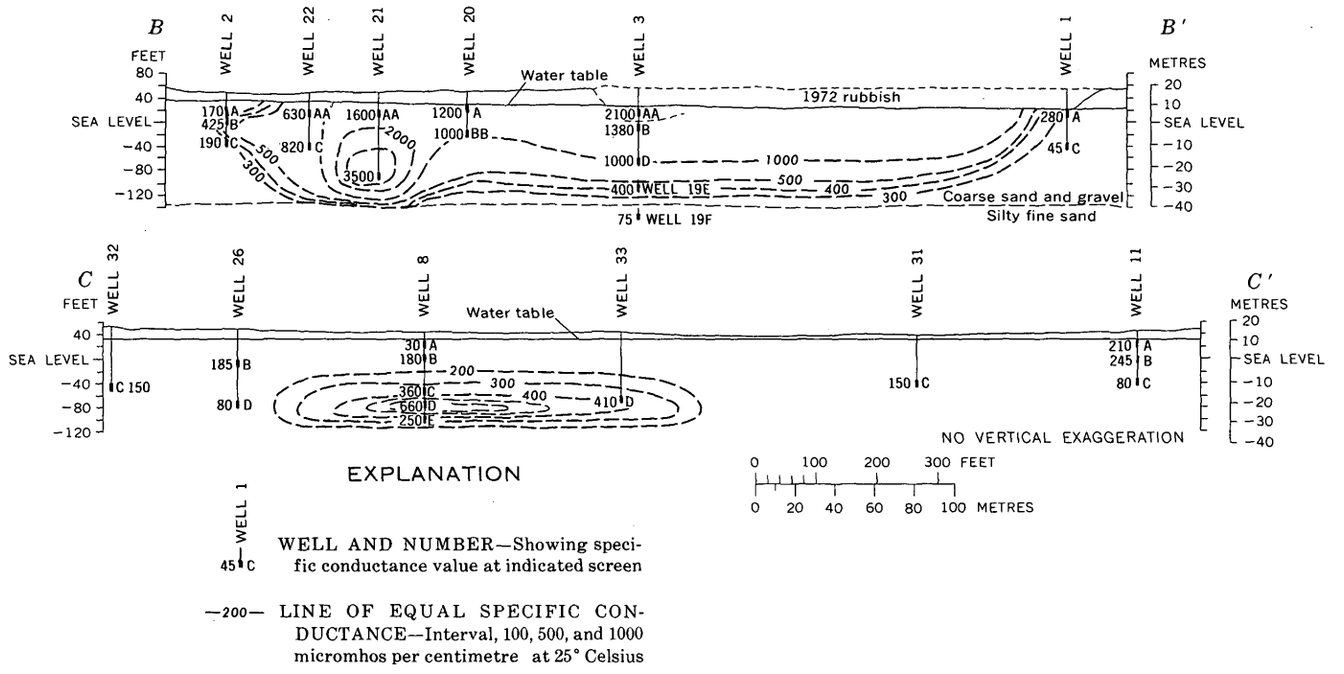

FIGURE 5.—Specific conductance of ground water in the upper glacial aquifer south of the Islip landfill. Conductance for wells 1A, 1C, and 3B in 1972; conductance for all other wells in 1973.

an apparently characteristic pattern for leachate in this environment in that water having the highest dissolved-solids concentration is generally near the bottom of the plume. Depth of the top of the plume increases with movement of this leachate-enriched water away from the landfill (figs. 4*A*, *B*, *C*; 5*B*). No hydrologic boundary was found in the sediments in section *C*–*C*′, but available geologic evidence from nearby wells suggests that the boundary is probably not more than a few feet below well 8E (section *C*–*C*′, fig. 5*B*). Specific conductance at section *C*–*C*′ shows that the greatest solute concentration in the plume is near the bottom. This condition also prevails at locations downgradient from the landfill at the Babylon site, though it is not as well developed as at the Islip site.

The silty fine sand 190 ft (58 m) below land surface seems to control the position of the bottom of the plume (fig. 5). The sinking of the leachate-enriched water across the normal flow path, which is parallel to the water table, in the aquifer is probably the result of a difference in density between the leachate and the ambient ground water.

CHEMICAL CHARACTER OF LEACHATE PLUME

The principal ions in the plume water are Ca^{+2}, Na^{+}, HCO_3^{-}, and Cl^{-}. These ions are also common in ambient water, but their concentrations are generally less than they are in plume water. HCO_3^{-} is a particularly distinctive ion in plume water, where its concentration usually exceeds 50 mg/l. The HCO_3^{-} concentration of ambient water is generally less than 20 mg/l, unless the water is unusually enriched with septic tank effluent.

Other ions common to both types of water include Mg^{+2}, NH_4^{+}, SO_4^{-2}, and NO_3^{-}. The concentration of Mg^{+2} in plume water varies directly with the distance from the landfill, and the concentration resembles that of ambient water near the end of the plume as mapped in figures 2 and 4. Chemical and biological reactions control the concentrations of NH_4^{+}, SO_4^{-2}, and NO_3^{-}. Near the landfill sites, where the Eh is low, N occurs in its reduced species NH_4^{+}. Farther out from the landfills, the water becomes oxidative and the oxidized form, NO_3^{-}, occurs. Water highly enriched in leachate is further identified by a pH of about 7, whereas water surrounding the leachate has a pH ranging from 4 to 6.

Ground water containing high concentrations of N species is a potential health hazard because of NO_3^{-} or the convertibility of other N species to NO_3^{-}. NO_3^{-} has received most attention because, in concentrations of more than 45 mg/l, it may cause methemoglobinemia in infants (U.S. Public Health Service, 1962, p. 48). Most of the N in ground water occurs as the species NH_4^{+} and NO_3^{-} and as organic N. NO_2^{-} is unstable in nature and only rarely accumulates in significant amounts in water. Total N concentration is

generally greater in the plumes than at most sample points in surrounding water. NH_4^+, the predominant N species in the plume, constitutes more than 10 percent of the cation concentration in most water samples from the leachate plumes, whereas, with a few exceptions, it constitutes less than 10 percent of total cations in water samples from outside the plumes. Concentration of NO_3^- is generally lower in the plume than in ambient water. NH_4^+ reflects the reducing conditions in the refuse and ground water near the landfills. Although Thornton and Blanc (1973) reported concentration of 845 mg/l NH_4^+ for leachate, the maximum concentration for leachate-enriched ground water in our study was 90 mg/l NH_4^+. If the NH_4^+ were oxidized to NO_3^-, the amount of NO_3^- produced would exceed the U.S. Public Health Service (1962) standard for drinking water; however, the NO_3^- concentration of water from one well only was found to exceed the standard. Water from three wells outside the plume had NO_3^- concentrations that exceeded the drinking-water standard. Removal of N species from solution, dilution as the water moves downgradient, and incomplete conversion of NH_4^+ to NO_3^- probably account for concentrations of NO_3^- less than the U.S. Public Health Service standard near the distal end of the plume.

The only heavy metals dissolved in significant quantities in the leachate are Fe and Mn. These metals occur naturally in soil and sediment minerals and as coatings on the sediments that make up the aquifer. They are dissolved because of the reducing conditions in plume water in and near the landfills. Fe is also contributed by ferrous metals in the refuse. Moreover, microbial decomposition products from the refuse, such as organic acids (especially dicarboxylic, tricarboxylic, and amino acids) and polyphenols, are effective chelators of Fe and Mn. Significant amounts of the two metals could be solubilized by these organic ligands. These factors combined result in maximum Fe and Mn concentrations of 400,000 and 200,000 μg/l, respectively, near the landfill at Islip. However concentrations of Fe and Mn seem to be independent of one another.

Minor constituents of ground water were sought in most of the analyses, but none was found to exceed the U.S. Public Health Service (1962) standards. The metals Cd, Cr, Co, Cu, Pb, Hg, and Ni were detected in only a few samples. Refuse contains Cd, Cr, Cu, Ni, and Pb in the elemental form, but the corrosion-dissolution rates of these metals are very slow. Moreover, the metals once solubilized must percolate through landfill-covering materials and decomposing organic matter before entering the ground-water reservoir. Adsorptive and complexing reactions throughout the system could remove metal cations from solution. At any rate, the resulting concentrations of metal ions in leachate are very low, but some of them would be slowly released over the span of centuries.

Zn concentrations were as much as 220 μg/l in leachate-enriched water and 30 μg/l in ambient water. In the refuse, Zn is primarily in elemental form as ferrous-metal coating.

Determinations of minor nonmetallic constituents in leachate-enriched ground water near the landfills showed as much as 0.3 mg/l P, 0.6 mg/l F, 7 μg/l As, 38 μg/l Se, and 2,000 μg/l B.

CONCLUSIONS

The solid-waste landfills at Babylon and at Islip yield leachate to the upper glacial aquifer. Plumes of leachate-enriched ground water have formed downgradient from the landfills for at least 10,600 ft (3,200 m) at Babylon and 5,000 ft (1,500 m) at Islip. A characteristic of the plumes is that they sink to and travel along a hydrologic boundary directly below the landfill. Water near the bottom of the plume has the maximum solute concentration.

Neither plume exhibits significant lateral spreading; however, the vertical distribution of the plume seems to be related to the thickness of the aquifer. At Babylon, where thickness of the aquifer ranges from 71 to 77 ft (22–24 m), the plume extends the full thickness of the aquifer, but at Islip, where the thickness of the aquifer is 170 ft (52 m), the top of the plume declines below the top of the aquifer as the distance from the landfill increases.

Specific conductance and concentrations of HCO_3^-, Cl^-, and SO_4^{-2} are the best indicators of the plume. These three ions and most other ions in the contaminated water are also common to ambient water. However, their concentrations are significantly greater in plume water than in ambient water, and they may be several hundred times greater.

Except for Fe, Mn, and Zn, which are ubiquitous in refuse, soil, and aquifer sediments, there are no noteworthy concentrations of heavy metals in leachate-enriched ground water. Fe and Mn are especially enriched in the concentrated zones of the plumes.

N is a minor component in the leachate plumes. The predominant N species in the leachate-enriched ground water is NH_4^+. Concentration of NH_4^+ in leachate-enriched ground water exceeds that in ambient water. Conversely, NO_3^- in ambient water in many places exceeds the concentration of NO_3^- within the plumes.

The quantity of water in the plume at Islip is estimated to be one-half that in the plume at Babylon.

This difference is proportional to the volume of refuse at the two sites. Even though the Islip landfill is 14 yr older than the Babylon landfill, its volume is slightly less than one-half that of the Babylon landfill. Refuse accumulation has been significantly slower at Islip than at Babylon, and one could deduce that leachate production has been significantly less at Islip than at Babylon.

Ions in ground water travel at the same rate as the water if they are not removed from solution by adsorption or chemical reaction. Therefore, the ground-water velocity should determine the plume length. Dispersion of the ions takes place as solute-bearing ground water moves downgradient. This process dilutes the concentration of the ions, but the approximate position of the leading edge of the plume should be predictable from calculations of ground-water velocity.

On the basis of the calculated range in ground-water velocity, from 400 to 1,000 ft/yr (120–300 m/yr), the length of the plume at Babylon, after 25-yr traveltime, is estimated to be within the range of 10,000 to 25,000 ft (3,000–10,000 m). The measured distance from pile 1 to the 400-μmho/cm specific conductance contour is 10,600 ft (3,200 m) which falls within the range of the estimated velocities. Although leachmate-enriched water extends beyond the 400 μmho/cm line, the distance traveled by this water probably is closer to the low end of the ground-water velocity range. At Islip the calculated range in ground-water velocity suggests that the plume length would be 16,000 to 39,000 ft (3,900–16,000 m) after 39 yr, whereas the measured plume length is 5,000 ft (1,500 m). A well 130 ft deep, the same depth as the plume, located 5,500 ft (1,700 m) from the landfill, yields uncontaminated water. These data preclude leachate-enriched water at a distance of 5,500 ft (1,700 m), which is one-third the distance calculated from the lower end of the range in ground-water velocity.

Although the difference in volume of refuse may account for the difference in quantity of leachate-enriched ground water from the two landfills, it does not explain the discrepancy in the length of the plume at Islip. This phenomenon may result from differences in thickness in the upper glacial aquifer at the two sites. Although the vertical gradient below the landfills is not known, it may be that much of the traveltime for the Islip plume was consumed in the downward movement and that the horizontal part of the plume has taken about 10 yr to form at a velocity of 400 ft/yr.

REFERENCES CITED

Cohen, Philip, Franke, O. L., and Foxworthy, B. L., 1968, An atlas of Long Island's water resources: New York State Water Resources Comm. Bull. 62, 117 p.

Jensen, H. M., and Soren, Julian, 1971, Hydrogeologic data from selected wells and test holes in Suffolk County, Long Island, New York: Long Island Water Resources, Bull. 3, 35 p.

McClymonds, N. E., and Franke, O. L., 1972, Water-transmitting properties of aquifers on Long Island, New York: U.S. Geol. Survey Prof. Paper 627–E, 24 p.

Miller, J. F., and Frederick, R. H., 1969, The precipitation regime of Long Island, New York: U.S. Geol. Survey Prof. Paper 627–A, 21 p.

Thornton, R. J., and Blanc, F. C., 1973, Leachate treatment by coagulation and precipitation: Am. Soc. Civil Engineers Proc. Jour. Environmental Eng. Div., v. 99, no. EE4, p. 535–544.

U.S. Public Health Service, 1962, Drinking water standards: U.S. Public Health Service Pub. 956, 61 p.

Zanoni, A. E., 1972, Ground water pollution and sanitary landfills—a critical review: Ground Water, v. 10, no. 1, p. 3–13.

Jour. Research U.S. Geol. Survey
Vol. 3, No. 3, May–June 1975, p. 281–283

STRAIN-GAGE MEASUREMENTS IN CARLSBAD CAVERNS, NEW MEXICO

By J. S. McLEAN, Albuquerque, N. Mex.

Work done in cooperation with the U.S. National Park Service

Abstract.—Displacement transducers installed on a near-vertical joint in the lunchroom in Carlsbad Caverns measured small movements along the joint with a resolution of 3.7×10^{-6} in (9.4×10^{-6} cm). During 1973 the maximum annual displacement horizontally, vertically, and perpendicularly to the plane of the joint was 4.7×10^{-4}, 4.0×10^{-4}, and 1.1×10^{-4} in (1.2×10^{-3}, 1.0×10^{-3}, and 2.8×10^{-4} cm), respectively.

In March 1971 the U.S. Geological Survey, in cooperation with the U.S. National Park Service under NPS Research Project CACA–001a, began a project to measure small displacements in a joint in the rock wall of the lunchroom of Carlsbad Caverns (fig. 1). The output signal from the transducers was measured daily with a digital millivoltmeter by Park Service personnel.

In this report values are given in both English and metric units of measurement. The following table lists the factors used for conversion of the English units to the metric International System (SI) units:

Inch (in)	× 2.54	= centimetre (cm)
	× 2.54×10^{-4}	= micrometre (μm)
Foot (ft)	× 0.3048	= metre (m)

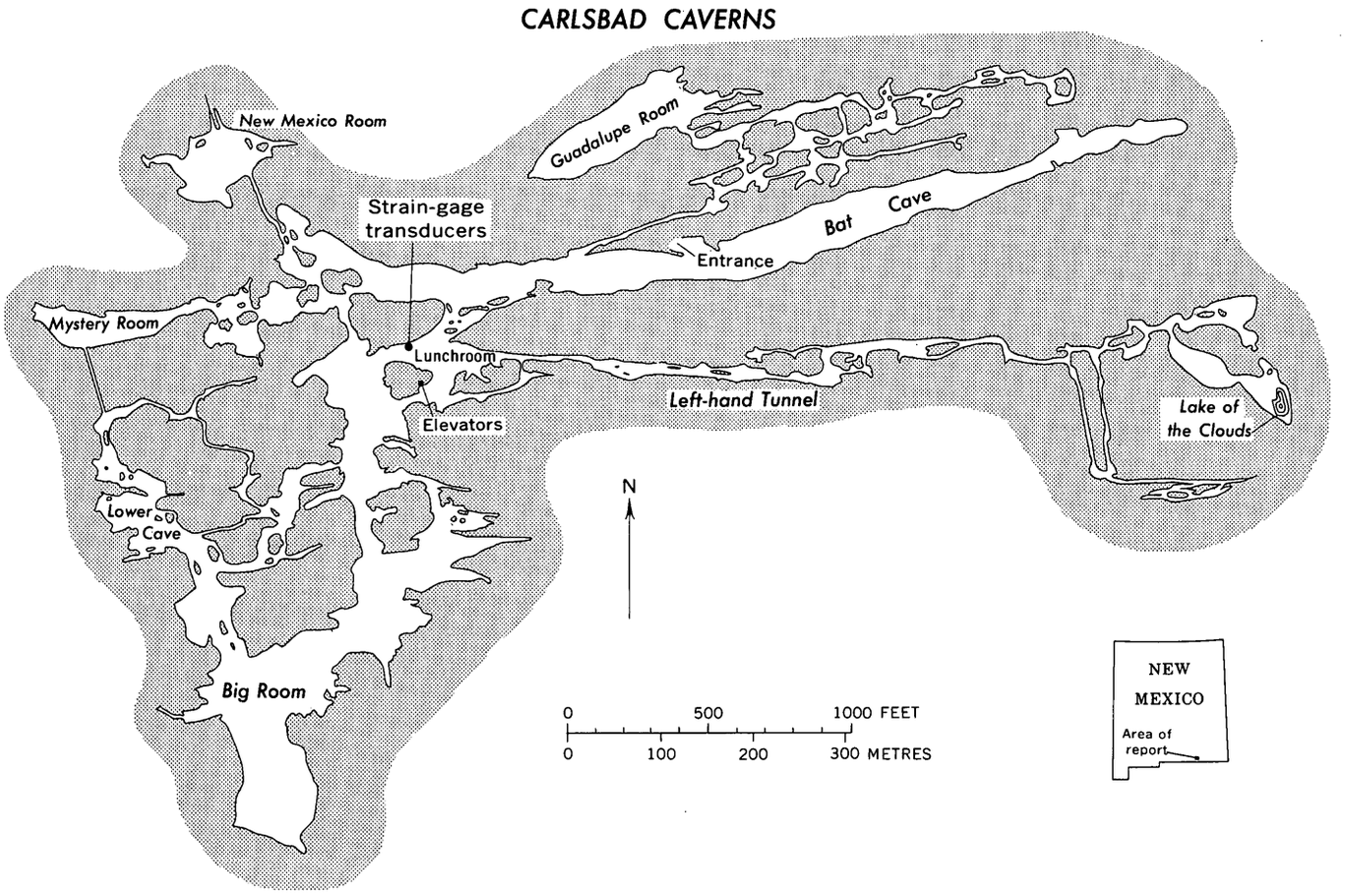

FIGURE 1.—Location of strain-gage transducers. Base modified from Moore (1960).

LOCATION OF STRAIN-GAGE TRANSDUCERS

Three transducers were installed on the conspicuous near-vertical joint in the rock wall on the north side of the lunchroom at a depth of about 750 ft (229 m) below the land surface. One transducer was installed vertically; another, horizontally in the plane of the joint; and the third, perpendicularly to the plane of the joint.

PREVIOUS INVESTIGATIONS

Strain gages have not previously been placed in Carlsbad Caverns. Davis and Moore (1965) studied the motion along a steeply dipping joint in Wool Hollow Cave in California. They recorded diurnal movements of 0.4 and 0.6 μm parallel to the dip and strike of the joint, respectively. An earthquake during the course of the study produced abrupt, steplike displacements of as much as 0.03 μm.

MEASURED DISPLACEMENTS

The strain-gage transducers were read with a digital millivoltmeter by National Park Service personnel, usually once a day. The results of these measurements are shown in figure 2. The transducers were calibrated prior to installation. Marks on the transducer mounting plate provided a rough check on the meter readings. The meter used is accurate to 0.1 mV, which is equivalent to a displacement of 3.7×10^{-6} in (9.4×10^{-6} cm), or roughly 1 mV/μm of displacement. The maximum displacements during 1973 are summarized below:

Transducer	Displacement	
	Inch	*Centimetre*
Horizontal	4.7×10^{-4}	1.2×10^{-3}
Vertical	4.0×10^{-4}	1.0×10^{-3}
Perpendicular	1.1×10^{-4}	2.8×10^{-4}

The vector sum of these movements was therefore 0.00063 in (0.0016 cm) during 1973.

CAUSES OF MOTION

Movement along the joint appears to consist of a slow, irregular creep that has a series of short-term fluctuations superimposed. The record is infrequently disturbed by abrupt "steps." The long-term creep may represent the response of the rocks in the vicinity of the cave to unloading by removal of overburden and to local erosion.

The short-term fluctuations noted are of the same order of magnitude as the earth-tide induced fluctuations noted by Davis and Moore (1965). They probably represent the effects of earth tides, small earthquakes, and local effects such as blasting. They do not appear to induce permanent displacement in the joint, although they may act to release preexisting stress.

Some of the steps in the record are due to equipment malfunction and to disturbance of the sensors by people in the cave, particularly during 1972. However, some of the large steps took place when there was no

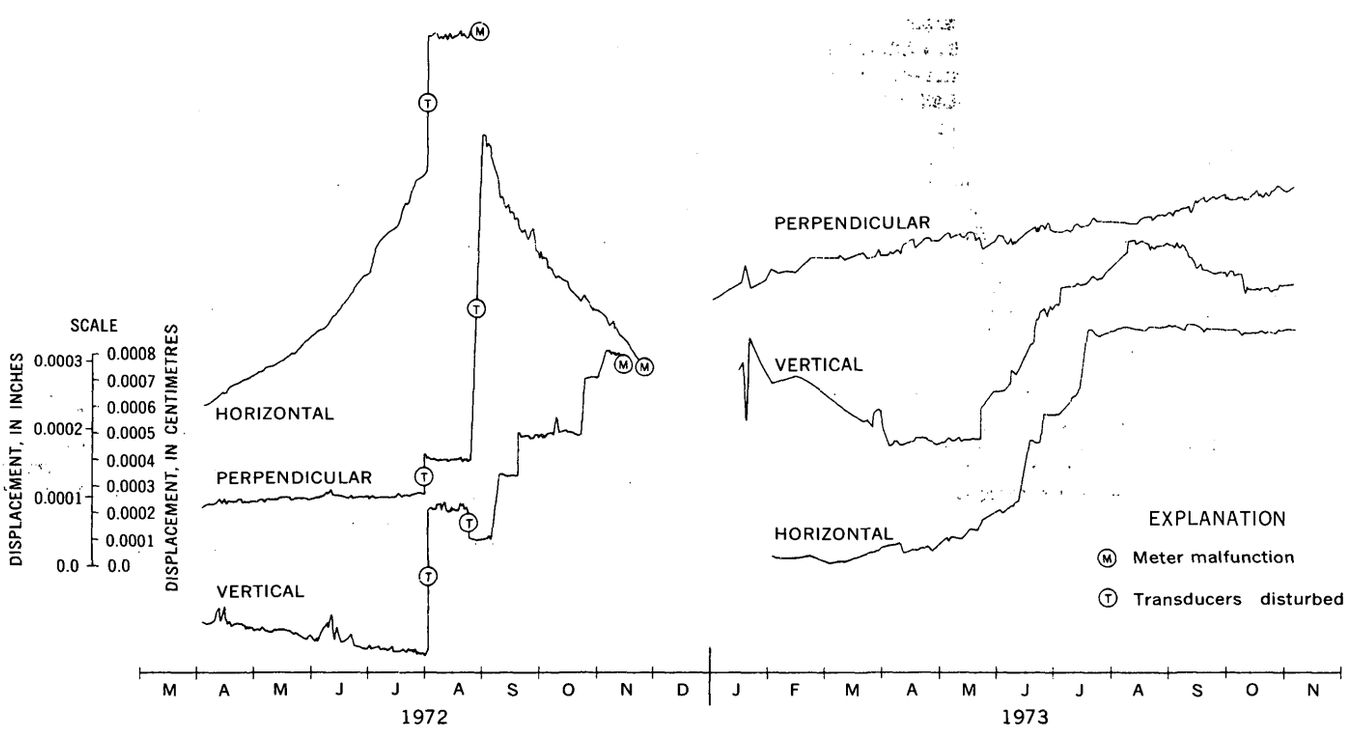

FIGURE 2.—Movement of a joint in Carlsbad Caverns.

equipment malfunction or disturbances. These seem to represent abrupt movement along the joint. Some of these steps appear to coincide with major earthquakes and may represent the triggering of the release of stress in the joint by earthquakes. The data are inadequate to allow a detailed correlation between earthquakes and abrupt displacements.

REFERENCES CITED

Davis, S. N., and Moore, G. W., 1965, Semidiurnal movement along a bedrock joint in Wool Hollow cave, California: Natl. Speleol. Soc. Bull., v. 27, no. 4, p. 133–142.

Moore, G. W., 1960, Geology of Carlsbad Caverns, New Mexico, *in* A guidebook to Carlsbad Caverns National Park: Natl. Speleol. Soc. Guidebook Ser., no. 1, p. 10–17.

Jour. Research U.S. Geol. Survey
Vol. 3. No. 3, May–June 1975, p. 285–293

APPLICATIONS OF REMOTE SENSING TO STRUCTURAL INTERPRETATIONS IN THE SOUTHERN APPALACHIANS

By J. E. JOHNSTON, R. L. MILLER, and K. J. ENGLUND, Reston, Va.

Abstract.—Remote sensing is the technology of studying distant objects by measuring and recording energy from one or more segments of the electromagnetic spectrum. Imaging sensors which operate from medium- and high-altitude aircraft or from spacecraft can provide a synoptic view of large areas and of surface phenomena not evident in the field. Image-acquiring systems and instruments have been designed to partially automate data collection and to reduce the time devoted to analysis, information extraction, and detection of changes of surface phenomena. Among these phenomena are the surface distribution of heat, moisture, snow, water, vegetation, and cultural features. When coupled with ancillary data, including field surveys, sensor data provide useful information for the recognition and mapping of regional structure, jointing patterns, drainage patterns, fault and fracture traces, and rock types. The recognition of several major linear surface features, two of which proved to be traces of previously unrecognized faults (the Canebrake and the Coeburn faults) in the Appalachian Plateaus, demonstrates the pragmatic application of aircraft and spacecraft remote sensing to geological investigations in the Appalachians.

The purpose of this paper is to present three case histories of investigations that used remote-sensing methods for the interpretation of the structural geology of an area (in the southern Appalachians). Extensive literature is available which presents detailed discussions of methods and applications of remote sensing (Fischer, 1972), a technique which has been under development for several decades and is being increasingly used for the solution of geologic and related problems.

REMOTE SENSING

Generally, the term remote sensing is restricted to the sensing from a distance of emitted or reflected energy in some part of the electromagnetic spectrum. Sensing of phenomena such as the surface distribution of heat, moisture, snow, water, vegetation, and cultural features is included, whereas sensing of gravity and magnetism and detection of odors and chemicals is excluded.

Many types of sensors are available for measuring energy in the electromagnetic spectrum. One group includes scintillation counters, spectrometers, and radiometers, which take measurements from a fixed point. Another group of sensors includes photographic cameras, image orthicons (TV cameras), and optical-electronic scanners. These measure and record energy from the instantaneous field of view of the instrument. The familiar black-and-white aerial photographs are widely used in topographic and geologic mapping. Many geologists are now also using color or color infrared aerial photographs where available.

Sensors that measure or record and display energy variations on photographic film or through a cathode-ray tube as images are most compatible with conventional photointerpretation methods. The data from these sensors are easily analyzed and are proving very useful to a large sector of the natural science community. Image-acquiring systems and instruments have been designed to partially automate data collection and to reduce the time devoted to analysis, information extraction, and detection of changes of surface phenomena. Sensor systems which produce image displays include the following:

1. Black-and-white (B/W) panchromatic and infrared photography, used as both single frames and stereographic pairs.
2. Color and color infrared (CIR) photography.
3. Multiband photography (MB).
4. Thermal infrared (TIR) scanner imagery.
5. Multispectral scanner (MSS) imagery (from ultraviolet to thermal infrared).
6. Side-looking aerial radar (SLAR) imagery.
7. Passive microwave scanner (PMS) imagery.

Several of these systems have provided imagery obtained from both medium- and high-altitude (7,600–>15,000 m) aircraft and from spacecraft (at a distance of about 916 km) over parts of the Appalachians and adjacent regions. They comprise SLAR imagery of parts of southeastern Kentucky, southern West Virginia, and southwestern Virginia declassified and released by the U.S. Army in 1964. In addition, CIR aerial photography has been flown over selected sites in this tristate area and satellite MSS imagery is being

acquired over this area every 18 days by the National Aeronautics and Space Administration (NASA) Earth Resources Technology Satellite (ERTS–1).

PREVIOUS GEOLOGICAL WORK

A large amount of geological work has been done in southwestern Virginia and adjacent parts of West Virginia and Kentucky. Small- and large-scale geologic mapping of this region has continued intermittently for more than 80 yrs. Starting near the end of the last century much of the region was mapped geologically by the U.S. Geological Survey at 1:125,000 scale in a program that lasted more than 10 yrs. As 1:62,500-scale topographic maps became available, the coal-bearing parts of the region were remapped geologically in a series of county reports in Virginia and West Virginia. Additional geologic mapping at 1:62,500 scale of some areas in the Valley and Ridge province has also been published. With the advent of topographic base maps at 1:24,000 scale, the geology of a considerable part of southwestern Virginia and eastern Kentucky has been investigated in even greater detail, and geologic maps of numerous quadrangles and some irregularly shaped areas have been published at this scale during the past 30 yrs. Because of this long history of wide-ranging geological investigations, it would seem unlikely that any major structures had escaped detection.

Remote-sensing techniques, however, have recently provided synoptic views of large parts of southwestern Virginia and adjacent States which have revealed some striking and previously unobserved linear features.

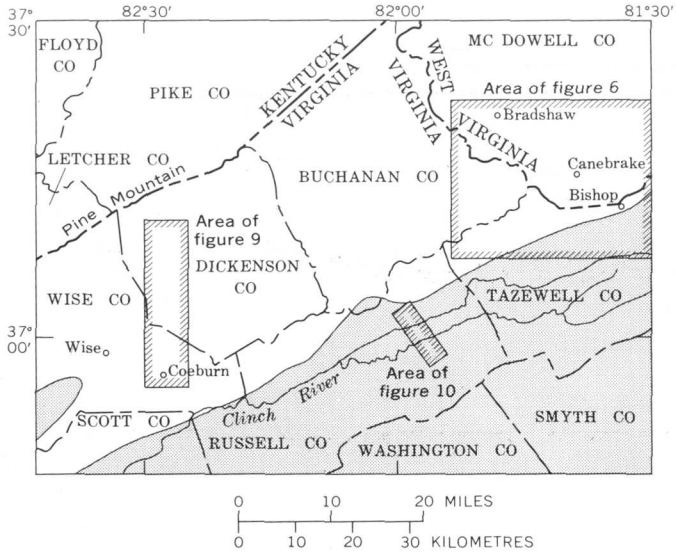

FIGURE 1.—Parts of the Appalachian Plateaus and of the Valley and Ridge province (shaded), showing areas (hachured) described in this report.

The lineaments appear principally as alinements of topographic features traversing areas of mainly flat-lying rocks in the Appalachian Plateaus or transverse to the regional structural trend in the Valley and Ridge province. These lineaments range in length from a few hundred metres to several tens of kilometres. Figure 1 shows areas in which the conspicous linear features that are discussed in this paper are located.

Lineaments were originally defined by Hobbs (1912) as "significant lines of landscapes which reveal the hidden architecture of the rock basement." Billings (1954) calls a lineament "a topographic line that is structurally controlled." These definitions stress structural control of the alinement of topographic and drainage features. In other more recent definitions, however, the term lineament is also applied to linear features of other origins. In this paper, all alinements that are visible on remotely sensed imagery are termed lineaments; those for which structural control can be demonstrated are termed structural lineaments.

PRESENT INVESTIGATION

Johnston first recognized known and suspected faults on SLAR imagery (fig. 2) prior to the public release of the imagery (1964). In November 1971, while indexing, he made a cursory inspection of medium- to high-altitude ektachrome infrared photography (figs. 3 and 4) of the tristate area and discerned these features, other lineaments, and anomalies of the drain-

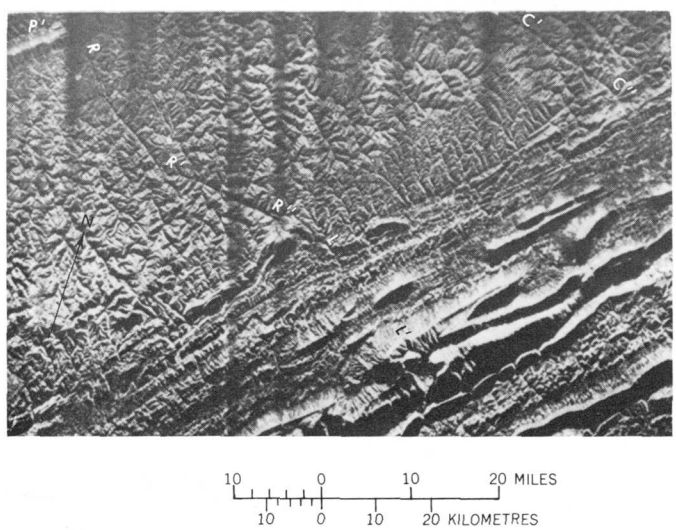

FIGURE 2.—Radar (SLAR) imagery of part of the area of figure 1 showing the Russell Fork fault (R–R'–R'') trending southeastward from the east end (P') of Pine Mountain, the Canebrake fault (C'–C''), and a lineament (L–L'). The aircraft flew along the northern boundary; note the northwest reflection of radar energy and the deep shadowing on the southeast side of the topography. U.S. Department of Defense SLAR imagery, released in 1964.

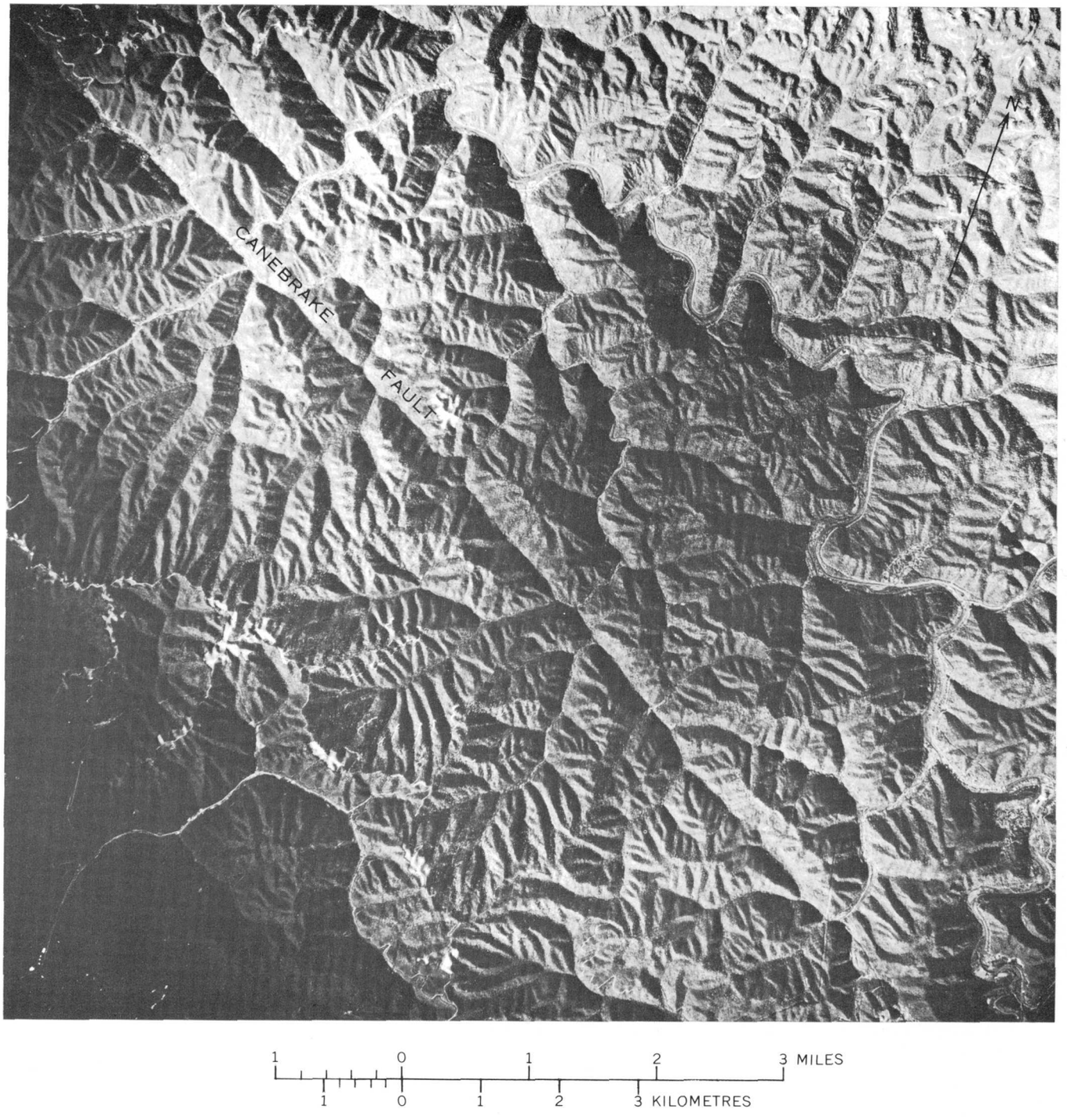

FIGURE 3.—A black-and-white copy of part of the CIR aerial photograph showing part of the Canebrake fault. The aircraft was flying at approximately 12,000 m over terrain with a mean elevation of 450 m. The camera had a 155-mm focal length lens. The original photographic scale is approximately 1:78,000, compared to the conventional photography which commonly ranges in scale from 1:20,000 to 1:40,000. CIR photograph provided by the Rome Air Force Development Group, Rome Air Force Base, November 3, 1971.

age patterns. These anomalies occured both in the Appalachian Plateaus and in the Valley and Ridge province to the southeast (Johnston, 1972). The observed features were discussed with Miller and Englund, each of whom has more than two decades of field experience near and within these areas. They agreed to check several of the more conspicuous lineaments in the field and to report their evaluations.

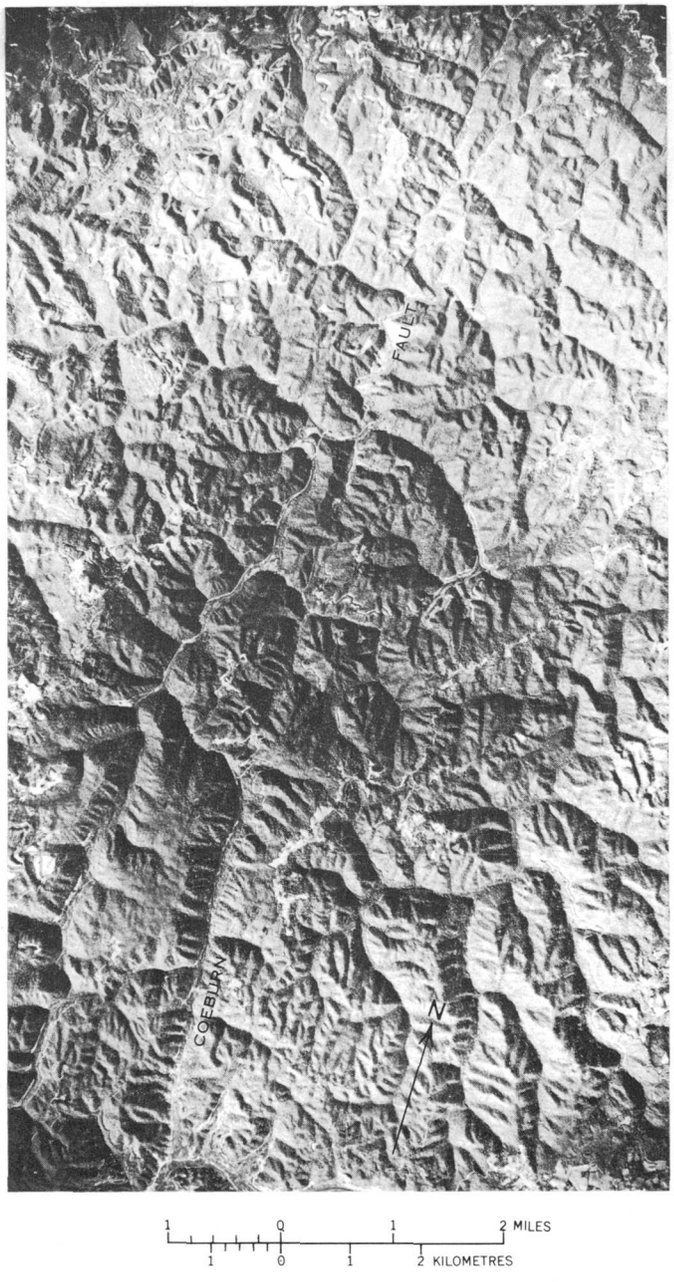

FIGURE 4.—A black-and-white copy of a CIR aerial photograph showing a segment of the Coeburn fault. This synoptic view of the region first allowed the authors to identify the lineament. CIR photograph provided by the Rome Air Force Development Group, Rome Air Force Base, November 3, 1971.

Subsequent cloud-free imagery from ERTS–1 (fig. 5) was compared with both the infrared photographs and the SLAR imagery to ascertain whether or not the lineaments identified by SLAR were also recognizable on the ERTS–1 imagery. As anticipated, major well-known structural features, such as the Pine Mountain and Russell Fork faults, were easily recognized. Most of the lineaments seen in the SLAR imagery were also recognizable.

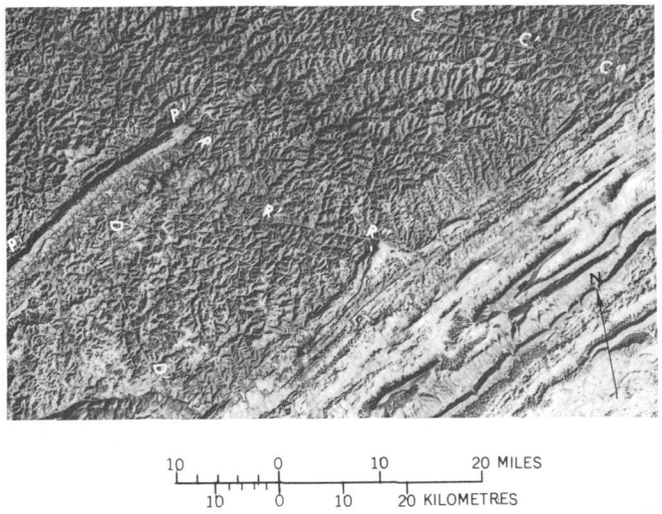

FIGURE 5.—Segment of ERTS near-infrared image, showing part of the study area about 9:30 a.m., January 12, 1973. Scale 1:1,000,000. Note shallow northwest shadowing. Image shows Pine Mountain (*P–P'*) left center, with the Pine Mountain fault on its northwest flank, and the Russell Fork fault (*R–R'–R''*) trending southeastward from the end of Pine Mountain. The lineament of the Canebrake fault (*C–C'–C''*) is in the upper right and that of the north-trending Coeburn fault (*D–D'*) at the lower left. ERTS–1–MSS image 1173–15371 band 7; NASA Goddard Space Flight Center, through the EROS Data Center.

Canebrake fault of southern West Virginia and southwestern Virginia

The principal mapped geologic structures in the Appalachian Plateaus of southern West Virginia and the adjacent part of southwestern Virginia consist of several northeast-trending, low-amplitude folds which parallel the Appalachian folded belt (Hennen and Gawthrop, 1915; Cardwell and others, 1968). The largest fold, Dry Fork anticline, extends northeastward about 72 km across parts of southwestern Virginia and southern West Virginia. It is as much as 10 km wide and attains a maximum amplitude of about 215 m. Faults have not been mapped previously in the Appalachian Plateaus of southern West Virginia, and the possible occurrence of large unmapped faults seemed unlikely because of the extent of underground and surface coal mining. However, prominent structural lineaments seen on medium- and high-altitude infrared photography command attention for economic as well as scientific reasons. One of these lineaments was recognized in the Bradshaw-Bishop area of McDowell County, W. Va., by Elder, Jeran, and Keck (1974, p. 20), who related it to a scissor fault exposed

in an underground mine at the southern end of the lineament. Exposure of a fault plane at the surface along the lineament was not reported.

The most conspicuous of several lineaments revealed by the aerial and satellite imagery trends N. 60° W. and extends from Bishop, Va., approximately 32 km across parts of Tazewell County, Va., and McDowell County, W. Va. (fig. 6). This area is underlain by relatively flat-lying, coal-bearing rocks of Pennsylvanian age. After this lineament was recognized on high-altitude infrared photography, it was readily delineated on low-altitude photography (approximate scale 1:27,000) and on topographic quadrangle maps (scale 1:24,000). An alinement of drainage courses and low gaps in intervening mountain ridges emphasizes the topographic expression of the trace. From its (apparent) southeastern terminus at the edge of the Appalachian Plateaus, this prominent lineament crosses a narrow strip of Tazewell County, Va., along the lower part of Crockett Cove. Northwestward from the state line it follows Jacobs Fork for approximately 5.6 km to Squire, W. Va.; from there, the lineament extends up an unnamed tributary and leaves the Jacobs Fork drainage at a low gap in the drainage between Jacobs Fork and Dry Fork. It then follows an unnamed tributary to Dry Fork and is occupied by this drainage course between the towns of Canebrake and Berwind. From Dry Fork the lineament parallels a short tributary to a gap into the War Creek drainage, which it crosses along northwesterly oriented tributaries to the head of Little Slate Creek. The lineation continues northwestward across the headwaters of Little Slate Creek and Hite Fork, along the lower part of Middle Fork, and up Bradshaw Creek. Northwest of Bradshaw Creek the drainage patterns are too randomly oriented to project or extend the trend. However, a subparallel lineation about 0.8 km southwest of the northwest end of the lineation on the ERTS–1 imagery extends westward toward the northeast end of the Pine Mountain fault (fig. 5).

To determine the significance of this conspicuous alinement of topographic features, Englund examined its trace in the field. The northwest 19 km of the trace from the head of Bradshaw Creek to Dry Fork is mostly occupied by drainage courses where the bedrock is concealed by a narrow strip of alluvium along the streams or by colluvium on the lower valley slopes. Consequently, a continuous exposure of rock strata across the lineament was not found northwest of Dry Fork. At a few localities, within 60 m of the trace, small exposures showed intensely sheared rock with closely spaced vertical fractures parallel to the trend of the lineament. However, a railroad cut in a bend of Dry Fork near Canebrake, W. Va., did present an excellent exposure of strata across the lineation and clearly revealed a fault (fig. 7), which is herein named the Canebrake fault for the locality. In this railroad cut a sandstone bed in the lower part of the Pocahontas Formation is cut by the fault plane which is nearly vertical and which strikes N. 60° W. Gouge, consisting of carbonaceous clay that is several inches thick, occurs along the fault plane, and adjacent sandstone is intensely sheared and fractured. Horizontal striations on the fault surface indicate that movement was entirely strike-slip. This interpretation is also supported

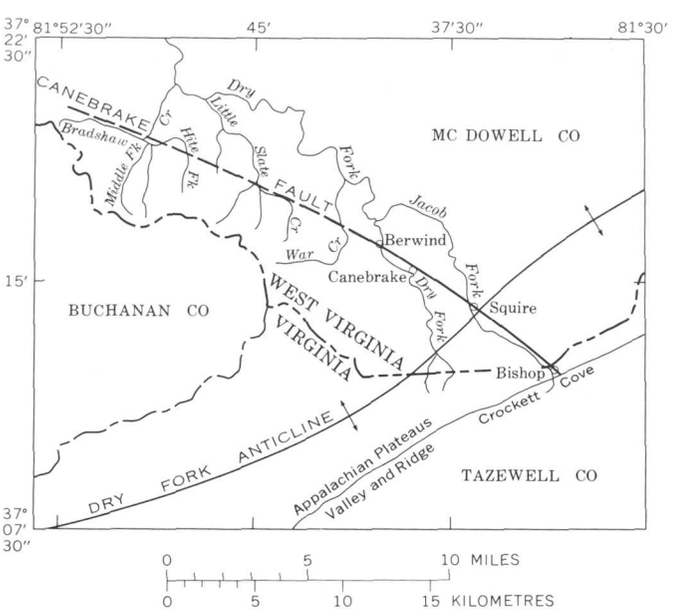

FIGURE 6.—Location of the Canebrake fault.

FIGURE 7.—Canebrake fault (parallel to head of hammer) in railroad cut at Canebrake, W. Va. The sandstone bed is not visibly offset because the movement was strike-slip.

by the lack of significant vertical displacement of the exposed sandstone bed and of mined coal beds in this vicinity.

Other exposures of the fault were found at several localities from Dry Fork southeastward to the end of the lineament near Bishop. One of these is in a railroad cut on the south side of Jacobs Fork about 2.4 km northwest of Bishop, Va. (fig. 8). Here the fault plane is vertical and includes about 0.6 m of gouge. The fault strikes N. 55° W., and an undetermined amount of horizontal movement is indicated by horizontal striations along the fault plane.

To assess the magnitude of strike-slip movement, detailed mapping and measurement of stratigraphic units on opposite sides of the fault will be needed. Movement on the Canebrake fault appears to be considerably less than on the major strike-slip faults of the Appalachian Plateaus such as the Jacksboro, Rocky Face, and Russell Fork faults. For example, movement on the Jacksboro fault was 18 km (Englund, 1968), on the Rocky Face fault was about 3.2 km (Englund, 1961), and on the Russell Fork fault was 6.4 km (Englund, 1971); in many places these faults consist of multiple tear faults with parallel folds. Such features are not evident along the Canebrake fault. However, the shearing and fracturing of strata within about 60 m of the Canebrake faults are sufficiently intense to be of concern to mining operations. Because along most of its extent the fault follows drainage courses and mining is largely above drainage levels, few mine workings to date have encountered the fault. At the few places where mines do cross the fault, miners report "faulting" and "broken rock" but minor vertical displacements of beds. During construction of a drainage tunnel to facilitate development of the Pocahontas No. 3 coal bed by drift mining in eastern McDowell County, W. Va., and Tazewell County, Va., fractured sandstone and enormous flows of water were encountered where the tunnel intersected the fault plane, 20 m beneath the surface stream that follows the lineament.

FIGURE 8.—Canebrake fault in railroad cut 2.4 km northwest of Bishop, Va. Man stands on talus-covered gouge zone with his hand on fault plane.

Coeburn fault in Wise and Dickenson Counties, Virginia

A lineament in Wise and Dickenson Counties, farther southwest in Virginia, was recognized in a high-altitude CIR photograph taken from an altitude of approximately 12,000 m (fig. 4). The scale of the print is about 1:74,000. The feature also shows up prominently on the ERTS–1 imagery (fig. 5). The lineament extends from the town of Coeburn almost exactly due north for about 24 km (fig. 9). It appears on the imagery as a nearly straight line made visible by straight segments of drainage lines and by gaps or saddles in the crests of linear ridges. This section of the Appalachian Plateaus is underlain by a nearly flat-lying coal-bearing sequence of clastic sediment. It has an average relief of between 180 and 215 m in the area of the southern part of the lineament, decreasing to about 60 to 90 m in the northern part. The region is intricately dissected by a dendritic drainage pattern. Few, if any, normal stream courses are straight for as much as a mile; thus, an alinement of straight segments of streams and gaps for many miles becomes conspicuous in synoptic images. The high-altitude CIR photography made this alinement readily apparent; once the lineament was evident on the photography, it was readily recognizable on the 1:24,000 topographic maps. From south to north the lineament crosses the northern half of the Toms Creek quadrangle, all of the Caney Ridge quadrangle, and the southern half of the Clintwood quadrangle, It involves tributaries of three major rivers of the area—Pound River, Cranes Nest River, and Guest River. Geologic maps of the region have been published at 1:62,500 and 1:125,000 scales, but as yet none of the three quadrangles have been mapped geologically at 1:24,000 scale.

Miller field checked the lineament and found that it marks a normal, nearly vertical fault that is upthrown on the west side; thus this is a structural lineament. He was unable to determine any strike-slip movement, but if any occurred it was probably very small. In a traverse of the full length of the lineament, 11 localities were found where structure in outcrops near the lineament indicated the proximity of a fault (fig. 9). The actual fault plane was seen at only one locality, an abandoned drive-in theater, where excavation for the

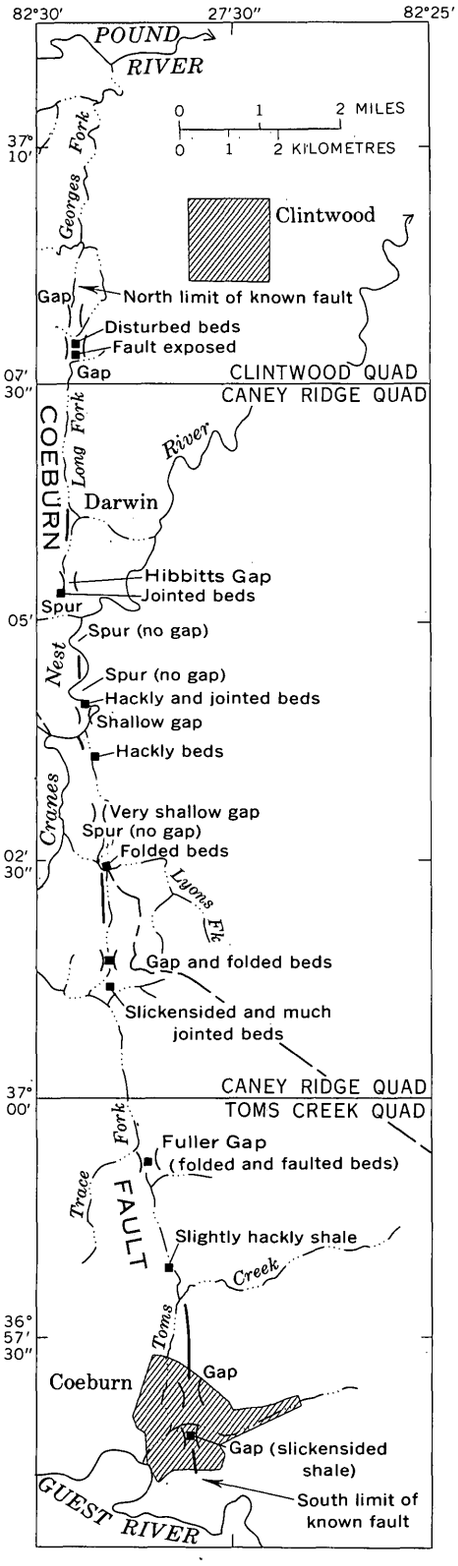

FIGURE 9.—The Coeburn fault trace across the Toms Creek, Caney Ridge, and Clintwood quadrangles (1:24,000). The fault is shown by a heavy line, interrupted where drainage lines closely follow the fault. Localities where evidence of faulting was found are indicated.

parking area had exposed bedrock on both sides of the fault. The fault consists of deeply weathered, crushed shale in a zone 1.5 m wide between nonmatching sandstone layers on opposite sides. Steep irregular dips occur within about 10 m of the fault zone, beyond which the beds are nearly flat.

Detailed mapping along the fault belt will be needed to determine the amount of vertical offset, which is probably a few tens of metres. Evidence of faulting at the other 10 bedrock localities (fig. 9) consists of folded, tilted, or abundantly jointed beds, slickensides formed by bedding plane slippage, and hackly shale.

The lineament seemed recognizable in the CIR aerial photography for approximately 3.2 km north of the northernmost recorded field evidence shown in figure 9. In this stretch the rectilinear course of the southern two-thirds of Georges Fork suggests that the structural disturbance extends that far, but bedrock evidence could not be found to substantiate this northward prolongation of the fault. Detailed mapping in this valley may, however, disclose evidence of faulting which the reconnaissance survey failed to reveal.

The fault is here named the Coeburn fault, for the town near the south end of the fault. Numerous coal beds and some mines are located on both sides of the fault. All the mines are, however, above drainage level so that to date mine workings have not crossed the fault. When deeper coal beds are mined in this area in shaft or slope mines, fractured or contorted strata may be encountered and the continuity of the coal beds may be lost where workings are extended to the fault. Hazardous roof conditions may exist for some distance laterally from the fault zone. Forewarning of this situation should aid the planning of deep mines. Core drilling or mining should also make it possible to determine accurately the amount of displacement on the fault.

Both the high-altitude CIR photography and ERTS imagery (figs. 4 and 5) show a lineament that diverges in a south-southwest direction from the Coeburn fault and approximately follows the upper course of Cranes Nest River, to and beyond the margin of figure 9. This possible fault was not field checked but merits future attention.

Lineament in Russell County, Virginia

An alinement of topographic features has also been recognized in SLAR imagery (fig. 2). This straight lineament in Russell County crosses, almost at right angles, belts of pre-Pennsylvanian rocks of the Valley and Ridge province. It is shown in figure 10 as a dotted line about 8 km in length. In the radar image it appears to join or almost join the southeast-trending

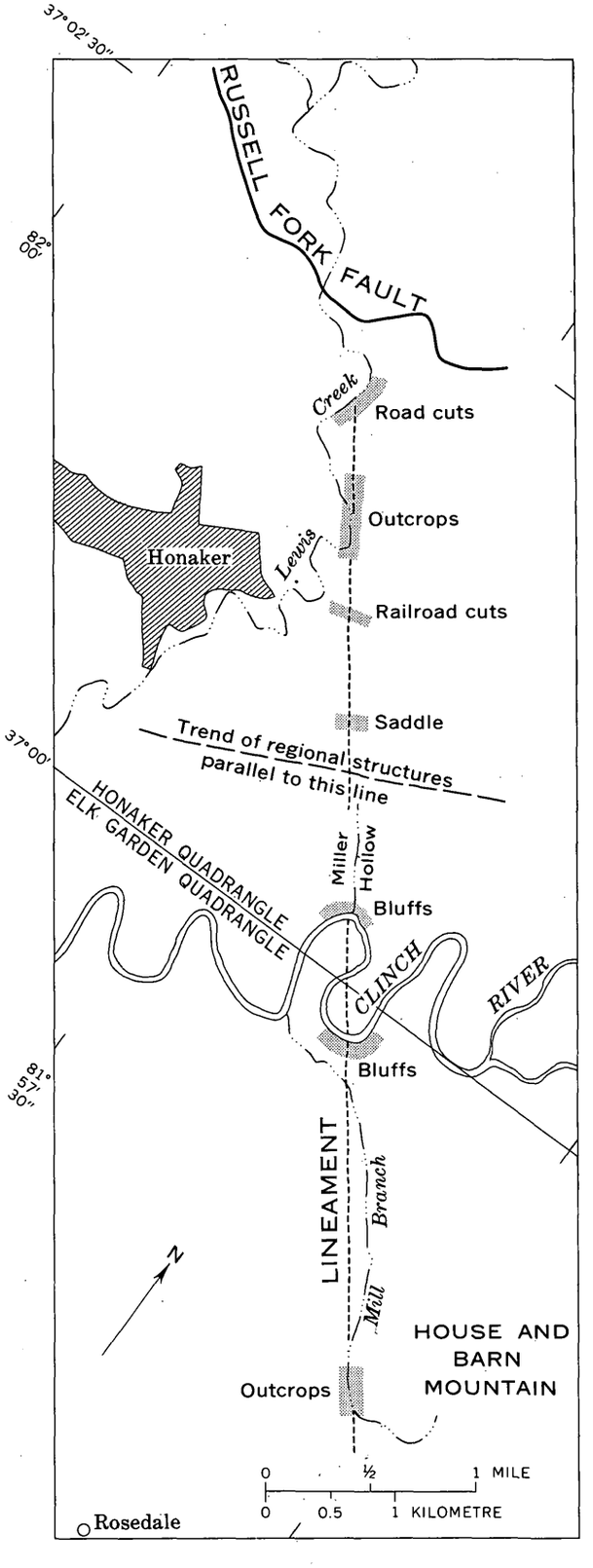

FIGURE 10.—The trace of a lineament in Honaker and Elk Garden quadrangles (1:24,000), and areas of abundant outcrops (shaded) that were examined in the field.

Russell Fork fault. The trace of the Russell Fork fault is clearly evident on any aerial photograph, SLAR, and ERTS–1 imagery, or on large- or small-scale topographic maps of the region. It thus attracts attention to an extended alinement seen in the radar image that continues in a somewhat more southerly direction. This line was plotted on the 1:24,000 topographic maps. In spite of its prominence on the radar image, the lineament has relatively little topographic expression. North of the Clinch River, one straight stretch of Lewis Creek 0.3 km long is exactly on the line (fig. 10), as is a saddle or sag in a conspicuous ridge line, and Miller Hollow, a short tributary of the Clinch River. South of the Clinch River the only topographic feature that falls on the line is a straight stretch of Mill Branch, where it cuts through a line of hills at the west tip of the high synclinal House and Barn Mountain.

Miller field checked this lineament, so prominent on the SLAR imagery and faintly recognizable on the ERTS imagery, fully expecting to find a fault. The areas of best exposures of bedrock crossing this line are shaded in figure 10. None of these bedrock exposures showed any evidence of a fault along or near the line. Neither was there abnormal jointing nor any other sign of structural disturbance or weakness. In the southern of the two sets of bluffs along the Clinch River, where all beds dip moderately to the southeast, bedrock clearly continues undisturbed across the line. In each of the other six areas examined, exposures of bedrock were so abundant that it seems impossible for an undetected fault to be present.

The explanation for the lineament on the radar image appears to be that the prominent topographic expression of the southeast-trending Russell Fork fault coupled with the abrupt westward termination of House and Barn Mountain at the water gap of Mill Branch causes the eye to seek an extension of the Russell Fork Fault lineament. Therefore, the alinement of the saddle marked in figure 10, and the straight stretches of Miller Hollow, Lewis Creek, and Mill Branch produce an image of a lineament. It is, however, entirely fortuitous that short segments of the three stream courses and a shallow sag or saddle in the low ridge fall in a nearly straight line.

Other lineaments in southwestern Virginia

Several other lineaments were noted in the imagery of southwest Virginia, but most were shorter and less distinct than the three that were field checked. One of special prominence, however, is parallel to and about 10 km west of the Coeburn fault. The lineament originates near the town of Wise, Wise County, Va., near

the south edge of the Appalachian Plateaus and is recognizable on the ERTS–1 imagery (fig. 5) northward for about 18 km. On the geologic map and in the report on Wise County, Eby (1923) recognized and drew structure contours on a very sharply flexed monocline along the southern half of this alinement. He also mentioned but did not interpret the unusual straightness of the valley of Indian Creek, which forms the northern half of the linear feature. Most likely this lineament represents a previously unrecognized fault of significant size throughout part or all of its 18-km extent. It certainly merits field investigation, particularly because of probable subdrainage coal mining in the future.

CONCLUSION

Remote-sensing imagery and photography can be used to locate and identify subtly expressed structures in the mountainous terrain of the southern Appalachians. Two examples of prominent lineaments proved to be previously unrecognized faults. Recognition of these features will aid in planning deep coal mining operations and in the exploration for oil and gas in the area (Ryan, 1974). On the other hand, not all lineaments seen in remote-sensing imagery are structural lineaments, as illustrated by the lineament in Russell County; laboratory interpretations of lineaments and other features seen in photographs and images from air and space must be field checked.

At a recent symposium (Freden and others, 1973) many geologists explained the use of ERTS–1 imagery as a pragmatic tool to study many types of geologic and related earth science problems. With the establishment of the Department of the Interior–U.S. Geological Survey EROS Data Center (1973) and with the availability of courses in remote-sensing methodology at many colleges and universities (Eitel, 1972), no field geologist should deprive himself of the opportunity to take a synoptic view of his field area.

REFERENCES CITED

Billings, M. P., 1954, Structural geology [2d ed.]: New York, Prentice Hall, 514 p.

Cardwell, D. H., Erwin, R. B., and Woodward, H. P., compliers, 1968, Geologic map of West Virginia: West Virginia Geol. and Econ. Survey, scale 1:250,000.

Eby, J. B., 1923, The geology and mineral resources of Wise County and the coal-bearing portion of Scott County, Virginia: Virginia Geol. Survey Bull. 24, 617 p.

Eitel, D. F., 1972, Remote sensing education in the U.S.A.: Photogrammetric Engineering, v. 38, no. 9, p. 900–906.

Elder, C. H., Jeran, P. W., and Keck, D. A., 1974, Geologic structure analysis using radar imagery of the coal mining area of Buchanan County, Virginia: U.S. Bur. Mines Rept. Inv. R.I., 7869, 29 p.

Englund, K. J., 1961, Rotational block of the Cumberland overthrust sheet in southeastern Kentucky and northeastern Tennessee: U.S. Geol. Survey Prof. Paper 424–C, p. C74–C76.

——— 1968, Geology and coal resources of the Elk Valley area, Tennessee and Kentucky: U.S. Geol. Survey Prof. Paper 572, 59 p.

——— 1971, Displacement of the Pocahontas Formation by the Russell Fork Fault, southwest Virginia: U.S. Geol. Survey Prof. Paper 750–B, p. B13–B16.

Fischer, W. A., 1972, Status of remote sensing: Cong. Internat. Soc. Photogrammetry, 12th, Ottawa, Canada, Proc.

Freden, S. C., Mercanti, E. P., and Becker, M. A., compilers and editors, 1973, Symposium on significant results obtained from the Earth Resources Technology Satellite–1, Goddard Space Flight Center, New Carrollton, Md., March 5–9, 1973, Technical Presentations (v. 1), sections A and B: Natl. Aeronautics and Space Adm., NASA SP–327, 1,730 p.

Hennen, R. V., and Gawthrop, R. M., 1915, Wyoming and McDowell Counties: West Virginia Geol. Survey, 783 p.

Hobbs, W. H., 1912, Earth features and their meaning: New York, The MacMillan Co., 506 p.

Johnston, J. E., 1972, Remote sensing as a tool for interpreting structural geology in the Appalachians [abs.]: Am. Assoc. Petroleum Geologists, Eastern Section, 1st Ann. Mtg., Columbus, Ohio, 1972, Program and Abstracts, p. 13.

Ryan, W. M., 1974, Structure and hydrocarbon production associated with the Pine Mountain thrust system in West Virginia [abs.]: Am. Assoc. Petroleum Geologists, Eastern Section, 3d Ann. Mtg., Pittsburgh, Pa., 1974, Program and Abstracts, p. 13.

U.S. Department of the Interior, 1973, The EROS Data Center: Washington, U.S. Govt. Printing Office, 18 p.

Jour. Research U.S. Geol. Survey
Vol. 3, No. 3, May–June 1975, p. 295–303

RELATIONS BETWEEN THERMAL, PHOTOGRAPHIC, AND TOPOGRAPHIC LINEARS AND MAPPED AND MEASURED STRUCTURES IN A PRECAMBRIAN TERRANE IN COLORADO

By BRUCE BRYANT, T. W. OFFIELD, and PAUL W. SCHMIDT, Denver, Colo.

Abstract.—Comparison of orientation of faults, foliations, and joints, observed during geologic mapping in Colorado, with thermal, photographic, and topographic linears shows that topographic linears are statistically useful indicators of mappable faults and fractures, photographic linears are less useful, and thermal linears, believed to represent zones of moisture concentration, are parallel to faults, foliations, and a statistically minor, but more open joint set.

Linears drawn from topographic maps, aerial photographs, and, more recently, other types of images, are commonly used to make geologic interpretations, especially where few data are available from field observations. We seldom have the information that allows a detailed comparison between data obtained in the field and linears observed in image analysis. The Evergreen 7½-min quadrangle, Colorado, furnishes an opportunity for such a comparison. This quadrangle has been the site of detailed geologic observations and compilations of data from remote sensing and other sources; these observations and compilations have led to a folio of maps (U.S. Geol. Survey Misc. Geol. Inv. Maps I–786A—G). Here we present geologic and remote sensing data from the Evergreen quadrangle in summary form, based on published (Sheridan and others, 1972; Reed and others, 1973; Offield and Pohn, 1975) and unpublished information, and attempt to interpret the significance of the linear features observed.

Comparisons have been made between photographic linears and joints and faults (Brown, 1961; Boyer and McQueen, 1964) and between topographic linears and bedrock structure (Gross, 1951). In a Precambrian and Paleozoic terrane in central Texas, Brown (1961) found that faults showed well as photographic linears but that one or more joint systems were not consistently reflected by linears. On the other hand, Boyer and McQueen (1964), in a similar comparison in a similar and nearby area, found a good correlation between photographic linears and faults and joints mapped and measured in a field study. Gross (1951) found that topographic linears reflected a number of geologic features including faults, schistosity, layering, dikes, and, possibly, moraines. No comparison with joint trends was made.

The Evergreen quadrangle is on the eastern flank of the Front Range, about 20 mi (32 km) west of Denver, Colo. (fig. 1). The rocks in the quadrangle are a Precambrian complex composed of interlayed and intergrading felsic gneiss, biotite gneiss, sillimanite mica schist and gneiss, amphibolite, calc-silicate rock, and marble intruded by granitic rock and pegmatite of two ages.

The major episode of deformation and sillimanite-grade metamorphism is dated as 1,750–1,700 m.y. ago (Hedge and others, 1967). Many of the metamorphic rocks were incipiently migmatitized and, locally, mappable areas of migmatite were produced. Small pegmatites, formed by metamorphic differentiation (Hedge, 1969), are numerous. Bodies of hornblende, biotite, and muscovite-biotite quartz monzonite to biotite granodiorite were emplaced during a late stage of the main metamorphism. They have numerous inclusions, and their contacts are locally indefinite because of migmatitization of the country rock.

Recent studies in areas adjacent to the Evergreen quadrangle have detected at least two episodes of folding that occurred before or during this metamorphic-plutonic event (Gable, 1968; Sheridan and others, 1967; Bryant and others, 1973). The metamorphic rocks trend northwest and generally have steep to moderate dips (fig. 1; Sheridan and others, 1972; Reed and others, 1973). Lack of marker horizons and the gradational contacts between rock units make well-defined fold noses difficult to locate. A few noses are shown on the geologic map (Sheridan and others, 1972), but no systematic succession of antiforms and synforms is detected. The scarcity of fold noses suggests that the axes of the folds controlling the outcrop pattern of the rock units must be nearly horizontal.

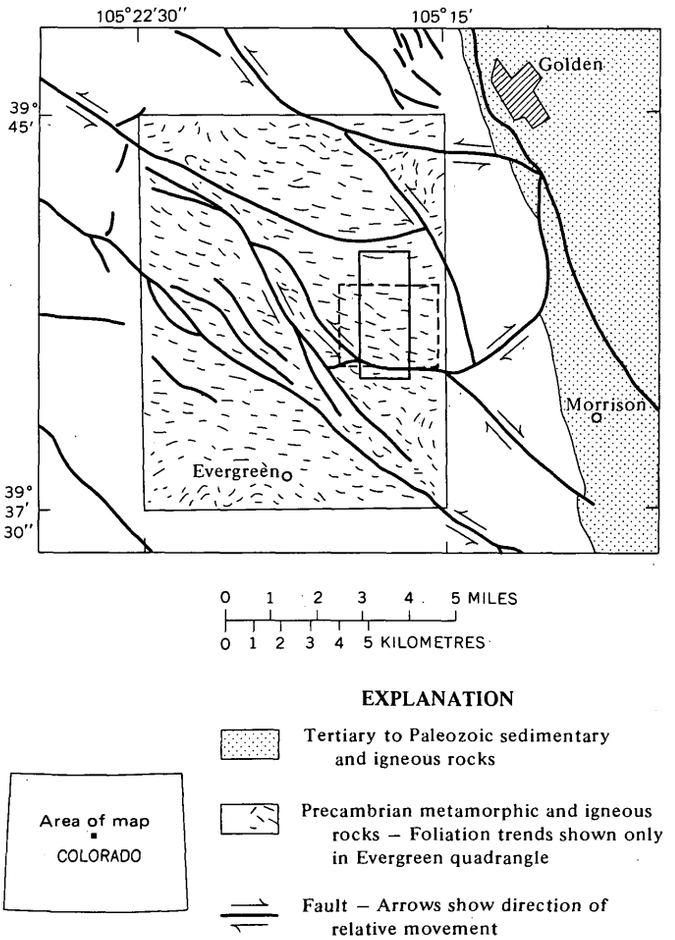

FIGURE 1.—Index map of the Evergreen quadrangle, showing major faults and foliation trends. From Sheridan, Reed, and Bryant (1972). Area of figure 3, outlined by dashes; area of figure 4, by solid line.

About 1,440 m.y. ago muscovite-biotite quartz monzonite, correlated with the Silver Plume Quartz Monzonite, was intruded in a number of irregular semiconcordant masses and numerous small dikes and sills in the southern part of the quadrangle.

The rocks were broken by a number of northwest- to west-trending faults, many of which have apparent left-lateral displacement of as much as a thousand feet (300 m). Movement along these fault zones probably took place at several times during the Precambrian and the Phanerozoic.

GEOLOGIC STRUCTURES

Faults and mapped fractures in the Evergreen quadrangle (Sheridan and others, 1972; Reed and others, 1973; fig. 2*A*) range from narrow zones of sheared or brecciated rock only a few feet thick to wide zones attaining a maximum thickness of 1,200 ft (400 m). Individual fault zones cover this range in thickness, for the zones pinch and swell in an irregular fashion. All gradations occur from unsheared country rock to breccia, in which the rock type from which the material in the fault zone was derived is not positively identifiable. Many of the best developed breccias, however, are apparently derived from felsic gneiss. The breccia fragments have iron oxide coatings which give their outcrops and the soil developed from them a distinctive yellowish-brown hue. No detailed mineralogical studies of the fault zones of the Evergreen quadrangle were made, but these zones are similar to those described by Sheridan, Maxwell, and Albee (1967) just to the north. Fluorite is locally conspicuous and, very locally, copper sulfide and uraninite occur. Inasmuch as the fault zones are generally not silicified, they tend to form valleys and saddles. Where they cross ridges, outcrops are lacking and the soil has fewer large rock fragments than soil on less fractured rock has. Exposures of fault zones are generally confined to roadcuts and streamcuts.

Foliation (fig. 2*A*), defined by alined platy minerals, principally biotite, is almost everywhere parallel to the compositional layering of the metamorphic rocks. This layering ranges in thickness from a fraction of an inch (about 1 cm) to a few tens of feet (about 10 m). The thickest layers are generally composed of felsic gneiss, and so the areas mapped as that rock type contain fewer thinly layered parts than other areas. Nonlayered rocks of Precambrian X age have variably developed foliation parallel to that of the layered rocks. The Silver Plume Quartz Monzonite of Precambrian Y age is weakly foliated or massive.

All rock units have well-developed joint systems (Reed and others, 1973; fig. 2*A*). Any differences in the spacing and distribution of joints in relation to rock type are difficult to identify because of the variations in sizes of exposures in different physiographic settings. Many of the joints spaced less than 5 ft (1.5 m) apart (Reed and others, 1973) are in areas of steep topography or in sizable roadcuts. In many of the areas of gentler slope, joint spacing cannot be determined, because the outcrops are too small. The distribution of joints spaced 5–50 ft (1.5–15 m) is extremely sparse because of the small size of individual outcrops and the highly jointed character of the rocks of the region.

LINEAR STRUCTURES

The photographic linears were compiled from aerial photographs (scale 1:26,800) that were taken at a mean distance above the ground of 13,400 ft (4,400 m) with a camera having a focal length of 153.68 mm.

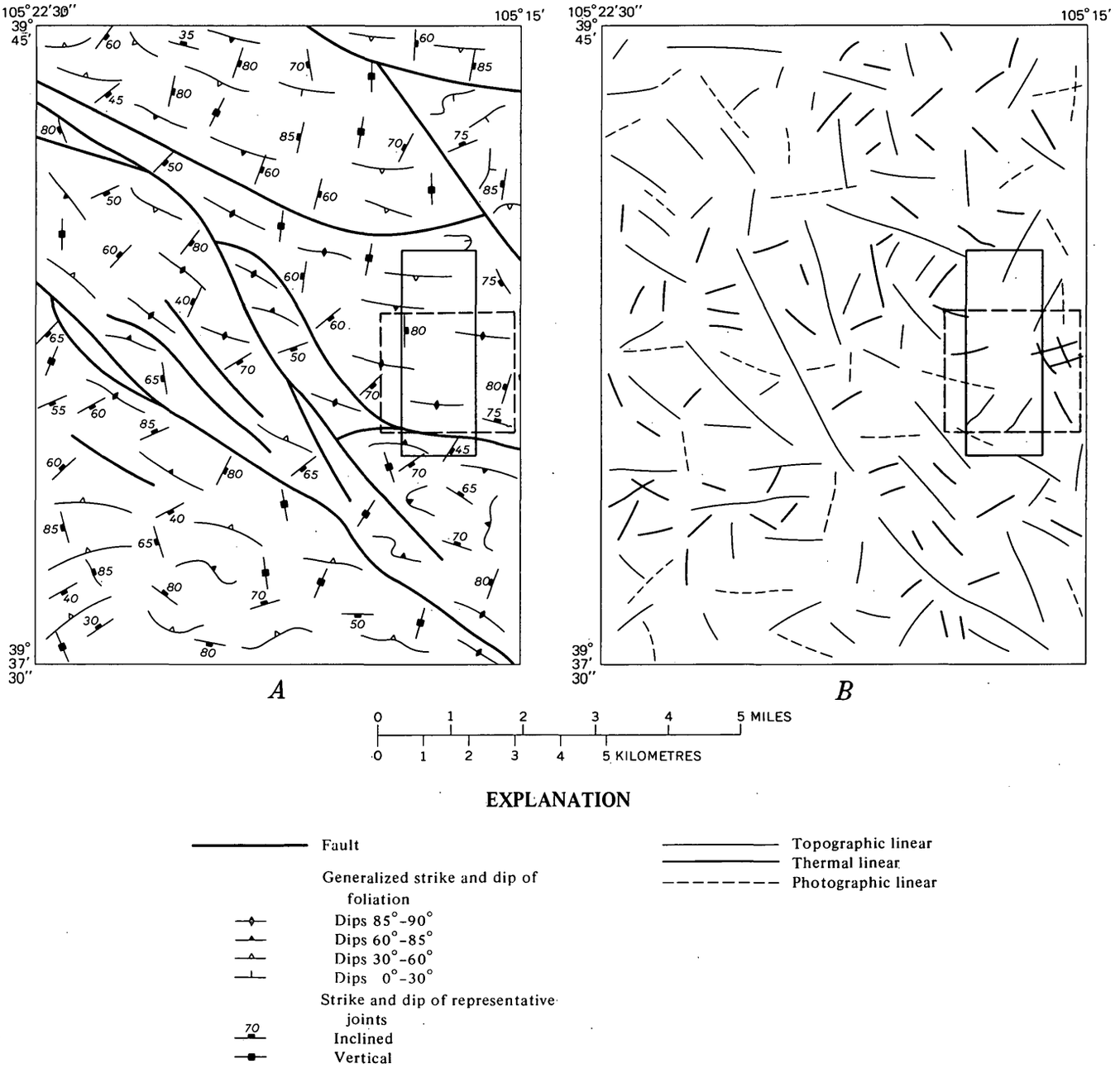

FIGURE 2.—Sketch maps of the Evergreen quadrangle. Area of figure 3, outlined by dashes; area of figure 4, by solid line. *A*, Geologic structures: Faults, foliation, and joints from Reed, Sheridan, and Bryant (1973). *B*, Linear features: Topographic, photographic, and thermal linears.

They were taken at 10:00 a.m., August 8, 1971. The Sun at that time shines from S. 62° E. at 57° above the horizon (figs. 2*B*, 3). The photographic linears are relatively straight lines marked by the alinement of ridges, streams, gullies, trees, or differences in vegetation. They range in length from 1,000 ft (100 m) to 2.5 mi (4 km); many of them fall in the range from 1,500 ft to 1 mi (0.5 to 1.6 km) in length.

Topographic linears were compiled from the U.S. Geological Survey Evergreen 7½ min quadrangle, 1965 edition. They are marked by straight valleys, long valleys, and ridges, and short straight stretches of gullies tributary to the larger valleys (figs. 2*B*, 4*B*). They range in length from 3 mi (5 km) to about 1,000 ft (300 m). A large number of these topographic linears are 1,500 to 2,500 ft (0.5 to 0.8 km) long.

Thermal linears are linear features expressed by ground-surface temperature contrasts. They are map-

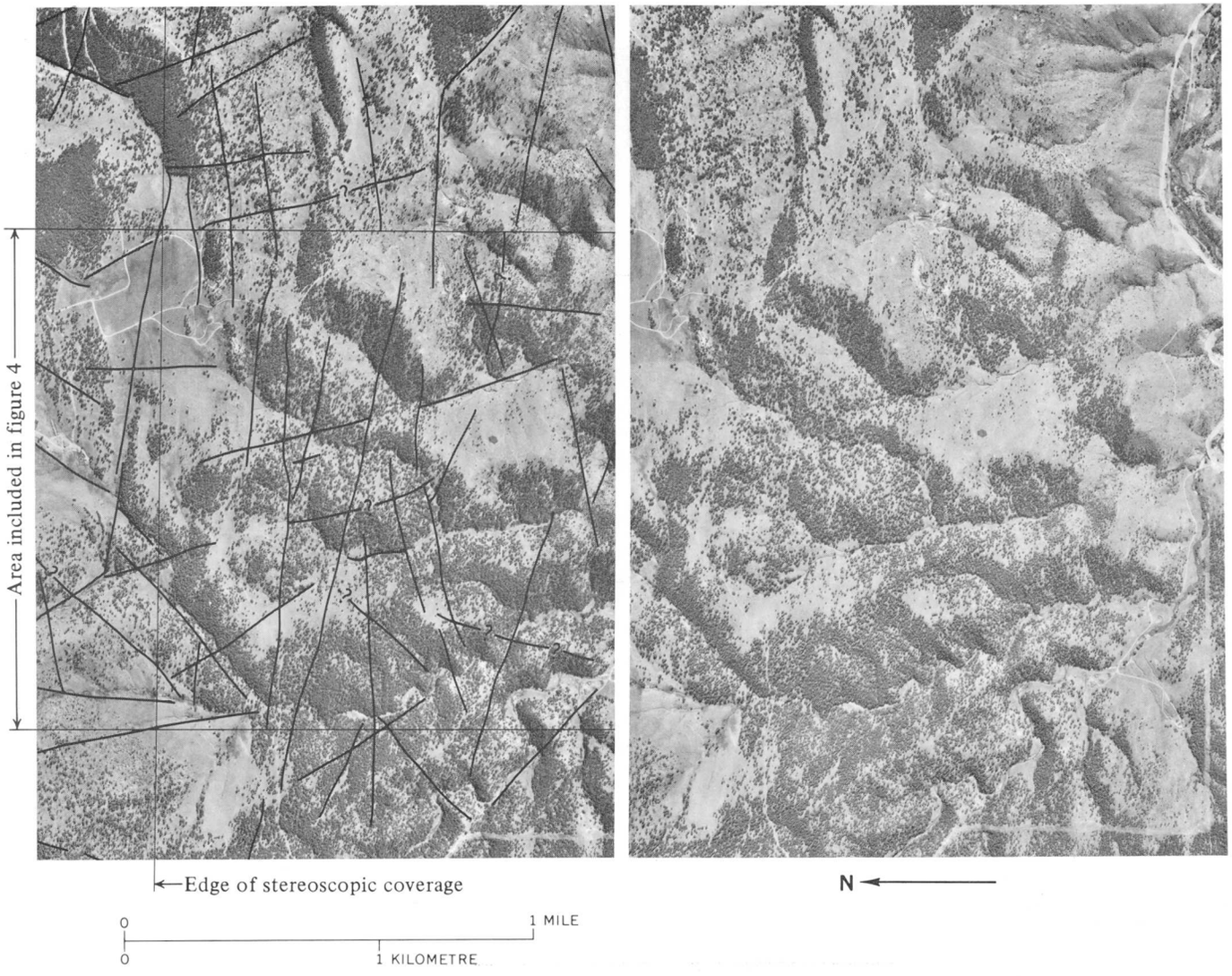

FIGURE 3.—Stereopair of aerial photographs in the east-central part of the Evergreen quadrangle, showing photographic linears. U.S. Geological Survey photographs GS–VCUC–3–200 and –201 taken at 10:00 a.m., August 8, 1971.

ped from thermal infrared images of about two-thirds of the Evergreen quadrangle (fig. 2*B*). The images were obtained predawn in the 3- to 5-μm-wavelength range and midday in the 11- to 13-μm range during July 1971, on flights about 3,000 ft (1,000 m) above mean terrain. The thermal images were geometrically distorted and precise plotting of linears on a map was difficult in many areas; the plotting is considered to be accurate to better than ±5 degrees in azimuth (figs. 2*B*, 4*A*). The thermal linears range in length from 300 ft (100 m) to 1.5 mi (2.5 km). Many of them fall within a length range of 1,000 to 2,000 ft (0.3–0.7 km).

ORIENTATION OF LINEARS AND STRUCTURES

Foliation, faults and mapped fractures, joints, thermal linears, photographic linears, and topographic linears are summarized in rose diagrams (fig. 5), as the linears lack a determinable dip. For ease of plotting, the geologic structures and the linears in the north and the south halves of the quadrangle were compiled separately and compared, except for the thermal linears. Also the structures and linears in an area of uniform foliation trend and thermal-image coverage in the east-central part of the quadrangle were compiled separately to see if the relations between linears and structures observed on the ground might be clearer in a small area. The patterns of the trends of the structures and linears for the three areas compiled separately are so similar that only the compilations for the whole quadrangle are shown in figure 5.

The faults and mapped fractures show a well-defined maximum at N. 40°–50° W. (fig. 5*A*) but many trend

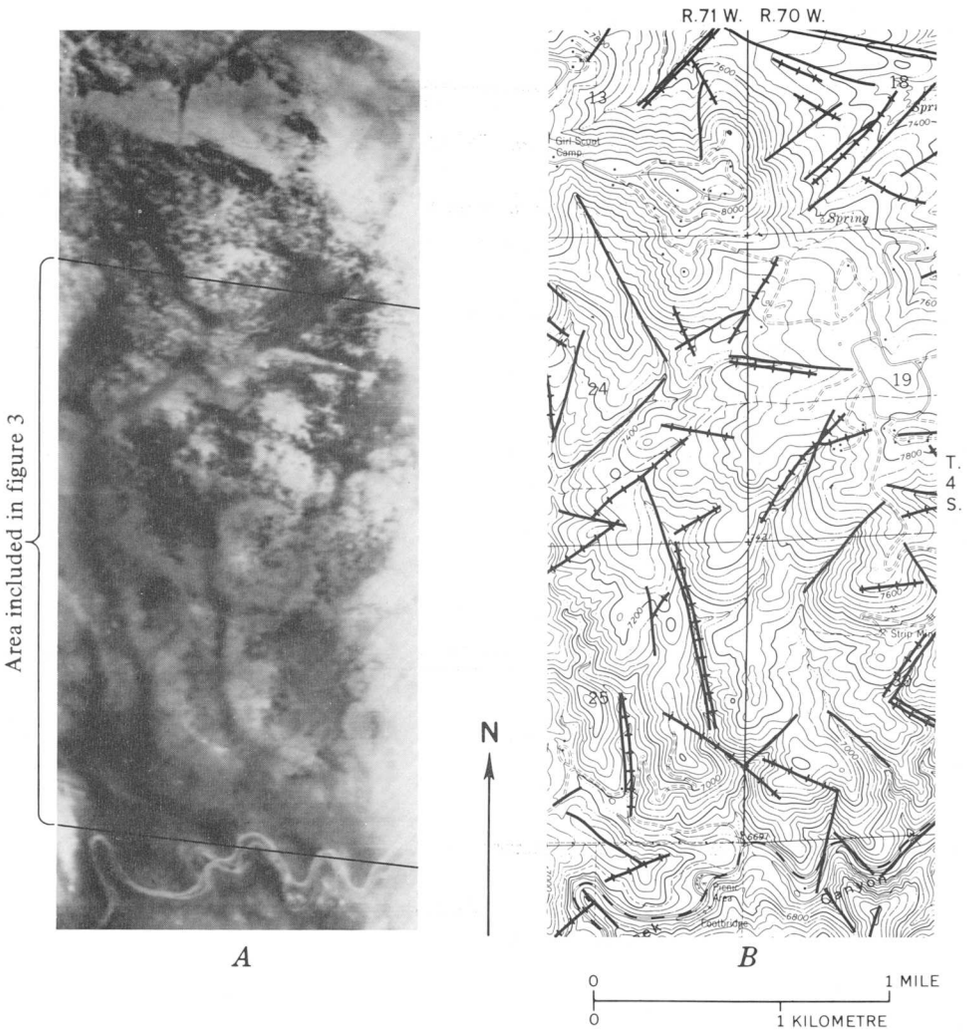

FIGURE 4.—Thermal imagery and thermal and topographic linears. *A*, Sample of predawn thermal imagery in east-central part of Evergreen quadrangle. Bear Creek at bottom; segment of Interstate Highway I–70 at northeast corner. Dark areas are relatively cool; light areas, relatively warm. Image is not orthographic. *B*, Part of Evergreen topographic map reduced to approximate scale of thermal image. Lines with crossbars are thermal linears derived from *A* and a midday thermal image. Single lines are topographic linears. Double lines are topographic and thermal linears that coincide; these are not included in the rose diagram of figure 8.

E–W to N. 20° W. These trends were established during the Precambrian (Tweto and Sims, 1963, p. 1001). The northwest-trending maximum cuts the foliation at an angle of about 20°.

Many of the faults were reactivated during uplift of the ancestral Rockies in Pennsylvanian time and of the present Front Range at the end of the Mesozoic. Both these uplifts, however, trend about 25° more northerly than the well-defined statistical maximum of the faults and fractures (fig. 1).

The foliations (fig. 5*B*) have a well-defined maximum of N. 60°–80° W., generally parallel to the boundaries of the mapped rock units. This trend was established during the deformation and metamorphism 1,700–1,750 m.y. ago.

The rocks of the Evergreen quadrangle are well jointed; the joints display a statistical maximum that trends N. 20° W. to N. 30° E. and has steep dips (figs. 5*C*, 6). This maximum is perpendicular to the trends of the foliation. Joints that trend N. 20° W. are parallel to the trend of the east margin of the Front Range and could be regional longitudinal joints. Few joints parallel mapped faults and fractures. Some joints, shown by the small N. 50°–70° E. maximum, are about perpendicular to them. They may be interpreted as cross joints in relation to either the faults and frac-

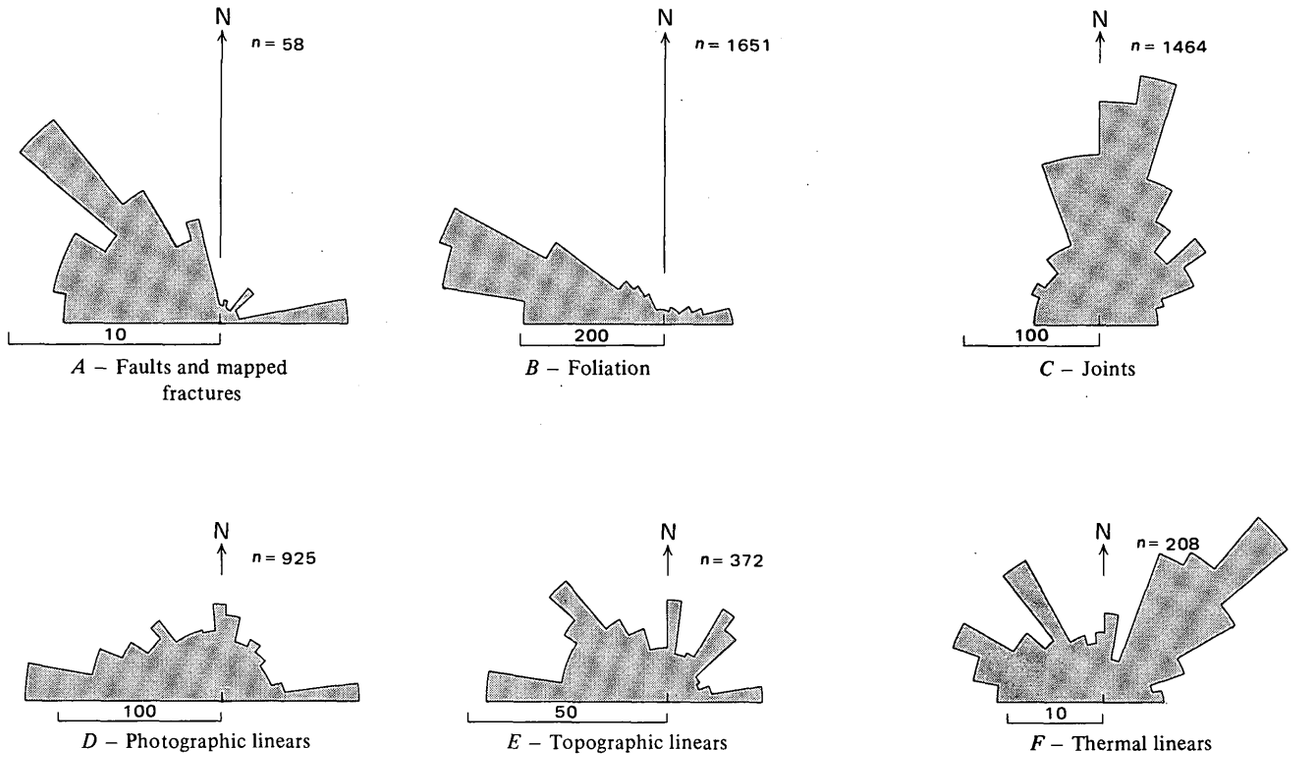

FIGURE 5.—Rose diagrams showing trends of structural features and linears in the Evergreen quadrangle. (*n* is number of measured features per diagram.)

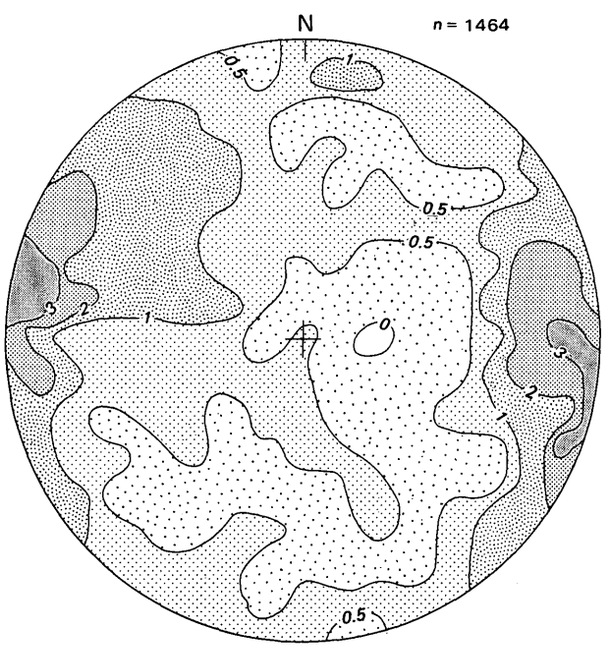

FIGURE 6.—Orientation of joints in the Evergreen quadrangle. Equal-area projection in the lower hemisphere with plane of projection horizontal and north at top. Contours show percentage of poles to joints falling within 1 percent of the area of the diagram. (*n* is number of joints measured.)

tures or the trend of the Phanerozoic Front Range uplifts, but some might be diagonal joints in relation to the Precambrian folds.

RELATION OF LINEARS TO STRUCTURES

The thermal, photographic, and topographic linears each have a distinct orientation pattern, but there is no well-defined statistical relation between the orientations of the separate linear types and any one of the structures mapped and measured on the ground. Yet, some of the geologic structures display distribution maxima that parallel maxima in the diagrams of linears.

The photographic linears (fig. 5*D*) have a prominent east-trending maximum, which is parallel to the maximum of none of the geologic structures, although a number of the mapped faults and fractures trend in that direction. Apparently this maximum also reflects the strongly developed east-west trend of foliation (fig. 5*B*). Some photographic linears are parallel to joints, as suggested by a small north-south maximum. An even smaller maximum parallels the maximum of the mapped faults and fractures.

The diagram summarizing topographic linears (fig. 5*E*) shows well-defined maxima N. 40°–50° W. and

east-west, parallel to mapped faults and fractures. The east-west maximum probably also shows development of linear topography along the principal foliation trend. Regional eastward drainage may serve to enhance the topographic effect of east-trending structures. Maxima at north to N. 10° E. and N. 30°–50° E. are joint controlled. The north-south joint set exercises a much smaller topographic control than the northeast-trending set in proportion to the number of joints of each set observed on the ground.

The lengths of the topographic linears range widely. A rose diagram was constructed by adding the total lengths rather than the number of linears of each orientation (fig. 7). This diagram enhances the N. 40°–50° W. maximum parallel to mapped faults and fractures and decreases the maxima related to the joint sets.

The photographic linears appear related in part to the topographic linears. If the statistical eastward drainage of the terrain has emphasized the effects of the east-west faults and foliation on the topographic linears, it appears to have further emphasized these east-west trending features on the statistical summary of the photographic linears. Could the Sun also somewhat enhance a photographic linear of a preferred direction? Wolfe and Bailey (1972, p. 24) believed that linears visible on aerial photographs at the Apollo 15 landing site on the Moon may have been caused by selective enhancement of fortuitous alinements of small topographic irregularities by oblique incident sunlight. What would be the effect of such sunlight on a terrain that has structures of numerous orientations? Would it be possible to obtain a statistically apparent enhancement of structures of one orientation over those of another? Not favorable to this hypothesis are the facts that the artificial linears showed two dominant trends bisected by the Sun's azimuth (Wolfe and Bailey, 1972, p. 21), whereas we cannot detect two directions of enhancement in the Evergreen quadrangle photographic linears (fig. 5*D*). Many of the linears pass through areas of dense forest cover; that might affect solar enhancement, if any, differently than if the ground were completely bare.

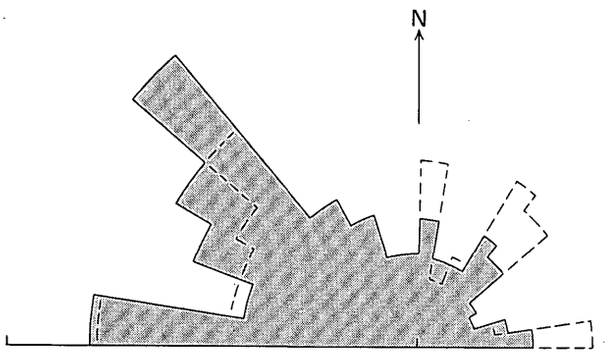

FIGURE 7.—Rose diagram of topographic linears, based on length of linears of each orientation. Dashed lines show distribution of orientation of linears based on number of linears from figure 5*E*.

The thermal linear features mapped in the Evergreen quadrangle are cooler than surrounding ground or forest during both day and night. This suggests that evaporation of surface moisture, particularly during daytime solar heating, is the dominant factor in producing the observed thermal contrasts. It is likely that many of the cool thermal linears reveal relatively moist zones or lines of fractures in unexposed bedrock.

The thermal linears (fig. 5*F*) show a strong N. 20°–60° E. maximum which matches many joints but not the main joint maximum, and which is in part parallel to a very small peak in the diagram of mapped faults and fractures. A N. 30°–40° W. maximum is parallel to the prominent maximum of mapped faults and fractures, and a N. 60° W. maximum is parallel to that of the foliation diagram.

About one-third of the linears lie along valleys or ridge crests where thermal contrasts probably are more a function of topography than of properties of the surface materials. Of these topographically controlled thermal linears, about two-thirds are parallel to structural elements mapped by Reed, Sheridan, and Bryant (1973), so even these thermal features have an indirect relation to structure.

In order to analyze more closely the origin of the thermal linears not associated with topographic elements, a separate rose diagram was made, from which the thermal linears that parallel topographic linears were omitted (fig. 8). The main differences between the modified and unmodified diagrams (compare fig. 5*F* with fig. 8) are the diminution of the maximum parallel with mapped faults and fractures and the enhancement of the maximum parallel with the foliation.

The linears in figure 8 can rarely be identified in the field. Many do not occur in areas of outcrop and thus cannot be directly identified as coinciding with structural directions. Nevertheless two-thirds of the nontopographic thermal linears are parallel to foliation or joints measured within 1,000 ft (300 m) of the linears. A majority of the linears have trends parallel to joints with spacing of less than 5 ft (1.5 m) (Reed and others, 1973), suggesting that intensity of jointing is a factor in the development of cool thermal lines. The linears do not match the joint maximum even though a majority of linears are parallel to nearby joint sets. This suggests that although those sets are not the most

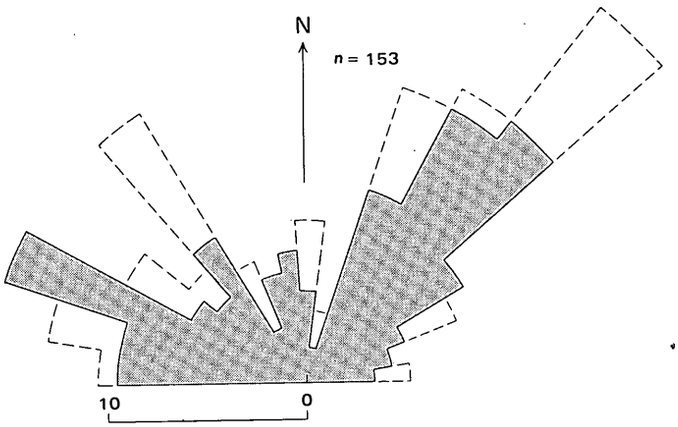

FIGURE 8.—Rose diagram showing trends of thermal linears not associated with topographic elements. For comparison, dashed lines show figure 5F at same scale. (n is number of linears.)

abundant joints, they may be the most open fractures and therefore loci of moisture concentration. The main linear maximum is normal to the maximum for faults; it is reasonable for open fractures to develop normal to faults.

One of the possible practical considerations of a study of thermal linears is to discover what structural element most strongly controls storage and movement of ground water. In the Evergreen quadrangle many people obtain domestic water supplies from wells in bedrock and also dispose of wastes into the rock through leaching fields. Unfortunately, the method by which the location of wells is reported to the Colorado State Engineer does not allow one to determine correlation between well yield and specific structural features, whether the features be mapped faults or possible water-bearing fractures suggested by thermal linears (Schmidt and Reed, 1972).

If the suggestion from the thermal data is valid, that cool linears mark zones of moisture concentration, then it appears from figures 5 and 8 that joints trending northeast, foliations trending west-northwest, and faults trending northwest are the most promising structures in prospecting for ground water. The correlation of each of these types of structures with the thermal linears is variable within the quadrangle. Because these structural elements commonly are not vertical, determination of the dip of the structures at each location for a new well and drilling the well perpendicular to the target structure would give a better statistical chance of intersecting more of the potentially water-bearing zones than would a simple vertical well.

Over the whole quadrangle, the apparently more water-bearing northeast-trending joint set, as suggested by the thermal linears, has a statistical moderate southeast dip as compared to a statistical near-vertical dip for the north-south joint set (fig. 6). Consequently, wells drilled in a northwest direction inclined at about 60° from the horizontal would appear to have a better statistical chance of intersecting members of the more open joint set than would a vertical hole. As inclined wells are seldom, if ever, drilled in this area, the utility of this suggestion cannot now be evaluated.

CONCLUSIONS

Topographic, photographic, and thermal linear features mapped in the Evergreen quadrangle are related to structural elements in the rocks. The relationship is complex, however, and interpretation of linears is greatly enhanced by detailed knowledge of the structure of the area. Statistically, topographic linears furnish the best indicators of faults, but in some instances the topographic linears are controlled by joint trends. Photographic linears are strongly coincident with east-west faults and foliation trends and do not statistically represent the joints very well. Thermal linears have maxima parallel to a statistically minor joint set, the major foliation trend, and some faults or fractures. These thermal linears are believed to reveal zones of moisture concentration along relatively open structural planes and may be of interest in studies of water or drainage problems.

REFERENCES CITED

Boyer, R. E., and McQueen, J. E., 1964, Comparison of mapped rock fractures and airphoto linear features: Photogramm. Eng., v. 30, no. 4, p. 630–635.

Brown, C. W., 1961, Comparison of joints, faults, and airphoto linears: Am. Assoc. Petroleum Geologists Bull., v. 45, no. 11, p. 1888–1892.

Bryant, Bruce, Miller, R. D., and Scott, G. R., 1973, Geologic map of the Indian Hills quadrangle, Jefferson County, Colorado: U.S. Geol. Survey Geol. Quad. Map GQ–1073, 7 p. (text) [1974].

Gable, D. J., 1968, Geology of the crystalline rocks in the western part of the Morrison quadrangle, Jefferson County, Colorado: U.S. Geol. Survey Bull. 1251–E, 45 p.

Gross, W. H., 1951, A statistical study of topographic linears and bedrock structures: Geol. Assoc. Canada Proc., v. 4, p. 77–87.

Hedge, C. E., 1969, Petrogenetic and geochronologic study of migmatites and pegmatites in the central Front Range: Colorado School of Mines Ph. D. thesis, 158 p.

Hedge, C. E., Peterman, Z. E., and Braddock, W. A., 1967, Age of the major Precambrian regional metamorphism in the northern Front Range, Colorado: Geol. Soc. America Bull., v. 78, no. 4, p. 551–557.

Offield, T. W., and Pohn, H. A., 1975, Map showing thermal linears in the Evergreen quadrangle, Jefferson County, Colorado: U.S. Geol. Survey Misc. Geol. Inv. Map I–786–G.

Reed, J. C., Jr., Sheridan, D. M., and Bryant, Bruce, 1973, Map showing faults, joints, foliation, and surficial deposits in the Evergreen quadrangle, Jefferson County, Colorado: U.S. Geol. Survey Misc. Geol. Inv. Map I–786–F.

Schmidt, P. W., and Reed, J. C., Jr., 1972, Map showing approximate locations, depths, and estimated yields of water wells in the Evergreen quadrangle, Jefferson County, Colorado: U.S. Geol. Survey Misc. Geol. Inv. Map I–786–E [1973].

Sheridan, D. M., Maxwell, C. H., and Albee, A. L., 1967, Geology and uranium deposits of the Ralston Buttes district, Jefferson County, Colorado, *with sections on* Paleozoic and younger sedimentary rocks, by Richard Van Horn: U.S. Geol. Survey Prof. Paper 520, 121 p.

Sheridan, D. M., Reed, J. C., Jr., and Bryant, Bruce, 1972, Geologic map of the Evergreen quadrangle, Jefferson County, Colorado: U.S. Geol. Survey Misc. Geol. Inv. Map I–786–A [1973].

Tweto, Ogden, and Sims, P. K., 1963, Precambrian ancestry of the Colorado mineral belt: Geol. Soc. America Bull., v. 74, no. 8, p. 991–1014.

Wolfe, E. W., and Bailey, N. G., 1972, Lineaments of the Apennine Front—Apollo 15 landing site, *in* King, E. A., Jr., ed., v. 1, Mineralogy and petrology *of* Lunar Science Conf., 3d, Houston, Tex. 1972: Geochim. et Cosmochim. Acta, supp. 3, p. 15–25.

Jour. Research U.S. Geol. Survey
Vol. 3, No. 3, May–June 1975, p. 305–311

AN OCCURRENCE OF DISSEMINATED URANINITE IN WHEELER BASIN, GRAND COUNTY, COLORADO

By E. J. YOUNG and P. L. HAUFF, Denver, Colo.

Abstract.—Disseminated uraninite occurs in Wheeler Basin, Grand County, Colo., about 5 mi (8 km) southeast of Monarch Lake, in Precambrian metamorphic rocks consisting of migmatized gneiss and mixed gneiss and pegmatite. An intrusion of Precambrian Y Silver Plume Granite lies within 400 ft (122 m) of the occurrence. The disseminated uraninite is confined to parts of the host rock that are rich in biotite; highest grade found was 0.73 percent uranium. The disseminated uraninite occurs as cubes and grains, generally from 0.1 to 0.3 mm across. Unit cell edge of the uraninite, ≈5.48 A, suggests its pegmatitic origin. The origin of the uraninite disseminations is attributed by us to remobilization and concentration of elements during metamorphism caused by the intrusion of Silver Plume Granite. Uranium and lead isotopic analyses by K. R. Ludwig of uraninite and monazite from biotite concentrations confirm an apparent age of 1,450±20 m.y. for these minerals. This age is equivalent to that reported for the Silver Plume Granite. Although the Wheeler Basin occurrence is small in size, it has many similarities to the Rössing uranium deposit in South-West Africa.

Wheeler Basin is a U-shaped, glacially scoured valley, tributary to the larger glacially scoured valley of Arapaho Creek, which flows into Monarch Lake and thence into Lake Granby. Wheeler Basin lies within the Indian Peaks Wilderness at an altitude above 10,400 ft (3,170 m) and was formerly known as the Hellhole. The Monarch Lake 7½-minute topographic quadrangle, 1958, uses the name Wheeler Basin, thus honoring Alfred T. Wheeler (1868–1938) of Boulder, Colo., who prospected for many years in the basin. The location of a log cabin built by him and his prospecting companion, Jonas Bennett, is shown in figure 1. It is currently used by Wheeler's descendants.

Prospecting in Wheeler Basin is difficult owing to its relative inaccessibility. Pack trips by horse can be outfitted at Arapaho Valley Ranch, 1 mi (1.6 km) northwest of Monarch Lake, or at Nederland across the Continental Divide.

The first development work was done in 1956 by Jonas Bennett of Nueva, Calif., who opened a 32-ft (9.8-m) adit (Fred Bogart, oral commun., 1973) which is referred to as the Bennett mine by local people. At the time of the senior author's investigation in 1973, several tons of uraninite-bearing biotite concentrations (ore) lay on the dump on each side of the adit portal. Our work was prompted by discussions with Frank Krein of Lakewood, E. P. Beroni of the Atomic Energy Commission at Grand Junction, and Glenn Culver of the Texas Gulf Sulphur Co. Geologists of Texas Gulf Sulphur have made an investigation of this occurrence, but their report is not available.

GEOLOGIC SETTING

The geologic sketch map of the area surrounding the uraninite occurrence (fig. 1) has been taken directly from the field maps of R. C. Pearson and J. C. Ratté, with their kind permission. The uraninite occurrence is in Precambrian metamorphic rocks consisting of migmatized gneiss, mixed gneiss and pegmatite, and small but discrete pegmatites. These metamorphic rocks are probably correlative with the metasedimentary Idaho Springs Formation, which is about 1.7 b.y. old. A pluton of Precambrian Silver Plume Granite lies to the northeast, and a lobe of this granite lies within 400 ft (122 m) to the south and presumably underlies the metamorphic rocks. Although the Silver Plume is called granite, it ranges from granodiorite to granite and probably averages quartz monzonite. It is fine- to medium-grained (0.1–5 mm) in the lobe and is slightly but noticeably magnetic.

At several places in the lobe of Silver Plume Granite, radioactivity is 3–4 times greater than the background radioactivity in Wheeler Basin (metamorphic gneiss), as shown in table 1. Counts per second were made with a portable scintillation counter.

The Silver Plume Granite, though not dated in this area, has been assigned an age of 1.39–1.45 b.y. in nearby areas (Peterman and others, 1968).

Regional foliation in the metamorphic rocks generally strikes northwest and dips northeast at moderate to steep angles (fig. 1).

A large-scale geologic map of the uraninite occurrence is shown in figure 2*A*, and a plan of the Bennett

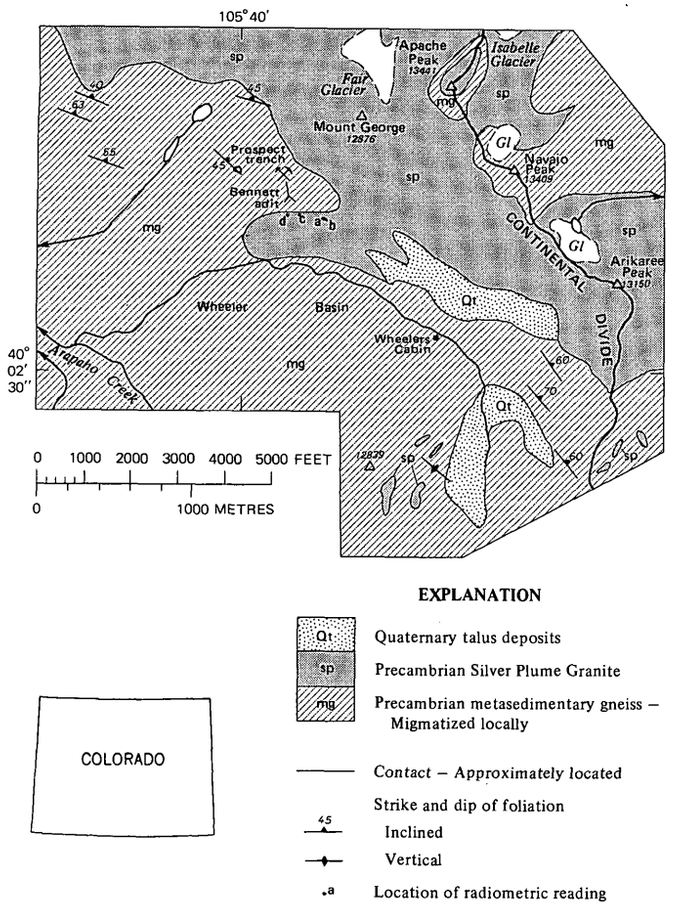

FIGURE 1.—Geologic sketch map of Wheeler Basin. Geology mapped by R. C. Pearson and J. C. Ratté in 1973.

TABLE 1.—*Radioactivity, measured in counts per second, of selected localities compared with the background radioactivity of 200–210 c/s in Wheeler Basin (metamorphic gneiss), Colorado*

Locality [1]	Rock type	Radioactivity
a	Silver Plume Granite	640–830
b	----do	620–720
c	----do	560–680
d	----do	700–900
([2])	Migmatite	300–320

[1] Localities a, b, c, and d are shown in figure 1.
[2] Near contact with Silver Plume Granite.

adit is shown in figure 2*B*. On the surface the most radioactive rock invariably is that in which biotite is concentrated. Two views of these biotite concentrations are shown in figure 3.

MINERALOGY AND PETROGRAPHY

Host rocks for the biotite concentrations are gneiss, migmatite, and pegmatite, in complex relation and variable proportions. Biotite concentrations and isolated small pegmatite bodies are irregularly disposed without conformity to regional foliation. Migmatized gneiss is generally fine grained (<1 mm) and consists largely of plagioclase and quartz and small amounts of biotite and sillimanite. Pegmatite, both in isolated bodies and as an important component of the mixed gneiss and pegmatite unit, consists mostly of pink perthite, quartz, and much smaller amounts of biotite and muscovite.

The uraninite-bearing biotite concentrations are irregular but have swirled, sharp contacts with pegmatite, migmatized gneiss, or mixed gneiss and pegmatite. Dimensions of the biotite concentrations are normally less than 10 ft (3 m) but may be more. These uraninite-bearing biotite concentrations are very radioactive, recording >10,000 c/s. Because of glacial scouring in the late Pleistocene, exposed rock has not yet had time to become chemically altered or to have the uranium leached from it.

Grain size in the biotite concentrations ranges mostly from >1 mm to 5 mm; a few biotite books are >1 cm across. Bright yellow and orange encrustations of uranophane on blocks of biotite concentrations or on the outcrop indicate that uranium is at least one of the radioactive elements. Yellow-brown rounded crystals of monazite are easily seen under a hand lens or binocular microscope, but the black, small uraninite cubes and grains are virtually invisible because of the black biotite matrix.

From thin-section, polished-section, and mineral-separation study, the uraninite-bearing biotite concentrations are seen to consist of the following primary minerals:

	Volume percentage		*Volume percentage*
Biotite	40–80	Hematite	Tr–2
Sillimanite	15–40	Uraninite	Tr–1
Quartz	5–10	Zircon	Tr
Pyrite	1–4	Molybdenite	Tr
Muscovite	Tr–3	Chalcopyrite	Tr
Monazite	Tr–2	Fluorite	Tr, rare

and the following secondary minerals, generally in trace amounts: Chlorite (iron-rich), hematite (red, earthy), uranophane, curite, and fourmarierite. The iron-rich chlorite and the uranium secondary minerals were determined by X-ray methods. Although appearing black in hand specimen, the biotite is pleochroic from dark brown to yellow under the microscope. Evidently it is moderately titaniferous, and as no ilmenite or sphene were noted, the biotite may be the source of the titanium present in the rock (table 2). The sillimanite is fibrous. Quartz and muscovite are decidedly minor in amount. Hematite, pyrite, monazite, zircon,

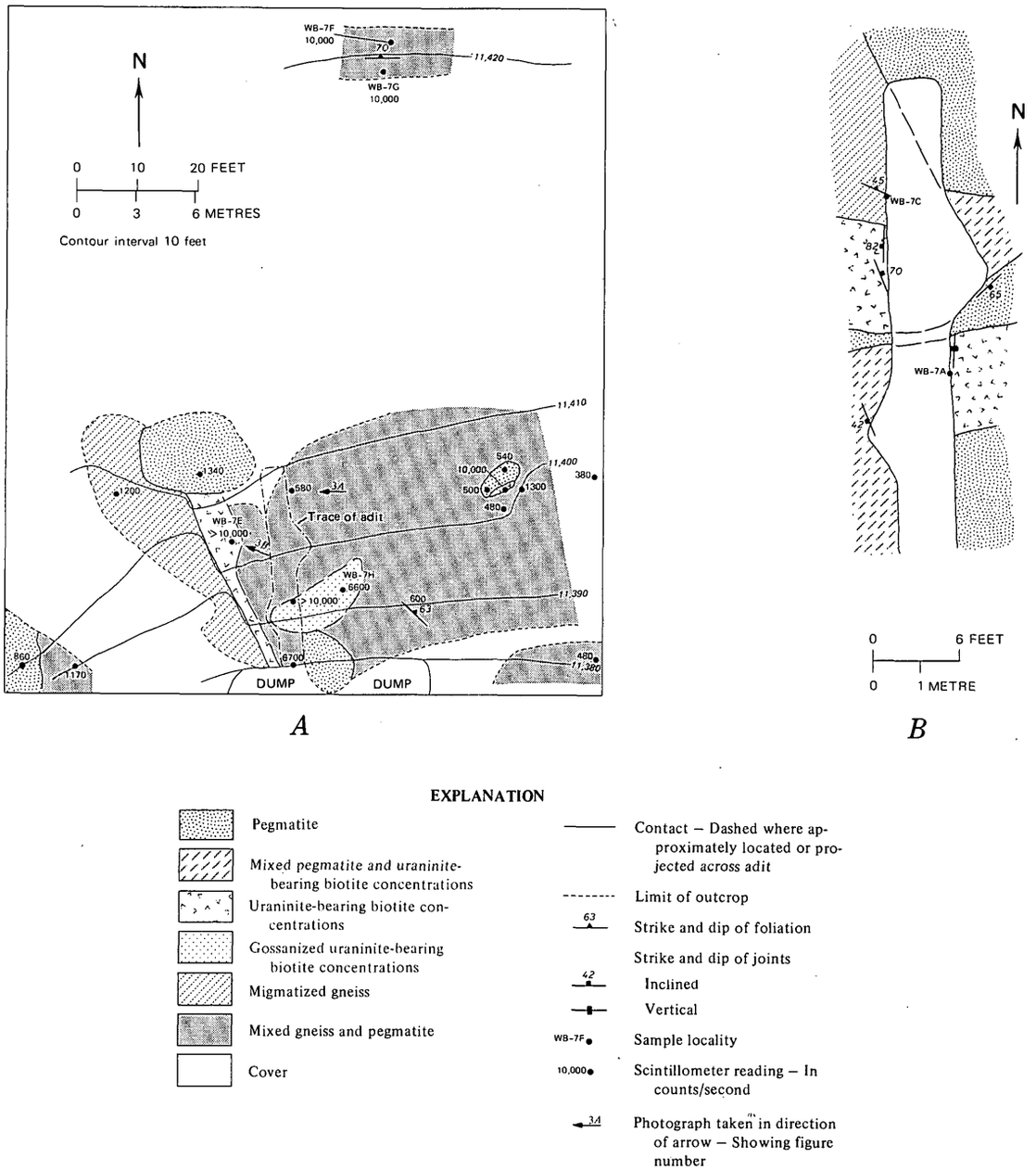

FIGURE 2.—Geologic map of area around Bennett adit (*A*) and plan of adit (*B*).

molybdenite, chalcopyrite, and uraninite are disseminated as small grains and crystals. Fluorite was seen in only one hand specimen from the dump.

Spectrographic analyses of major, minor, and trace elements and additional analyses for uranium of seven samples of uraninite-bearing biotite concentrations—four from surface outcrop, one from the adit, and two from the dump—are given in table 2. The relative importance of the contribution of equivalent uranium (eU) radioactivity from monazite is seen in samples WB–7H and WB–7F, which show larger eU's than U's. Samples containing more than 0.1 percent U tend to overshadow the relatively small contribution of radioactivity from monazite.

Although the uraninite is disseminated, there is a tendency for local concentrations to occur as shown in figure 4*A*. Figure 4*B* shows a malformed cube of uraninite in polished section. The uraninite cubes and grains almost invariably display alteration rims, in contrast to the hematite which does not. Most uraninite is embedded in biotite, but locally it is in contact with hematite. Uraninite causes pleochroic halos in the bio-

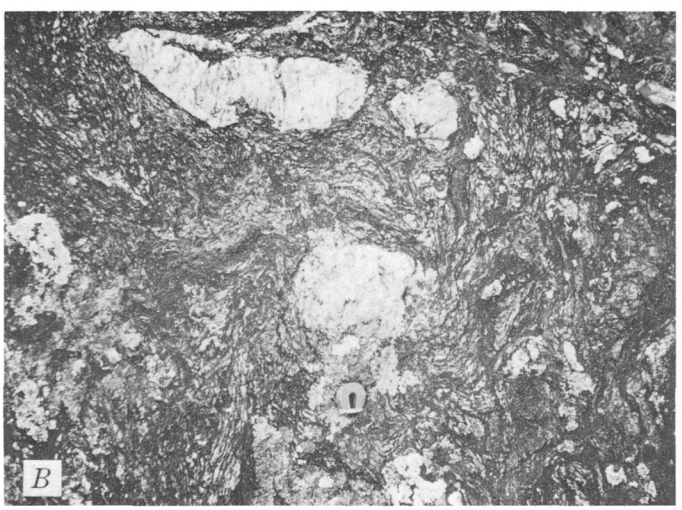

FIGURE 3.—Uraninite-bearing biotite concentrations. *A*, Note boulder of mixed gneiss and pegmatite in foreground, small pegmatite body on right, and biotite concentrations in middle ground extending downhill to left. View is to the west, see fig. 2). Area of closeup *B* is in center of lower left quarter. *B*, Closeup of biotite concentration. Light inclusions are quartz segregations. Largest dimension of magnet is 1 in.

TABLE 2.—*Analyses of seven uraninite-bearing biotite concentrations from Wheeler Basin, Grand County, Colo.*

[Semiquantitative six-step spectrographic analysis by N. M. Conklin. The following elements (detection limits given in parts per million) were looked for but not found: Ag, 0.5; As, 1,000; Au, 20; B, 20; Bi, 10; Cd, 50; Er, 50; Eu, 100; Ge, 10; Hf, 100; Ho, 20; In, 10; Li, 100; Lu, 30; P, 2,000; Pd, 2; Pt, 50; Re, 50; Sb, 200; Ta, 500; Tb, 300; Te, 2,000; Tl, 50; Tm, 20; W, 100; Zn, 300]

	WB–2	WB–11	WB–7A	WB–7E	WB–7F	WB–7G	WB–7H
Spectrographic analysis[1] in weight percent							
Al	7	>10	>10	>10	>10	>10	>10
Ca	.07	.03	.2	.03	.03	2	.03
Fe	7	>10	10	7	>10	7	>10
K	5	7	7	7	10	5	7
Mg	3	5	5	3	7	3	3
Na	.3	.3	.2	.2	.3	7	.3
Si	>10	>10	>10	>10	10	>10	10
Ti	1.5	1.5	1.5	1.5	1.5	.7	1.5
Spectrographic analysis in parts per million							
Ba	1,000	1,000	700	700	1,000	700	500
Be	<1.5	3	3	<1.5	<1.5	1.5	7
Ce	700	1,500	700	300	700	1,500	150
Co	70	70	70	50	70	30	30
Cr	300	700	300	700	1,000	200	700
Cu	150	150	200	70	100	15	300
Dy	<50	50	<50	<50	<50	<50	<50
Ga	30	50	70	50	70	50	70
Gd	<70	70	<70	<70	<70	<70	<70
La	500	1,500	700	200	700	700	50
Mn	700	700	700	700	700	500	500
Mo	300	300	30	300	300	300	150
Nb	70	50	50	70	70	50	50
Nd	700	1,500	700	300	700	1,500	<70
Ni	150	150	150	150	300	70	70
Pb	1,500	2,000	300	700	300	1,000	70
Pr	70	200	70	<70	70	200	<70
Sc	70	70	70	70	100	70	50
Sm	<100	300	150	<100	200	150	<100
Sn	15	15	<15	<15	15	<15	<15
Sr	30	30	30	20	30	700	15
Th	500	700	<200	300	300	500	<200
U	7,000	7,000	1,000	2,000	<500	1,500	<500
V	300	700	700	500	700	300	700
Y	150	200	150	50	70	100	15
Yb	15	20	15	3	5	7	2
Zr	1,500	700	700	1,000	1,500	200	700
Analyses for uranium[2] in parts per million							
eU	4,500	7,300	970	2.000	780	1,300	220
U	5,600	7,300	970	1,800	180	1,400	30

[1] WB–2 and WB–11 are samples from the dump; WB–7A is from the adit (fig. 3); and WB–7E, WB–7F, WB–7G, and WB–7H are from surface outcrop (fig. 2).

[2] eU was determined by G. D. Shipley using beta-gamma scaler; U was determined fluorometrically by E. J. Fennelly.

tite, as does monazite. A 67-h autoradiograph taken on Polaroid 55P/N film is shown in figure 5. The disseminated nature of the Wheeler Basin uraninite is clearly indicated, as contrasted to vein pitchblende from the Schwartzwalder mine, Jefferson County, Colo.

The largest uraninite crystal seen was 0.4×0.7 mm. Most grains and crystals are between 0.1 and 0.3 mm; many have a well-developed cubic habit. However, in those samples containing uraninite altered to curite and fourmarierite, deterioration of this habit occurs. The alteration process is evidenced by a change in color from black to dull gold and by the progressive breakdown of the cubic form to rounded or irregular grains. The radioactivity of these altered grains is lower than that for the uraninite cubes, which individually read four to six times above background in a micro alpha counter. (See Young and others, 1966, p. 659.)

Uraninite from five samples was concentrated by heavy liquids and the Frantz magnetic separator. With a sideslope of 5° and a forward slope of 20°, the best retrieval occurred at 0.5 amperes. Table 3 shows the unit cell dimensions of the five uraninites and the uranium-thorium ratios found in these samples. The cell dimensions were obtained by using the method of Evans, Appleman, and Handwerker (1963). The uraninites are notably low in thorium according to the uranium-thorium ratios, and the remarkable similarity of their cell edges probably reflects their chemical similarity, which in turn implies common genesis. The

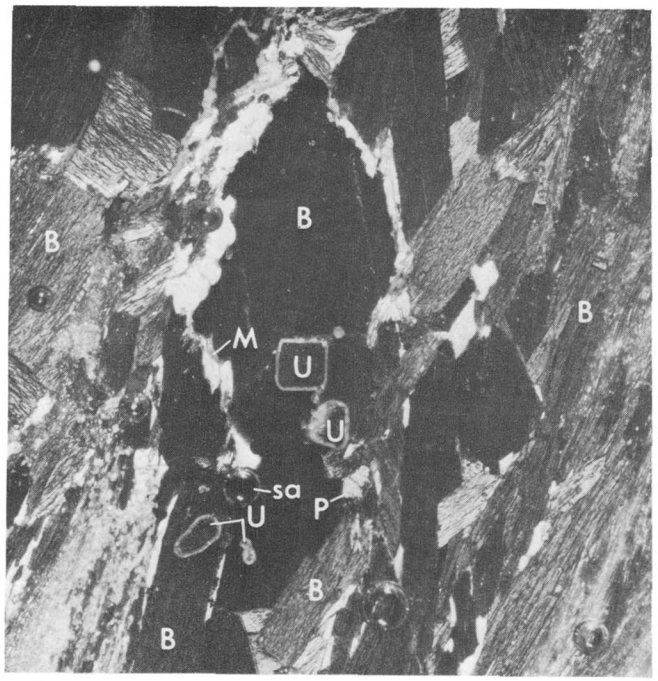

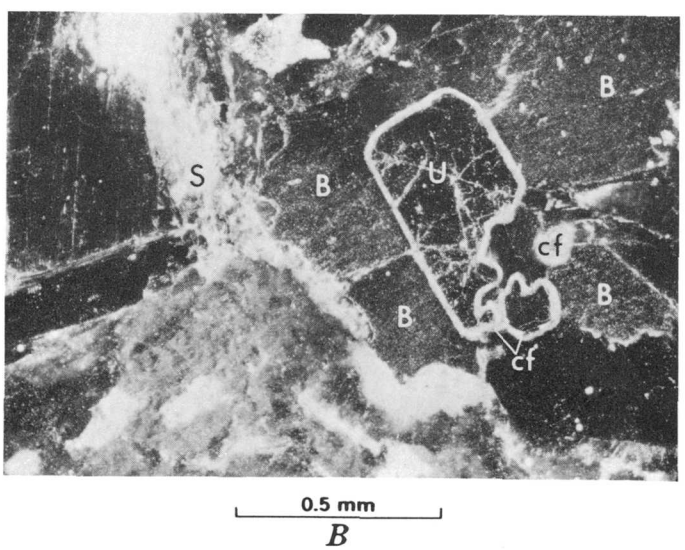

FIGURE 4.—Photomicrographs. *A*, Anhedral grains and cubic crystals of uraninite (U) in biotite (B) in thin section; secondary uranium minerals form light rims around uraninite; spherical areas (sa) are bubbles in mounting medium; P, pyrite; M, muscovite; combined transmitted light and oblique reflected light. *B*, Malformed cube of uraninite (U) in polished section; uraninite is rimmed by secondary uranium minerals curite and fourmarierite (cf), all enclosed in biotite (B); S, sillimanite; oblique reflected light.

relatively large size of the unit cell, ≈5.48 A, is commonly shown by uraninite from pegmatites and is also indicative of tetravalent rather than hexavalent uranium (Brooker and Nuffield, 1952; Berman, E., 1955; Berman, R. M., 1957; Frondel, 1958; Kašpar and Hejl, 1970).

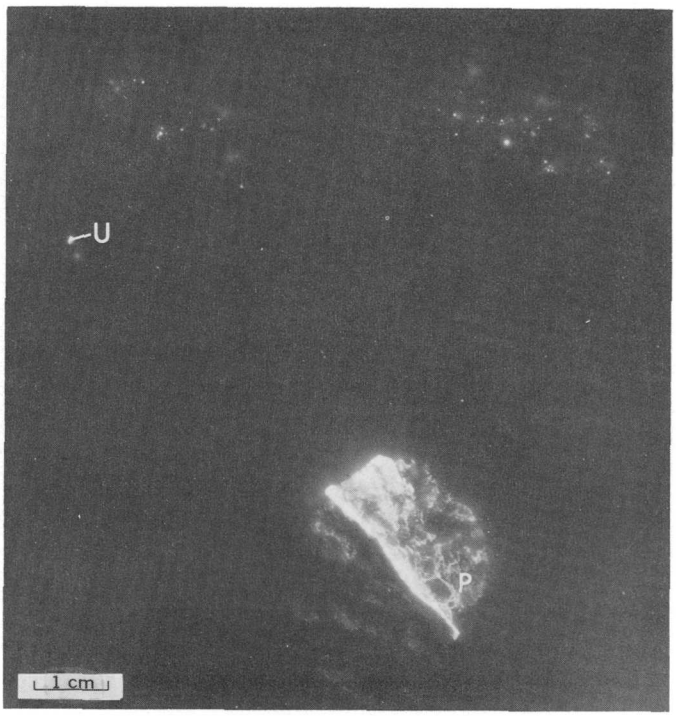

FIGURE 5.—Autoradiograph of uraninite-bearing biotite concentrations from Wheeler Basin. The sharp bright points of light result from uraninite cubes and grains on the surface of the polished section. Fuzzy patches of light denote uraninite just below the surface of the polished section. U, malformed uraninite cube of figure 4*B*. Vein pitchblende (P) from the Schwartzwalder mine, Jefferson County, Colo., is shown for comparison.

TABLE 3.—*Unit cell dimensions and uranium-thorium ratios of uraninite from Wheeler Basin*

Sample	Locality	Unit cell dimensions		Uranium-thorium ratios [1]
		a_0 (A)	Volume (A^3)	
WB–2	Dump	5.484	164.90	30.3
WB–3	do	5.484	164.91	45.5
WB–7A	Adit (see fig. 3)	5.484	164.97	35.7
WB–7G	Outcrop (see fig. 3)	5.481	164.64	33.3
WB–11	Dump	5.482	164.72	35.7
Average		5.483	164.81	36.1

[1] Ratios determined by J. S. Wahlberg.

Several fractions of uraninite and monazite were analyzed for their uranium and lead concentrations and lead isotopic composition by K. R. Ludwig. These data (unpub. data, 1974) indicate that the monazite and uraninite are cogenetic. Preliminary interpretation suggests an apparent time of formation of 1,450±20 m.y. and a subsequent disturbance of the uranium-lead systems at roughly 900±130 m.y. This interpretation

corroborates the timespan 1,390—1,450 m.y., the time of intrusion that Peterman, Hedge, and Braddock (1968) gave for the Silver Plume and Sherman Granites.

SIMILAR OCCURRENCES OF URANINITE

The Wheeler Basin occurrence of uraninite, though in metamorphic rocks, has intimate affinities with pegmatite and migmatite. The large intrusion of Silver Plume Granite, <1,000 ft (305 m) to the northeast and <400 ft (122 m) to the south, provided the heat, and possibly the solutions, to mobilize many elements in the metasediments. Monazite can be a metamorphic mineral (Overstreet, 1967; Young and Sims, 1961), and uraninite may show a similar behavior (Narayan Das and others, 1971).

In contrast to uraninite occurrences in pegmatites, which are relatively common, disseminated uraninite in migmatites and other metamorphic rocks either are not as common or remain mostly undetected. Heinrich (1958) listed several such occurrences from Canada. Harshman and Bell (1970) described a uraninite occurrence from Wyoming that is somewhat similar, although most of the disseminated uraninite occurs in a syenitic phase of an intrusive Precambrian granite and smaller amounts occur in chlorite schist close to the contact with the syenite. Smith (1965) and von Backström (1970) described an occurrence of disseminated uraninite from South-West Africa that has similarities to the Wheeler Basin occurrence. It is called the Rössing uranium deposit and is considered to have economic potential as a low-grade source of uranium. Complex intrusions of pegmatite into gneiss, migmatite, amphibolite, and limestone comprise the host rocks, which are of medium grain size (1–5 mm). The pegmatite consists almost entirely of quartz-alkali feldspar and is called alaskite by them. Smith (1965) stated that the uranium occurs in the form of complex oxides as well as in fine-grained euhedral uraninite, generally as inclusions in biotite selvages in the pegmatite. Age determinations on uraninite, davidite, and biotite indicate an age of 510±40 m.y. (von Backström, 1970). Associated minerals are zircon, monazite, minor pyrite, chalcopyrite, molybdenite, and ilmenite intergrown with magnetite, and, rarely, fluorite and hematite.

A comparison of the Rössing deposit with the occurrence in Wheeler Basin shows more similarities than differences. In tabular form the attributes of both deposits are the following:

	Rössing deposit	*Wheeler Basin occurrence*
Host rock	Pegmatite and metamorphic rocks.	Metamorphic rocks and pegmatite.
Grain size (rock)	1–5 mm	<1–5 mm, rarely larger.
Mineralogy:		
Primary	Quartz	Quartz.
	Microcline	Microcline.
	Microcline perthite	Microcline perthite.
	Biotite	Biotite.
		Sillimanite.
		Muscovite.
	Uraninite	Uraninite.
	Betafite	
	Davidite	
	Monazite	Monazite.
	Zircon	Zircon.
	Pyrite	Pyrite.
	Chalcopyrite	Chalcopyrite.
	Molybdenite	Molybdenite.
	Ilmenite	None(?).
	Magnetite	Not now present.
	Fluorite (rare)	Fluorite (rare).
	Hematite (rare)	Hematite.
Secondary	Uranophane	Uranophane.
	Beta-uranophane	?
	Metatorbernite	
	Metahaiweeite	
	Carnotite	
		Curite.
		Chlorite (iron-rich).
Uraninite habit and size.	Cubes and grains, few micrometres to 0.3 mm.	Cubes and grains, 0.1–0.3 mm.
Uraninite unit cell edge.	?	5.483 A.
Age	510±40 m.y.	1450±20 m.y.
Grade and tonnage.	As much as 0.55 percent U in small and patchy amounts; several million tonnes of 0.05 percent U.	As much as 0.73 percent U in probably small amounts; tonnage in terms of 0.05 percent U is not known.

REFERENCES CITED

Backström, J. W. von, 1970, The Rössing uranium deposit near Swakopmund, South West Africa—A preliminary report, *in* Uranium exploration geology: Vienna, Internat. Atomic Energy Agency, Panel Proc. Ser., p. 143–150.

Berman, E. R., 1955, Unit cell dimensions of uraninite: Am. Mineralogist, v. 40, nos. 9–10, p. 925–927.

Berman, R. M., 1957, The role of lead and excess oxygen in uraninite: Am. Mineralogist, v. 42, nos. 11–12, p. 705–731.

Brooker, E. J., and Nuffield, E. W., 1952, Pitchblende from Lake Athabaska, Canada, [Pt.] 4 *of* Studies of radioactive compounds: Am. Mineralogist, v. 37, nos. 5–6, p. 363–385.

Evans, H. T., Jr., Appleman, D. E., and Handwerker, D. S., 1963, The least-squares refinement of crystal unit cells with powder diffraction date by an automatic computer indexing method [abs.]: Am. Crystallog. Assoc. Ann. Mtg., Program and Abs., Cambridge, Mass., 1963, p. 42–43.

Frondel, Clifford, 1958, Systematic mineralogy of uranium and thorium: U.S. Geol. Survey Bull. 1064, 400 p.

Harshman, E. N., and Bell, K. G., 1970, Uraninite-bearing contact metamorphic deposits, Heaths Peak, Carbon County, Wyoming: Econ. Geology, v. 65, no. 7, p. 849–855.

Heinrich, E. W., 1958, Mineralogy and geology of radioactive raw materials: New York, McGraw-Hill, Inc., 654 p.

Kašpar, Jan, and Hejl, Václav, 1970, Thermodynamic conditions of the origin of uraninites, *in* Uranium exploration geology: Vienna, Internat. Atomic Energy Agency, Panel Proc. Ser., p. 301–314.

Narayan Das, G. R., Parthasarathy, T. N., and Taneja, P. C., 1971, Uranium mineralization in the pelitic schists in the Kulu Himalaya and its probable origin: Indian Acad. Sci. Proc., Pt. A, v. 37, no. 4, p. 267–276.

Overstreet, W. C., 1967, The geologic occurrence of monazite: U.S. Geol. Survey Prof. Paper 530, 327 p.

Peterman, Z. E., Hedge, C. E., and Braddock, W. A., 1968, Age of Precambrian events in the northeastern Front Range, Colorado: Jour. Geophys. Research, v. 73, no. 6, p. 2277–2296.

Smith, D. A. M., 1965, The geology of the area around the Kahn and Swakop Rivers in South West Africa: South Africa Geol. Survey Mem., South West Africa Ser. 3, 113 p.

Young, E. J., and Sims, P. K., 1961, Petrography and origin of xenotime and monazite concentrations, Central City district, Colorado: U.S. Geol. Survey Bull. 1032–F, p. 273–299.

Young, E. J., Weeks, A. D., and Meyrowitz, Robert, 1966, Coconinoite, a new uranium mineral from Utah and Arizona: Am. Mineralogist, v. 51, p. 651–663.

Jour. Research U.S. Geol. Survey
Vol. 3, No. 3, May–June 1975, p. 313–327

GEOLOGY, GEOCHEMISTRY, AND FLUID-INCLUSION PETROGRAPHY OF THE SAPO ALEGRE PORPHYRY COPPER PROSPECT AND ITS METAVOLCANIC WALLROCKS, WEST-CENTRAL PUERTO RICO

By DENNIS P. COX, ILEANA PÉREZ GONZÁLEZ,[1] and J. THOMAS NASH,
Reston, Va., San Juan, Puerto Rico, Denver, Colo.

Prepared in cooperation with the Commonwealth of Puerto Rico, Department of Natural Resources

Abstract.—The Sapo Alegre prospect, a small porphyry copper-molybdenum occurrence in west-central Puerto Rico, is characterized by distinct zones of alteration and mineralization of quartz diorite porphyry. A biotite-chlorite zone in the porphyry near its contact with surrounding metavolcanic rocks contains copper, molybdenum, gold, silver, selenium, and tellurium. A quartz-sericite-pyrite zone within the porphyry contains abundant sulfur and traces of selenium, but metals of the biotite-chlorite zone are nearly absent and zinc, manganese, nickel, sodium, calcium, and magnesium contents are very low. Quartz grains in the biotite-chlorite zone contain abundant fluid inclusions in which halite crystals are common, whereas in the quartz-sericite-pyrite zone inclusions are less abundant and rarely contain halite inclusions. Metavolcanic rocks northwest of the mineralized porphyry are altered to amphibolitic hornfels near the contact. Biotitic alteration is strong outward from the hornfels and grades into chlorite alteration. The hornfels has very low sulfide content, and the biotite zone has moderate amounts of copper and sulfur, decreasing outward. The chlorite zone is characterized by an abrupt increase in zinc and manganese content. Fluid-inclusion data suggest temperatures between 300° and 400°C for hydrothermal fluids in the biotite-chlorite zone of the porphyry and 250° to 300°C for fluids in the quartz-sericite-pyrite zone. Pressures equivalent to about 1.5 km of burial are indicated.

The porphyry copper-molybdenum occurrence chosen for this study includes the discovery outcrop that first drew attention to the copper resource potential of west-central Puerto Rico. In 1957, W. R. Bergey, seeking the source of strong copper and molybdenum anomalies in stream sediments in the Río Viví, discovered mineralized porphyry in the walls of a canyon 8 km southeast of Utuado. Subsequent geologic, geochemical, and drilling work, mainly by American Metals Climax Corp., showed that this mineralized zone, which was given the name Sapo Alegre, was too small for economic mining. However, over 100 million tons of 0.8 percent copper ore was proved in two nearby deposits, Piedra Hueca and Cala Abajo. Aside from being smaller, Sapo Alegre differs from these two main deposits and from most other deposits in Puerto Rico in having a high molybdenum content. Figure 1 shows the relationship of the Sapo Alegre prospect to these two subsequently discovered ore deposits in the Río Viví area.

The Sapo Alegre prospect is one of two places in Puerto Rico where stream erosion has exposed porphyry copper mineralization. Elsewhere, extensive development of deep saprolite makes direct study of the deposits impossible. These two exposures (the second is on the Río Coabey at the Helecho deposit, 13 km to the northwest) provide relatively fresh bulk samples and a three-dimensional view of rocks and structures, giving this type of study a distinct advantage over diamond-drill-core logging.

Detailed mapping, sampling, and chemical analysis of rocks in the Sapo Alegre zone have provided a fairly coherent picture of the relationship of more than 20 chemical elements to porphyry intrusion, mineralization, and hydrothermal alteration. Trace-element levels have served as a guide for interpretation of soil-geochemical data, and experience gained in this study has been helpful in the design of similar studies of other Puerto Rican deposits.

Acknowledgments.—We wish to express our appreciation to Roger A. Bradley of Ponce Mining Co. for his generous sharing of information on the Sapo Alegre deposit and to J. J. Hemley for critical review of the manuscript and stimulating discussion. Success of the field phase of this project was largely due to the enthusiastic assistance of Carlos Cram and Isidro Toro, of the Puerto Rico Department of Natural Resources, and of Gustavo Gonçalves, of the Companhia

[1] Puerto Rico Department of Natural Resources.

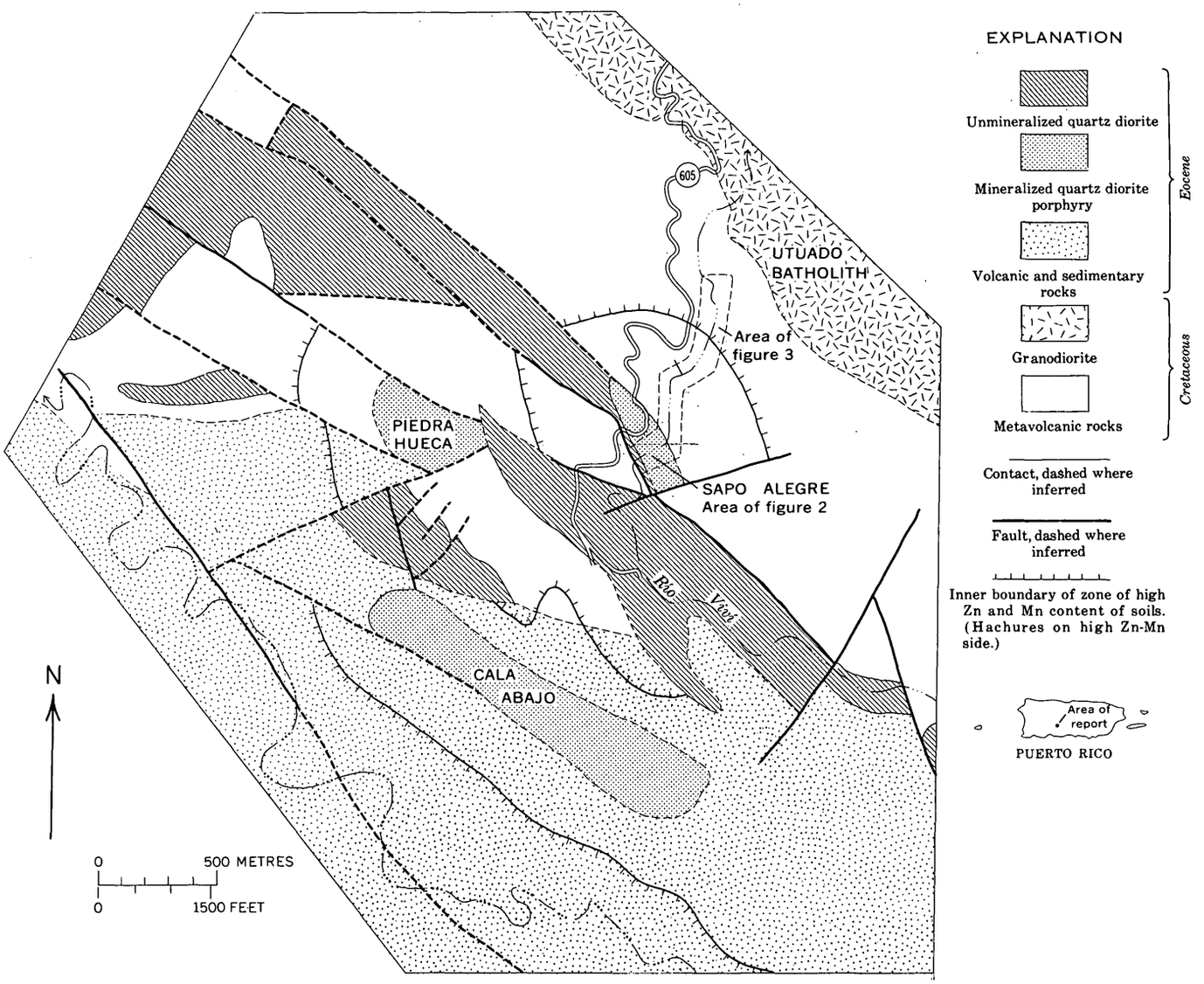

FIGURE 1.—Map of the Río Viví district, Puerto Rico, showing geology (modified from Mattson, 1968), zinc-manganese geochemistry (from Learned and Boissen, 1973), and the location of the Sapo Alegre prospect and study area in relation to the two main deposits, Piedra Hueca and Cala Abajo.

de Pesquiza de Recursos Minerais of Brazil, who was visiting Puerto Rico at the time of the study. Thin- and polished-section preparation and most of the chemical analyses were carried out by the Laboratory of Geology, Puerto Rico Department of Natural Resources, whose staff includes Raphael Boissen, Carmen Anna Abrahamson, Sara Cortés, Lizbeth Hyman, Juan Martínez, and the second author as present director.

SAMPLING METHODS

A total of 65 rocks samples was collected during the detailed mapping of the Río Viví canyon where it crosses the Sapo Alegre deposit and nearby volcanic rocks. Chip samples at 3-m (10 ft) intervals were taken in the porphyry and in the metavolcanic rocks within 75 m of the contact. Grab samples at 30-m (100 ft) intervals were collected in the metavolcanic rocks along a 500-m traverse to the northeast. At each locality, an effort was made to minimize the amount of oxidized or secondarily enriched material in the sample. Most samples contain less than 1 percent limonite and other weathering products, and, except for two samples (87 and 93), secondary chalcocite is negligible.

One or two rocks, judged to be typical of each sample interval, were selected for thin- and polished-section microscopy.

ANALYTICAL PROCEDURES

Samples were crushed and pulverized and analyzed semiquantitatively for 30 elements in a 1.5-m emission spectrograph, according to methods developed by Grimes and Maranzino (1968). Spectrographic data for Cu, Mo, Ag, Ni, and Co were used in the study.

Atomic-absorption determinations for Cu, Zn, Pb, Au, Fe, K, Na, Ca, Mg, and Mn were made with a Perkin Elmer 403 spectrophotometer, using an air-acetylene flame. Standards were prepared by dilution from 1,000 ppm stock solutions. Cu, Zn, and Pb content was determined according to the method of Ward and others (1969). For gold analysis, a 10-g sample was ignited at 700°C overnight, then digested with hydrobromic acid–bromine solution. After cooling, gold was extracted by MIBK (methyl isobutyl ketone) and determined by atomic absorption (Thompson and others, 1968). For Fe, K, Na, Ca, Mg, and Mn, samples were digested twice to dryness with hydrochloric–hydrofluoric acid solution and the residue dissolved in nitric acid. Final acid concentration was 10 percent HNO_3.

Sulfur was determined by combustion analysis using a Leco induction furnace and an automatic sulfur titrator. Standards were prepared by mixing sulfur with silica at different percentages and homogenizing in a paint shaker for 1 h. Samples of 0.1 and 1.0 g were analyzed. A potassium iodate 4.444-g/l titrant solution was used for samples with high sulfur content.

Selenium and tellurium analyses were performed by G. L. Crenshaw and A. E. Hubert, respectively, both of the U.S. Geological Survey. For selenium, samples were fused with sodium carbonate and digested in nitric–phosphoric acid solution. Solution was reacted with 2,3-diaminonaphtalene, and extracted in cyclohexane. Selenium present was measured by means of a fluorimeter (Crenshaw and Lakin, 1974).

Tellurium was estimated by its catalytic action in the reduction of gold, after digesting sample with hydrobromic acid–bromine solution. Tellurium was extracted with MIBK and extracted from the ketone in distilled water. Aliquots from these solutions were added to gold chloride solution and filtered through 0.45-μm Millipore filters. Intensity of colored filter disks was compared to standards run in the same way (Hubert, 1971).

Thallium and indium analyses performed by G. L. Crenshaw consisted of digestion of the sample in hydrofluoric acid followed by solution in hydrobromic acid and bromine. Metals were extracted in MIBK and read by atomic absorption (Hubert and Lakin, 1973).

Uranium and thorium were determined by C. M. Bunker of the U.S. Geological Survey using gamma-ray spectrometry. The samples were placed on and around a sodium iodide crystal detector, and the uranium and thorium spectra were compared with those of standards measured by isotope dilution and mass or alpha spectrometry. Uranium concentrations were determined indirectly by measuring the radium daughters to obtain radium-equivalent uranium values. Because of the possibility of disequilibrium between uranium and its daughter products, these values may differ somewhat from the true uranium concentration. Thorium is also measured from daughter products but their half lives are short and disequilibrium is improbable. The value shown can be considered a direct measurement of thorium concentration.

GEOLOGY OF THE RÍO VIVÍ AREA

The geology of the Adjuntas 7½-min quadrangle, which includes the study area, was mapped and described by Mattson (1968). Bradley (1971) has described the geology of the Piedra Hueca and Cala Abajo deposits. The geochronology of volcanism, intrusion, and mineralization was studied by Barabas (1971). Cox (1972) and Cox, Larsen, and Tripp (1973) have described the mineralogy and hydrothermal alteration of the deposits.

The Río Viví area is underlain by altered basaltic lavas and tuffs of probable Cretaceous age that were intruded by the Utuado batholith at about 66 million years before present. During Eocene time, andesitic to dacitic lavas were erupted along a trough extending northwesterly across the island and underlying the south side of the Río Viví area. At the same time (about 42 m.y. B.P.), numerous small stocks of quartz diorite porphyry intruded the volcanic and batholithic rocks. These stocks locally contain disseminated chalcopyrite, and biotitic and propylitic alteration is common. Sericitic and argillic alteration are present but have not yet been noted as widespread zones around deposits. Stocks and dikes of quartz diorite, quartz diorite porphyry, and minor granodiorite and quartz monzonite locally intrude the mineralized and altered porphyries but are themselves barren and unaltered. Ages of these later intrusions are radiometrically indistinguishable from the earlier mineralized porphyries. This late Eocene volcanic and intrusive activity was the last stage of magmatism in the development of Puerto Rico. It was followed by uplift, erosion, and deposition of middle and upper Tertiary marine sediments.

GEOLOGY OF THE SAPO ALEGRE DEPOSIT

Rock types

Rock types exposed in the Sapo Alegre deposit include (1) metavolcanic rocks of probable Cretaceous age, (2) mineralized quartz diorite porphyry of Eocene age, and (3) postmineralization grandiorite, quartz monzonite, and diorite in small dikes also of Eocene age. Figures 2 and 3 show the distribution of these rock units along the canyon of the Río Viví. The northeast contact of the quartz diorite porphyry is graditional through a 25-m zone of mixed porphyry and partly assimilated blocks of volcanic hornfels. The fault-breccia zone on the southwest side probably is of large displacement relative to the size of the mineralized zone because no dikes or apophyses of mineralized porphyry have been found south of it.

Soil-geochemistry studies and diamond drilling have delimited the strike length and depth of the Sapo Alegre deposit (fig. 3). The deposit extends about 270 m northwest and 120 m southeast; it is cut off by a northeast-trending fault at the southeast. At depth, the postmineralization granodiorite dike that cuts the porphyry just northeast of the fault-breccia widens abruptly, and the mineralized zone narrows to a few metres (R. A. Bradley, oral commun., 1972).

The quartz diorite porphyry, in which the copper-molybdenum mineralization is found, is a greenish-gray rock containing zoned plagioclase (An_{35-45}) and quartz phenocrysts and clusters of chlorite or biotite after original hornblende phenocrysts. Primary biotite and potassium feldspar are apparently absent. The groundmass is aphanitic, sucrose in texture, and composed of rounded to interlocking grains of quartz, and rounded to subhedral plagioclase (An_{20-30}). The groundmass plagioclase has a dusty appearance from small inclusions and is rarely twinned.

The northeast contact of the porphyry is gradational beginning near sample interval 97, where small blocks of metavolcanic rock are enclosed in porphyry. Northeastward, these blocks become more abundant and porphyry becomes rarer. At sample intervals 102 and 106, small dikes of porphyry are found in the metavolcanic rocks. Thermal metamorphism of the metavolcanic rocks has produced a zone of amphibolitic hornfels extending 55 m outward from the northeast from the main body of quartz diorite porphyry. Outcrops southwest of the fault breccia are similarly metamorphosed, but the source of heat is probably a different intrusion lying to the south. The hornfelses are composed mainly of pale-green, weakly pleochroic amphibole and small amounts of plagioclase. Relict augite phenocrysts largely replaced by pale-green amphibole are common, as are relict plagioclase phenocrysts converted to unzoned oligoclase. Thin veinlets and small irregular patches of potassium feldspar and traces of biotite are present in the hornfels. Magnetite is abundant, and sulfides are rare to absent. To the northeast, the hornfels gives way gradationally to fine-grained porphyritic lava and breccia with strong biotitic alteration. The biotitic alteration zone extends 400 m northeast, where it passes into strong chloritic alteration containing abundant epidote.

Postmineralization dikes in the Sapo Alegre zone differ from the larger postmineralization intrusives in the district as a whole in that they are anomalously rich in primary potassium feldspar. A biotite quartz monzonite dike 0.3 to 0.6 m wide cut by a northeast-trending fault was noted southeast of the fault-breccia zone. A 4.5-m dike of biotite-hornblende granodiorite intrudes quartz diorite porphyry just northeast of the fault breccia. This dike widens to more than 30 m a short distance below the surface, as shown by diamond drilling. Black andesitic dikes 0.3 to 0.6 m thick were noted in a few places cutting sericitized porphyry and chloritized volcanic rocks.

Mineralization and hydrothermal alteration of the porphyry

Throughout the Sapo Alegre zone, the quartz diorite porphyry is hydrothermally altered and contains varying amounts of pyrite, chalcopyrite, and molybdenite. Copper values between 0.5 and 1.2 percent are mainly confined to a 20-m-wide zone of disseminated chalcopyrite along the northeast side of the porphyry body (fig. 2). Molybdenum grades of 0.07 to 0.1 percent are found in a 9-m-wide zone of abundant quartz-molybdenite-sericite veinlets just inside the porphyry contact.

Four types of hydrothermal alteration are present in the porphyry: Kaolinite-pyrite, quartz-sericite-pyrite, sericite-albite-chlorite, and biotite-chlorite. Biotite-chlorite alteration coincides closely with the copper- and molybdenum-rich zones near the contact and is found in the dikes of porphyry, which extend from the contact out into the hornfels. Biotite is very fine grained and pale brown; it commonly forms clusters replacing mafic phenocrysts but may occur as patches, veinlets, or streaks. Plagioclase is largely unaltered and zoned but may contain small amounts of sericite. Chlorite is abundant in patches and veinlets and locally may contain inner cores of relict biotite, suggesting it is an alteration product of the biotite. Pyrite to chalcopyrite ratio is low in the biotite-chlorite zone, and magnetite is present in trace amounts.

Potassium feldspar is very rare in the porphyry. Its occurrence in veinlets and patches with chlorite

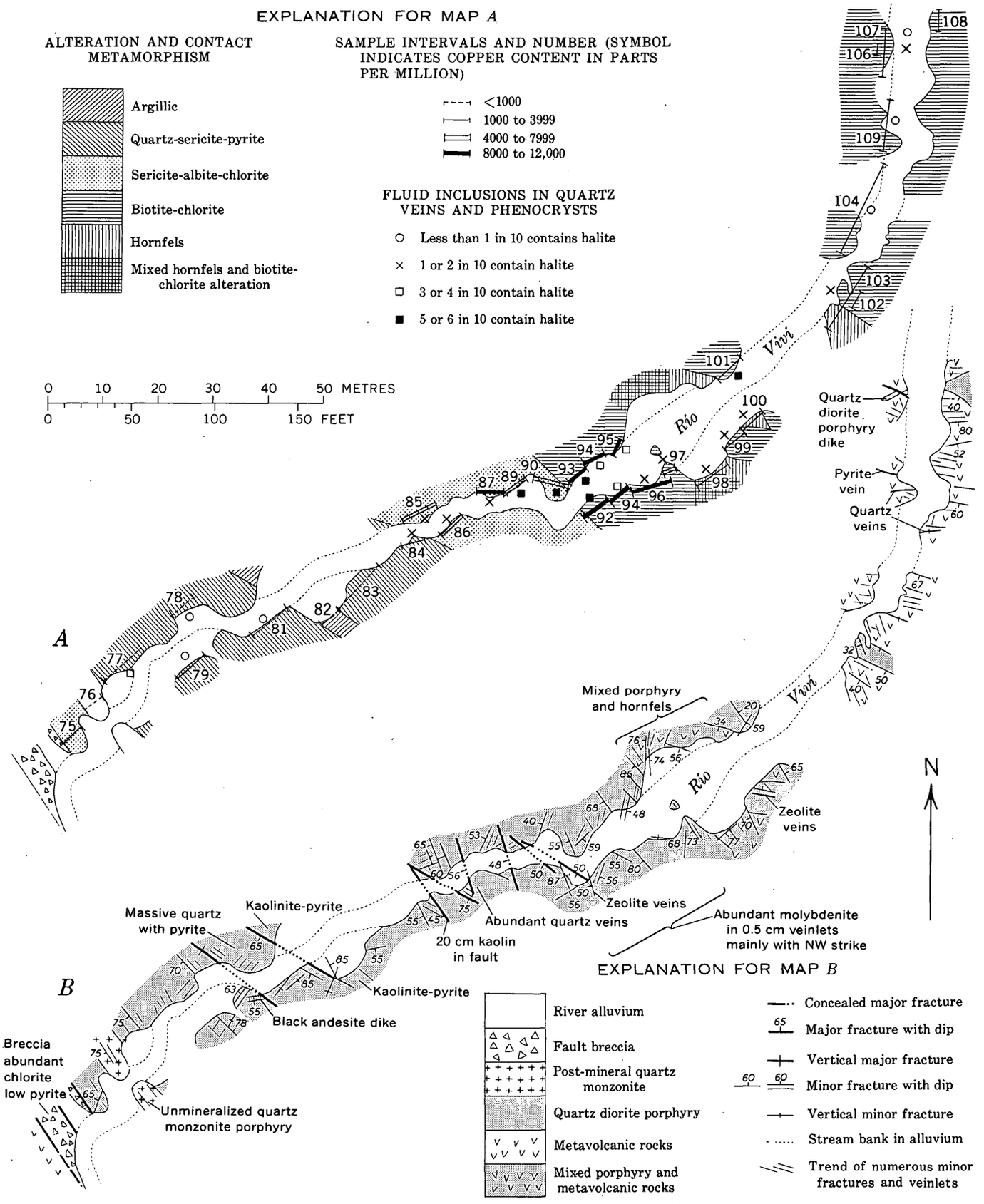

FIGURE 2.—Maps of the Sapo Alegre prospect showing geology, hydrothermal alteration, fluid-inclusion petrography, sample intervals, and copper content.

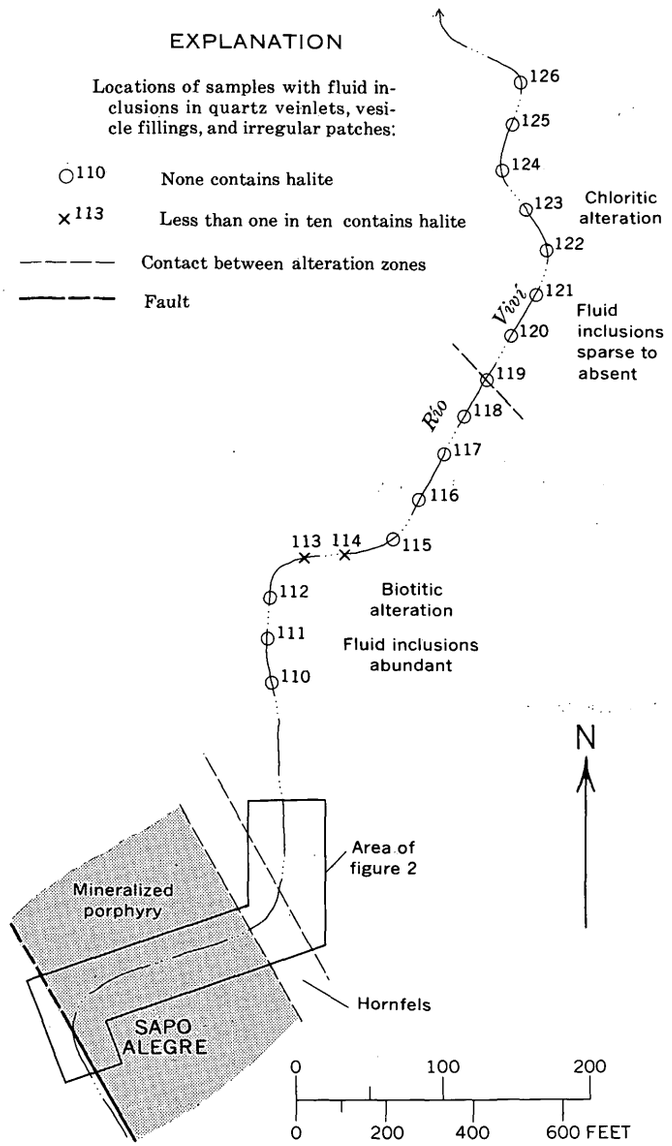

FIGURE 3.—Alteration zones, fluid-inclusion petrography, and sample locations in metavolcanic rocks north of the Sapo Alegre prospect.

may be a byproduct of the alteration of biotite to chlorite (Cox and others, 1973).

To the southwest is a zone of sericite-albite-chlorite alteration. All the biotite in this zone has been altered to chlorite, and a large part of the chlorite and plagioclase is replaced by sericite, especially along the borders of interlacing quartz veinlets. The unreplaced plagioclase is albitic. Epidote is common in veins and clusters and is everywhere partly replaced by sericite.

Farther to the southwest, quartz veins are abundant and sericitization is complete. The porphyry is composed entirely of quartz, sericite, pyrite, and sparse remnants of epidote. Quartz phenocrysts and groundmass grains are preserved, and rectangular patches of sericite mark the sites of original feldspar and hornblende phenocrysts. These textural features serve to identify this quartz-sericite-pyrite rock as the altered equivalent of quartz diorite porphyry.

Within the quartz-sericite-pyrite zone is a zone 6 m wide of intense argillic alteration composed of kaolinite and pyrite. This argillic zone and other thin kaolinite veins follow steeply dipping faults trending N. 55° W.

An outcrop of highly sheared porphyry with sericite-albite-chlorite alteration lies on the extreme southwest side of the porphyry body, between the fault-breccia zone and dike of postmineralization granodiorite. The transition from this zone to the quartz-sericite-pyrite zone to the northeast is obscured by the granodiorite intrusion.

Veinlets of leonhardite, a zeolite, with or without calcite and without hydrothermal alteration envelopes, are abundant in the copper-rich zone of the porphyry, present elsewhere in the porphyry, and generally absent in the metavolcanic rocks.

Age relations between the alteration types can be derived from detailed textural and structural features. Chlorite rims biotite, and biotitic alteration is cut by veinlets with chloritic selvages. Biotite-chlorite and sericite-albite-chlorite zones are cut by quartz-pyrite veinlets with sericite selvages. All alteration types are cut by kaolinite-pyrite and zeolite veins.

Structure

Geologic structure of the Sapo Alegre prospect is dominated by a northwest-striking fault-breccia zone containing angular fragments of metavolcanic rock in a fine chlorite-rich matrix. Pyrite is rare, and copper mineralization is absent in this breccia.

The mineralized zone is cut by abundant faults and mineralized fractures spaced a few decimetres apart. A plot of 57 fractures in the Sapo Alegre porphyry indicates a slight predominance of south-dipping fractures striking between N. 20° E. and N. 70° W. and a near absence of east-west north-dipping fractures. These orientations are in general agreement with attitudes of major and minor faults mapped by Mattson (1968) in the surrounding region. Northeast-striking fractures at Sapo Alegre offset postmineralization quartz monzonite and andesite dikes and rarely are mineralized. Northwest-striking fractures contain (1) granular quartz and sulfides, (2) pyrite, sericite, and molybdenite, (3) kaolinite and pyrite, and (4) zeolites.

A plot of 60 fractures cutting metavolcanic rocks north of the intrusion showed a nearly random arrangement of steeply dipping surfaces. Planes striking

generally east-west, which are rare in the intrusion, are abundant in the metavolcanics. These attitudes may represent planes of bedding in the volcanics. but no geologic evidence to identify bedding was found during this study. Quartz veins, quartz-pyrite veins, and zeolite veins were noted in the metavolcanics, but these did not show any preferred orientation.

Fluid-inclusion studies

Fluid inclusions of three general types are readily observed in quartz phenocrysts and quartz veinlets in spite of their small size, generally 1 to 10 μm. The most common type consists of liquid plus about 15 percent vapor; birefringent daughter minerals are small and rare. These inclusions have moderate salinity, judging from the absence of halite daughter minerals and similarity to inclusions of known composition elsewhere (Nash and Theodore, 1971). Another type is characterized by small cubic crystals of halite and commonly hematite, plus liquid and 10 to 15 percent vapor. The halite cubes occupy about 5- to 10-volume percent; hence, the salinity of these inclusions is estimated to be at least 35 percent. Inclusions containing predominant vapor are present in some samples; the gas-rich compositions suggest that they represent trapped steam. No liquid carbon dioxide was observed in any inclusion type. The small size of the inclusions precludes study on the heating stage, but estimates of likely homogenization temperature are possible from considerations of phase proportions and general compositions. Moderate-salinity inclusions have vapor fractions suggesting they would homogenize in the temperature range about 250° to 300°C for most samples. Halite-bearing inclusions probably would homogenize in the range 300° to 400°C; the higher temperature estimate is for many secondary inclusions in quartz phenocrysts, and the lower estimate is for typical halite-bearing inclusions in quartz veins.

Data for fluid-inclusion occurrence and abundance are in table 1. Inclusion population is an estimate of relative abundance in parts per ten of halite-bearing (H-type), gas-rich (G-type), and moderate-salinity (M-type) inclusions. In table 1, only H and G types are entered, and the remainder, M type, is implicit.

TABLE 1.—*Chemical and petrographic data for the Sapo Alegre quartz diorite porphyry*

[In percent for Fe, S, K_2O, and Na_2O and in parts per million for other data except where noted in boxheads. N.d., not determined; N, not detected; L, detected at lowest levels of sensitivity: Mo and Ni, 5 ppm; Ag, 0.5 ppm; Te, 0.05 ppm; and Au, 0.02 ppm]

Sample	Cu	Fe	S	Mo	Au	Ag	Se	Te	Mn	Ni	Zn	K_2O	Na_2O	Halite-bearing (H) and gas-rich (G) fluid inclusions in parts per ten of the inclusion population		Inclusion abundance	Pyrite-chalcopyrite ratio	
														In veins	In phenocrysts		Polished section	Calculated
Kaolinite-pyrite																		
82	---	190	6.2	4.5	15	L	N	4.5	0.34	150	L	12	1.8	0.3	N.d.	N.d.	N.d.	N.d.	124.0
Quartz-sericite-pyrite alteration																		
77	---	110	3.3	5.9	L	L	N	2.5	L	50	L	L	2.2	0.3	0	3H, 1G	Sparse	High	282.0
78	---	360	5.4	4.3	L	L	N	4.6	L	150	L	10	2.0	.4	0	0	---do	33.0	625.0
79	---	1,200	6.8	5.5	7	L	0.7	5.5	0.05	150	5	8	2.1	.4	0	N.d.	---do	1.1	23.7
81	---	490	5.7	5.0	20	L	N	5.0	.05	70	L	8	1.1	.3	<1	N.d.	Moderate	67.0	52.8
83	---	680	4.9	2.7	L	L	.7	2.7	L	70	L	8	1.9	.6	N.d.	N.d.	N.d.	High	20.6
Sericite-albite-chlorite alteration																		
75	---	1,700	6.0	3.5	30	L	1.0	6.2	0.20	200	15	15	1.4	1.2	N.d.	N.d.	N.d.	N.d.	12.7
84	---	2,700	3.0	2.3	30	L	.7	5.0	.25	100	7	13	2.8	.3	<1H	1H, <1G	Moderate	0.75	3.97
85	---	4,300	2.5	1.5	150	0.09	1.5	5.0	.25	200	30	18	2.5	1.8	N.d.	2H, 2G	Moderate to high.	.80	1.26
86	---	6,200	2.4	1.6	150	.12	1.0	5.5	.25	100	30	26	2.6	1.4	N.d.	1H	Moderate	.40	.86
87	---	10,000	3.0	1.9	200	.09	1.5	4.7	.05	150	20	7	2.5	.8	N.d.	1H	Moderate to high.	2.7	.46
89	---	4,300	4.0	1.6	150	.07	3.0	7.0	.40	70	5	14	3.3	.4	2H	6H, 1G	High	1.2	1.38
90	---	6,900	2.4	1.5	150	.14	1.5	4.5	.25	150	30	21	1.9	1.9	N.d.	5H, 2G	---do	.89	.59
Biotite-chlorite alteration ("ore" zone)																		
92	---	8,100	2.3	1.9	1000	0.15	2.0	6.0	0.25	300	30	31	1.2	2.1	5H	4H	High	.17	.71
93	---	9,000	3.0	3.3	700	.11	3.0	6.0	.60	700	30	47	1.9	2.1	N.d.	5H, 2G	---do	.34	1.40
94	---	12,000	3.5	2.5	700	.21	7.0	8.0	.66	700	70	50	1.9	2.7	N.d.	4H	---do	.30	.56
95	---	8,800	4.3	4.1	1000	.16	3.0	7.5	.40	300	50	41	1.2	1.4	4H, 4G	4H, 2G	---do	.33	1.92
96	---	10,000	2.9	1.7	300	.20	3.0	5.5	.46	300	70	46	1.4	2.4	2H	N.d.	---do	.16	.35
Dikes in metavolcanic rocks																		
101	---	1,100	4.0	0.6	5	L	0.5	1.0	0.20	1,500	15	46	1.0	2.7	5H, 2G	N.d.	Very sparse	1.32	2.34
102	---	1,100	7.3	.5	5	L	.5	.3	.20	1,000	70	87	3.1	3.0	N.d.	1H	Moderate	1.61	2.06
106	---	1,400	3.7	2.0	7	L	.7	3.5	.05	700	7	61	1.9	2.7	N.d.	1H, 1G	---do	5.26	7.16

The population estimates are based on inclusions of all ages. Inclusion abundance, an estimate of the relative total abundance of all fluid inclusions, is a descriptive parameter because considerable variation is noted which appears to correlate with factors such as intensity of fracturing and degree of alteration.

Several generalizations can be made from the fluid-inclusion observations (table 1 and fig. 2). Secondary halite-bearing and gas-rich inclusions are relatively abundant in quartz phenocrysts of the quartz diorite porphyry. The occurrence of these inclusions is interpreted to mean that the porphyry generated a boiling, highly saline brine having a temperature of 300° to 400°C. Many quartz veins in the porphyry contain similar fluid inclusions, indicating that the hot brine circulated in the consolidated porphyry. Halite-bearing and gas-rich inclusions are less abundant in quartz veins in metavolcanic host rocks to the north; moderate-salinity fluids, probably of somewhat lower temperature, appear to have been predominant in the wallrocks. Correlations with hydrothermal alteration include the following: The quartz-sericite-pyrite alteration zone contains generally small numbers of halite-bearing inclusions, particularly in quartz veins with sericitic envelopes; hence, this alteration is believed to have been produced by moderate-salinity fluids. Rocks of the sericite-albite-chlorite zone contain relatively more halite-bearing inclusions, but paragenetic control is not sufficient to specify whether high- or moderate-salinity fluids produced all or part of the alteration. The biotite-chlorite zone of alteration within the porphyry, which contains the highest grade of copper and molybdenum, is characterized by abundant halite-bearing inclusions; high-salinity fluids are believed to have caused this alteration and metallization. The hornfels zone of the intruded wallrocks is not well understood on the basis of only two thin sections; moderate-salinity fluids appear to have prevailed. Altered wallrocks to the north generally contain small numbers of halite-bearing inclusions, and rocks in the chlorite zone north of location 119 contain no halite-bearing inclusions, so the high-salinity brine probably did not extend this far.

Samples collected by R. E. Learned from the Sapo Alegre zone exposed in a road cut to the northwest of the river exposure were examined for fluid-inclusion content of quartz grains. Although the samples were completely oxidized and friable, fluid-inclusion abundance and halite content were found to be the same as in the unweathered samples. If halite-bearing inclusions are everywhere associated with porphyry copper mineralization as they are at Sapo Alegre and at other deposits (Roeder, 1971; and Nash, 1971), then fluid-inclusion content of quartz grains in soils might prove to be a useful guide to copper ore, especially when used in conjunction with geochemical sampling and analysis.

Geochemistry and mineralization of the quartz diorite porphyry

In the biotite-chlorite zone, copper, molybdenum, gold, and silver all show at least a tenfold increase in concentration compared with their concentration in quartz diorite porphyry dikes in the metavolcanic rocks (see table 1). Sulfur, selenium, and tellurium (fig. 4) also show an increase but not as great a one. Iron, manganese, nickel, and zinc do not show any increase. Other metals, not shown in the table, likewise show no increase in concentration. They are lead (<2–14 ppm), cobalt (<5–30 ppm), and mercury (<0.03–8 ppm).

K_2O and Na_2O are shown for each porphyry sample in table 1 and data for K_2O, Na_2O, CaO, and MgO are summarized in table 2. These values are roughly the same in the biotite-chlorite alteration zone as in the porphyry dikes and the postmineralization quartz monzonite, although the latter is relatively deficient in magnesia. The porphyry dikes and the postmineralization quartz monzonite are distinctly higher in K_2O and deficient in Na_2O, CaO, and MgO compared to eight quartz diorite samples analyzed by Chen (1969) and presumed from their map location to be Eocene in age. K_2O content of the biotite-chlorite zone in the porphyry is low relative to that of the other rocks in the area, reflecting the predominence of chlorite over biotite in that mineral assemblage.

In distinct contrast, samples from the quartz-sericite-pyrite zone show a marked decrease in copper, tellurium, manganese, nickel, and zinc and a virtual absence of molybdenum, gold, and silver. Mercury, cobalt, and lead do not change in this zone. Iron, sulfur, and selenium content of the quartz-sercite-pyrite zone is much larger than that of the porphyry dikes but is roughly the same as that of the biotite-chlorite alteration zone. Samples from the quartz-sericite-pyrite zone are depeleted in Na_2O, CaO, and MgO, but K_2O remains about the same as in the porphyry dikes and biotite-chlorite alteration zone (see table 2). An apparent increase in FeO in this zone may be the result of depletion of other elements rather than of introduction of iron.

Rocks from the sericite-albite-chlorite zone appear to be intermediate chemically between the biotite-chlorite and quartz-sericite-pyrite zones.

Pyrite to chalcopyrite ratios shown in table 1 are low in the copper-rich, biotite-chlorite alteration zone and

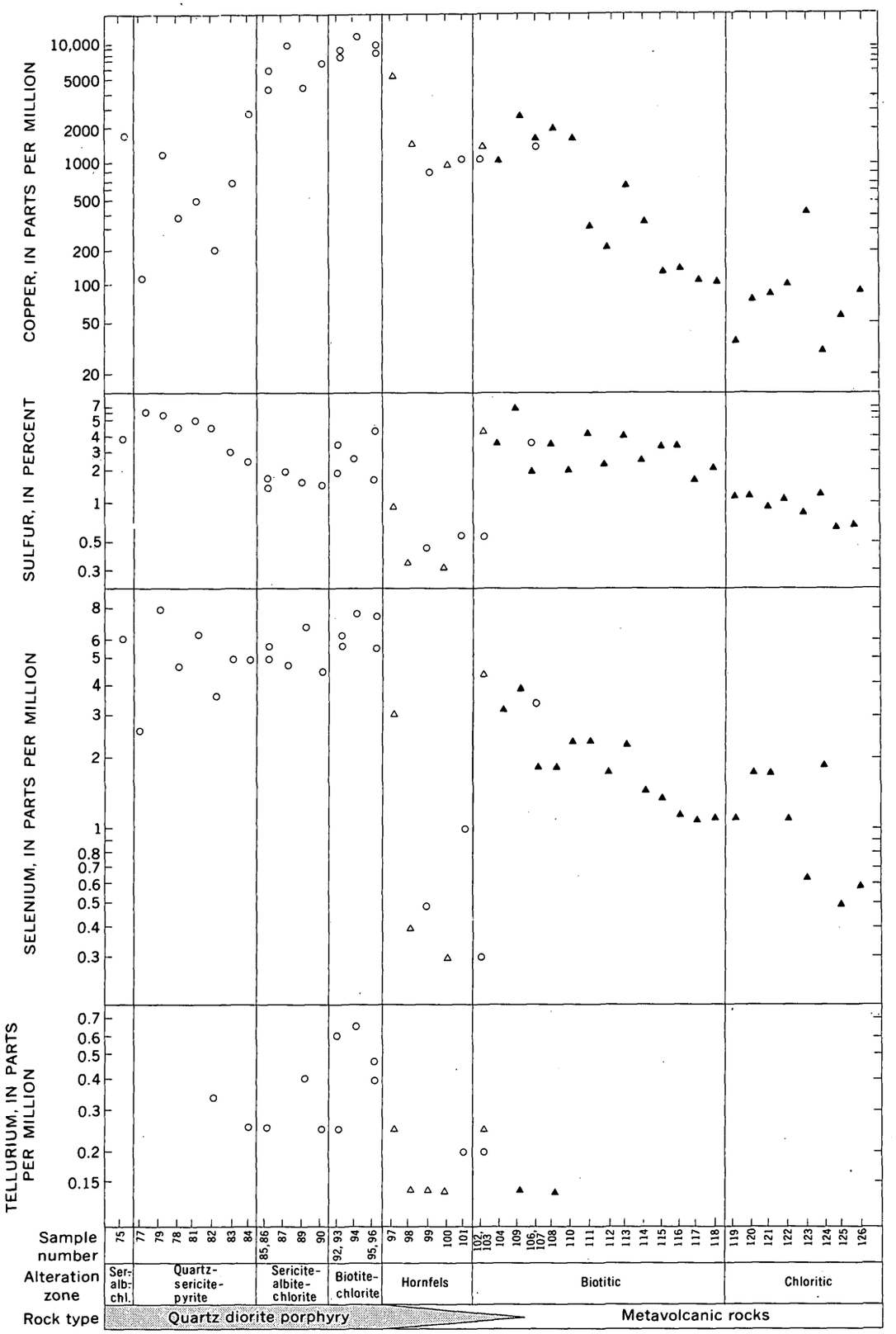

FIGURE 4.—Distribution of copper, selenium, and tellurium (in parts per million) and sulfur (in percent) along a traverse across the Sapo Alegre porphyry and metavolcanic host rocks. Sample points along the abscissa are not plotted to scale; see figures 2 and 3 for location. Open circles indicate samples of porphyry; open triangles, mixed porphyry and metavolcanics; and solid triangles, metavolcanic rocks. Missing values are below limit of detectability.

TABLE 2.—*Chemical data for the Sapo Alegre porphyry and other quartz diorites*

[In weight percent. FeO, total iron]

Geology	Number of samples	K_2O	Na_2O	CaO	MgO	FeO
Quartz-sericite-pyrite zone.	6	2.0	0.4	0.3	0.5	6.2
Kaolinite-pyrite zone	1	1.8	.3	.1	.9	7.9
Sericite-albite-chlorite zone.	6	2.4	1.2	1.3	1.2	4.3
Biotite-chlorite zone	5	1.5	2.1	2.4	1.6	4.1
Dikes of porphyry in amphibolite.	3	2.0	2.8	3.8	1.8	4.5
Postmineralization quartz monzonite (sample 76).	1	2.2	2.7	1.7	.7	3.8
Eocene quartz diorite (Chen, 1969).	6	1.0	3.6	5.7	1.6	4.2

very high in the quartz-sericite-pyrite zone. Two sets of ratios are shown, one estimated from a single polished section, selected from each sample, and one calculated from the copper and sulfur analyses of the bulk sample.[1] As expected, large discrepancies exist between these estimates due, in part, to sampling error. The pyrite to chalcopyrite ratio of the bulk sample, however, is higher than that of the single polished section in more than 80 percent of the samples, suggesting that pyrite may be relatively more abundant as fracture fillings than is chalcopyrite. Rocks chosen for polishing are generally bounded by fractures but not cut by them. Thus, the polished-section ratio is more representative of the disseminated pyrite and chalcopyrite between fractures.

Molybdenite was rarely found in the polished sections suggesting that this mineral, like pyrite, may have formed preferentially in fractures rather than disseminations.

A plot of gold and copper values (fig. 5) shows that most samples fall along a line in which gold is consistently about 2×10^{-5} of the copper content. This suggests that gold was deposited with chalcopyrite and may be contained in that mineral. In samples 87 and 93, finely divided secondary chalcocite along fractures is noticeably more abundant than in other samples. Thus, secondary enrichment is presumed to account for their high copper to gold ratio.

Gold also occurs in quartz-pyrite veinlets having low copper and molybdenum content. These veinlets cut the metavolcanics at sample locality 103, and their relation to the main copper mineralization is not known.

[1] The mass ratio is calculated by assuming that all copper is in chalcopyrite and all sulfur is in pyrite and chalcopyrite and using the formula $\frac{1.87 \times \text{ppm sulfur} - 1.89 \times \text{ppm copper}}{2.89 \times \text{ppm copper}}$. This is then multiplied by 0.815 to obtain the volume ratio.

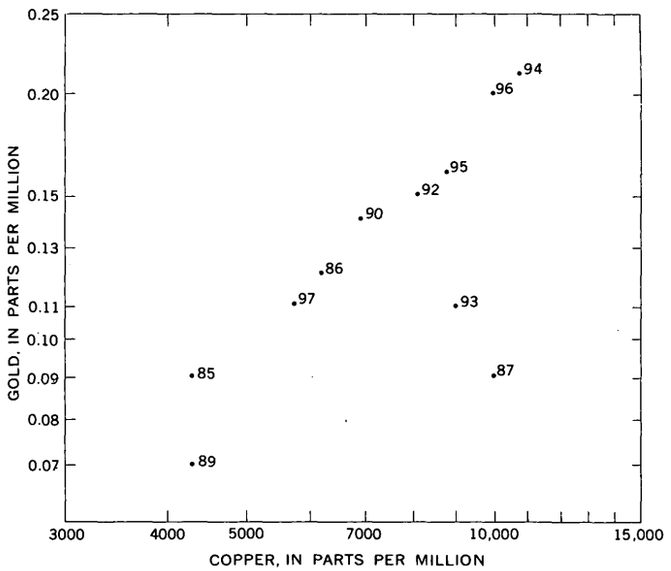

FIGURE 5.—Correlation of copper and gold values, Sapo Alegre prospect. Numbers refer to samples; see figure 2 for locations.

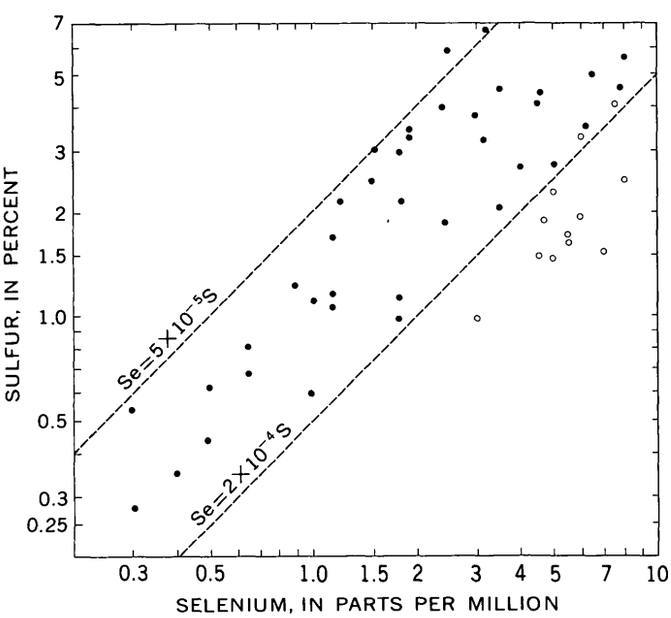

FIGURE 6.—Correlation of sulfur and selenium values, Sapo Alegre prospect. Samples containing more than 2,000 ppm copper, 150 ppm molybdenum, and 0.05 ppm gold are shown by open circles.

Figure 6 shows the relationship between selenium and sulfur values. Most of the samples fall in a zone on the graph in which selenium is between 5×10^{-5} and 2×10^{-4} of the sulfur content. The 10 samples falling outside of this zone and containing relatively higher selenium-sulfur ratios all contain high values of copper, molybdenum, and gold.

Geochemistry of the metavolcanic wallrocks

The distribution of elements and oxides through the mineralized porphyry and the 400 m of metavolcanic rocks sampled north of the porphyry is shown graphically as follows: Copper, sulfur, and selenium in figure 4; K_2O, Na_2O, uranium, and thorium in figure 7; and zinc, manganese, and thallium in figure 8. Sample numbers on the horizontal axis are the same as those shown in the maps (figs. 2 and 3). Samples 97 through 104 and 107 through 109 lie within 80 m of the porphyry contact. Between samples 108 and 110, rock exposures are absent in the stream valley. The aforementioned change from predominantly biotitic to chloritic alteration takes place gradationally between sample points 118 and 120.

Copper values (fig. 4) decrease abruptly at the porphyry contact from greater than 8,000 ppm to about 1,000 ppm. Another abrupt decrease takes place in the sample gap between 108 and 110, and values continue to decline irregularly. Sulfur decreases abruptly from a few percent in the ore zone to a few tenths of a percent in the magnetite-bearing hornfels zone near the porphyry contact. Sulfur increases again in the biotite zone with the appearance of pyrite and then decreases more or less continuously outward to about the 1-percent level in the chlorite zone. Selenium closely follows sulfur.

K_2O values (fig. 7) show a wide scatter and a barely perceptible decrease away from the porphyry. Na_2O shows a slight increase in the same direction. Uranium is distributed in a broad curve with low values in the quartz-sericite-pyrite zone of the porphyry and in the chloritic zone of the metavolcanics. Higher values (1.0–1.6 ppm) are in porphyry dikes cutting biotitic zone metavolcanics. Uranium content of the post-mineralization quartz monzonite was slightly more than 3 ppm.

Thorium shows a tenfold increase in the porphyry and hornfels compared to the biotitic and chloritic zone in the metavolcanics. Highest thorium values are in the argillic zone (28 ppm) and in the copper-rich zone (6–10 ppm) of the porphyry. The latter distribution may be partly dependent on the abundance of zeolite veinlets in the copper-rich zone. Samples of zeolite vein material were found to contain 16 ppm thorium. Zeolite-rich samples also contain 50 to 150 ppm lanthanum.

Zinc (fig. 8) shows a slight increase in the chlorite zone at a distance of about 350 m from the porphyry contact. Manganese (also shown in fig. 8) shows a similar increase from about 1,000 to 2,400 ppm at the same point along the traverse. This is in good agreement with the results of a soil geochemical survey published by Learned and Boissen (1973, p. 99–101) and summarized in figure 1. In that study, a zone of zinc, manganese, and lead enrichment in soils was found partly surrounding the Piedra Hueca and Cala Abajo deposit. The zone lies 200 to 400 m out from the contacts of the mineralized porphyries and, in several places, high (200 ppm) zinc values were found along the inner boundary of the zone. Our data support Learned's conclusion that the zinc and manganese distribution in the soils reflects a primary, hydrothermal zoning.

Thallium is most abundant (0.4–1.2 ppm) in the zone of biotitic alteration in the metavolcanics, but was not detected in the biotite-chlorite zone of the porphyry. Distribution of thallium may be dependent in part on the presence of biotite and in part on the temperature conditions in and near the intrusion and center of hydrothermal activity. More data are needed to verify that the thallium distribution is a product of hydrothermal zoning.

Indium near the limit of detectability (0.2 ppm) was noted in four samples distributed across the porphyry and metavolcanic sequence.

DISCUSSION

Conclusions to be drawn from this study are limited in their breadth by two factors: First, only rocks along a single stream traverse were mapped and sampled; and second, the traverse represents only one-half of a porphyry system, the southern part having been removed by faulting. The general coherence, however, of independently collected mineralogic, chemical, and fluid-inclusion data makes it possible to characterize at least two distinct zones within the mineralized porphyry and three zones in the metavolcanic host rock outward from the porphyry contact.

The biotite-chlorite zone in the porphyry near its contact contains stable plagioclase, secondary biotite, and chlorite after hornblende, and is characterized by high copper, molybdenum, gold, silver, and low pyrite to chalcopyrite ratio. Fluid inclusions indicate that a boiling, high-salinity brine was the predominant hydrothermal fluid in this zone. On the basis of estimated homogenization temperatures and general compositions of halite-bearing inclusions and on the interpretation that they coexisted with gas-rich inclusions, temperatures of 300° to 400°C and pressures of 100 to 150 bars are probable for this zone. This would correspond to a 1.5-km depth in a hydrostatic system.

Within the porphyry a quartz-sericite-pyrite zone is separated from the biotite-chlorite zone by an intermediate sericite-albite-chlorite zone. These zones appear to represent progressive chloritization of biotite

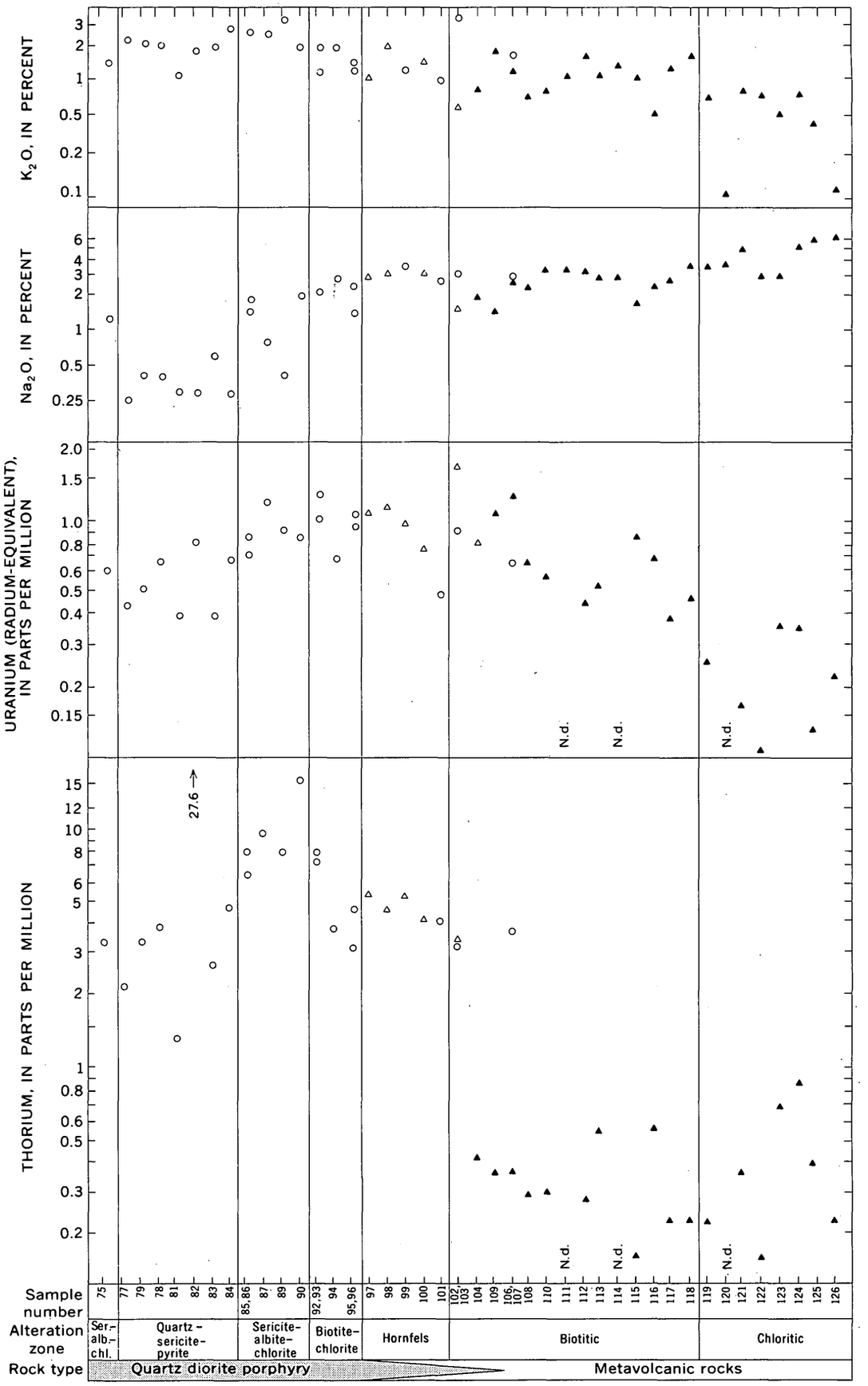
K_2O, IN PERCENT
Na_2O, IN PERCENT
URANIUM (RADIUM-EQUIVALENT), IN PARTS PER MILLION
THORIUM, IN PARTS PER MILLION
27.6
N.d.
Sample number
Alteration zone
Rock type
Ser.-alb.-chl.
Quartz-sericite-pyrite
Sericite-albite-chlorite
Biotite-chlorite
Hornfels
Biotitic
Chloritic
Quartz diorite porphyry
Metavolcanic rocks

and breakdown of plagioclase to albite and epidote and subsequent sericitization of the whole rock.

The quartz-sericite-pyrite zone is characterized by abundant sulfur, iron, and K_2O, and very low content of copper, gold, silver, zinc, lead, nickel, cobalt, Na_2O, CaO, and MgO. These data suggest that metals have been leached from the porphyry during sericitization in a manner strikingly similar to that described by Fountain (1972, p. 1058-1061) for the Panguna deposit, Bougainville Island, New Guinea. Fluid inclusions indicate that a low-salinity brine was the predominant hydrothermal fluid in the quartz-sericite-pyrite zone and that temperatures were near 250° to 300°C. There is no record of halite-bearing inclusions in the quartz-sericite-pyrite zone nor is there reason to suspect that they have been destroyed in these rocks. Hence it is concluded that high-salinity fluids were not present there.

Thus structural and mineralogical relations, on the one hand, indicate that sericitic alteration is superimposed on biotitic alteration. Fluid inclusion data, on the other hand, suggest that quartz-sericite alteration was not superimposed on a widespread biotite-chlorite alteration and that the two processes may have taken place independently. This apparent contradiction of evidence suggests that there is still much to be learned about the behavior of hydrothermal fluids in porphyries and (or) that the situation at Sapo Alegre cannot be fully understood by means of a single traverse across the prospect. It is possible, for example, that the quartz-sericite-pyrite zone is superimposed on a younger intrusion whose contact with the copper-rich porphyry is obscured by quartz veins and alteration.

Within the metavolcanic rocks northeast of the prospect, zones of amphibolitic hornfels, biotitic alteration, and chloritic alteration are arranged zonally outward from the mineralized porphyry. Outward across these three zones, copper, sulfur, selenium, K_2O, and uranium decrease, and Na_2O shows a barely perceptible increase. Sulfur and selenium contents are very low in the hornfels zone presumably because magnetite rather than pyrite was stable and insufficient copper was present to fix more than a small amount of sulfur. Zinc and manganese increase abruptly near the transition from biotitic to chloritic alteration and thallium appears to have affinities for the biotitic zone. Fluid inclusions in quartz veinlets in the metavolcanics suggest that small amounts of high-salinity brine may have circulated in the biotite zone of the metavolcanic rocks but not in the chlorite zone.

The fluid inclusions and alteration observed at Sapo Alegre are similar in many aspects to continual porphyry copper deposits of southwestern United States. In particular, the coincidence of highest copper and molybdenum values with potassic-biotitic alteration and high-salinity fluid inclusions is a recurring feature (Lowell and Guilbert, 1970; Nash, 1971; Moore and Nash, 1974; and others). Comparison of these fluid was involved. At Bingham, Utah, San Manuel, suggests that hydrothermal fluids at Sapo Alegre were different in two respects: temperatures were considerably lower than in many continental occurrences, and a greater proportion of moderate-salinity fluid was involved. At Bingham, Utah, San Manuel, Ariz., and several other deposits, temperatures in excess of 500°C were common during copper mineralization (Roedder, 1971; Moore and Nash, 1974; J. D. Davis, written commun., 1973), but there is no evidence for such temperatures at Sapo Alegre. Further, although the full original extent of the Sapo Alegre porphyry is not known, it seems clear that the very saline fluids circulated over a much smaller volume than in the deposits previously mentioned. Deposits at Bagdad and Mineral Park, Ariz. (Nash and Cunningham, 1974), possibly typify a different porphyry system which was considerably cooler (300–400°C) and dominated by moderate-salinity fluids, and which was possibly similar to that at Sapo Alegre. The pressure regime in all these deposits is a unifying element as all appear to have formed under less than 3.2 km of cover. The example at Sapo Alegre, although not economic, serves to remind us that a small intrusive body can generate saline fluids, metals, and sulfur, and set into motion a hydrothermal system in the porphyry and wallrocks that is characteristic of porphyry-type deposits.

Application of results to exploration

Results of this study bear to some extent on the problems of porphyry copper exploration. We have demonstrated that the halite content of fluid inclusions in quartz correlates directly with copper content of the rock and that these inclusions are probably unaffected during weathering and formation of soils. We suggest that, as a simple addition to soil-geochemical exploration programs, study of fluid inclusions in residual quartz grains might be of value. This is particularly true in tropical environments where intense leaching may remove most of the copper from the soils above an ore body (Learned and Boissen, 1973).

FIGURE 7.—Distribution of K_2O, Na_2O (in percent), and radium-equivalent uranium and thorium (in parts per million). Symbols and arrangement of samples same as for figure 4. N.d. indicates values not determined.

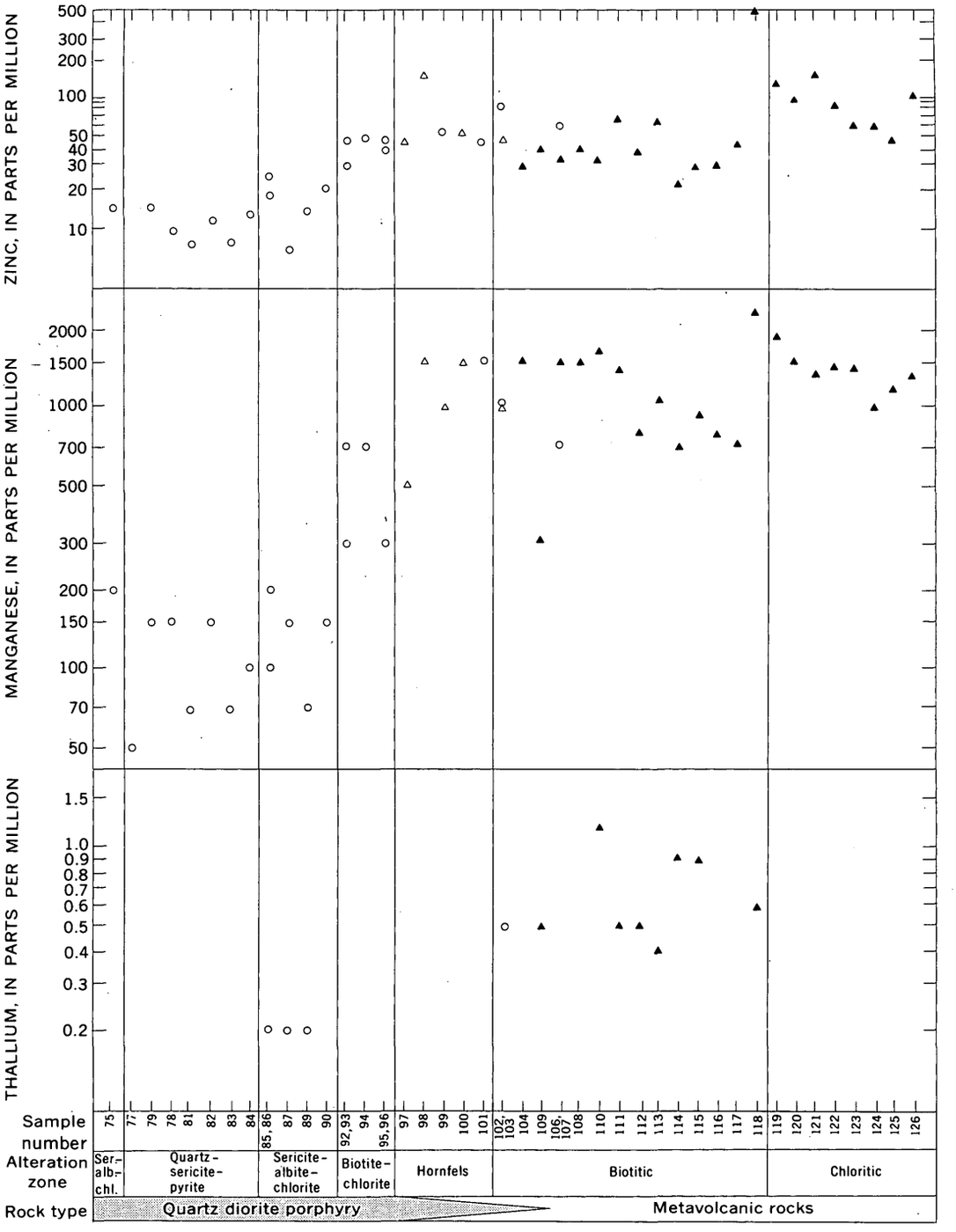

FIGURE 8.—Distribution of zinc, manganese, and thallium (in parts per million). Symbols and arrangement of samples same as for figure 4. Missing values are below limit of detectability. Spectrographic data for manganese are shown for samples 75 through 109. Atomic absorption data are shown for samples 110 through 126.

Secondly, we have shown that the zinc and manganese halo described by Learned and Boissen in soils surrounding Piedra Hueca and Cala Abajo can be detected in bedrock samples. This halo probably corresponds to the inner boundary of the chloritic alteration zone in metavolcanic rocks. Thallium may also be distributed in a halo of smaller diameter corresponding to the biotitic alteration zone.

REFERENCES CITED

Barabas, A. H., 1971 K-Ar dating of igneous events and porphyry copper mineralization in west central Puerto Rico [abs.]: Econ. Geology, v. 66, no. 6, p. 977.

Bradley, R. A., 1971, The geology of the Rio Vivi porphyry copper deposits, Puerto Rico [abs.]: Econ. Geology, v. 66, no. 6, p. 977.

Chen, Ju-Chin, 1969, Petrological and chemical studies of the Utuado Pluton, Puerto Rico: Acta Geol. Taiwanica, no. 13, p. 21–41.

Cox, D. P., 1972, Puerto Rican porphyry copper deposits, petrology and alteration [abs.], *in* Petzall, Cecily, ed., Caribbean Geol. Conf., 6th, Isla de Margarita, Venezuela, 1971, Trans.: p. 139–140.

Cox, D. P., Larsen, R. R., and Tripp, R. B., 1973, Hydrothermal alteration in Puerto Rican porphyry copper deposits: Econ. Geology, v. 68, no. 8, p. 1329–1334.

Crenshaw, G. L., and Lakin, H. W., 1974, A sensitive and rapid method for the determination of trace amounts of selenium in geologic materials: U.S. Geol. Survey Jour. Research, v. 2, no. 4, p. 483–487.

Fountain, R. J., 1972, Geological relationships in the Panguna porphyry copper district, Bougainville Island, New Guinea: Econ. Geology, v. 67, no. 8, p. 1049–1064.

Grimes, D. J., and Marranzino, A. P., 1968, Direct-current arc and alternating-current spark emission spectrographic field methods for the semiquantitative analysis of geologic materials: U.S. Geol. Survey Circ. 591, 6p.

Hubert, A. E., 1971, Determination of tellurium in geologic materials in the parts-per-billion range: U.S. Geol. Survey Prof. Paper 750–B, p. B188–B190.

Hubert, A. E. and Lakin H. W., 1973, Atomic absorption determination of thallium and indium in geologic materials, *in* Jones, M. J., ed., Geochemical Exploration, 1972: Internat. Geochem. Explor. Symposium, 4th, London, England, 1972, Proc., p. 383–387.

Learned, R. E., Boissen, Rafael, 1973, Gold—a useful pathfinder element in the search for porphyry copper deposits in Puerto Rico, *in* Jones, M. J., ed., Geochemical Exploration, 1972: Internat. Geochem. Explor. Symposium, 4th, London, England, 1972, Proc., p. 93–103.

Lowell, J. D., and Guilbert, J. M., 1970, Lateral and vertical alteration-mineralization zoning in porphyry ore deposits: Econ. Geology, v. 65, no. 4, p. 373–408.

Mattson, P. H., 1968, Geologic map of the Adjuntas quadrangle, Puerto Rico: U.S. Geol. Survey Misc. Inv. Map I–519.

Moore, W. J., and Nash, J. T., 1974, Petrologic and fluid inclusion studies of the porphyry copper ore body at Bingham Canyon, Utah: Econ. Geology, v. 69, no. 5, p. 631–645.

Nash, J. T., 1971, Fluid inclusions as a guide to porphyry-type mineralization [abs.]: Econ. Geology, v. 66, no. 8, p. 1268.

Nash, J. T., and Cunningham, C. G., Jr., 1974, Fluid-inclusion studies of the porphyry copper deposits at Bagdad, Arizona: U.S. Geol. Survey Jour. Research, v. 2, no. 1, p. 31–34.

Nash, J. T., and Theodore, T. G., 1971, Ore fluids in the porphyry copper deposit at Copper Canyon, Nevada: Econ. Geology, v. 66, no. 3, p. 385–399.

Roedder, Edwin, 1971, Fluid inclusion studies on the porphyry-type ore deposits at Bingham, Utah, Butte, Montana, and Climax, Colorado: Econ. Geol. v. 66, no. 1, p. 98–120.

Thompson, C. E., Nakagawa, H. M., and VanSickle, G. H., 1968, Rapid analysis for gold in geologic materials: U.S. Geol. Survey Prof. Paper 600–B, p. B130–B132.

Ward, F. N., Nakagawa, H. M., Harms, T. F., and VanSickle, G. H., 1969, Atomic-absorption methods of analysis useful in geochemical exploration: U.S. Geol. Survey Bull. 1289, 45 p.

Jour. Research U.S. Geol. Survey
Vol. 3, No. 3, May–June 1975, p. 329–335

WIDESPREAD LATE GLACIAL AND POSTGLACIAL TEPHRA DEPOSITS FROM MOUNT ST. HELENS VOLCANO, WASHINGTON

By DONAL R. MULLINEAUX, JACK H. HYDE, and MEYER RUBIN,
Denver, Colo., Tacoma, Wash., Reston, Va.

Abstract.—Pumice layers composing four different groups of tephra beds (termed "sets"), whose stratigraphy, age, and trend away from Mount St. Helens are fairly well known, are potentially valuable stratigraphic markers in the northwestern United States and adjacent parts of Canada. All four tephra sets are less than about 18,000 yr old. The oldest set described (set S) is between about 18,000 and 12,000 yr old; the most extensive pumice layers of the set, however, probably are no more than about 13,000 yr old. Relatively voluminous layers in the next younger tephra unit (set J) probably range from slightly less than 12,000 to slightly more than 8,000 yr old; in the overlying set Y, the most extensive layers range from about 4,000 to 3,400 yr old. The largest tephra layers in the youngest tephra set described, set W, are apparently all about 450 yr old. All the extensive tephra deposits were carried chiefly east of Mount St. Helens, and the bulk of them form an arc which extends from north-northeast of the volcano clockwise around to the southeast.

Mount St. Helens, in southern Washington (fig. 1), has been an intermittent but prolific source of pyroclastic airfall deposits, called tephra, for more than 35,000 yr. The sequence of many tephra layers, which is being studied as part of an appraisal of volcanic hazards at Mount St. Helens, provides an excellent record of explosive eruptive activity. Some of these deposits are also useful marker beds for stratigraphic correlation and dating because they are distinctive and widespread. One pumice deposit erupted by Mount St. Helens, for example, has been identified in Mount Rainier National Park (Crandell and others, 1962) and in western Canada near Kamloops and Edmonton (Fulton and Armstrong, 1965; Westgate and others, 1970). The thicknesses and distribution of several other pumice deposits near Mount St. Helens suggest that they are similarly widespread and could serve as valuable marker beds in the northwestern United States and adjacent parts of Canada.

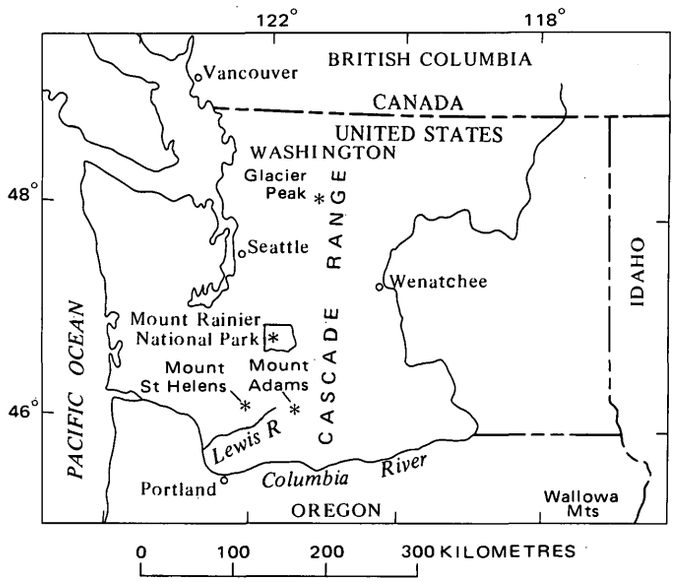

FIGURE 1.—Location of Mount St. Helens, southern Washington.

The content of ferromagnesian minerals in pumice erupted by Mount St. Helens has changed significantly from one eruptive episode to another on several occasions (table 1). As a result the layers can be grouped into several sets, each of which has a characteristic suite of Fe-Mg phenocrysts (Mullineaux and others, 1972). Each of these sets except the youngest contains more than one layer of tephra. A few layers are distinctive enough to be recognized individually and traced from one outcrop to another, but most layers are identifiable only as a part of a certain set. A single

TABLE 1.—*Age and* Fe-Mg *phenocryst content of tephra sets*

Set	Approximate ages [1] (radiocarbon years)	Fe-Mg phenocrysts	
		Predominant	Subordinant
T	150	Hypersthene, hornblende.	Augite.
W	1,150–450	----do----------	None.
B	2,500–1,600	Olivine, augite, hypersthene.	Do.
P	3,000–2,500	Hypersthene, hornblende.	Do.
Y	4,000–3,000	Cummingtonite, hornblende.	Biotite (in layer Yb).
J	<12,000, >8,000	Hypersthene, hornblende.	None.
S	<18,000, >12,000	Cummingtonite, hornblende.	Hypersthene.
Unnamed	37,600–18,000	Cummingtonite, hornblende, biotite.	Do.

[1] Years before 1950. Age of pumice here called set T determined from tree-ring counts by Lawrence (1954). Younger date for set W determined from tree-ring counts by Crandell (1971). All other dates are in radiocarbon years.

letter, such as Y, has been assigned to each set as a whole. Tephra layers that can be individually recognized and traced for some distance are further designated by adding a second letter—for example, layer Yn.

Selection of the letters used has no significance other than convenience. When the sets are arranged according to age, for example, the sequence of letters does not follow an alphabetical or other ordered sequence. The system we use arose during study of tephra in Mount Rainier National Park, where names for important marker beds were needed long before the tephra study was complete. The tephra layers recognized early in that study were known to be only a fraction of the total number of layers present, and no orderly sequence for all the tephra deposits could be established at that time. Instead, letters were assigned arbitrarily as needed, commonly from some word used in field descriptions. Thus, the letter Y was used for a yellow pumice, and W for a white one. Similarly, the second letter assigned to a distinctive layer within a set may be taken arbitrarily from field descriptions—for instance, layer Yn is a pumice bed in set Y that extends generally northeast of the volcano.

This report presents preliminary data on the stratigraphy, distribution, and age of four tephra sets, namely, sets S, J, Y, and W, which are expected to form recognizable marker beds over broad areas. The other tephra sets listed in table 1 either have been less fully studied or form less useful marker beds. Tephra units older than set S range in age from at least 37,600 to less than 20,000 radiocarbon years, but neither their stratigraphy nor their distributions have yet been determined. Set P, a preliminary description of which is presented in another report (Crandell and Mullineaux, 1973), is relatively thin and may be difficult to distinguish from ash beds from other volcanoes in the Cascade Range. Set B consists largely of scoria layers that are of relatively local extent. Set T contains only one moderately extensive pumice layer and has been described briefly in previous reports (Mullineaux, 1964; Mullineaux and Meier, 1965; Okazaki and others, 1972).

DESCRIPTION OF TEPHRA DEPOSITS

Tephra-set S

Set S consists chiefly of beds of yellow to brown pumice lapilli and ash with lesser amounts of lithic fragments. Ten km east-northeast of the present summit of Mount St. Helens, the set as a whole is as much as a metre thick and contains several separate lapilli beds (fig. 2). Irregularly stratified beds of chiefly ash- and lapilli-size pumice that make up the lower part of the set are more variable in thickness than most tephra layers around Mount St. Helens; these deposits may have been reworked after initially falling onto snow or ice. The middle part of the set contains at least three thin, relatively well defined beds of lapilli that are separated by even thinner ash beds. The upper part consists of two relatively coarse and thick lapilli layers. The lower of these, designated "Sg," commonly is 25–50 cm thick at 10 km from the volcano, and the upper, designated "So," is 10–20 cm thick.

Set-S tephra has been identified in virtually all directions from Mount St. Helens, but most of it lies in the quadrant extending from northeast to southeast of the volcano. Although one thin bed in the middle part of the set extends mainly southeast, the other well-defined layers in the set extend chiefly east-northeast from the volcano. The most voluminous beds of this set are the layers Sg and So, and they probably extend for considerable distances east and northeast of Mount St. Helens.

Close to Mount St. Helens, set S can be distinguished fairly readily in the field from younger pumice deposits; pumice in set S generally is lighter in color and finer grained than pumice in the overlying set J, and more weathered than pumice in set Y and younger deposits. Set S is less readily distinguished from older pumice deposits, and is identified in the field chiefly by its stratigraphic position under set J. It is separated stratigraphically from set J by lithic pyroclastic-flow deposits in some places, and elsewhere by lithic tephra and eolian material that commonly form a massive bed of silt and fine sand. Set S is separated from the next older pumiceous tephra unit by two beds of fine-grained lithic tephra and eolian material, each of which has a weak soil profile developed in it.

Ferromagnesian mineral suites further distinguish

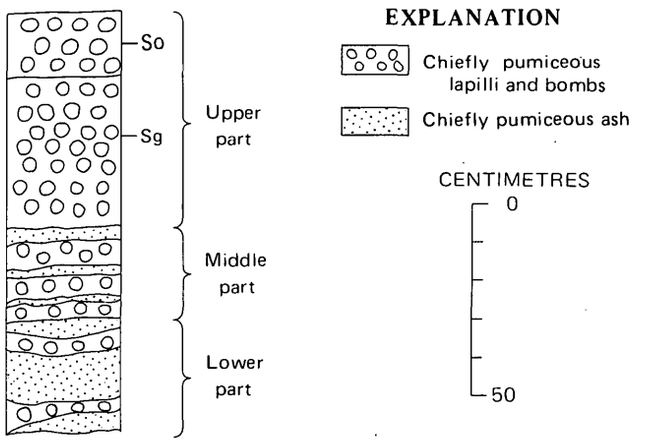

FIGURE 2.—Columnar section of set S, at a point about 10 km east-northeast of the summit of Mount St. Helens.

pumice in set S. The predominant Fe-Mg minerals in set-S pumice are cummingtonite and olive to brown hornblende, but pumice in this set typically also contains small amounts of hypersthene (table 1). The abundance of cummingtonite distinguishes set S from all younger pumice except that of set Y; set S can be distinguished from set Y by the presence of hypersthene, as well as by the character of its hornblende constituent, which is browner and has a higher refractive index than that found in the younger set. Likewise, the pumice in set S differs from most older pumice by the virtual absence of biotite, an abundance of brown rather than green hornblende, and the greater abundance of hypersthene.

Four radiocarbon dates for samples from pyroclastic-flow or lahar deposits that overlie layer So east of the volcano establish that set S is older than about 12,000 yr; stratigraphic positions of two of these dated samples are shown in figure 3. An age of less than 18,500 yr is indicated by a dated charcoal sample taken from another pyroclastic flow that underlies the set (fig. 3). One other dated charcoal sample suggests that part of the set is approximately 13,000 yr old; a radiocarbon date of 13,100±350 yr has been obtained for charcoal from a pyroclastic flow south of the volcano whose constituent pumice is like that in set S, and which underlies several thin beds of set-S pumice. This was a hot pyroclastic flow, which may have been erupted at the same time as some set-S tephra. Thus, the set-S layers above the dated pyroclastic flow, although they have not been correlated with individual layers elsewhere, show that at least part of the set is no more than about 13,000 yr old. At present, it seems likely that the voluminous layers Sg and So are about 13,000 yr old or perhaps even slightly younger.

Tephra-set J

Near Mount St. Helens, set J consists chiefly of reddish-brown to yellow pumice lapilli and small bombs. Southeast of the volcano three separate beds can be recognized in the set (fig. 4), and at least two beds can be distinguished to the northeast. Bedding in the set is obscure in most places, however, and we have not yet been able to trace individual layers from the southeast side of the volcano to the northeast.

Set J has been identified as a whole from north of the volcano clockwise around to the south. It is thickest in the quadrant that extends from the northeast to southeast; in those directions it is nearly a metre thick at a distance of about 10 km from the summit of Mount St. Helens and probably extends for considerable distances over a broad arc. Further southeast of Mount St. Helens, set-J pumice is as much as 20 cm thick at a distance of 40 km.

Near the volcano, pumice in set J commonly is darker and redder than pumice in sets S and Y. In addition, a brown oxidized zone is developed in the upper part of set J, and it commonly is separated from set Y by a thin discontinuous layer of charred vegetation.

The only common Fe-Mg minerals in set-J pumice are hypersthene and hornblende. Thus, this pumice differs markedly from that in sets S and Y in its

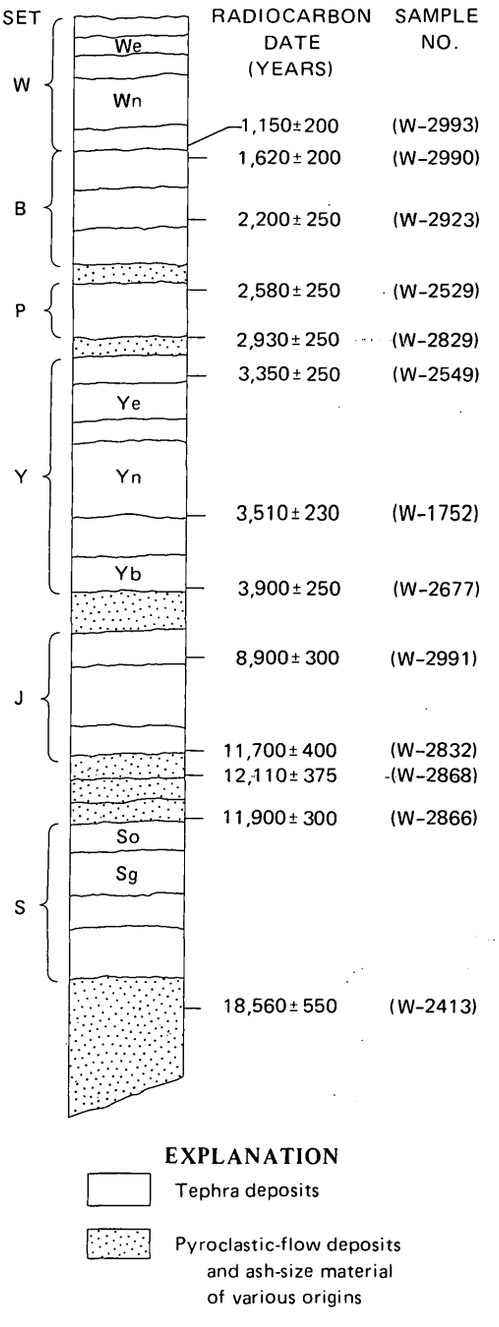

FIGURE 3.—Diagrammatic section showing stratigraphic positions of some key radiocarbon samples used to determine ages of tephra sets.

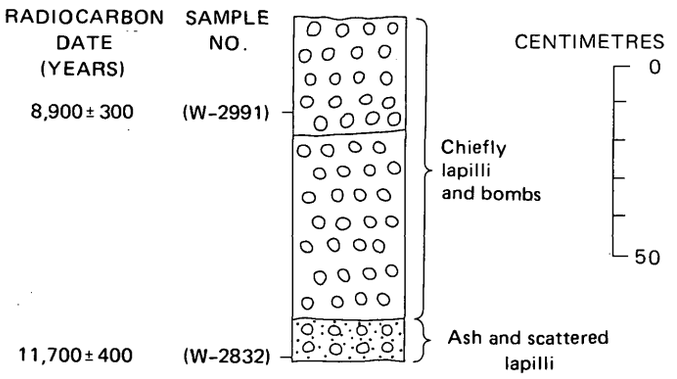

FIGURE 4.—Columnar section of set J, at a point about 10 km southeast of the summit of Mount St. Helens.

abundance of hypersthene and absence of cummingtonite. It is similar in mineral content to pumice in set W, but the hypersthene of set J has a lower refractive index (see "Tephra-set W"). In Fe-Mg mineral content and character of glass, it is also similar to pumice from Glacier Peak that is reported to be about 12,000 yr old (Fryxell, 1965); however, according to R. E. Wilcox and J. A. Westgate (oral commun., 1973), set-J pumice can be distinguished from that of Glacier Peak by their differing compositions of glass as determined by electron-probe methods.

Tephra beds in set J may have been the products of eruptions at widely spaced intervals throughout most of the period from slightly less than 12,000 yr to slightly more than 8,000 yr ago. A radiocarbon date of 11,700±400 yr for a sample from the basal bed of the set on the southeast flank of Mount St. Helens may approximate the eruption of that fine-grained layer (fig. 4). A date from the upper bed of set J there (fig. 4) shows that one coarse and thick pumice bed had been erupted about 9,000 yr ago, and another somewhat before that time. Two other dates from set-J pumice on the northeast flank of the volcano indicate that two more set-J eruptions occurred as late as about 8,430 (W-2702) and 8,300 (W-2587) yr ago. These two dates from the northeast flank, when compared to the one date in the upper layer of set J on the southeast flank of the volcano, also suggest that all the coarse and thick pumice on the northeast is younger than the uppermost coarse bed on the southeast side of the mountain. It has not yet been possible, however, to confirm their stratigraphic relation in the field.

Tephra-set Y

Set Y, the thickest and coarsest of the late glacial and postglacial tephra units, consists of many beds of white to yellowish-brown pumice and a few beds of lithic fragments. It includes more than a dozen discrete layers of pumice (fig. 5), two of which have been

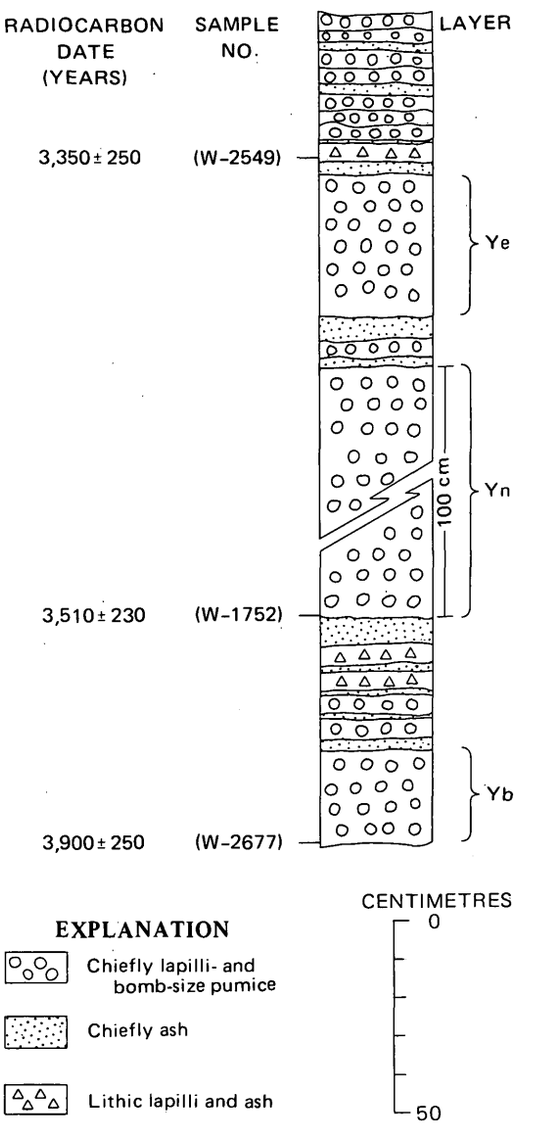

FIGURE 5.—Composite columnar section of set Y at a distance of about 10 km from the summit of Mount St. Helens. Thickness shown for layer Ye occurs east-southeast of the volcano; thicknesses for other layers are to the northeast.

found hundreds of kilometres from the source (fig. 6).

The layer designated Yn, the thickest and coarsest bed in the set, extends in a long narrow lobe that leads north-northeastward from the volcano (fig. 6). Within about 10 km of the mountain, it commonly consists of a metre or more of bombs and lapilli along the thickest, axial part of its lobe. At a distance of 80 km, layer Yn makes up a bed of lapilli and ash as thick as 30 cm in the southwestern part of Mount Rainier National Park, where it is the "layer Y" of Crandell, Mullineaux, Miller, and Rubin (1962). Still farther northeast, it has been identified near Kamloops in British Columbia (Fulton and Armstrong, 1965), and in Alberta where it is about 900 km from its

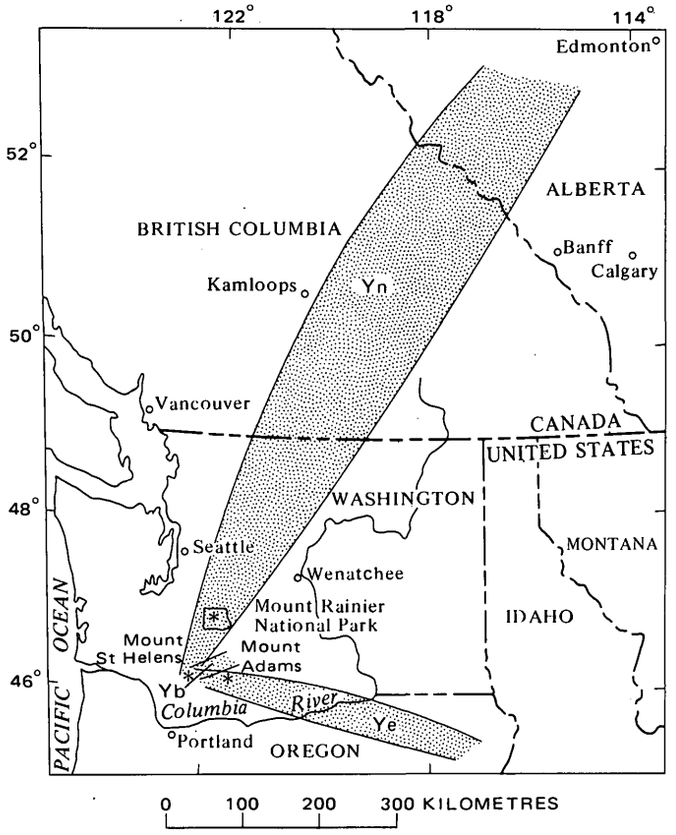

FIGURE 6.—Minimum distribution inferred from known occurrences of layers Yb, Yn, and Ye. Information from Crandell, Mullineaux, Miller, and Rubin (1962); Westgate, Smith, and Nichols (1970); and Borchardt, Norgren, and Harward (1973).

source (Westgate and others, 1970).

Layer Ye is a coarse thick bed that extends mainly east-southeast from the volcano (fig. 6). It is about 35 cm thick at a distance of 10 km from the summit, and as much as 20 cm thick at a distance of 50 km. Layer Ye probably is the 5-cm-thick "Mount St. Helens Y ash" identified in northeastern Oregon, at a distance of about 400 km from Mount St. Helens (Norgren and others, 1970; Borchardt and others, 1973).

A few other beds of set Y have also been found at considerable distances from Mount St. Helens. Layer Yb, for example, which lies at the base of the set northeast of the volcano, is as much as 5 cm thick at a distance of 50 km northeast of the mountain. In addition, at least two of the beds that are above layer Yn are ½–1 cm thick in Mount Rainier National Park at a distance of 80 km from their source (Mullineaux, 1974).

Set-Y pumice near Mount St. Helens is fairly easily distinguished from older pumice deposits by its relatively firm, unweathered condition. Set-Y pumice is stained yellowish brown, and this color distinguishes it from most younger pumice deposits, which are white. In addition, set-Y pumice differs from younger Mount St. Helens pumice and from other known tephras from Cascade Range volcanoes by its abundance of cummingtonite. Set-Y deposits far from the volcano might be differentiated from older cummingtonite-bearing tephras of Mount St. Helens by the absence of hypersthene in pumice fragments; however, because hypersthene is common as a contaminant in ash beds, recognition of ash beds of set Y may depend on their stratigraphic position. The Fe-Mg mineral content of most beds in set Y does not vary appreciably; layer Yb, however, contains small amounts of biotite (table 1).

Charcoal dated at about 4,000 and 3,000 radiocarbon years (fig. 3) underlies and overlies, respectively, set-Y pumice directly east of the volcano. Two other dates that bracket the two most extensive layers, Yn and Ye, indicate that they are between about 3,500 and 3,350 radiocarbon years old (fig. 3). Still other dates that are pertinent to the age of layer Yn include one of 3,500 yr from below layer Yn at Mount Rainier (Crandell and others, 1962); another of about 3,500 yr, regarded as from "the same stratigraphic position" as that same layer in Alberta (Westgate and others, 1970); and three dates of about 3,400 yr, two from below the layer and another from above it, in British Columbia (Fulton, 1971). Layer Yn originally was arbitrarily assigned an age of 3,200 yr on the basis of two limiting radiocarbon ages of about 3,500 and 3,000 yr (Crandell and others, 1962); the dates now available indicate that it is slightly older, perhaps about 3,400 radiocarbon years. However, curves that compare radiocarbon dates to calendar ages as indicated by bristlecone-pine tree rings suggest that organic material as young as about 3,600 calendar years or as old as about 4,000 calendar years could give a radiocarbon age of between 3,500 and 3,350 yr (Suess, 1970). Thus, the ages assigned to these tephra layers must be regarded as approximate, and the eruption of layers Yn and Ye might have been separated by a longer period of time than is indicated by the 3,500- and 3,350-year radiocarbon dates.

Tephra-set W

Set W consists mostly of a group of coarse white to light-gray pumice beds. The basal coarse bed of the set, however, is made up of relatively dense fragments of lapilli and ash (fig. 7). It is overlain by at least five pumice layers, two of which are known to extend many tens of kilometres from the volcano. Layer Wn, the coarsest and thickest pumice layer in the set, extends mostly to the northeast (fig. 8). At a distance of 10 km from Mount St. Helens, it consists chiefly of bombs and lapilli a metre or more thick; at a

distance of about 80 km, in the southeastern part of Mount Rainier National Park, the layer is as much as 8 cm thick and consists of small lapilli and ash. In the park, it is the "layer W" of Crandell, Mullineaux, Miller, and Rubin (1962).

Another relatively thick bed in the set, layer We (fig. 7), extends east of the volcano (fig. 8). It is about half a metre thick at a distance of 10 km from Mount St. Helens, and as much as 5 cm thick 50 km east of the volcano. This, or perhaps another, similar, bed of set W, is also 20–25 cm thick on the south flank of Mount St. Helens. The other pumice beds in the set are much thinner, and seem to be distributed mostly northeast and east of the volcano. Tephra of set W is known as far as 100 km northeast of Mount St. Helens (Mullineaux and Meier, 1965; Okazaki and others, 1972), and as far as 70 km east of the volcano (J. A. Norgren, written commun., 1971).

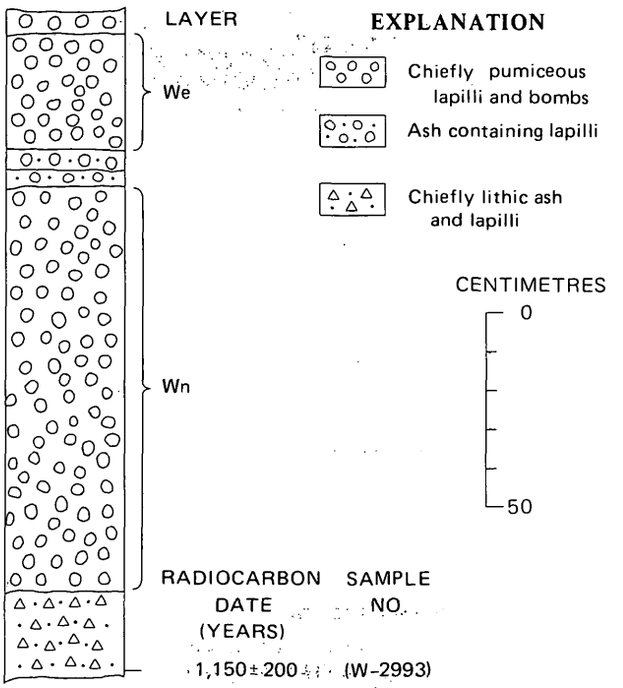

FIGURE 7.—Composite columnar section of set W at a distance of about 10 km from the summit of Mount St. Helens. Thickness shown for layer We occurs east of the volcano; thicknesses for other layers are to the northeast.

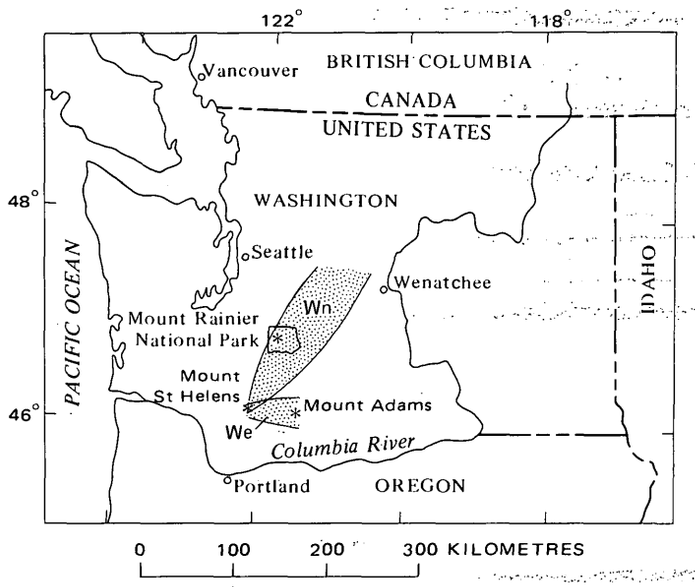

FIGURE 8.—Minimum distribution of layers Wn and We inferred from known occurrences

Set W is distinguished in the field from older pumice deposits of Mount St. Helens chiefly by color and stratigraphic position. It can also be readily differentiated from set Y by its hypersthene content and from pumice in set T by the absence of augite (table 1). Set W contains the same Fe-Mg mineral suite as set P (table 1), but generally is thicker and coarser. In addition the lowest refractive index of hypersthene in set W pumice is higher than 1.70, whereas that of hypersthene in set P is less than 1.70.

Set-W tephra beds appear to range from slightly more than 1,000 to about 450 yr old. A single charcoal sample from the basal coarse bed in the set has been dated as 1,150±200 yr old. Vegetation was reestablished on top of that basal bed before eruption of the overlying layer Wn, which has been dated as about 450 yr old by tree-ring counts (Crandell, 1971). Set W beds younger than layer Wn probably were erupted just shortly after layer Wn, for a tree as old as 435 yr has been found growing over layer We.

USE OF MOUNT ST. HELENS TEPHRA LAYERS FOR DATING AND CORRELATION

The tephras from Mount St. Helens should be especially useful for deciphering and dating glacial and volcanic sequences and for correlating those sequences from place to place. Because these tephras occur on and are interbedded with a wide variety of natural and artificial deposits, they can also be useful in geomorphic and archeologic investigations.

Tephra-set S in the Lewis River valley southeast of Mount St. Helens provides an example of application of these tephras to glacial studies. In this area, the middle and upper parts of set S occur on an outwash terrace formed during or shortly after the maximum stand of a valley glacier of Fraser age (Crandell and Mullineaux, 1973, p. A12). The lower part of the set is missing from the terrace, even though conditions for preservation seem to be favorable; thus, the outwash deposits presumably are younger than the lower part of the set, but older than the middle part. Close

dating of the tephra would provide a relatively precise date for the maximum stand of the glacier in the Lewis River valley. Moreover, determination of the distribution of various parts of the set on glacial deposits in nearby valleys would allow correlation of glacier positions from one valley to another. At progressively higher altitudes above valley floors eastward from Mount St. Helens, the upper beds of set S become discontinuous or absent altogether, and from their distribution it may be possible to determine approximately the extent of alpine glaciers at the time those tephra layers fell.

Knowledge of each of the younger tephra sets described can also be applied to glacial problems in the Cascade Range. Set-J tephra is a marker deposit that separates late Pleistocene from Neoglacial deposits wherever the tephra can be identified, and sets Y and W have been used to subdivide Neoglacial drift as far north as Mount Rainier National Park (Crandell and Miller, 1964). Discovery of set-Y tephra in the glaciated Wallowa Mountains of northeastern Oregon (Norgren and others, 1970; Borchardt and others, 1973) indicates that the tephra might be helpful in unraveling the Neoglacial sequence there.

The tephras may be very useful for determining the ages, especially the minimum limiting ages, of young lava flows, which do not commonly include carbon from which direct dates can be obtained. In many places in the Cascade Range of southern Washington, the four tephra sets described should allow subdivision of late glacial and postglacial lavas into at least four categories: those older than about 8,500 yr, those younger than 8,500 but older than 3,000–4,000 yr, others that are younger than 3,000 but older than about 500 yr, and still others that are less than about 500 yr old.

East of the Cascade Range, the Mount St. Helens tephra deposits provide information applicable to a variety of problems in the Columbia River basin. Three ash layers that are strongly similar to set-S tephra, for example, occur in the upper part of a widespread lacustrine fill in that basin. Confirmation of the three layers as part of set S, and closer dating of that tephra set, would provide a critical date for the geomorphic history of that region. Set-J tephra may be useful for unraveling the history of draining of the same lake and incision of the lake beds; tephra layers of sets Y and W have already been identified on younger deposits in the area (Fryxell, 1972).

Although the limits of distribution of these tephra sets are not yet known, the extent of a few layers such as Yn and Ye indicates that they could prove useful as much as several hundred kilometres from their source.

REFERENCES CITED

Borchardt, G. A., Norgren, J. A., and Harward, M. E., 1973, Correlation of ash layers in peat bogs of eastern Oregon: Geol. Soc. America Bull., v. 84, no. 9, p. 3101–3108.

Crandell, D. R., 1971, Postglacial lahars from Mount Rainier volcano, Washington: U.S. Geol. Survey Prof. Paper 677, 75 p.

Crandell, D. R., and Miller, R. D., 1964, Post-Hypsithermal glacier advances at Mount Rainier, Washington, *in* Geological Survey research 1964: U.S. Geol. Survey Prof. Paper 501–D, p. D110–D114 [1965].

Crandell, D. R., and Mullineaux, D. R., 1973, Pine Creek volcanic assemblage at Mount St. Helens, Washington: U.S. Geol. Survey Bull. 1383–A, 23 p.

Crandell, D. R., Mullineaux, D. R., Miller, R. D., and Rubin, Meyer, 1962, Pyroclastic deposits of Recent age at Mount Rainier, Washington, *in* Geological Survey research 1962: U.S. Geol. Survey Prof. Paper 450–D, p. D64–D68.

Fryxell, Roald, 1965, Mazama and Glacier Peak volcanic ash layers—Relative ages: Science, v. 147, no. 3663, p. 1288–1290.

———1972, Relationship of late Quaternary volcanic ash layers to geomorphic history of the Columbia Basin, Washington [abs.]: Geol. Soc. America Abs. with Programs, v. 4, no. 3, p. 159.

Fulton, R. J., 1971, Radiocarbon geochronology of southern British Columbia: Canada Geol. Survey Paper 71–37, 28 p.

Fulton, R. J., and Armstrong, J. E., 1965, Day 11, *in* Schultz, C. B., and Smith, H. T. U., eds., Internat. Assoc. [Union] Quaternary Research Cong., 7th, Guidebook Field Conf. J, Pacific Northwest, 1965: p. 87–98.

Lawrence, D. B., 1954, Diagrammatic history of the northeast slope of Mount St. Helens, Washington: Mazama, v. 36, no. 13, p. 41–44.

Mullineaux, D. R., 1964, Extensive Recent pumice lapilli and ash layers from Mount St. Helens volcano, southern Washington [abs.]: Geol. Soc. America Spec. Paper 76, p. 285.

———1974, Pumice and other pyroclastic deposits in Mount Rainier National Park, Washington: U.S. Geol. Survey Bull. 1326, 83 p.

Mullineaux, D. R., Hyde, J. H., and Rubin, Meyer, 1972, Preliminary assessment of upper Pleistocene and Holocene pumiceous tephra from Mount St. Helens, southern Washington [abs.]: Geol. Soc. America Abs. with Programs, v. 4, no. 3, p. 204–205.

Mullineaux, D. R., and Meier, M. F., 1965, Day 1, *in* Schultz, C. B., and Smith, H. T. U., eds., Internat. Assoc. [Union] Quaternary Research Cong., 7th, Guidebook Field Conf. J, Pacific Northwest, 1965: p. 6–12.

Norgren, J. A., Borchardt, G. A., and Harward, M. E., 1970, Mount St. Helens Y ash in northeastern Oregon and south-central Washington [abs.]: Northwest Sci., v. 44, no. 1, p. 66.

Okazaki, Rose, Smith, H. W., Gilkeson, R. A., and Franklin, Jerry, 1972, Correlation of West Blacktail ash with pyroclastic layer T from the 1800 A.D. eruption of Mount St. Helens: Northwest Sci., v. 46, no. 2, p. 77–89.

Suess, H. E., 1970, Bristlecone-pine calibration of the radiocarbon time-scale 5200 B.C. to the present, *in* Olsson, I. U., ed., Radiocarbon variations and absolute chronology—Nobel symposium, 12th, Uppsala Univ., 1969 Proc.: New York, John Wiley & Sons, Inc., p. 303–311.

Westgate, J. A., Smith, D. G. W., and Nichols, H., 1970, Late Quaternary pyroclastic layers in the Edmonton area, Alberta, *in* Symposium on pedology and Quaternary research, Edmonton, 1969, Proc.: Alberta Univ. Press, p. 179–187.

Jour. Research U.S. Geol. Survey
Vol. 3, No. 3, May–June 1975, p. 337–343

THE INFLUENCE OF LATE CENOZOIC STRATIGRAPHY ON DISTRIBUTION OF IMPOUNDMENT-RELATED SEISMICITY AT LAKE MEAD, NEVADA-ARIZONA

By R. ERNEST ANDERSON and R. L. LANEY,
Denver, Colo., Phoenix, Ariz.

Abstract.—At Lake Mead, contrasts in permeability of upper Cenozoic sediments show a better correlation with irregularly distributed impoundment-related seismicity than do contrasts in structure. An evaluation of structures developed during the late Cenozoic fails to explain the erratic distribution of seismicity. An evaluation of the late Cenozoic stratigraphy, however, shows a concentration of relatively impermeable evaporite beds and fine-grained clastic strata in the less seismic part of the lake basin; therefore, the authors conclude that a hydraulic connection between the lake water and the deep aquifer system that includes buried faults is needed in the Lake Mead area to cause the release of seismic energy. Where hydraulic connection is prevented by continuous or quasi-continuous upper Cenozoic basin-fill strata of low permeability, as in the eastern basin area, seismicity does not occur.

Lake Mead, one of the major reservoirs of the world, was created in the middle 1930's by the construction of Hoover Dam across the Colorado River at Black Canyon. Soon after Lake Mead began to fill, local earthquakes were felt in the vicinity of the lake (Carder, 1970) and since then over 10,000 events have been recorded.

The impoundment of water in some reservoirs stimulates the release of seismic energy. W. V. Mickey (NOAA Environmental Research Laboratories, written commun., 1973) summarized the impoundment-related seismicity in the United States and found that indirect and inconclusive evidence relating seismic activity to reservoir impoundment is available for more than 40 reservoirs. However, seismic data are available for only 18 reservoirs and at only 10 of these is there an indication of possible cause and effect. Lake Mead is the only reservoir for which there are sufficient seismic data to allow significant comparisons between water impoundment and local seismicity. It is clear that reservoir filling results in increased seismic activity (Carder, 1970).

The Lake Mead area lies along part of the common border of Arizona and Nevada (fig. 1). For purposes of reference the lake can be divided into three parts which, from east to west, are (1) the upper lake, a narrow body that clearly reflects the sinuous course of the Colorado River, (2) the eastern basin, the large body that includes Virgin Basin and Overton Arm, and (3) the western basin north of Hoover Dam (fig. 2). The western basin has been variously referred to as Boulder Basin or Callville Basin.

Carder (1945, 1970) and Carder and Small (1948) prepared maps of earthquake epicenters in the Lake Mead area covering the period from 1940 through 1947.

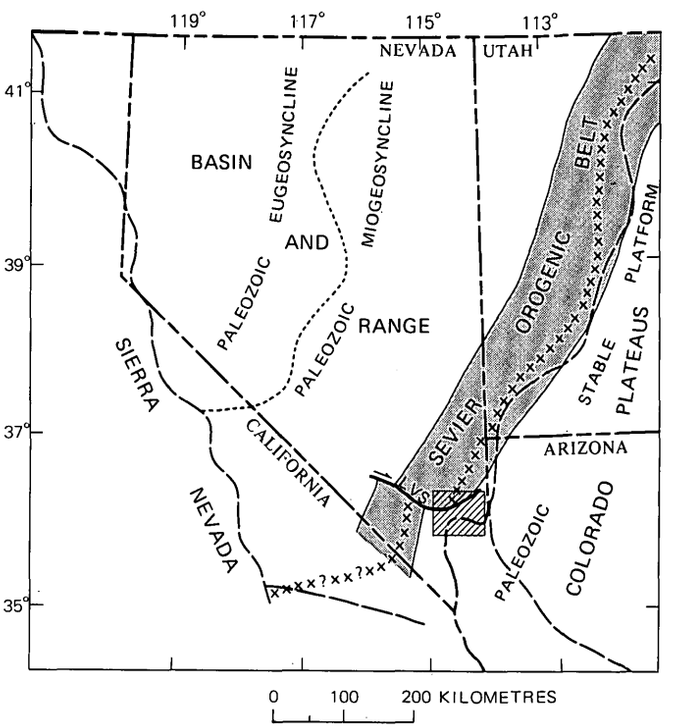

FIGURE 1.—Map showing the location of the Lake Mead area (diagonally ruled) relative to the boundary between the Paleozoic miogeosyncline and stable platform (X's), the Mesozoic Sevier orogenic belt, the boundary between the Colorado Plateaus and Basin and Range provinces (long-dashed line), and the Las Vegas Valley shear zone (LVS).

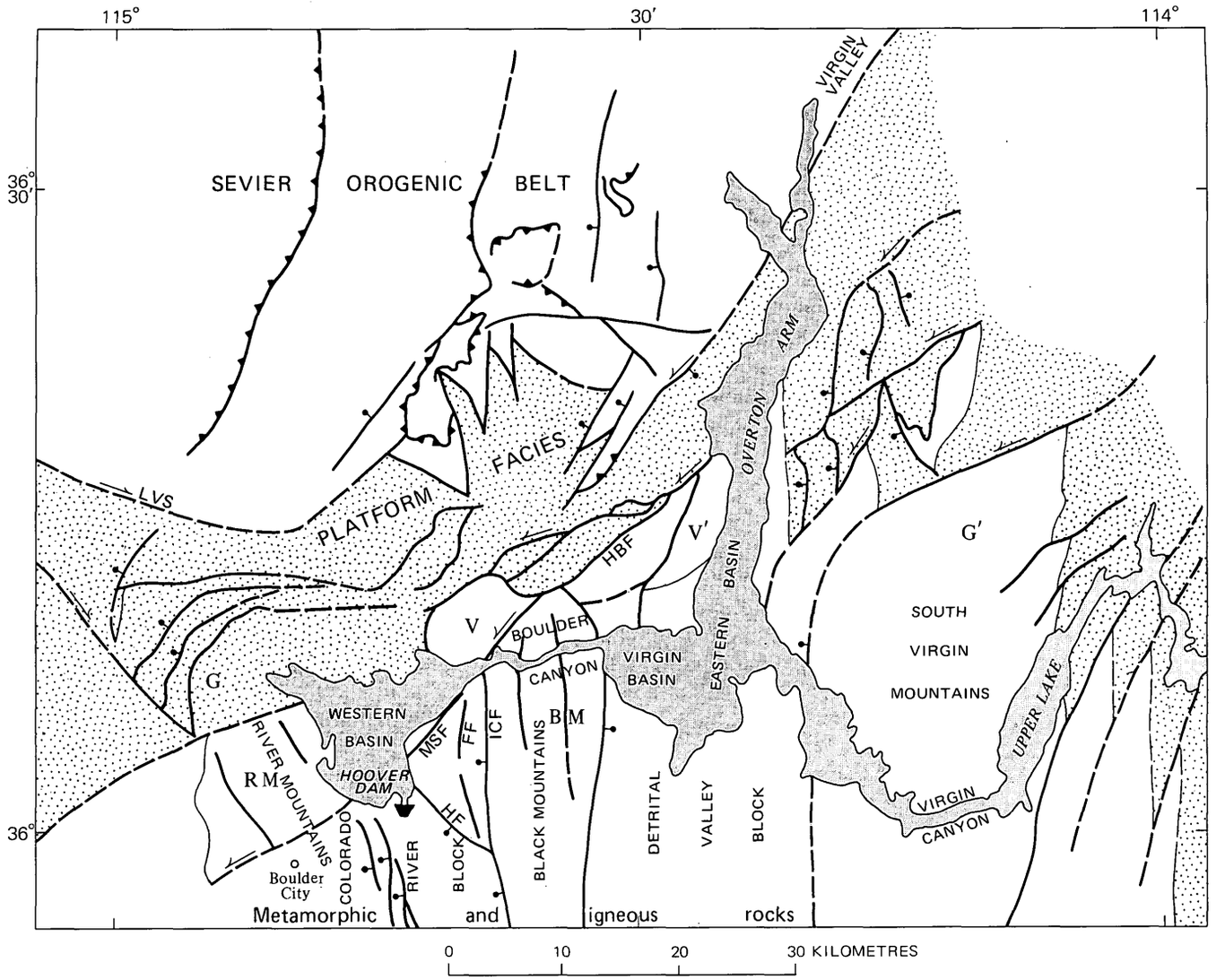

FIGURE 2.—Map showing Lake Mead (shaded) and its principal basins relative to some of the major tectonic features of the area including (1) Sevier orogenic belt and its complexly faulted south boundary, (2) area of Precambrian metamorphic rocks and Cenozoic igneous and volcanic rocks, and (3) structural corridor (stipple pattern) between 1 and 2 composed of tectonically transported Paleozoic platform facies rocks and Mesozoic and Cenozoic strata of continental origin. Two offset parts of a late Cenozoic volcano, indicated by V and V′; the River Mountains (RM) probably represent the offset northern part of the Black Mountains (BM); unique rapakivi granite widely exposed at G′ is found as landslide masses at G, indicating the approximate cumulative displacement on the left-lateral shear system. Las Vegas Valley shear zone, LVS; Hamblin Bay fault, HBF; Mead Slope fault, MSF; Fortification fault, FF; Indian Canyon fault, ICF; Horsethief fault, HF. Faults are dashed where approximately located and have bar and ball on downthrown side; arrow shows relative direction of movement; sawtooth edge indicates east-directed overthrusts.

The distribution of epicenters is extremely irregular; epicenters are highly concentrated in the vicinity of, and south of, the western basin, with a subordinate concentration in the area of the upper lake (fig. 3). No epicenters are reported in the eastern basin although it contains the largest area and volume of water. According to A. M. Rodgers, Jr. (Environmental Research Corp., written commun., 1973), microearthquakes are now occurring in the western basin area at the rate of one or two per day at depths typically less than 5 km. Most of the epicenters in the vicinity of the western basin lie northeast of Boulder City, Nev., and many are concentrated near four major faults that were described by Longwell (1963, pl. 1)—the Mead Slope fault, the Fortification fault, the Indian Canyon fault, and the Horsethief fault (figs. 2, 3).

Carder (1945) suggested that the irregular distribution of seismicity is related to a contrast in the type of

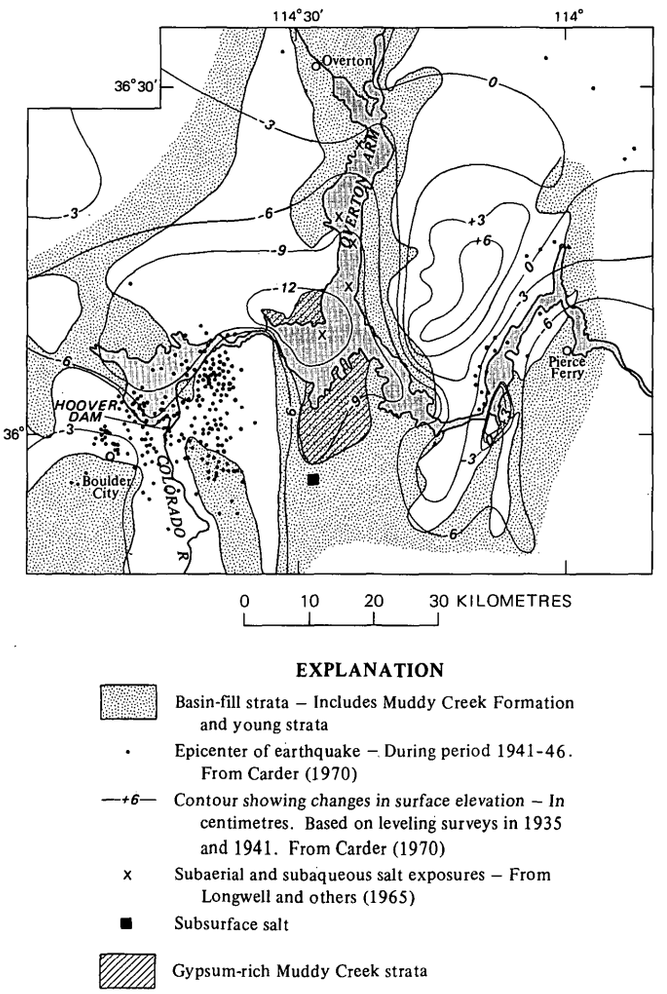

FIGURE 3.—Map of the Lake Mead area showing locations of epicenters, changes in surface elevations, highly generalized distribution of basin-fill strata, occurrences of subaerial and subaqueous salt exposures in the Overton Arm area, location of subsurface salt, and area of gypsum-rich strata in Muddy Creek Formation in Detrital Valley.

impoundment-related deformation between the two major basins: flexuring in the aseismic eastern basin and faulting in the seismic western basin. The purpose of the present report is to summarize the geologic setting and late Cenozoic geologic history of the Lake Mead area, to evaluate Carder's suggestion in terms of that summary, and to suggest, instead, that the irregular distribution of seismicity is related to contrasts in basin stratigraphy and not to structure. In particular, the distribution of relatively impermeable evaporite beds and fine-grained clastic strata in the eastern basin seems to have produced an aseismic area by preventing hydraulic connection between the waters of Lake Mead and the system of faults that is believed to be present beneath the impermeable strata.

GEOLOGIC SETTING

Lake Mead occupies the critical junction of several major geologic features, some of which are offset and others of which either intersect or adjoin in the vicinity of the lake. The location of the lake relative to these features is shown in figures 1 and 2. The boundary between the Paleozoic miogeosynclinal and platform facies rocks projects toward the lake area from the northeast as does the broad belt of east-directed Cretaceous overthrusts, the Sevier orogenic belt. However, neither feature quite reaches the main area of the lake (fig. 1). Both were offset many kilometres to the west during the late Tertiary by displacements on a complex system of faults, one of which is the Las Vegas Valley shear zone (Longwell, 1960; Fleck, 1970). The approximate location of the faulted margin of the Sevier orogenic belt, which embraces the miogeosyncline-platform facies boundary, is shown in figure 2. Although the late Tertiary truncation of these features may be of importance to understanding the geology of the lake area, the features themselves are not and therefore will not be given additional consideration.

The eastern extremity of the upper lake lies across the faulted transition zone between the Colorado Plateaus and the Basin and Range structural provinces (figs. 1, 2). The lake extends westward from the transition zone about 80 km into the Basin and Range province. As the lake reaches westward it transects one basement ridge at Virgin Canyon; farther west the lake lies athwart the northern extremities of two north-trending basins and one intervening range each of which is very well defined for more than 70 km south of the lake (south of the area of fig. 2). From east to west these latter three features are (1) the Detrital Valley downdropped block, (2) the uplifted Black Mountains, and (3) the structural trough that has had much of its sediment fill scoured out by the Colorado River south of Hoover Dam (fig. 2). Bedrock in these areas consists of Precambrian crystalline rocks and Tertiary volcanic and plutonic rocks (Longwell, 1963; Wilson and Moore, 1959). The structural corridor situated between the north ends of these Basin and Range structures and the southern faulted margin of the Sevier orogenic belt (fig. 2) consists of a fantastic array of faulted ridges composed of rocks that were carried into that area from the northeast, piggyback style, on a relatively fast moving current of mantle and lower crustal materials during the late Tertiary (Anderson, 1973). This structural corridor consists of platform-facies Paleozoic strata, Mesozoic strata that include the Moenkopi and Chinle Formations and the Aztec Sandstone, and a thick sequence of continental

basin strata, the lower part of which may be as old as Late Cretaceous or early Tertiary.

In summary, the most important stratigraphic units that shape the geologic setting of Lake Mead are (1) the Precambrian and Tertiary metamorphic and igneous rocks in the south and the younger sediment prisms that partially fill the basins that developed there later, and (2) the Paleozoic, Mesozoic, and Tertiary sedimentary strata located in the structural corridor to the north. The most important structures are (1) the faulted transition zone between the Colorado Plateaus and the Basin and Range areas, (2) the Basin and Range structures that extend into the lake area from the south, and (3) the corridor of complex strike-slip structures along which the belt of sedimentary rocks has been shifted many kilometres to the southwest. In the section that follows we attempt to sort out these stratigraphic and structural units in terms of their sequence of development.

LATE CENOZOIC GEOLOGIC HISTORY

The late Cenozoic geologic history of the area can be divided into three main events. During the first episode, which occupied a 7-m.y. period that ended about 13 m.y. ago, there was eruption of predominantly andesite lava to form piles as much as 4,000 m thick, simultaneous emplacement of hypabyssal plutons of batholithic proportions in the southern part of the area, and deposition of clastic, carbonate, and evaporite strata in broad basins to the northeast [1] (Anderson and others, 1972). The plutonism occurred during the latter part of this period and was accompanied by extreme thin-skinned extensional tectonism that continued into the next main event (Anderson, 1971). The Colorado Plateaus and Basin and Range areas probably began to be structurally and physiographically distinguishable during this period. However, all available evidence suggests that drainage was to the north or northeast from the Lake Mead area during most of this period (Lucchitta, 1972).

The second episode occurred between 13 and 5 m.y. ago. During the first part of this 8-m.y. period, the intensity of volcanism and thin-skinned extensional tectonism in the southern part of the lake area decreased rapidly. Structural activity changed with time from displacements on low-angle shingling normal faults to displacements on higher angle normal faults that blocked out basins which began to fill with sediments and minor intercalated lavas. More than 1.5 km of vertical displacement eventually developed between the Black Mountains and the flanking basins (Anderson and others, 1972). In the area to the northeast the early formed broad basins were broken up by large-magnitude displacements on interrelated strike-slip and normal fault systems that began to transport the rocks to the southwest. The boundary between the southern metamorphic-igneous area and the central sedimentary corridor (fig. 2) developed early during this period as a major left-lateral strike-slip fault zone that eventually acquired about 60 km of displacement (Anderson, 1973). There was undoubtedly much fault interaction across this boundary because displacements on the strike-slip faults were in part compensated for by simultaneous west-directed extensional tectonics in the area to the south. As in the south, new basins formed in the north and they too began to fill with sediments. The basin-fill sediments in both areas have been mapped widely as the Muddy Creek Formation, which includes coarse to fine clastic rocks, lavas, tuffs, landslide deposits, and more significantly, evaporites and chemical precipitates. Basalt lavas at the top of the Muddy Creek sediments have been dated isotopically at about 5 m.y. (Anderson and others, 1972). These lavas flowed down the flanks of the Black Mountains across the range-front faults and out over the alluviated valleys. The lavas predate the Colorado River in the area and postdate all but a small amount of normal faulting.

The geologic record for the final period, between 5 m.y. ago and the present, is fragmentary largely because much of what might have served as evidence has been removed by erosion. The period may have begun with continued basin sedimentation under conditions of greatly reduced structural activity. Sedimentation was interrupted early and abruptly when the Colorado River entered the area and began breaching the basins and carrying their sedimentary fill southward out of the Lake Mead area. Potassium-argon data reported by Lucchitta (1972) indicate that the Colorado River had cut its channel to approximately its present level by about 3.3 m.y. ago. This age value, together with those reported by Anderson, Longwell, Armstrong, and Marvin (1972), seems to compress the period of canyon cutting by the Colorado River into too short an interval (less than 1.7 m.y.). Nevertheless, the data probably approximate the age of that event, if not its precise duration.

Anderson (1969) reported the presence of the effects of a fossil water table exposed at altitudes more than 0.5 km above present grade of the Colorado River in the vicinity of Hoover Dam. This is undoubtedly the youngest pre-Colorado River feature in the area, but

[1] Although the sedimentary rocks of this period are now located to the north of the western and eastern Lake Mead basins, they were transported to that position tectonically from the northeast and not deposited there (Anderson, 1973). The true nature of the prefaulting transition between predominantly igneous rocks in the south and the sedimentary rocks is not known.

its age has not been precisely determined. Contrasting layers produced by different amounts of water-table-related cementation are traceable for a few kilometres. They are not cut by faults (Anderson, 1969, fig. 2), whereas the youngest nearby basalt lavas are (R. E. Anderson, unpub. data, 1974). These relationships suggest pronounced structural stability over the past 3.3 m.y. in the general area of the most intense impoundment-related seismicity.

The level to which the western basin was filled with sediment near its edges is determined by the level of the fossil water table. Thus, it is clear that a thickness of as much as 0.5 km of basin-fill sediment was stripped from the western basin by the Colorado River. A similar thickness may have been removed from parts of the eastern basin. This denudation event and the accompanying reduction of ground-water level could have acted in the direction of stabilizing the area seismically by reducing hydraulic pressure at hypocentral depths. If this is so, the fact that seismic activity has been triggered by reservoir impoundment would suggest that the rocks at hypocentral depths are maintained in a critical or near-critical state of stress by mild but active tectonic forces. Despite the indications of increased structural stability during the past 5 m.y., the intense late Tertiary tectonism could reasonably be followed by residual tectonic forces of a much lower but still significant magnitude extending to the present.

HYPOTHESIS OF SEISMICITY RELATED TO STRUCTURE

Contoured leveling data reported by Carder and Small (1948, fig. 2) for the period extending from prior to the filling of Lake Mead to 1941 show that the maximum differential displacement measured in the vicinity of the lake occurred between the Detrital Valley block, which subsided 12 cm, and the bedrock area of the South Virgin Mountains to the east, which rose 6 cm (fig. 3). Contours representing changes in elevation for the period from 1935 to 1963 show a similar pattern of subsidence in the area of the Detrital Valley block although some rebound had occurred from 1949 to 1963 (Lara and Sanders, 1970, figs. 2-2 and 2-3). These data, together with the map of epicenter locations reported by Carder and Small (1948), show that impoundment-related deformation was greatest in the aseismic part of the lake area where the largest volume of water occurred. We therefore assume that seismicity is not the direct result of loading by the mass of lake water but instead reflects a reduction in effective stress on fractures in the focal region due to direct hydraulic connection with surface water. Also, if the irregular distribution of seismicity is related to contrasting styles of structural response to loading, as suggested by Carder (1945) and as outlined in the introduction to this report, we should expect to find some contrast in structural setting or pattern between the aseismic and seismic areas.

High-angle normal faults that cut and bound the Black Mountains block extend beneath the waters of Lake Mead in the aseismic as well as the seismic areas (Longwell, 1936; Anderson, 1973). Individual strike-slip faults also extend into both aseismic and seismic areas. In particular, the southernmost strike-slip fault north of Boulder Canyon (the Hamblin Bay fault of Anderson, 1973) has had about 20 km of left-lateral displacement since about 12.7 m.y. ago (offset indicated in fig. 2). This fault projects beneath the aseismic Overton Arm to the northeast and the seismic western basin to the southwest (fig. 2). Its trace is largely buried beneath strata of the Muddy Creek Formation in the Overton Arm area. Other late Tertiary strike-slip faults having displacements of several kilometres have been mapped in the South Virgin Mountains east of Overton Arm (Longwell and others, 1965; Morgan, 1968). These faults also must extend beneath the lake, although their traces are concealed by basin-fill strata that flank the lake. Late Tertiary normal and related strike-slip faults of large displacement are very abundant along the canyon of the Colorado River south of Hoover Dam (Longwell, 1963; Anderson, 1969, 1971, and unpub. data, 1974). They are visible there only because the river has removed much of the basin fill. Faults of similar size and abundance can be reasonably inferred to exist beneath the aseismic Detrital Valley block where the southern part of the eastern basin is located. Despite the fact that fault locations beneath the eastern basin are highly conjectural or unknown, available geologic maps provide no basis for suggesting that the abundance or pattern of large buried faults is any different there than in the seismic western basin.

INFLUENCE OF SALT BARRIER ON SEISMICITY

Surface exposures of rock salt in the area that is now occupied by Overton Arm (fig. 3) had been studied at several locations prior to the filling of Lake Mead (Longwell, 1936). The specific locations are shown on a mineral resources map of Clark County, Nev. (Longwell and others, 1965, pl. 2). The northernmost occurrence is still exposed along the western lakeshore southwest of Overton Beach (fig. 4).

The salt occurs within the Muddy Creek Formation and is as much as 500 m thick (Mannion, 1963). The Muddy Creek Formation in the area of Overton Arm

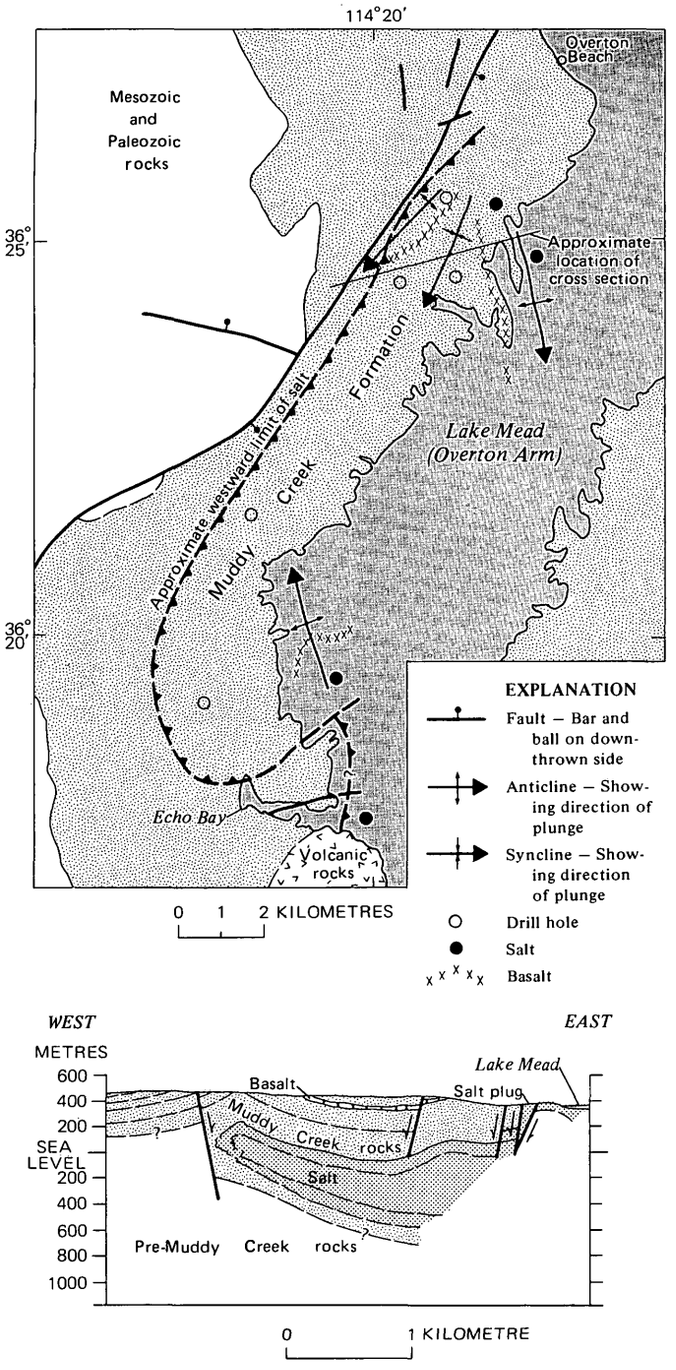

FIGURE 4.—Geologic sketch map of part of the Overton Arm area and generalized cross section south of Overton Beach showing the distribution of subsurface salt. From Mannion (1963).

is more than 800 m thick and consists mainly of siltstone, claystone, and sandstone, all of which are gypsiferous. A conspicuous basalt layer as much as 30 m thick occurs in the upper part of the section above the salt and serves as a useful marker in showing the structural deformation in the area (fig. 4). The salt exposures (all but two are now covered by Lake Mead) occur as domal bulges in the crests of anticlines. The anticlinal structures are complicated by faults, which increase in number and complexity near the salt bodies. Generally the nearly vertical flanks of the salt bulges are marked by high-angle faults. The side away from the axis of the fold usually is downthrown, thus indicating the upward movement of the salt in the anticline.

The entire Virgin Valley–Detrital Valley trough in the vicinity of Lake Mead contains salt deposits. In Detrital Valley about 50 km south of the northernmost exposure of salt in the Overton Arm area, a subsurface salt body has been defined by R. L. Laney using data from 10 drill holes (U.S. Geological Survey, 1972). The subsurface salt there covers an area of at least 13 km^2, is as much as 200 m thick, is within 130 m of the surface in places, and occurs as a northeast-trending mass that is about 2.4 km wide and at least 4.8 km long. The overlying clay, silt, and limestone beds of the Muddy Creek Formation, which are at least 450 m thick in the Detrital Valley block, have been upwarped into a south-plunging anticline. The east flank of the anticline forms a well-defined cuesta. The west flank is mostly concealed by alluvial deposits but, where exposed, appears to be complexly faulted.

To the north of the salt mass, Laney (unpub. data, 1973) mapped more than 90 km^2 where the surface exposures of the Muddy Creek Formation are rich in gypsum (fig. 3). Gypsum-rich beds commonly occur above salt in the Overton Arm area (Mannion, 1963) and in the Detrital Valley block, suggesting that salt may be present beneath the gypsum-rich beds south of the lake. Therefore, it is reasonable to infer from the available data that salt may underlie much of the eastern basin. Salt has not been reported in the western basin nor in the somewhat less seismic area of the upper lake where several large faults cut across the lake.

Salt is one of the least permeable natural rock-forming materials known, and it has a remarkable capacity to deform without fracturing. These physical properties could be responsible for preventing or greatly reducing hydraulic connection across a sequence of salt beds. We suggest that the presence of a continuous or quasi-continuous interval of bedded salt, in conjunction with deposits of gypsum and fine-grained clastic strata of low permeability beneath the eastern basin, is the single controlling factor in producing the aseismic area there; that is, a hydraulic connection between the lake waters and the system of faults in the pre-Muddy Creek rocks is apparently needed in the Lake Mead area to trigger the release of seismic energy by reduction of effective normal stress on fractures that are al-

ready sustaining shear stress near the point of failure. Our evaluation of the late Cenozoic geologic setting and history of the Lake Mead area indicates that nowhere should we expect to find a shortage of such fractures at hypocentral depths, but beneath the eastern basin the requisite hydraulic connection is missing.

An alternative explanation of the aseismic character of the eastern basin was suggested to us by R. C. Bucknam (written commun., 1974). The plastic yield of subsurface salt might result in a rather uniform redistribution of the concentrated surface load over the fractured bedrock at potential focal depths. Areas in which the concentrated load is not redistributed owing to plastic flow might be subjected to more localized loading, stress concentrations, and numerous small earthquakes.

In the eastern basin–Overton Arm area, the distance to which subsurface salt could tend to redistribute stress is limited by the contact between the bedrock and the basin-fill sediments (fig. 3), and in general it would be somewhat less than that distance. Where known, the actual distance is considerably less than the distance to which epicenters extend into areas of bedrock surrounding the western basin. The strongest vertical deformation reported by Carder (1970) occurred between the eastern basin and the bedrock area of the South Virgin Mountains (fig. 3). The maximum possible distance to which salt could tend to redistribute stress there is less than one-third of the distance to which seismicity extends beneath bedrock in the western basin area. Thus, even if the salt does serve to redistribute stress by plastic flow, the resultant stress would be sufficiently localized to produce seismicity if loading is the main cause of that seismicity. Because of these spatial relationships we favor an explanation related to fluid pressure as stated.

REFERENCES CITED

Anderson, R. E., 1969, Notes on the geology and paleohydrology of the Boulder City pluton, southern Nevada, *in* Geological Survey research 1969: U.S. Geol. Survey Prof. Paper 650–B, p. B35–B40.

———1971, Thin skin distension in Tertiary rocks of southeastern Nevada: Geol. Soc. America Bull., v. 82, p. 43–58.

———1973, Large-magnitude late Tertiary strike-slip faulting north of Lake Mead, Nevada: U.S. Geol. Survey Prof. Paper 794, 18 p.

Anderson, R. E., Longwell, C. R., Armstrong, R. L., and Marvin, R. F., 1972, Significance of K-Ar ages of Tertiary rocks from the Lake Mead region, Nevada-Arizona: Geol. Soc. America Bull., v. 83, p. 273–288.

Carder, D. S., 1945, Seismic investigation in the Boulder Dam area, 1940–1944, and the influence of reservoir loading on earthquake activity: Seismol. Soc. America Bull., v. 35, p. 175–192.

———1970, Reservoir loading and local earthquakes, *in* Adams, W. M., ed., Engineering seismology—The works of man: Geol. Soc. America Eng. Geology Case Histories, no. 8, p. 51–61.

Carder, D. S., and Small, J. B., 1948, Level divergencies, seismic activity, and reservoir loading in the Lake Mead area, Nevada and Arizona: Am. Geophys. Union Trans., v. 29, p. 767–771.

Fleck, R. J., 1970, Age and possible origin of the Las Vegas Valley shear zone, Clark and Nye Counties, Nevada: Geol. Soc. America Abs. with Programs, v. 2, no. 5, p. 333.

Lara, J. M., and Sanders, J. I., 1970, The 1963–64 Lake Mead Survey: U.S. Bur. Reclamation, Rept. REC–OCE–70–21, 162 p.

Longwell, C. R., 1936, Geology of the Boulder Reservoir floor, Arizona-Nevada: Geol. Soc. America Bull., v. 47, p. 1393–1476.

———1960, Possible explanation of diverse structural patterns in southern Nevada: Am. Jour. Sci., v. 258–A (Bradley volume), p. 192–203.

———1963, Reconnaissance geology between Lake Mead and Davis Dam, Arizona-Nevada: U.S. Geol. Survey Prof. Paper 374–E, 51 p.

Longwell, C. R., Pampeyan, E. H., Bowyer, Ben, and Roberts, R. J., 1965, Geology and mineral deposits of Clark County, Nevada: Nevada Bur. Mines Bull. 62, 218 p.

Lucchitta, Ivo, 1972, Early history of the Colorado River in the Basin and Range province: Geol. Soc. America Bull., v. 83, p. 1933–1948.

Mannion, L. E., 1963, Virgin Valley salt deposits, Clark County, Nevada, *in* Symposium on salt, Cleveland, 1962: Cleveland, Northern Ohio Geol. Soc., p. 166–175.

Morgan, J. R., 1968, Structure and stratigraphy of the northern part of the South Virgin Mountains, Clark County, Nevada: Albuquerque, New Mexico Univ., M.S. thesis.

U.S. Geological Survey, 1972, Geological Survey research 1972: U.S. Geol. Survey Prof. Paper 800–A, p. A43.

Wilson, E. D., and Moore, R. T., 1959, Geologic map of Mohave County, Arizona: Arizona Bur. Mines, scale 1:375,000.

Jour. Research U.S. Geol. Survey
Vol. 3, No. 3, May–June 1975, p. 345–361

ROCKFALL SEISMICITY—CORRELATION WITH FIELD OBSERVATIONS, MAKAOPUHI CRATER, KILAUEA VOLCANO, HAWAII

By ROBERT I. TILLING, ROBERT Y. KOYANAGI, and ROBIN T. HOLCOMB,
Hawaiian Volcano Observatory, Hawaii

Abstract.—During August 7–13, 1972, intense and sustained rockfall activity occurred in Makaopuhi Crater on the east-rift zone of Kilauea Volcano. In a 4-day period (August 7–10), approximately 270,000 m^3 of rockfall debris accumulated in Makaopuhi's west pit, representing a total kinetic energy release of about 10^{19} ergs. Because the rockfalls happened within an area with an established seismic network, it was possible to correlate the seismic record of the rockfalls with onsite field observations. The seismic signatures of rockfalls are generally distinguishable from those of earthquakes and other recorded events. Approximate magnitudes determined for some of the largest rockfalls range from 0.8 to 1.2, corresponding to calculated seismic energy releases of 2×10^{11} to 10×10^{11} ergs, if the magnitude-energy relationship for earthquakes is applicable to rockfalls. The August 1972 swarms of rockfalls at Makaopuhi correlate in time not with moderate or large earthquakes but rather with local eruptive activity and are inferred to have been caused by eruption-induced modifications of stress patterns of the crater walls. However, the amount and nature of the stress change required to exceed the threshold stability of the crater wall and to trigger a rockfall flurry cannot be determined. The Makaopuhi activity is typical of most major rockfall episodes in other Kilauean pit craters in recent years, which also have been associated with volcanic activity, particularly during times of changes in eruptive behavior.

Landslide phenomena (avalanches, earthflows, rockfalls) have been studied intensively by civil engineers, engineering geologists, and geomorphologists but have received scant attention from seismologists. To our knowledge, very few publications contain mention of instrumentally recorded seismicity presumed to be generated by landslides. Richter (1958, p. 155, 156) describes ground motions thought to have been produced by slumps related to petroleum-drilling operations near Terminal Island, Calif. Rockfalls have long been observed at Kilauea (for example, Jaggar, 1930a, b), and even with the rather crude seismic instruments in operation shortly after the Hawaiian Volcano Observatory was established in 1912, attempts were made to distinguish between "seisms" and "tremors" of the "avalanche type" and those clearly of earthquake origin (see any volume of the Hawaiian Volcano Observatory Bulletin). Records from the modern dense seismic network on the island of Hawaii (fig. 1) indicate that rockfalls generate characteristic seismic signals that may be used to monitor such activity on remote areas of the volcano. The seismic network consists of 35 telemetered stations and two independent stations (one at Hilo and the other at Haleakala, Maui).

This report describes some especially vigorous rockfall activity at Makaopuhi pit crater (fig. 2) during August 1972, the most intense and sustained such activity recorded in recent years. Some of the largest rockfalls were observed, timed, and photographed, thus permitting correlation of the on-the-scene observations with the seismicity generated by the rockfalls. This provided an opportunity to calibrate the response of the seismic network to the rockfalls and thereby interpret the seismic records for rockfalls not directly observed. This report is intended to draw special attention to the potential of using seismic techniques in investigations of landslide processes.

Acknowledgments.—We gratefully acknowledge the help of our colleagues at the Hawaiian Volcano Observatory, who have participated in some of the field excursions to Makaopuhi Crater and provided stimulating discussion regarding the nature and causes of the rockfalls observed. We also thank G. F. Kaye, National Park Service, and G. A. Macdonald, University of Hawaii. for field observations and photographs of rockfall activity on August 9.

SETTING OF THE ROCKFALLS

Makaopuhi is the largest of several craters that indent Kilauea's east rift zone (fig. 1). Although it may have been much more complex, the formation of Makaopuhi appears to have resulted principally from two episodes of prehistoric collapse of the south flank of the lava shield Kane Nui o Hamo (fig. 2). The first collapse probably produced an elliptical pit about 1.3 km long, 1.0 km wide, and 200 m deep. This pit was partly filled by a lava lake and later flows totaling about 90 m thick. Subsequent collapse centered on the

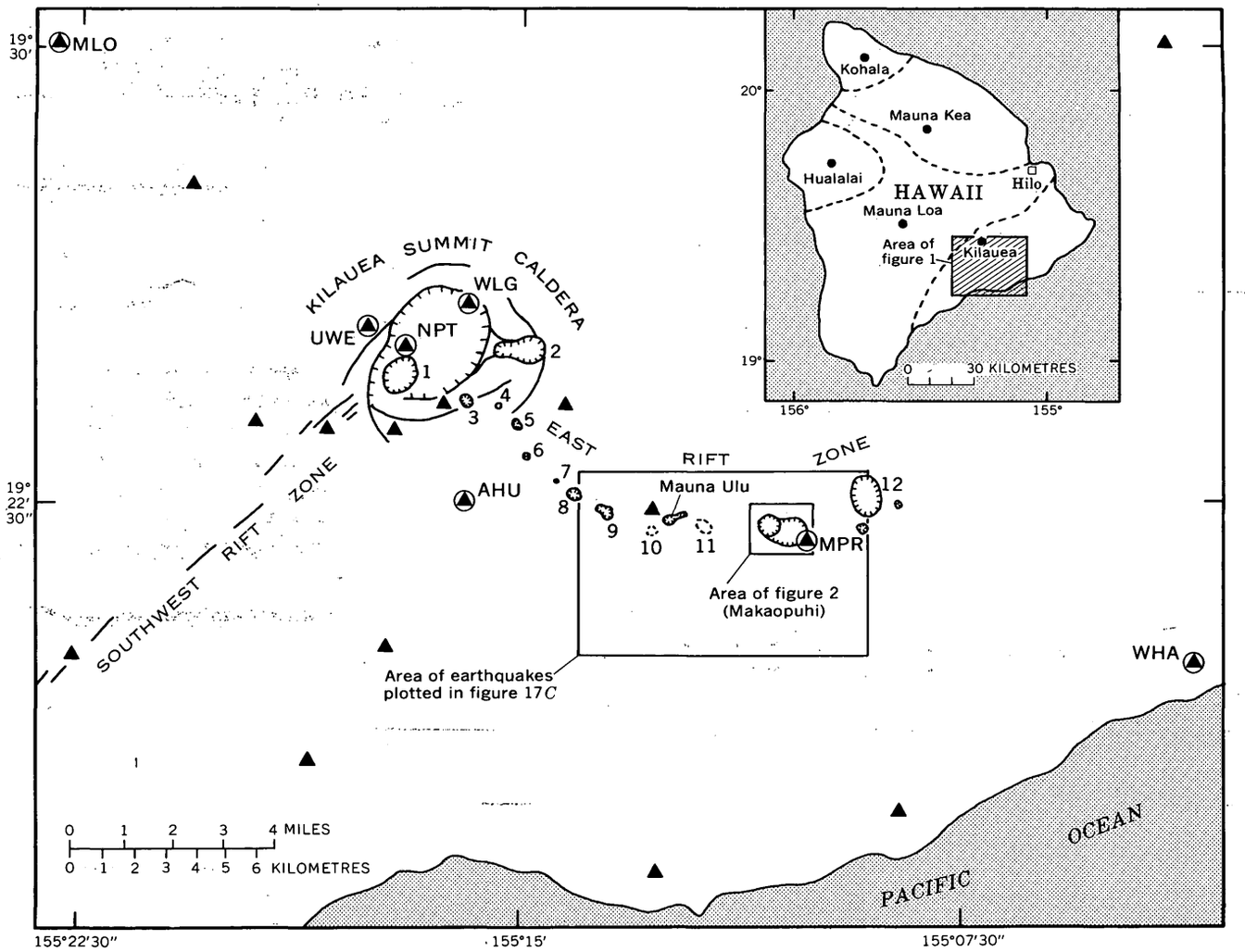

FIGURE 1.—Generalized map showing the location of Makaopuhi Crater relative to the summit caldera and rift zones of Kilauea Volcano. In addition to Makaopuhi, other Kilauean pit craters shown are 1, Halemaumau; 2, Kilauea Iki; 3, Keanakakoi; 4, Lua Manu; 5, Puhimau; 6, Kokoolau; 7, Devil's Throat; 8, Hiiaka; 9, Pauahi; 10, Aloi (buried); 11, Alae (buried); and 12, Napau. Twenty of the 35 telemetered seismic stations operated by the Hawaiian Volcano Observatory are shown by triangles; the stations (MLO, WLG, NPT, AHU, MPR, UWE, and WHA) mentioned specifically in the text are circled. Inset in upper right hand corner shows the five volcanoes that form the island of Hawaii; their summits are indicated by dots.

west rim elongated the crater to about 1.6 km and left the flat floor of the eastern compartment standing as a mezzanine about 200 m above the floor of the western pit.

In historic time Makaopuhi has been partly filled by lavas, and its steep-sided walls have been the site of many rockfalls. In 1922, lava that erupted from the northwest wall of the crater covered the floor of the western pit with a thin veneer (Stearns and Macdonald, 1946). In March 1965, lava that erupted from vents on the northwestern and northern walls produced a lava lake 83 m deep in the western pit and a small lava pad on the mezzanine (Wright and others, 1968). After the 1965 eruption, rockfalls began to litter the crust of the lava lake. Some rocks fell from the southern and eastern walls of the western pit, but most fell from the high north wall of the pit and accumulated as a talus cone adjacent to the main 1965 vent. In addition, a few larger rockfalls from the southeastern wall of the eastern pit littered the margin of the mezzanine. This activity peaked in late 1968 and early 1969 as eruptive activity and earthquakes in the east rift zone apparently triggered more rockfalls. Several rockfalls were recorded on the seismic network, and a few of the larger ones were observed and photographed by the Volcano Observatory staff (fig. 3). In February 1969, lava from fissures west of Makaopuhi cascaded over the western rim of the crater, and an aa

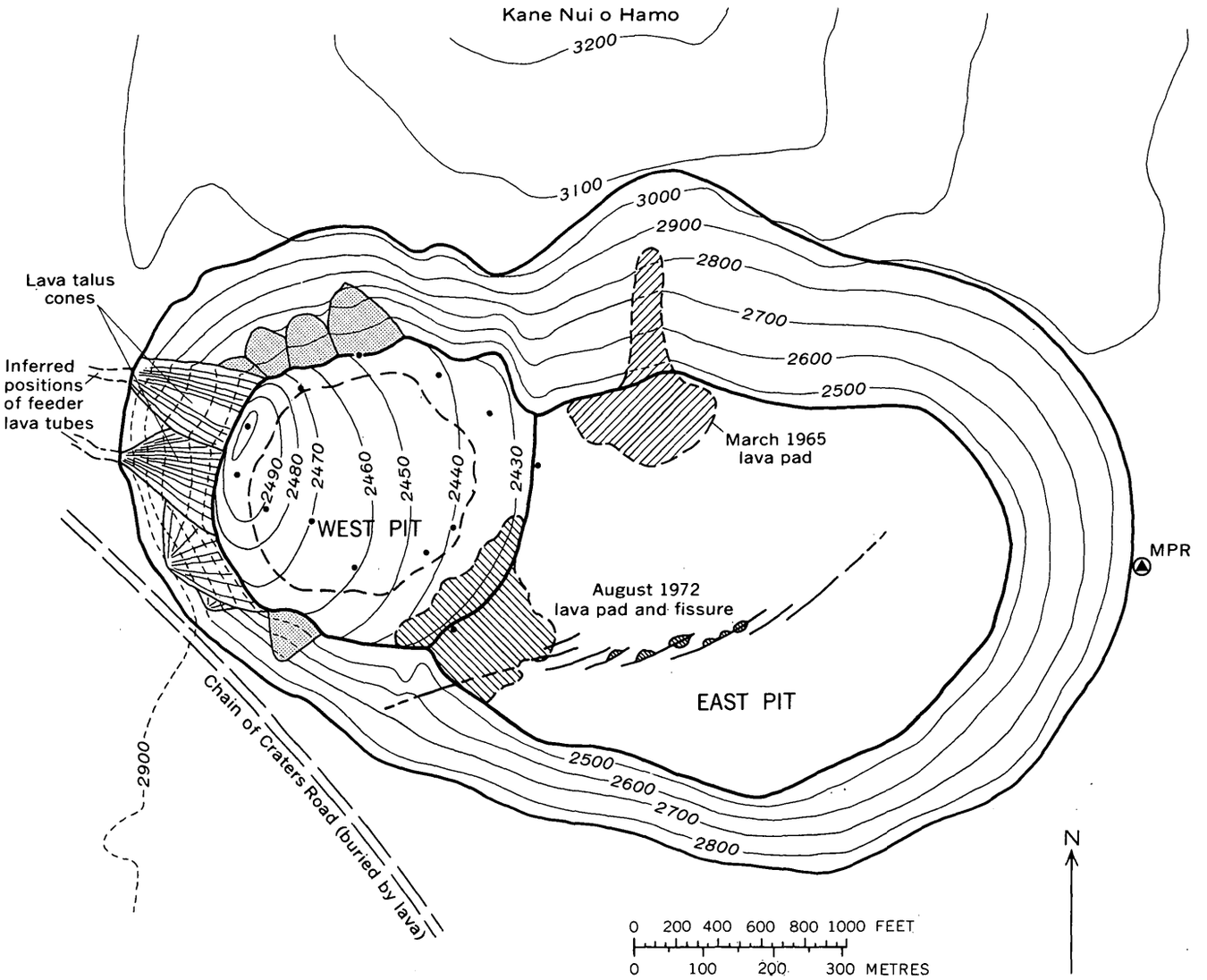

FIGURE 2.—Sketch map, refined by transit measurements and aerial photographs, showing the configuration of Makaopuhi Crater on August 10, 1972, and the distribution of rockfalls (shaded) in its west pit. The seismic station (MPR) closest to the site of rockfall activity is located on the eastern rim. The topographic base is from the Makaopuhi Crater 7½-min quadrangle (1:24,000) of the U.S. Geological Survey (1963) modified by elevation data obtained by transit measurements. The inferred buried perimeter of the west pit (dashed line) after the March 1965 eruption is estimated from the data of Wright, Kinoshita, and Peck (1968). Stations in the west pit used for repeated transit measurements are indicated by dots.

flow about 3 m thick covered much of the 1965 lake surface (Swanson and others, 1975). In 1969 eruptive activity was localized at Mauna Ulu (Swanson and others, 1971) about 3 km west of Makaopuhi, and rockfalls in Makaopuhi temporarily ceased.

From March 1972 to March 1973, the west pit of Makaopuhi intermittently received tube-fed lavas from the Mauna Ulu–Alae region (Tilling and others, 1973). Inflow continued, with variations in rate but no interruptions, from mid-June through late August of 1972 and almost filled the west pit to the level of the mezzanine (fig. 4). All the lava filling the west pit originated from the Alae vent, except possibly for lava fed by a brief, small-volume fissure eruption on the mezzanine observed on August 9 and 10 (fig. 4). (The precise beginning of the mezzanine eruption is not known but can be bracketed between late afternoon of August 7 and early morning of August 9.) Peak rockfall activity coincided with the eruptive outbreak on the mezzanine, suggesting a genetic association between them. Inflow from Alae vent apparently stopped in late August but then resumed sporadically and less copiously in succeeding months. At the end of the final inflow in March 1973, the west pit was completely filled by a

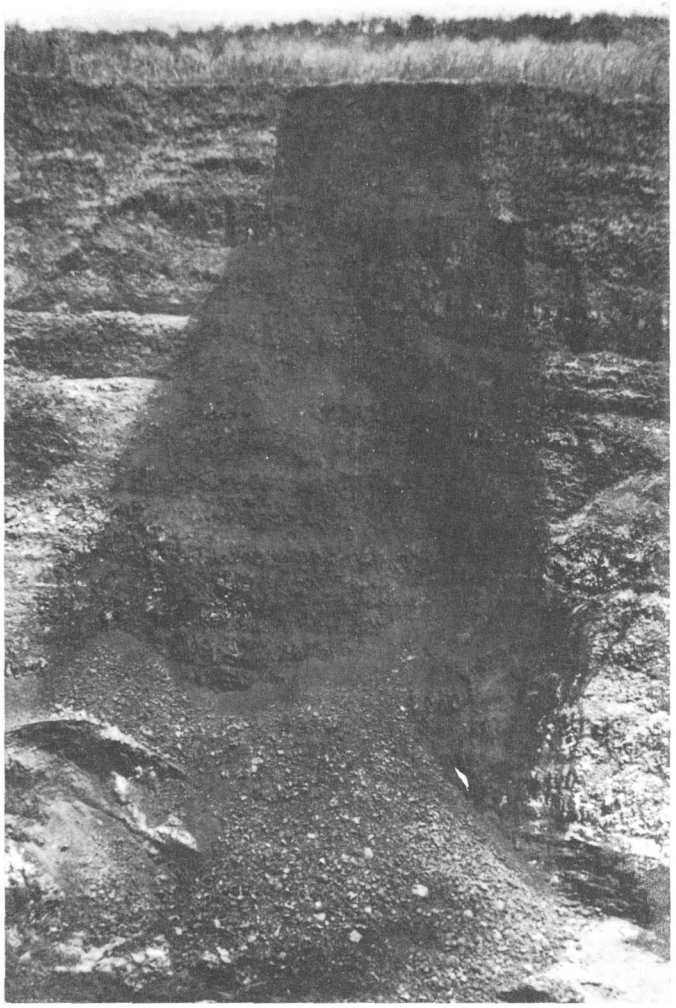

FIGURE 3.—View of the north wall of Makaopuhi's west pit immediately after a rockfall in March 1969, showing the dark fresh scar and rockfall talus. The vertical distance from the rim to the crater floor is approximately 220 m. Part of the March 1965 spatter cone can be seen in the lower left corner. (Photograph courtesy of J. C. Forbes.)

lava pile which spread over nearly two-thirds of the east-pit floor. This partial filling of Makaopuhi Crater, like the earlier complete filling of Alae Crater (Swanson and others, 1972), was complex.

FIELD OBSERVATIONS OF THE ROCKFALLS

During June–August 1972, periodic observations were made to measure the rate of filling of the west pit of Makaopuhi and to document the accumulation of lava-talus cones by the infalling of lava against the west wall of the crater. A few rockfalls occurred during June and July, but not until early August did we begin to take special notice of the rockfall activity. Table 1 summarizes all observed and inferred rockfall activity in Makaopuhi during August. Observations

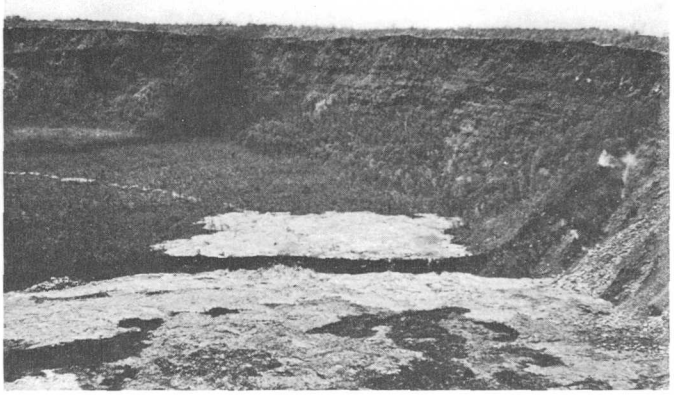

FIGURE 4.—View of Makaopuhi on the morning of August 10, 1972, from its west rim showing the fissure and lava pad related to the eruptive outbreak in its east pit (mezzanine). Two active lava cascades over the mezzanine brink into the west pit may be seen in the southern (right hand) part of the August 1972 lava pad. The surface of the lava in the west pit (foreground) was approximately 9 m below the mezzanine at this time.

were made from vantage points along the rim of Makaopuhi, from the mezzanine, and from the floor of the west pit itself during a leveling survey on August 10 (during which wary glances were cast at the crater walls).

Rockfall activity on August 10, 1972

The most complete observations of rockfalls were made on August 10. We consider the activity on that day to be representative of the more vigorous activity during the August 7–13 period. On the morning of August 10, Makaopuhi had the general configuration shown in figures 2 and 4. Three coalescing rockfall-talus cones against the north wall had accumulated since late afternoon of August 7 (fig. 5); another large cone lay against the south wall. Numerous small rockfalls trickled down the north wall nearly continuously. Lava from the mezzanine fissure vent, first observed on August 9, continued to spill into the southeastern part of the west pit, while lava entered the west part of this pit via the tube system leading from Alae (figs. 2 and 4). The floor of the west pit was a broadly domical surface gently sloping toward the mezzanine; much of the floor periphery consisted of a low moatlike area several meters wide into which lava tended to flow.

Observed rockfalls on August 10 typically began as a cohesive mass that slowly but perceptibly peeled away from the wall. Within seconds after the onset of downslope movement, however, the mass fragmented as it fell (fig. 6), forming a shower of debris ranging from blocks measuring several meters in diameter (fig. 7) to

TABLE 1.—*Summary of rockfall activity in the west pit of Makaopuhi Crater during August 1972*

[N.o., no observations]

August	Onsite observations			Large rockfalls recorded seismically			
	Rockfall time [1]	Rockfall location	Remarks	Time [2]	Approximate duration (s)	Magnitude [3] (M_b)	Seismic energy [4] release (ergs)
1	------	N.o	N.o	-------	------	------	--------
2	------	Scattered	Very infrequent and small	-------	------	------	--------
3	------	N.o	N.o	-------	------	------	--------
4	------	Mainly west wall	Few and small	-------	------	------	--------
5–6	------	N.o	N.o	-------	------	------	--------
7	≈1130	Mainly north wall, but widespread.	During observation period (morning and afternoon) rockfalls generally small but nearly continuous.	1938 S	54	1.1	7×10^{11}
	≈1200			2022 S	45	1.1	7×10^{11}
	≈1600						
8	------	N.o	N.o	-------	------	------	--------
9	------	All around pit, but mainly north wall.	Many rockfalls some very large; photographed but not timed by observers.	1120 M	62	0.8?	2×10^{11}
				1244 M?	64	0.8?	2×10^{11}
				1501 M	72	0.8?	2×10^{11}
				1837 S	49	0.8?	2×20^{11}
				1844 M	76	0.8?	2×10^{11}
10	1055	North wall	Nearly continuous rockfalls in various parts of the pit, but mainly off north wall.	0021 M?	94	0.8?	2×10^{11}
	1107			0640 M?	50	0.8	2×10^{11}
				0704 M	57	0.8	2×10^{11}
	1155*			1156 M	113	1.2	1×10^{12}
	1205*			1206 M	242	1.1	7×10^{11}
	1213	South wall	-------	------	------	--------	
	≈1230	Nose of northern lava tube, west wall.	Large rockslide. As impressive visually as many of the rockfalls, but little seismicity recorded.	-------	------	------	--------
	1625	South wall, near west edge of mezzanine.	-------	1340 M	151	1.1	7×10^{11}
11	≈0900	North wall	Many small falls closely spaced in time.	0528 M?	65	0.8?	2×10^{11}
	1053	Northern lava tube, west wall.	Scattered smaller falls elsewhere, but mainly the north and south walls.	-------	------	------	--------
	1058						
12	0900	Uncertain	Evidenced by large dust cloud observed upon approach to pit.	-------	------	------	--------
13	------	N.o	N.o	0655 S?	56	1.0	7×10^{11}
14–15	------	N.o	N.o	-------	------	------	--------
16	------	N.o	None seen during period of observation.	-------	------	------	--------
17–22	------	N.o	N.o	-------	------	------	--------
23	------	N.o	No obvious activity	-------	------	------	--------
24–31	------	N.o	N.o	-------	------	------	--------

[1] Beginning times (Hawaiian standard time) of moderate or large rockfalls (relative to others observed for a given day). Rockfalls denoted by * were recorded seismically as large falls; time shown may not agree exactly with the more precise timing from the seismic record.
[2] Beginning times of large rockfalls recorded at seismic station MLO, 26 km distant (see text); S, single event; M, multiple event.
[3] Determined from seismic amplitudes measured on Uwekahuna (UWE) Sprengnether short-period records.
[4] Calculated from magnitudes of events after Richter's (1958) equation: $\log E = 9.9 + 1.9\ M_b - 0.024\ M_b^2$, where E is energy in ergs and M_b is magnitude of the local earthquake.

dust-size particles. As they fell onto the talus cone, these fragments were sorted crudely by size so that the coarser debris was concentrated near the base of the cone. During the observed rockfalls, most of the descending debris remained near the crater wall, sliding or bouncing down it. However, many blocks, especially those produced by shattering of originally larger blocks upon secondary impact (against the wall or other blocks) during descent, fell freely for several to many meters before striking the wall again or the floor of the pit. Some blocks traveled considerably farther than other debris and came to rest as much as 10 m beyond the toe of the talus, appearing as isolated blocks on the lava surface. As debris continued to fall from the crater walls, sluggish lava flows slowly engulfed the toes of the cones. Rockfall and eruptive activity overlapped complexly; field relations show that some blocks fell into or were partly buried by molten lava (fig. 8), whereas others came to rest on solidified lava crust.

The rockfalls were accompanied by tremendous crashing sounds and copious clouds of dust, some of which rose 100 m or more into the air. We were too close to the source to photograph the large dust plumes originating at Makaopuhi, but figure 9 shows a similar rockfall-generated dust cloud at Mauna Ulu in May 1973. The large rockfalls generally were preceded and followed by flurries of smaller rockfalls. On one occasion a rockfall from the north wall was followed within seconds by a flurry of smaller rockfalls, not only in the vicinity of the original fall but also elsewhere along

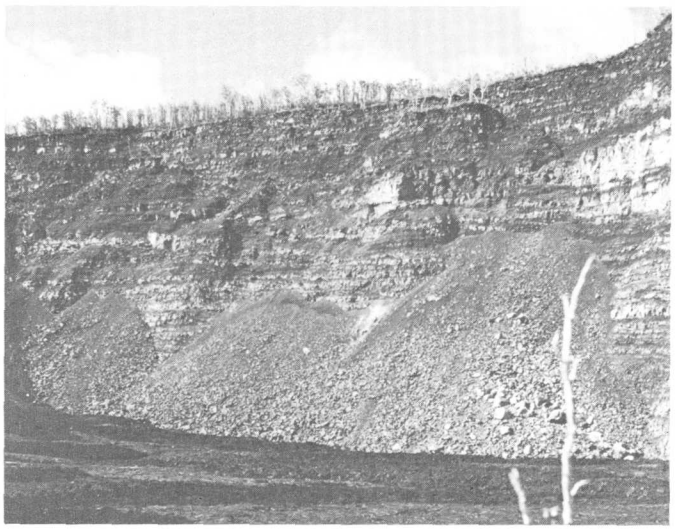

FIGURE 5.—View of the north wall of Makaopuhi's west pit on August 12, 1972, showing the three rockfall-talus cones, which were well developed by August 10 as a result of vigorous rockfall activity that began on August 7 (see fig. 2). Note the small rockfall in progress between the two cones near center of photograph. The vertical distance from the rim to the crater floor is approximately 150 m.

the north wall and, to a lesser extent, the south wall. These observations suggest that large rockfalls may trigger smaller rockfalls. Because of the overlapping nature of the rockfalls, it was not possible in the field to determine precisely the duration of any given rockfall; hence, we recorded only the beginning times of rockfalls visually larger than background activity (table 1). However, in general the larger rockfall episodes lasted about 1 to several minutes.

Estimate of mass of rockfall debris

Because rockfalls were virtually continuous and overlapping during periods of peak activity at Makaopuhi, it was impossible to obtain the repeated field measurements necessary to determine the mass of any given rockfall or series of rockfalls. However, field observations and photographic evidence prove that the major rockfalls shown in figure 2 took place during August 7–10; a much smaller but unknown amount of material was added to these rockfall-talus cones between August 11 and 13. Measurements from a topographic map of the talus cones along the north wall yield a calculated aggregate volume of about 2.7×10^5 m^3 of debris (adjusted for 20 percent open spaces)[1] accumulated during August 7–10. This estimate is crude but probably accurate to within a factor of two or less. Assuming the average bulk density of the rock to be about 2.6 g/cm^3, the total mass of rocks that fell during the 4-d period would be approximately 7.0×10^8 kg, or 7.0×10^5 metric tons.

Assuming complete transformation of gravitational potential energy to kinetic energy, the rockfall debris would represent a total maximum energy release of about 10^{19} ergs. Some of the large individual blocks (for example, those shown in fig. 7) have volumes on the order of 10 m^3 and could generate about 4×10^{14} ergs. Similarly, using the same assumptions, the estimated volume of the debris produced in the large rockfall (8,000 m^3) shown in figure 6 would represent an energy release of about 3×10^{17} ergs. A rockfall episode at Mauna Ulu crater on August 31, 1971, that involved about 5,000 m^3 of debris falling approximately 70 m could generate about 9×10^{16} ergs (Hawaiian Volcano Observatory, unpub. data, 1974).

ROCKFALL SEISMICITY

Seismic network

Details concerning the seismic network and instrumentation of the Hawaiian Volcano Observatory have been published elsewhere (Endo and others, 1972; Koyanagi and others, 1972; Koyanagi, 1969); hence only a brief description is given here. Most seismometers in the network are battery-operated, short-period vertical instruments, whose signals are transmitted to the observatory via radio or cable; a few stations are not linked to the observatory. Signals received at the observatory are recorded on 16-mm film by two Develocorders and on smoked paper as well for a few selected stations. The seismic records are read daily, and foci of earthquakes, depending on magnitude or urgency of need for information, are located either manually at the observatory or by computer in Menlo Park or both.

Standard Hawaiian Volcano Observatory telemetered seismic recording systems on the Develocorder film viewer have a peak magnification of 2×10^5 at a period of 0.1 s. For periods between 0.1 and about 1.0 s, the response falls off 6 dB per octave (Endo and others, 1972). With the instrumental response and preset recording speed, our reading capability to differentiate seismic wave frequencies is limited to periods of about 0.1 to 1.0 s (or about 10 to 1 c/s).

Seismic signature of rockfalls

Natural seismic events recorded and analyzed at the Hawaiian Volcano Observatory include local earthquakes, teleseisms, harmonic tremor, and, if pronounced and prolonged, rockfall activity. Other disturbances recorded but not routinely analyzed include

[1] The unadjusted figure (that is, for no open spaces) would be $3.4\times10^5 m^3$; regardless of the amount of open spaces assumed, the calculated kinetic energy rounds out to 10^{19} ergs.

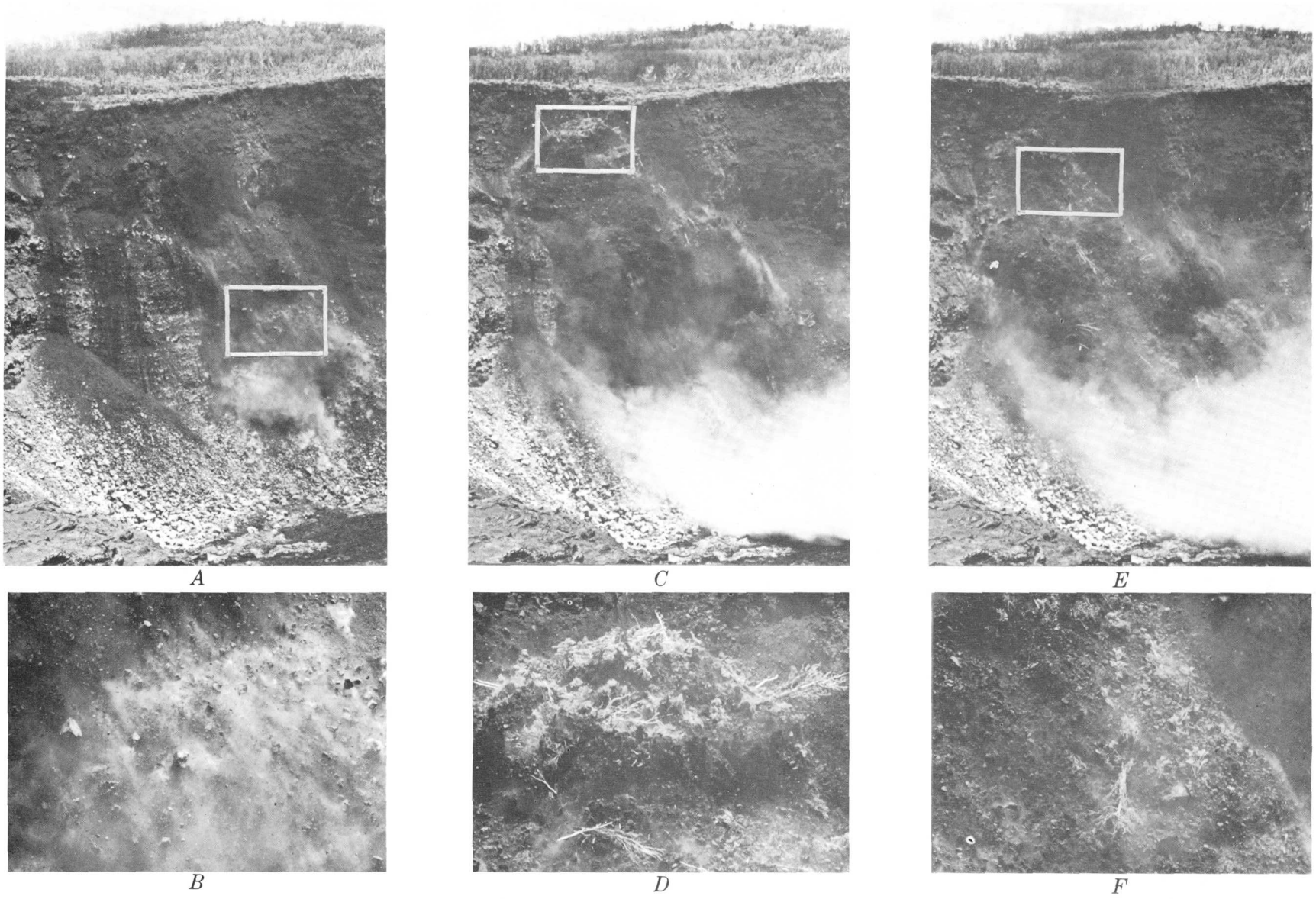

FIGURE 6.—Sequential views of the large rockfall flurry at 1205, August 10, 1972. (See figs. 13, 15, 16, and table 2 for the seismic data recorded for this event.) Trees at the rim are between 6 and 10 m tall. *A*, Photograph taken at 1204 showing a rockfall in progress prior to the collapse of the western half of the block which was already detached from the wall (top center); inset gives the approximate area shown in *B*, a telephoto view taken at about the same time. *C*, Photograph taken at 1205 showing the downward movement and disintegration of detached crater-wall block; inset gives the area shown in *D*, a telephoto view taken a few seconds later. *E*, A view of the rockfall a few seconds later showing complete disintegration of block; inset gives the approximate area shown in *F*, a telephoto view taken at about the same time.

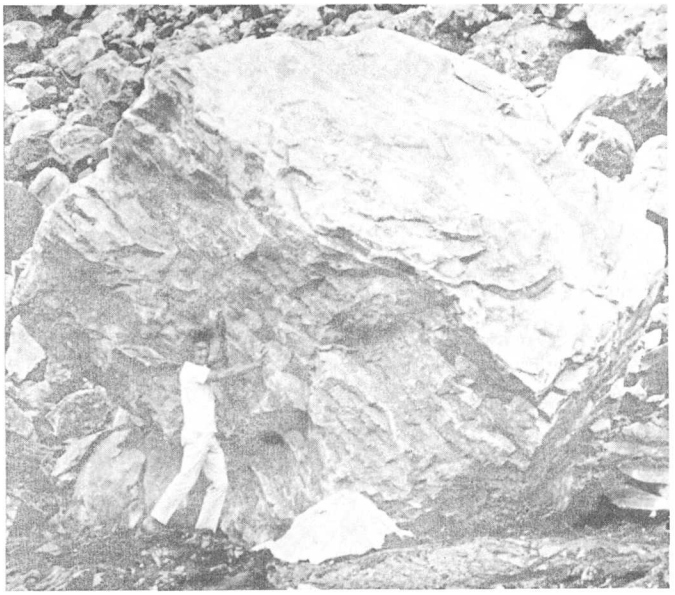

FIGURE 7.—One of the large blocks that fell during the rockfall episode shown in figure 6.

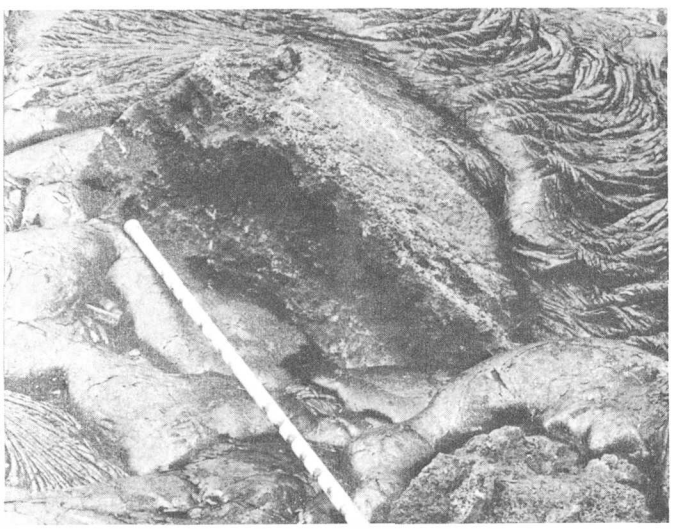

FIGURE 8.—Closeup view showing lava oozing around a block that probably fell into molten, or at least still plastic, lava; markings on range pole are about 3 cm.

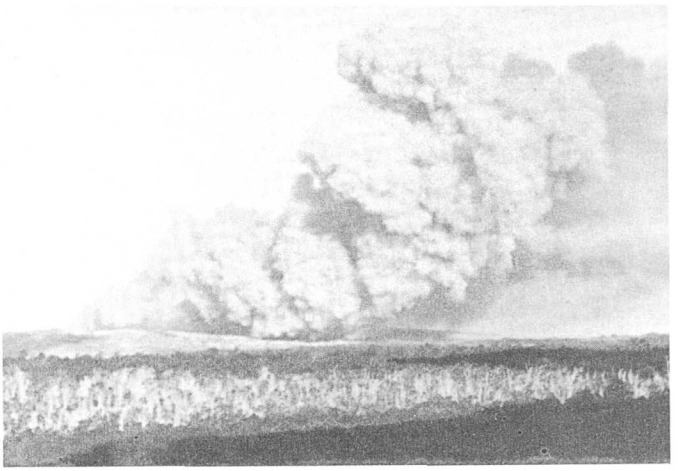

FIGURE 9.—A dust cloud generated by a large rockfall that occurred at Mauna Ulu during May 1973, (photograph taken by J. C. Forbes from the Hawaiian Volcano Observatory approximately 11 km away). The top of the cloud is about 540 m above the ground; this dust cloud was larger than similar clouds generated during the August 1972 rockfall activity in Makaopuhi.

seismic noise related to extreme weather conditions (wind, rain, high surf, lightning, thunder), occasional large quarry blasts, vehicular and pedestrian traffic, and sonic disturbances caused by military firing exercises.

Seismic events are commonly recorded at frequencies varying from about 1 to 10 c/s with diverse amplitude characteristics. Local short-period (S–P) earthquakes occurring near a station yield patterns characterized by very high frequency, large amplitude, relatively short duration, and sharp onset, giving a single-cone appearance to the seismic trace (fig. 10*A*, *a*). More distant but still local earthquakes produce a double-cone pattern characterized by high frequency and distinction between primary (P) and secondary (S) waves (fig. 10*A*, *a*). For local long-period (L–P) quakes, the onset of the seismic phase is emergent (that is, gradual), commonly with some high-frequency waves preceding or superimposed on the predominant low-frequency waves (fig. 10*A*, *b*). The trace for a teleseism shows long-period, nearly sinusoidal P-waves recorded at about 1 c/s; deep events generally have sharper onset (fig. 10*B*, *a*). The waterborne teleseismic phase (T-phase) gives a cigar-shaped pattern with nearly sinusoidal waves recorded at a frequency of about 2 c/s that is generally recorded widely across the seismic network (fig. 10*B*, *b*).

Harmonic (volcanic) tremor (see Finch, 1949; Omer, 1950; Shimozuru and others, 1966), typically recorded before and during eruptive activity, is believed to be caused by movement of lava (surface) or magma (subsurface). This type of continuous microseismic disturbance (fig. 10*C*) may last from several minutes to many days or even many months; recorded frequencies commonly range from about 2 to 5 c/s. Disturbances due to extreme weather conditions, blasting, gunfire, or traffic are not discussed here, but their seismic traces (fig. 10*F–J*), in general, can be readily distinguished from earthquakes, harmonic tremor, and rockfalls (see also Krivoy and others, 1967; Krivoy and Eppley, 1964).

The seismic signature of a rockfall (fig. 10*D*) is characterized by relatively emergent (that is, gradual)

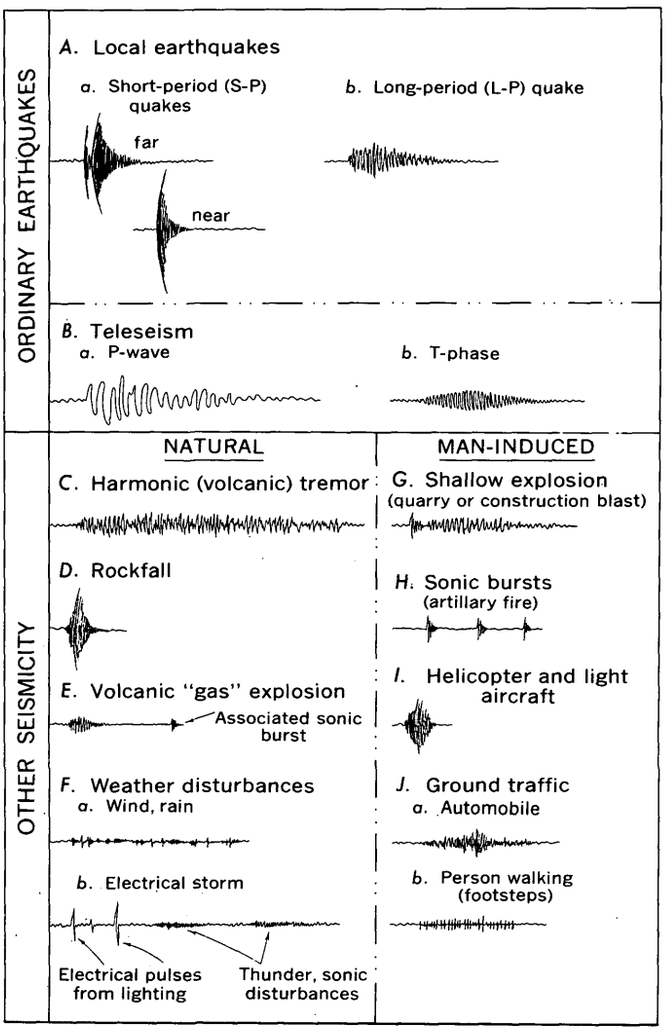

FIGURE 10.—A schematic comparison of various seismic traces of natural and man-induced events. These sketches portray seismic disturbances often observed on 60 mm/min smoke-drum recordings from the stations located around the summit of Kilauea.

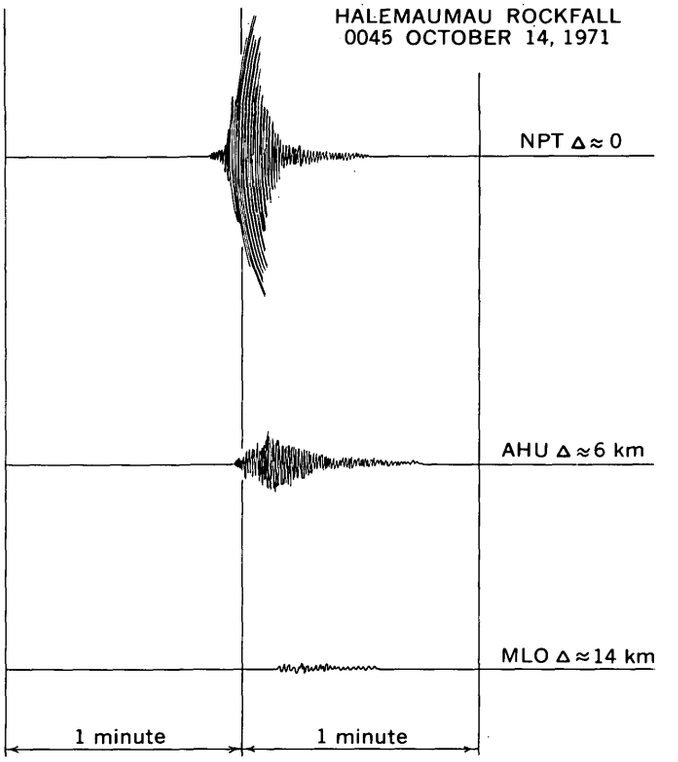

FIGURE 11.—Smoke-drum traces of a rockfall in Halemaumau pit crater, October 1971, showing the differences in seismic signature as recorded by three instruments located at increasing distances from the rockfall site (fig. 1): NPT (≈0 km); AHU (≈6 km); and MLO (≈14 km).

onset, frequencies ranging from 1 to 5 c/s, and high attenuation of signal with increasing distances, especially for the higher frequencies. Figures 11–13 show the actual traces or quantitative depiction of seismic signals as recorded for some rockfalls and earthquakes. The relatively low propagation velocities of rockfalls, as implied by the lag time of the first arrival across the seismic net, reflect the predominance of surface waves. At some stations, the signature of a rockfall may superficially resemble that of an L–P quake. However, on a network-wide basis, the decrease of trace amplitude with distance is noticeably more pronounced for rockfalls than for L–P quakes.

We chiefly analyzed the seismic records of five stations at increasing distances from the west pit of Makaopuhi Crater: (1) MPR, 1 km, (2) AHU, 9 km, (3) WLG, 11 km, (4) WHA, 17 km, and (5) MLO, 26 km (fig. 1). Events recorded only at MPR are defined as small, those recorded at stations from MPR to WLG moderate, and those recorded from MPR to MLO large. However, even large rockfalls were not recorded at stations more distant than MLO.

Velocity, frequency, and duration of rockfall-induced seismic waves

The recorded rockfall-generated seismic waves generally showed emergent arrival times, so that determination of velocity was difficult. Nonetheless, by measuring onset times as well as maximum-amplitude times recorded on various stations we were able to obtain rough apparent velocities. The apparent velocity at distances of several kilometers to about 26 km from Makaopuhi ranges from less than 1 km/s to nearly 2 km/s. This is appreciably lower than body-wave velocities determined from the region beneath the island of Hawaii (Eaton, 1962; Hill, 1969). Surface waves are probably dominant in the wave group observed on the seismograms.

For rockfalls, the seismic waves attenuate rapidly with distance traveled, as expected for shallow seismic

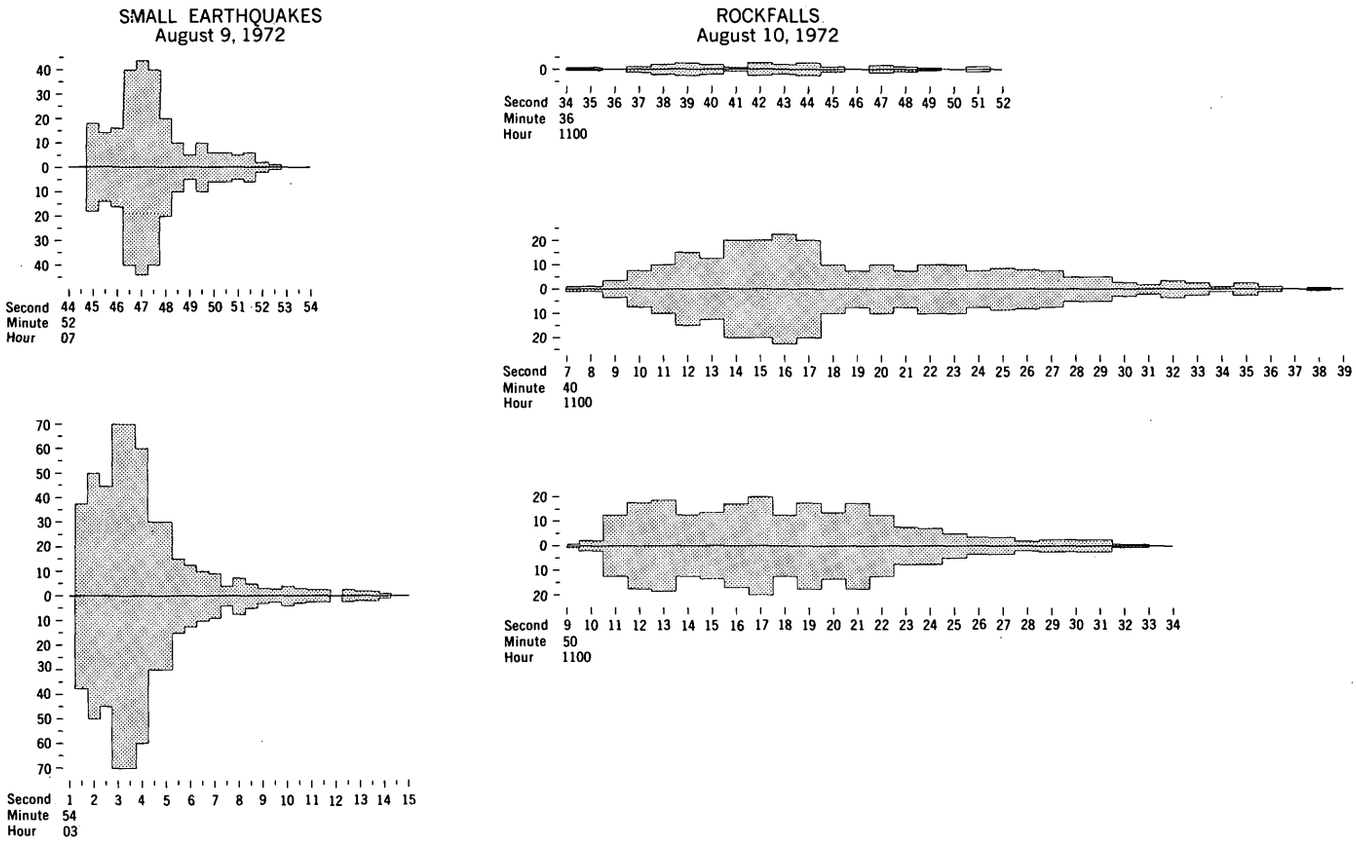

FIGURE 12.—Comparison of the amplitude-duration patterns of small earthquakes of August 9 and rockfalls of August 10, 1972, recorded on the seismograph (MPR) located on the east rim of Makaopuhi Crater (fig. 2). Amplitude readings were made from 16-mm strip-film (Develocorder) recordings magnified to 60 cm/min. The amplitudes were averaged at ½- or 1-s intervals plotted consecutively above and below a zero-amplitude reference line to quantitatively depict the amplitude-duration pattern of the seismic signal.

events (figs. 11, 13). The higher frequency component of the seismic waves attenuates much more rapidly than the lower frequency component. For example, at MPR station the predominant recorded frequency appears to be about 10 c/s, or about our reading threshold for high frequencies, but at AHU station about 9 km away the predominant recorded frequency is about 4 c/s. At MLO station, approximately 26 km from the site of rockfalls, the predominant recorded frequency is still lower, about 1.5 c/s. In general, the recorded predominant frequencies appear to decrease exponentially with distance of the recording stations from Makaopuhi (fig. 14).

Seismic waves generated by small, single rockfalls at Makaopuhi are generally less than a minute in duration, but larger events may last more than 1 min, in general accord with field observations. However, many of the events, especially the large ones, are complicated by the related occurrences of smaller events that tend to prolong the seismic disturbance at nearby stations. In addition, we speculate that the recorded duration also may depend on the nature of the rockfall. For example, a limited number of large, free-falling blocks impacting against a solid surface could result in a seismic trace of relatively large amplitude but short duration. In contrast, an event primarily involving the sliding and breaking up of material might produce a seismic signal of relatively small amplitude but long duration. Although the field and seismic data are inadequate to test these speculations, the lack of obvious correlation between duration and magnitude of large rockfalls (table 1) suggests that the recorded duration does not simply reflect rockfall size.

Seismic energy release of rockfalls

Approximate magnitudes for the large rockfalls were calculated from seismic amplitudes read on Uwekahuna (UWE) Sprengnether short-period records (fig. 1 and table 1). During the interval August 7–13, the fifteen largest rockfalls were 0.8 to 1.2 in magnitude. Using the magnitude-energy relation of Richter

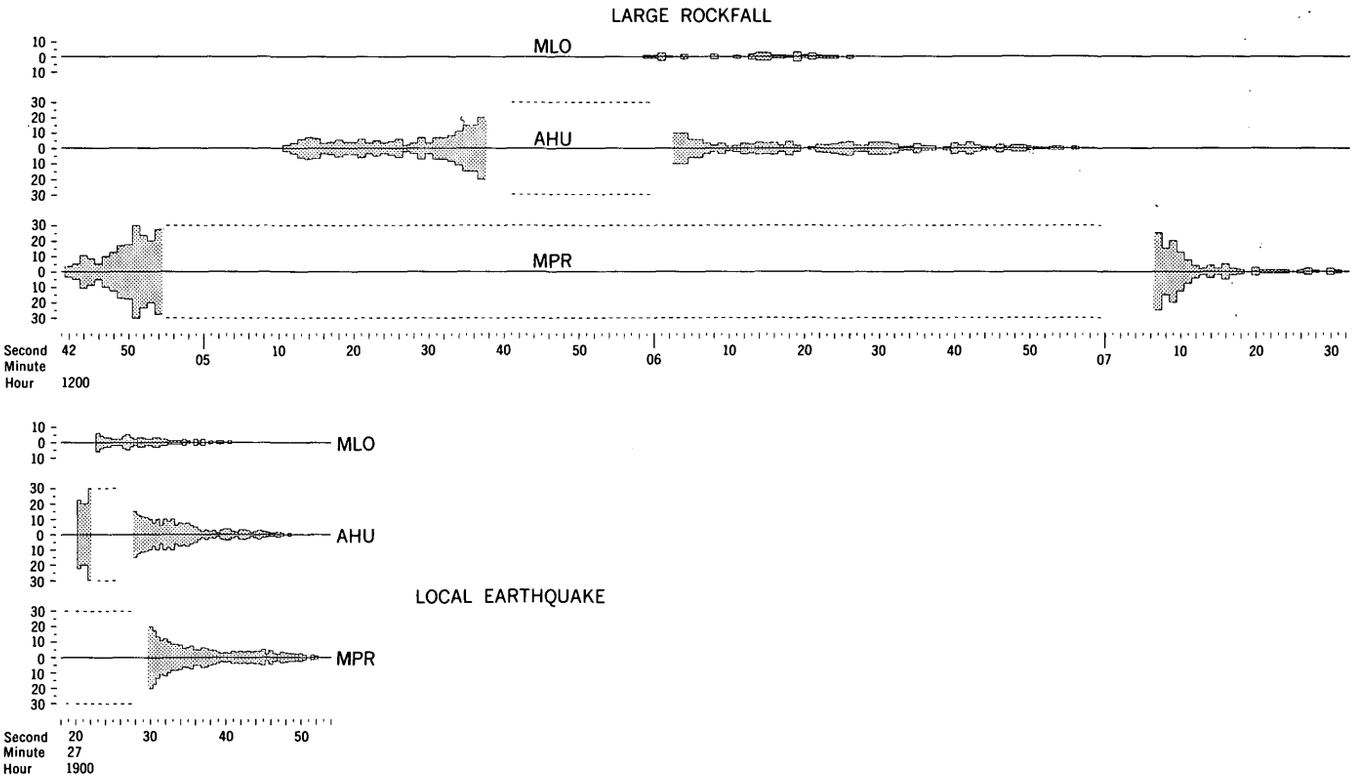

FIGURE 13.—Comparison of the amplitude-duration patterns of the large rockfall at 1206, August 10, 1972 with those of a local earthquake in the Makaopuhi area as recorded by three seismic stations at different distances from the site of the events (fig. 1): MLO, 26 km; AHU, 9 km; and MPR, 1 km. Amplitudes were determined from Develocorder 16-mm film traces and were averaged at 1-s intervals. The dashed portions of the AHU and MPR records indicate clipping of the seismic trace because of high amplitude.

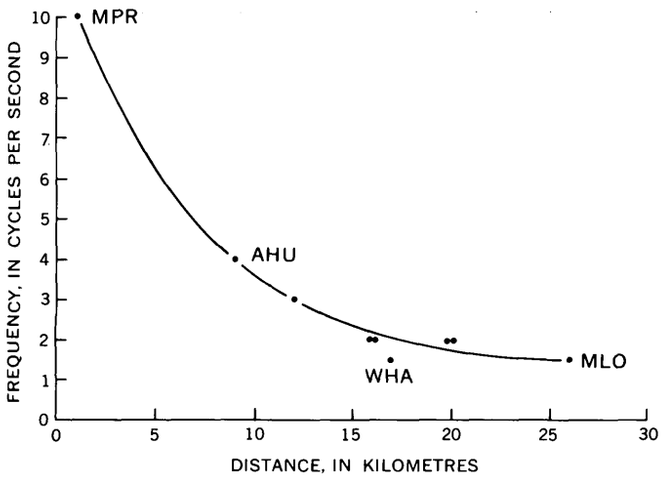

FIGURE 14.—Plot of predominant frequency (cycles per second) against distance of recording seismic station for a rockfall at Makaopuhi Crater, August 1972. See figure 1 for locations of stations denoted by MPR, AHU, WHA, and MLO.

(1958, p. 366) we estimated that the energy release of these events ranges from 2×10^{11} to 1×10^{12} ergs (table 1). If only these large events are considered, a minimum value of total seismic energy generated by the August 1972 rockfalls at Makaopuhi would be about 6×10^{12} ergs. A comparison of the seismic energy release and the kinetic energy release of some observed rockfalls shows no systematic relation between rockfall mass, kinetic energy, and seismic energy (table 2). Although the data given in table 2 are imprecise, they suggest a rather low efficiency of conversion of kinetic energy into seismic energy during rockfalls. The differences between the estimates of kinetic and seismic energies by several orders of magnitude stem partly from the assumptions used in their estimation. The values for kinetic energy are maxima because they assume complete transformation of gravitational potential energy to kinetic energy in frictionless freefall. On the other hand, the seemingly low estimates of seismic energies suggest that rockfall-generated seismicity for any given part largely reflects the impact of a relatively small number of large blocks against solid ground, rather than the total mass involved in downslope movement. Also, because of inherent differences in efficiency of energy transmission between earthquakes (deep) and rockfalls (surficial), Richter's (1958) magnitude-energy relation for earthquakes simply may be inapplicable for estimating the seismic energy of rockfalls.

TABLE 2.—*Comparison of seismic energy release and kinetic energy release of some rockfall events Kilauea Volcano, Hawaii*

Time and place of event(s)	Estimated volume (m^3)	Estimated mass [1] (kg)	Kinetic energy [2] (ergs)	Seismic energy [3] (ergs)
Aug. 31, 1971, at Mauna Ulu summit crater	5,000	1.3×10^{7}	9×10^{16}	4×10^{12}
1206 on Aug. 10, 1972, at Makaopuhi (see fig. 6)	8,000	2.1×10^{7}	3×10^{17}	7×10^{11}
Aug. 7–13, 1972, at Makaopuhi (all rockfalls)	[4] 270,000	7.0×10^{8}	1×10^{19}	[5] 6×10^{12}

[1] Calculated from volume assuming bulk density of rock to be 2.6 g/cm³.
[2] Assumes complete transformation of gravitational potential energy to kinetic energy in frictionless freefall; height of freefall for the Mauna Ulu event is 70 m and for the Makaopuhi events, 150 m.
[3] Calculated from energy-magnitude relation of Richter (1958); see table 1.
[4] Adjusted for assumed 20 percent open spaces in rockfall-talus cones.
[5] Sum of seismic energy for the large rockfalls given in table 1; because the seismic energies of the small and moderate rockfalls cannot be calculated, the value given is a minimum figure.

Seismic record of rockfalls

The proximity of rockfalls to station MPR made continuous monitoring possible, and this seismic record (fig. 15) indicates that rockfall activity, relatively minor between August 4 and 6, increased dramatically on August 7, both in number and in size of falls. The activity, except for a lull on August 11, remained at a high level through the afternoon of August 13 but waned noticeably that evening. Rockfall activity ceased by noon of August 14, but, after a 5-d respite, resumed weakly and intermittently during August 19–22 (fig. 15).

Figure 15 does not distinguish between small and moderate rockfalls but does indicate the times of large events. (See text, last paragraph under "Seismic signature of rockfalls," for size designations.) However, data shown in figure 16 illustrate that relative sizes of rockfalls can be readily determined by detailed study of records from more than one station. Larger rockfalls tend to be more common when the frequency of falls is high (figs. 15 and 16); this is compatible with some field observations that large rockfalls generally are associated with flurries of smaller rockfalls, some of which themselves are possibly induced by the large falls.

The large rockfalls at 1156 and 1206, August 10, that were well recorded seismically were also sufficiently impressive visually to cause onsite observers to take special notice. The seismic record, however, indicates another large rockfall at 1340 that escaped the attention of the observers and was not timed in the field as a large event (table 1). Conversely, the visually and audibly conspicuous rockslide on the west wall observed, photographed, and timed at ≈1230 apparently produced little seismicity; examination of the record for the interval 1215–1245 revealed no significant event, only the background seismicity generated by lava movement and the many small rockfalls from the north and south walls. The 1230 event well illustrates the fact that field and seismic evaluations of comparative rockfall intensity do not always agree.

The feeble seismicity of the 1230 event is puzzling but perhaps reflects one or both of the following factors: (1) The material moved down the gentler lava-talus slope of the west wall primarily by sliding and tumbling instead of free falling, and (2) various parts of the crater floor receiving rockfalls may have differed in gross elasticity related to varying proportions of solidified lava, molten lava, and unconsolidated lava-talus or rockfall-talus debris. If so, these observations imply that the rockfall seismicity is generated mainly by the impact energy of falling rocks striking the wall, crater floor, or previously fallen blocks, rather than by the energy released by fracturing, sliding, and jostling preceding and during the fall. A rockfall into mushy sluggish lava flows would have caused a weaker seismic response than a rockfall of comparable size onto solidified lava crust or unconsolidated but solid debris. Our observations also demonstrate that it might be difficult to attempt to correlate rockfall volume with seismic trace without supporting field observations. The fact that high-energy events can occur unnoticed by onsite

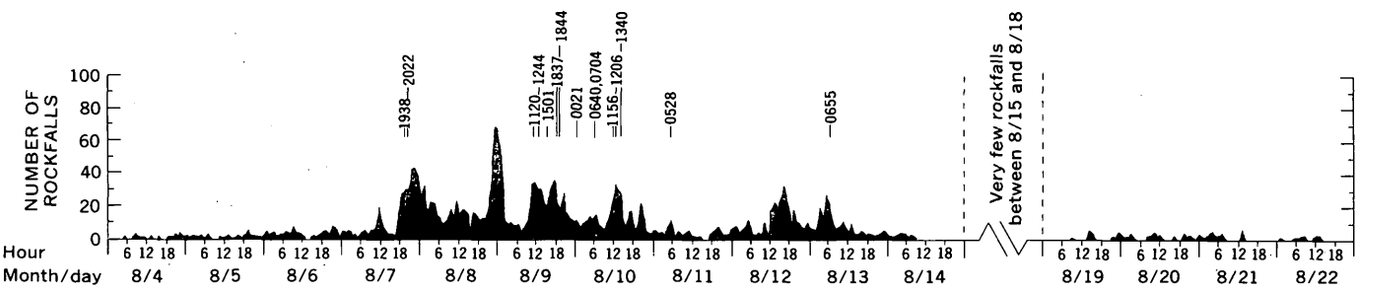

FIGURE 15.—The frequency of rockfalls between August 4 and 22, 1972, at Makaopuhi as recorded at the seismic station (MPR) on the east rim of the crater. The number of rockfalls, plotted on an hourly basis, includes all events regardless of size. However, the times of the large rockfalls (table 2) are indicated above the frequency curve. No rockfalls sufficiently large to be recorded even at MPR, only about 1 km from site, occurred between August 15 and 18.

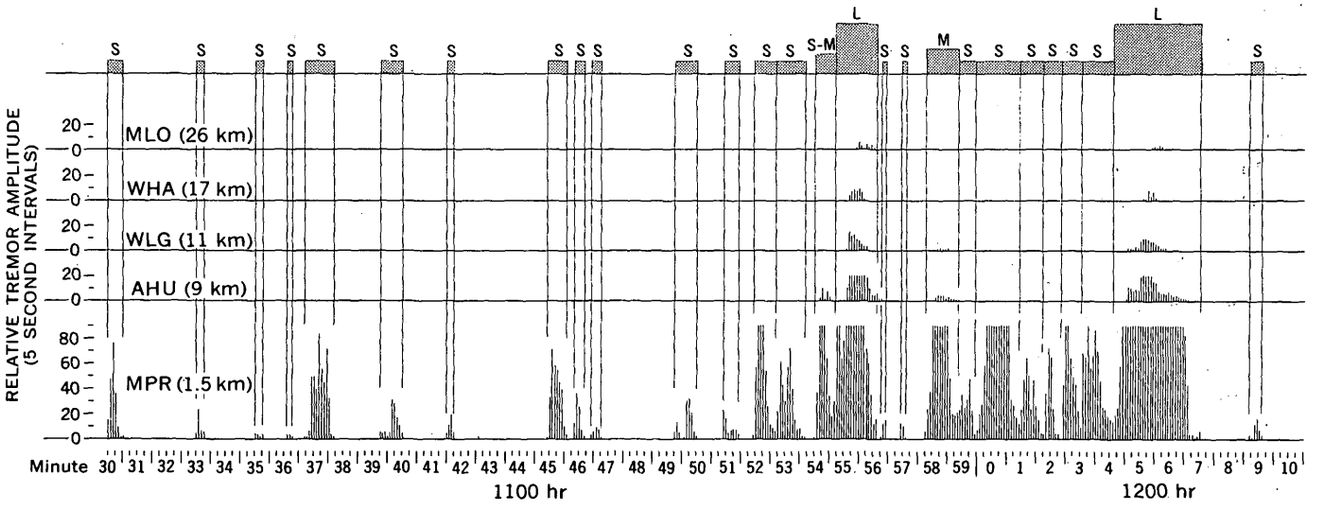

FIGURE 16.—Detailed seismic record of the rockfall activity at Makaopuhi between 1130 and 1210, August 10, 1972, as registered on five selected seismic stations at different distances from Makaopuhi's west pit (see fig. 1 for locations of stations). The letters S, M, and L refer to the arbitrary size classification (small, moderate, and large) based on the seismic trace amplitude. (See text.) In general, the size classifications based on seismicity were confirmed by field observations. Part of the large event at ≈1206 was documented photographically (fig. 6).

Amplitudes were read at 1-s intervals on the 16-mm Develocorder film recordings. To compensate for varying levels of background introduced on the seismic recordings from harmonic (volcanic) tremor in the Mauna Ulu-Alae area and from various microseismic noises, amplitude readings were reduced to an appropriate threshold for each station. The 1-s readings were compiled and averaged for consecutive 5-s intervals; the 5-s averages were then plotted chronologically.

The conspicuous pickup of amplitude for signals from the Makaopuhi station (MPR) is due to the impact of rockfall at Makaopuhi Crater. In general, larger events were recorded at more distant stations, with attenuation, and amplitude peaks delayed according to distance from Makaopuhi. Seismic traces that approached high amplitude and that were inappropriately placed on the film made some measurements difficult. As a partial compensation for this problem, an upper limit of measurement was placed for the purpose of plotting, depending on the readability of each station read.

observers primed to watch for them indicates that seismic instruments may be superior to human observations in identifying such events during periods of intense and overlapping rockfall activity.

CAUSE OF THE ROCKFALLS

The rockfall activity at Makaopuhi Crater during August 7–13, 1972, relative to other recent Kilauean rockfall episodes, was particularly vigorous and sustained. Why did the rash of rockfalls occur there at that time, with only minor activity before and since? Can seismic and other evidence provide clues to possible causes of the abnormally intense rockfall activity?

We recognize that many processes may have acted to weaken or "work" the walls of Makaopuhi prior to the rockfall activity in 1972. One important process probably was the collapse that formed the west pit of the crater itself, resulting in steep-sided, probably oversteepened, walls. In addition, a few relatively incompetent strata (clinkery parts of aa flows, cinder deposits, and other rubbly zones) interlayered with the more massive, ledge-forming lavas have been weathered to form notched, locally undercut areas on the crater walls. Since the initial collapse, doubtless the combined processes of mechanical weathering, mass wasting, deformation associated with pre-1972 eruptions in and near Makaopuhi, and previous minor rockfalls further contributed to slope instability. On the supposition that the walls of Makaopuhi's west pit had been significantly weakened prior to 1972, we have considered the following hypotheses regarding factors that might have triggered the intense rockfall activity: (1) Chain reaction, (2) heavy rainfall, (3) strong earthquakes, and (4) magma movement.

Chain reaction

According to this model, a few small rockfalls of unknown origin undermined and shook the crater wall, triggering larger rockfalls that in turn triggered still larger ones until the peak activity on August 9 and 10. We disfavor this hypothesis because seismic data indicated an abrupt rather than gradual increase of rockfall activity the evening of August 7 (fig. 15). Moreover, field observations showed that the occasional small rockfalls prior to August 7 were distributed widely on both the north and the south walls and not

localized in any one area, as might be expected from chain-reaction processes. It is unlikely that small rockfalls from one wall could initiate rockfalls on the opposing wall 500 m away, although some field evidence suggests that large rockfalls can trigger minor activity on the opposite wall. (See "Rockfall activity on August 10, 1972.")

Heavy rainfall

This process requires vigorous percolation of rainwater into fractured ground to lubricate the contact points between individual blocks until the frictional threshold is exceeded to allow slip and, eventually, fall of the blocks. Minor rockfalls have occurred in Halemaumau and other Kilauean pit craters during and immediately after abnormally heavy rainfalls. However, precipitation records for the observatory area, which generally receives precipitation similar to that received by the Makaopuhi area (Taliaferro, 1959), indicate no precipitation in excess of normal; in fact, records for May–August 1972 show the rainfall to be slightly below average. Also, our field observations at Makaopuhi in August generally were made under sunny conditions or sometimes under intermittent light showers.

Strong earthquakes

The hypothesis that the Makaopuhi rockfalls were caused by an unusually high incidence of moderate to large earthquakes preceding or during the intense rockfall activity is not tenable because seismic data clearly show that the months of July and August were not anomalous in earthquake activity. Only two earthquakes of magnitude 2 to 2.5 (both located within 5 km of Makaopuhi) were recorded in August, which also was low in the total number of quakes (all magnitudes), especially during the interval of intense rockfall activity. (Compare figs. 15 and 17.)

Magma movement

The prime agent in causing the rockfalls may be the deformation associated with surface or subsurface

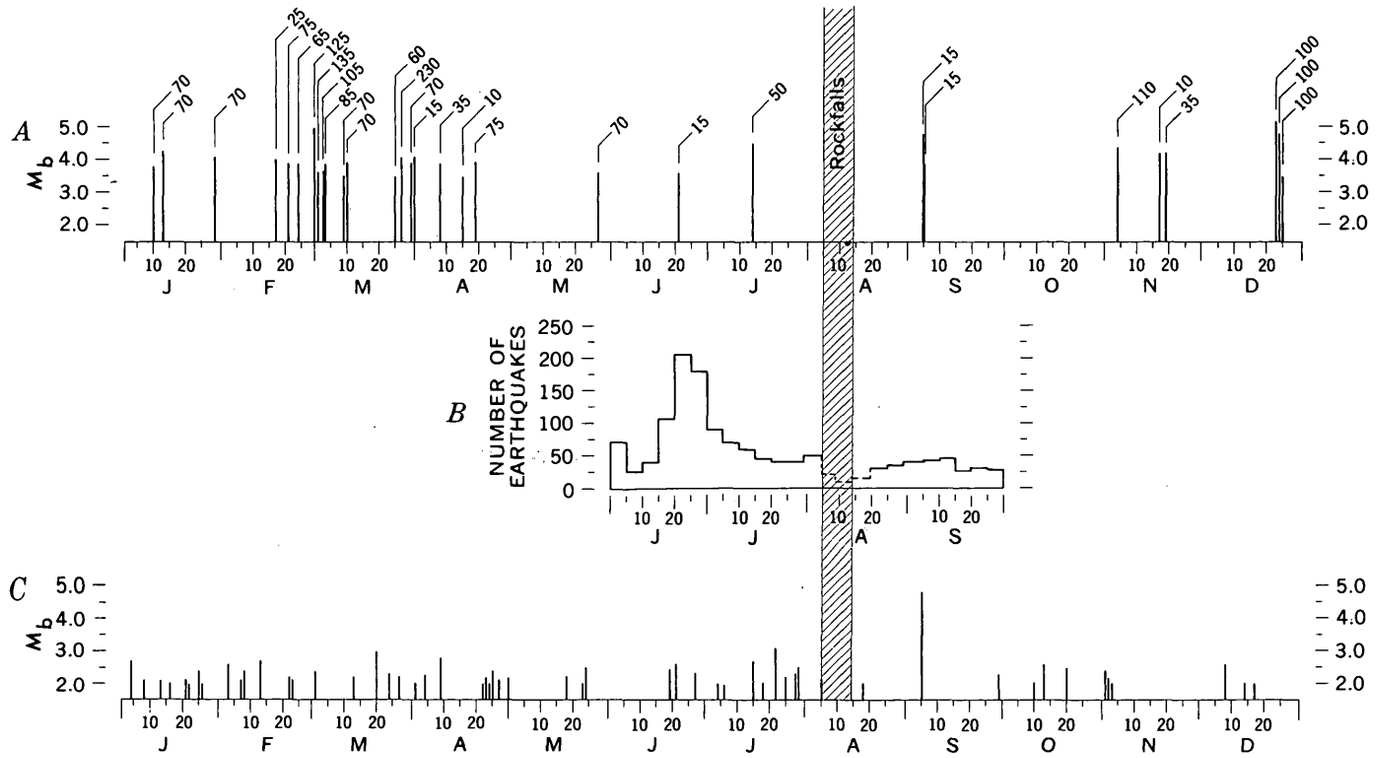

FIGURE 17.—Plot of island-wide earthquakes of magnitude (M_b) ≥3.5 for the calendar year 1972; approximate focal distances in kilometres relative to Makaopuhi's west pit are given by the numbers above each event. *B*, Plot of total number of earthquakes (5-d averages) on Kilauea's upper east rift and adjacent south flank regardless of magnitude. Precise counts of the earthquakes during August 6–14 were not possible because intense rockfall activity and high winds obscured the record. Thus, only large earthquakes that could readily be identified in the seismic records were counted for the August 6–14 interval. The actual total count probably would not exceed the minimum count (shown by dashed line) by more than a factor of two. *C*, Plot of earthquakes of magnitude ≥2 and depths ≤15 km located near the rockfall area within the coordinates lat 19° 20′–23′ N. and long 155° 09′–14′ W. for 1972. (See fig. 1 for location of area relative to Makaopuhi Crater.)

magma movement. Because most major rockfall episodes in Kilauea's caldera and pit craters in the past have been associated with volcanic activity (table 3),

TABLE 3.—*Some notable episodes of rockfall activity at Kilauea Volcano in recent years in pit craters other than Makaopuhi Crater*

[See fig. 1 for locations of sites]

Date	Site	Remarks
December 1962	Aloi Crater (later buried by 1969–70 lavas).	One large rockfall immediately after the short eruption (Dec. 7–9, 1962) and many smaller ones on the next day.
July 1963	Devil's Throat	Numerous small rockfalls during earthquake swarm and ground cracking associated with inferred intrusive event (no lava erupted in the Koae-upper east rift area).
December 1967–July 1968	Halemaumau pit (summit).	Several rockfalls, observed as well as recorded seismically, during the 1967–68 summit eruption (Nov. 5, 1967–July 13, 1968). Also a few rockfalls at Makaopuhi.
February 1969	Alae Crater	Moderate rockfall activity during the February 1969 east-rift eruption. Also some rockfalls at Makaopuhi.
May 1969–summer 1971	Mauna Ulu Crater (and the numerous smaller pits which preceded it).	Rockfalls, commonly observed either directly or indicated by dust cloud (see fig. 9), throughout the eruption, particularly after abrupt lowering of lava-lake levels.
October–November 1971	Halemaumau pit (summit).	Apparently no significant rockfall activity during the September 24–29 eruption; however, the number of rockfalls recorded increased significantly in early October. Moderate activity continued sporadically through November.
February 1972–June 1973	Mauna Ulu Crater and fissure trough; Alae shield (site of former Alae Crater).	With resumption of eruptive activity at Mauna Ulu-Alae, (Feb. 4, 1972), rockfall activity has also resumed.

we favor this hypothesis. Commonly, rockfall activity begins or increases during times of significant changes in eruptive behavior, such as the opening of new vents, changes in old vents, fluctuations in lava-lake levels, and increase in harmonic tremor (Tilling, 1974). Deformation produced by intrusive activity could probably trigger rockfalls. Subsurface magma movement is known to measurably deform the volcanic edifice (for example, Fiske and Kinoshita, 1969; Swanson and others, 1971a, b; Koyanagi and others, 1972), and the persistent jostling of rocks accompanying such deformation should not only prepare the ground for rockfalls but could also trigger them.

Assuming that the Makaopuhi rockfalls, like most Kilauean rockfalls, were produced by volcanic processes, we have speculated on several mechanisms that could have altered the stress patterns in the crater walls to cause them. These mechanisms all assume a genetic link between the rockfalls and the mezzanine eruption but differ according to the following volcanic-structural settings: (1) A local surface lava reservoir, (2) a local subsurface magma reservoir, and (3) a general east-rift dilation.

Local surface lava reservoir.—The rockfalls were triggered by stress changes related to the accumulation of lava in Makaopuhi's west pit. By August 7 lava filling the pit began to exert sufficient hydrostatic pressure to affect the crater walls, exceeding their threhold stability and initiating rockfalls. The increased hydrostatic pressure also caused breakout on the mezzanine of lava injected laterally from the west pit. This mechanism is appealing because it invokes only the observed filling of the west pit; no other structural complexities or volcanic processes are required.

Local subsurface magma reservoir.—Both the rockfalls and mezzanine eruption were caused by local stress-pattern shifts associated with the inflation or deflation of a subsurface magma reservoir near Makaopuhi. (Evidence presented by Jaggar (1930b) and by Richter, Moore, and Haugen (1962) indicates that the widening of cracks around craters, eventually leading to rockfalls, can be caused by either inflation or deflation.) The mezzanine lava was derived from the same reservoir. This mechanism is considered plausible because several lines of evidence suggest that such a subsurface reservoir may have existed and was operative as late as 1969 (Jackson and others, 1975; Swanson and others, 1975; Hawaiian Volcano Observatory, unpub. data, 1975).

General east-rift dilation.—Changes in stress patterns to induce rockfalls and to cause the mezzanine eruption were local responses to a more general dilation of the east-rift zone in the vicinity of Makaopuhi. The fundamental cause of the gross dilation was the movement of magma from Kilauea's summit reservoir into the east-rift zone. This mechanism is attractive because repeated dilations of Kilauea's east rift zone and related mobility of its south flank have been well documented (for example, Fiske and Kinoshita, 1969; Swanson and others, 1971a, b; and Koyanagi and others, 1972).

Several approaches can be used in evaluating the three mechanisms outlined above: (1) Comparison of ground-deformation effects in the vicinity of Makao-

puhi before and after the rockfall swarms in August 1972, (2) comparison of mineralogy and chemistry of the lava erupted on the mezzanine with the mineralogy and chemistry of the 1965 Makaopuhi lavas and 1972 Mauna Ulu–Alae lavas, and (3) analysis of seismicity (earthquake and rockfall) before, during, and after the August activity. Unfortunately, because the previously monitored deformation network in the Makaopuhi area has been destroyed and not reestablished owing to eruptive activity during and since 1969, critical evidence regarding ground deformation is lacking. Although chemical analyses of the mezzanine and other 1972 lavas are not yet available, we anticipate that they could be used to determine whether or not the mezzanine lava is petrologically relatable to lava in Makaopuhi's west pit, thereby providing a test of the local surface reservoir mechanism. At present, however, in lieu of other data, only the approach involving seismic evidence can be considered.

For many weeks prior to the rockfall swarms in August, seismic data for the upper east rift showed an increase in harmonic tremor and, possibly, small earthquakes. Then tremor level decreased beginning about midmorning of August 6 and remained comparatively low throughout the week of intense rockfall activity (August 7–13). We interpret these observations to suggest a period of heightened local dilation and ground vibration caused by near-surface magma movement and injection before vigorous rockfall activity. The overall decrease in tremor after the onset of rockfall flurries may indicate that the stressed areas were relaxing as pressure was relieved when lava eventually broke through to the surface on the mezzanine. However, this interpretation is compatible with any of the three hypothesized mechanisms involving magma movement.

Therefore, presently available data suggest that the Makaopuhi rockfalls in 1972 were caused by ground deformation related to magma movement but are insufficient to pinpoint the exact nature of such deformation and the actual mechanisms that trigger and sustain the intense rockfall activity. Ground-deformation data and more detailed seismic information before, during, and after the activity are essential to identify unambiguously the causes of the rockfalls. In this respect, the deployment of a dense seismic net around Makaopuhi would have been most useful to better determine the locations of small earthquakes and to analyze harmonic tremor more accurately.

A denser seismic network around Makaopuhi would have enabled us to locate more precisely the small earthquakes detected on the MPR station before the major rockfalls. If magma had forced itself along a confined shallow zone from near Alae to the Makaopuhi mezzanine, the hypocentral distribution of the small quakes may provide evidence for such magma movement. A more quantitative analysis of harmonic tremor would probably involve more sensitive and sophisticated instrumentation because of the need to distinguish between the nearly continuous but fluctuating tremor related to activity at the Mauna Ulu–Alae vents approximately 3 km to the west and the tremor reflecting magma movement local to Makaopuhi.

SUMMARY

In about a week's time during August 1972, rockfall activity at Makaopuhi Crater deposited about 2.7×10^5 m^3 of debris in its west pit, representing a maximum total kinetic energy release of about 10^{19} ergs. The calculated combined seismic energy release for the 15 largest events during this interval is about 6×10^{12} ergs, which is a minimum estimate because the seismic energies for many hundreds of small to moderate rockfalls cannot be considered.

Seismic signatures of rockfalls are distinct from those of other seismic events, natural or man-induced, and large falls are recorded at seismic stations as much as 26 km distant. Rockfall seismicity apparently registers mainly the impact energy of blocks falling against solid material (crater wall, floor, or previously fallen blocks) and only subordinately the energy released by fracturing, jostling, and sliding immediately preceding and during downslope movement.

The immediate cause of the rockfalls at Makaopuhi pit crater was sustained local deformation related to volcanism. The rockfall activity in the west pit of Makaopuhi and the eruptive outbreak on the floor of its east pit (mezzanine) were genetically related and were caused by the same dynamic forces. Changes in stress configurations of the crater walls to induce rockfalls are not known but are believed to be related to local deformation caused by magma movement on or beneath the surface in the Makaopuhi area.

Seismic data provide an accurate chronology of rockfalls, estimates of their relative impact energies, and other key information about landslide mechanisms. The seismic network employed in this study was established primarily to record earthquakes and harmonic tremor related to volcanism, but nonetheless we believe our results show the potential of studying rockfall seismicity in certain geomorphology, engineering geology, or geologic hazards investigations. Seismic studies with use of a specially designed network could constitute an important adjunct in systematic research on rockfalls and other landslide phenomena, particularly in areas not amenable to repeated direct field observations because of remoteness or logistic difficulties.

REFERENCES CITED

Eaton, J. P., 1962, Crustal structure and volcanism in Hawaii: Am. Geophys. Union Geophys. Mon. 6, p. 13–29.

Endo, E. T., Koyanagi, R. Y., Okamura, A. T., 1972, Hawaiian Volcano Observatory summary 57, January, February, March 1970: U.S. Geol. Survey, 54 p.

Finch, R. F., 1949, Volcanic tremor, part I: Seismol. Soc. America Bull., v. 39, p. 73–78.

Fiske, R. S., and Kinoshita, W. T., 1969, Rift dilation and seaward displacement of the south flank of Kilauea Volcano, Hawaii, *in* Volume of abstracts *of* Symposium on volcanoes and their roots: Internat. Assoc. Volcanology Chemistry Earth's Interior, Oxford, England, 1969, p. 53–54.

Hill, D. P., 1969, Crustal structure of the island of Hawaii from seismic-refraction measurements: Seismol. Soc. America Bull., v. 59, p. 101–130.

Jackson, D. B., Swanson, D. A., Koyanagi, R. Y., and Wright, T. L., 1975, The August and October 1968 flank eruption of Kilauea Volcano, Hawaii: U.S. Geol. Survey Prof. Paper 890. (In press.)

Jaggar, T. A., 1930a, Meaning of crater avalanches: The Volcano Letter, no. 269, p. 1–3.

——— 1930b, Rim cracks and crater slides: The Volcano Letter, no. 283, p. 1–3.

Koyanagi, R. Y., 1969, Hawaiian seismic events during 1968, *in* Geological Survey research 1969: U.S. Geol. Survey Prof. Paper 650–D, p. D168–D171.

Koyanagi, R. Y., Swanson, D. A., and Endo, E. T., 1972, Distribution of earthquakes related to mobility of the south flank of Kilauea Volcano, Hawaii, *in* Geological Survey research 1972. U.S. Geol. Survey Prof. Paper 800–D, p. D89–D97.

Krivoy, H. L., and Eppley, R. A., 1964, T-phase of May 11, 1962, recorded in Hawaii, *in* Geological Survey research 1964: U.S. Geol. Survey Prof. Paper 501–B, p. B105–B107.

Krivoy, H. L., Johnson, C. G., and Koyanagi, R. Y., 1967, An usual example of pseudo-seisms resulting from military exercises: Pacific Sci., v. 21, p. 119–128.

Omer, Guy C., Jr., 1950, Volcanic tremor, Part 2, The Theory of volcanic tremor: Seismol. Soc. America Bull., v. 40, p. 175–194.

Richter, C. F., 1958, Elementary seismology: San Francisco, W. H. Freeman, 768 p.

Richter, D. H., Moore, J. G., and Haugen, R. T., 1962, Recent growth of Halemaumau, Kilauea Volcano, Hawaii, *in* Short papers in geology, hydrology, and topography: U.S. Geol. Survey Prof. Paper 450–B, p. B53–B56.

Shimozuru, Daisuke, Kamo, Kosuke, and Kinoshita, W. T., 1966, Volcanic tremor of Kilauea Volcano, Hawaii, during July–December 1963: Earthquake Research Inst. Bull., v. 44, p. 1093–1133.

Stearns, H. T., and Macdonald, G. A., 1946, Geology and groundwater resources of the island of Hawaii: Hawaii Div. Hydrography Bull. 9, 363 p.

Swanson, D. A., Duffield, W. A., Jackson, D. B., and Peterson, D. W., 1972, The complex filling of Alae Crater, Kilauea Volcano, Hawaii: Bull. Volcanol., v. 36, p. 105–126.

Swanson, D. A., Duffield, W. A., and Okamura, R. T., 1971a, Seaward displacement of the south flank of Kilauea Volcano [abs.]: Am. Geophys. Union Trans., v. 52, no. 4, p. 372.

——— 1971b, Mobility of Kilauea's south flank related to rift intrusion [abs.], *in* Symposium on volcanism and upper mantle earthquakes: Internat. Union Geodesy and Geophys., 15th Gen. Assembly, Moscow, U.S.S.R., Program, p. 29.

Swanson, D. A., Jackson, D. B., Duffield W. A., and Peterson, D. W., 1971, Mauna Ulu eruption, Kilauea Volcano: Geotimes, v. 16, no. 5, p. 12–16.

Swanson, D. A., Jackson, D. B., Koyanagi, R. Y., and Wright, T. L., 1975, The February 1969 east-rift eruption of Kilauea Volcano, Hawaii: U.S. Geol. Survey Prof. Paper 891. (In press.)

Taliaferro, W. J., 1959, Rainfall of the Hawaiian Islands: Hawaii Water Authority, 394 p.

Tilling, R. I., 1974, Rockfall activity in pit craters, Kilauea Volcano, Hawaii, *in* Volume of abstracts *of* International Symposium on Volcanology: Internat. Assoc. Volcanology Chemistry Earth's Interior, Santiago, Chile, 1974, p. 71–72.

Tilling, R. I., Peterson, D. W., Christiansen, R. L., and Holcomb, R. T., 1973, Development of new volcanic shields at Kilauea Volcano, Hawaii [abs.]: Internat. Union Quarternary Research, 9th Cong., Christchurch, New Zealand, Dec. 2–10, 1973, Program, p. 366–367.

Wright, T. L., Kinoshita, W. T., and Peck, D. L., 1968, March 1965 eruption of Kilauea Volcano and the formation of Makaopuhi lava lake: Jour. Geophys. Research, v. 73, p. 3181–3205.

Jour. Research U.S. Geol. Survey
Vol. 3, No. 3, May–June 1975, p. 363–368

A CHARACTERISTIC PATTERN OF DISEQUILIBRIUM IN SOME URANIUM ORE DEPOSITS

By ELMER S. SANTOS, Denver, Colo.

Abstract.—A redistribution of radium-226 in uranium ore deposits produces a characteristic pattern of disequilibrium in which uranium is greater than equivalent uranium in high-grade samples and equivalent uranium is greater than uranium in low-grade samples. The redistribution is a continuous process in uranium deposits, and the resulting pattern of disequilibrium is itself a system in equilibrium.

Samples of rock from uranium deposits are often analyzed both chemically and radiometrically to determine their uranium contents. If the uranium content determined chemically does not equal that determined radiometrically, the sample is said to be out of equilibrium. This report concerns a distinctive pattern of disequilibrium in uranium ore deposits. In the discussion that follows, use is made of a number of symbols which are defined below.

Equivalent uranium, eU, is a measure of the beta-gamma radioactivity of a sample, reported as the percentage of uranium, in equilibrium, that would produce the measured radioactivity. Equivalent concentrations of certain radioisotopes, denoted as ΣTh^{230}, ΣRa^{226}, and ΣPb^{210}, are expressed, in percentage, as the amount of uranium in radioactive equilibrium required to sustain the measured amounts of these daughter products. Thus, $\Sigma Th^{230} = 0.2$ indicates that the amount of thorium of atomic weight 230 present is that which would be in equilibrium with 0.2 percent uranium.

Acknowledgments.—The interpretations regarding the nature of processes involved in the creation of a pattern of disequilibrium are based largely on chemical and radiochemical analyses of 87 samples from ore deposits in the Ambrosia Lake district, New Mexico. Radiochemical analyses for Pa^{231}, Th^{230}, Ra^{226}, Rn^{222}, and Pb^{210} were made by J. N. Rosholt, Jr.; eU analyses were made by L. M. Lee; U analyses by the volumetric method were made by H. H. Lipp; and U analyses by the fluorometric method were made by D. L. Ferguson. These same analyses were used as the basis of a report on radium migration by Granger (1963).

DISCUSSION

The analyses of samples from many uranium deposits in sandstone display a characteristic pattern of disequilibrium in which U>eU in samples that contain more than 0.1 percent uranium and eU>U in samples that contain less than 0.01 percent uranium. Samples whose content is in the range of 0.01 to 0.1 percent uranium have U≈eU. For some reason, migration of one or more radioelements has peculiarly resulted in consistent radioactive equilibrium only for samples that contain about 0.01 to 0.1 percent uranium and in consistent radioactive disequilibrium in samples whose uranium contents are outside this range. Somehow, the rocks in apparent radioactive equilibrium were not affected by the migration of radioelements or they gained and lost radioelements at the same rate. The object of this paper is to present a conceptual model that explains the pattern of disequilibrium and to show that it is the result of a long-term, continuous process.

Plots of U and eU pairs of analyses illustrating the characteristic pattern were published by Granger, Santos, Dean, and Moore (1961, p. 1206), Finnell, Franks, and Hubbard (1963, p. 35), and Harshman (1972, p. 61). By plotting U and eU pairs of analyses from published and unpublished data, the author found the same pattern in uranium deposits of Texas, Utah, Colorado, Wyoming, and South Dakota. The deposits occur in permeable sandstone host rocks as old as Pennsylvanian and as young as Pliocene age. The source of the data, together with the location of the deposits from which the samples were collected, is shown in table 1.

To test for the possibility that the pattern may be the result of flaws in analytical techniques, using barren rocks, I successively diluted splits of a sample containing 0.75 percent uranium for which analyses indicated U>eU. Analyses of seven splits ranging down to a uranium content of 0.0015 percent showed a consistent pattern in which U>eU. I concluded that

TABLE 1.—*List of localities where ore deposits display a characteristic pattern of disequilibrium*

Mine or district	State	Age of host rock	Source of data
Palangana Dome	Texas	Pliocene	Unpublished.
Pumpkin Buttes	Wyoming	Eocene	Sharp and others (1964).
Mrak mine	do	do	Unpublished.
Crooks Gap	do	do	Stephens (1962).
Gas Hills	do	do	Unpublished.
Hulett Creek	do	Cretaceous	Robinson and Rosholt (1961).
Black Hills	South Dakota	do	Cuppels (1962).
Ambrosia Lake	New Mexico	Jurassic	Granger (1966).
Happy Jack mine	Utah	Triassic	Rosholt (1959).
Garo mine	Colorado	Pennsylvanian and Permian.	Wilmarth (1959).

the natural pattern of disequilibrium seen in many deposits is real.

The pattern of disequilibrium in all the deposits tested could result from a redistribution of uranium in such a way that low-grade parts of a deposit are depleted and high-grade parts are enriched. The pattern could also result from the redistribution of one or more daughter products in such a way that low-grade parts of deposits are enriched and high-grade parts are depleted, or from the redistribution of both uranium and its daughter products. The redistribution could be either a continuous or an episodic process.

The plot of analyses shown by Granger (1963, p. B61, fig. 17.1) indicates that a fair degree of equilibrium exists between U and ΣTh^{230}. Equilibrium between U and ΣTh^{230} would not be likely had there been an enrichment of uranium in the high-grade parts of a deposit and a depletion in the low-grade parts. Such a redistribution of uranium would be expected to produce a pattern in which $U > \Sigma Th^{230}$ in high-grade and $\Sigma Th^{230} > U$ in low-grade parts of a deposit. My interpretation, therefore, is that the characteristic pattern of disequilibrium in the uranium deposits of Ambrosia Lake and elsewhere is not due to the redistribution of uranium. The alternative, then, is to attribute the pattern to the redistribution of one or more daughter products in the decay series of U^{238} and U^{235}.

With but few exceptions, analytical data on the 87 samples indicate that, just as with comparisons of U and eU pairs, $U > \Sigma Ra^{226}$ in high-grade and $\Sigma Ra^{226} > U$ in low-grade samples. Granger (1963, p. B61, fig. 17.2) showed the relative abundances of these two elements in sandstone adjacent to ore (low-grade) and in ore. Th^{230}, the precursor of Ra^{226}, shows no similar abundance relationship with U so it is clear that a redistribution, mainly of Ra^{226}, is the most likely cause for the pattern of disequilibrium. Some losses and gains of other daughter products are indicated by the analytical data, but nothing in the data suggests that these are being systematically depleted in one part and enriched in another part of a deposit.

That uranium deposits other than those at Ambrosia Lake owe their pattern of disequilibrium mainly to the redistribution of Ra^{226} is indicated by the analyses listed by Rosholt (1959, table 2). In all but 3 of 147 samples collected from 15 States $\Sigma Ra^{226} > U$ when $eU > U$ and $U > \Sigma Ra^{226}$ when $U > eU$. There is also a good correlation in the degree of disequilibrium; $\Sigma Ra^{226} \gg U$ when $eU \gg U$.

In order to create a condition in which $\Sigma Ra^{226} > \Sigma Th^{230}$, as in most low-grade samples, an episode of redistribution would have had to occur more recently than 10,000 yr ago. In 10,000 yr, or about six times the half-life of Ra^{226} (1,620 yr), any excess of Ra^{226} not supported by an equivalent quantity of Th^{230} would have decreased by more than 98 percent because of its decay, and the two isotopes would be virtually in equilibrium. To attribute the pattern of disequilibrium to an episodic process would require that more recently than 10,000 yr ago an episode of Ra^{226} redistribution occurred in deposits as widely separated as those in Utah, Texas, and South Dakota, deposits in different geologic settings and in host rocks of different ages. Because such a coincidence is considered highly improbable, I propose that the redistribution of Ra^{226} is a continuous rather than an episodic process.

I tested various conceptual models based on the assumption of continuous redistribution to determine whether a continuous process could produce the characteristic pattern of disequilibrium. The pattern can be produced if it is assumed (1) that some portion of a daughter product in the solid phase goes into solution in all parts of a deposit, and (2) that in equal intervals of time the same percentage of the remaining daughter product in the solid phase is moved. Some or all of the dissolved daughter product is then redeposited uniformly in and near the deposit. The amount redeposited is assumed to be equal to that lost only in rocks that contain 0.01 to 0.1 percent of the redistributed daughter product's precursor. Equilibrium is thus maintained at some value in the range of 0.01 to 0.1 percent. The general equation for a computation based on these assumptions, when losses and gains due to the decay of the redistributed daughter product and its precursor are accounted for, is

$$A\left(\frac{N_o}{2}+\frac{N_a}{2}+\frac{P}{2}\right)=N$$

where A is a fraction related to the rate of loss by solution, N_o equals the initial amount of daughter product in the solid phase, N_a equals the amount of

daughter product redeposited, P equals the amount of the redistributed daughter product's precursor, and N equals the net amount of daughter product in the solid phase after one half-life of the redistributed daughter product. Units of N_o, N_a, P, and N are equivalent percentages. The factor A is related to the fraction lost to solution by $1.0-A=$fraction of the solid phase lost during one half-life of the redistributed daughter product. Thus, when $A=1.0$, the fraction lost to solution is zero and no redistribution occurs.

The fraction related to the rate of loss is an empirical factor determined from pairs of analyses by

$$A=\frac{2\cdot\Sigma Ra^{226}}{U+\Sigma Ra^{226}}$$

where $U>\Sigma Ra^{226}$. The amount of daughter product that must be redeposited uniformly to maintain equilibrium at 0.1 percent is determined by

$$N_a=\frac{0.2}{A}-0.2$$

and for equilibrium at 0.01 percent by

$$N_a=\frac{0.02}{A}-0.02.$$

For a pair of analyses where U=15.2 percent and $\Sigma Ra^{226}=7.02$ percent, $A=0.63$ and $N_a=0.117$ for equilibrium at 0.1 percent and $N_a=0.0117$ for equilibrium at 0.01 percent.

Using $A=0.63$, two sets of calculations were made for $P=0.001$, 0.005, 0.01, 0.05, 0.1, 0.5, 1.0,5.0, 10.0, and 15.2. In one set $N_a=0.117$ to maintain equilibrium at 0.1 percent and in the other set $N_a=0.0117$ to maintain equilibrium at 0.01 percent. In each set of calculations the initial value of N_o, the amount of redistributed daughter product in the solid phase, was assumed to equal zero. The calculations were repeated six times (six half-lives of the redistributed daughter product) for each value of P and with each calculation beginning with the substitution of N for N_o in the next calculation.

The resulting computed values of N approach, asymptotically, a constant value for each value of P. Figure 1 shows the curves generated by connecting successive values of N for $P=0.01$, 0.1, and 1.0. Thus, redistribution of any daughter product according to the model outlined above will result in a pattern of disequilibrium which, after sufficient time, will itself constitute a system in equilibrium.

That the factor A reflects a reasonable approximation of the rates of loss that actually occur is indicated

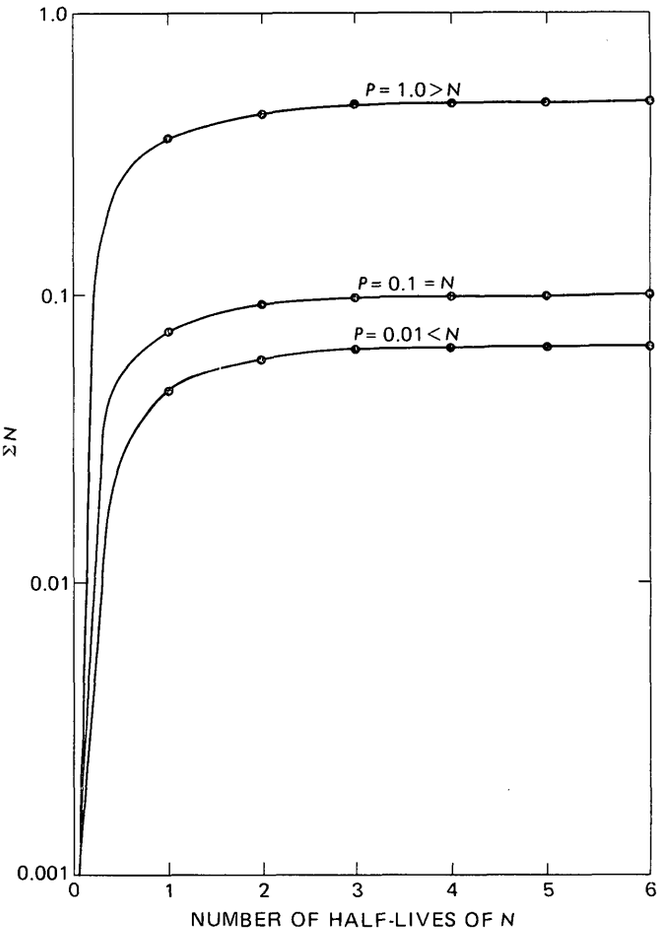

FIGURE 1.—Curves connecting successive computed values of N for $P=0.01$, 0.1, and 1.0.

by the curves in figure 2. Curve A connects successive values of N for $P=15.2$ where the initial value of $N_o=0$; that is, where the redistributed daughter product had never reached equilibrium with its precursor. Curve B connects successive values of N for $P=15.2$ where the initial value of $N_o=15.2$; that is, where the redistributed daughter product was in equilibrium with its precursor at some time before 10,000 yr ago. In both curves N approaches a constant near 7.02 percent, the actual value of ΣRa^{226} from the pair of analyses used to determine A and N_a.

Table 2 shows the selected values of P compared to the constant values of N attained after redistribution, during the course of six half-lives of Ra^{226}. Substituting U and eU for P and N, respectively, results in a pattern of disequilibrium like that observed in the deposits tested; U>eU when U>0.1 or 0.01 and eU>U when U<0.1 or 0.01. That this is so reflects the fact that eU values depend mainly on excesses and deficiencies of Ra^{226} and its decay products and of the fact that $\Sigma Th^{230}\approx U$.

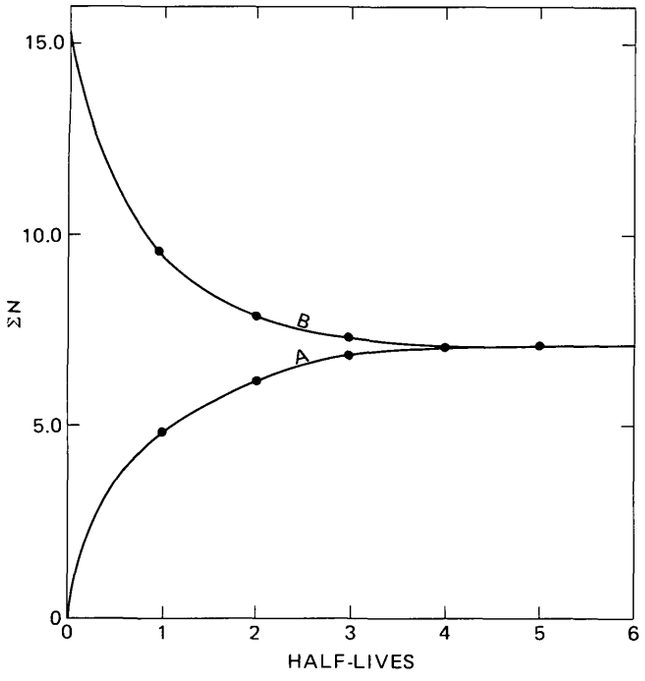

FIGURE 2.—Curves connecting successive computed values of N for P=15.2. Curve A starts with initial value of N_o=0. Curve B starts with initial value of N_o=15.2

TABLE 2.—*Computed values of* eU *for selected values of* U
[All data in percent]

U or P	eU or N (equilibrium at 0.1)	eU or N (equilibrium at 0.01)
15.2	7.04	6.99
10.0	4.67	4.62
5.0	2.36	2.32
1.0	.516	.467
.5	.285	.235
.1	.10	.051
.05	.077	.028
.01	.059	.010
.005	.056	.008
.001	.054	.006

Pairs of these computed values of U and eU, when plotted, yield the two curves shown in figure 3. In curve A, U=eU=0.1; in curve B, U=eU=0.01. Between these two, various curves might be drawn to represent U=eU somewhere in the range of 0.1 to 0.01. The equilibrium line C represents no redistribution, where N_a=0 and A=1.0 in the general equation. Values of A between 0.63 and 1.0 in the general equation would then yield pairs of values of U and eU that would fall between line C and curves A and B. Also plotted in the figure are pairs of U and eU analyses of the 87 samples from the Ambrosia Lake ore deposits.

From figure 3, it is apparent that the curves generated by the computations fit very well the plots of actual analyses. Of the few analyses that do not fit, one has a greater than usual excess of Ra^{226} and the others, of Th^{230}. The close fit indicates that the assumptions made about continuous redeposition of

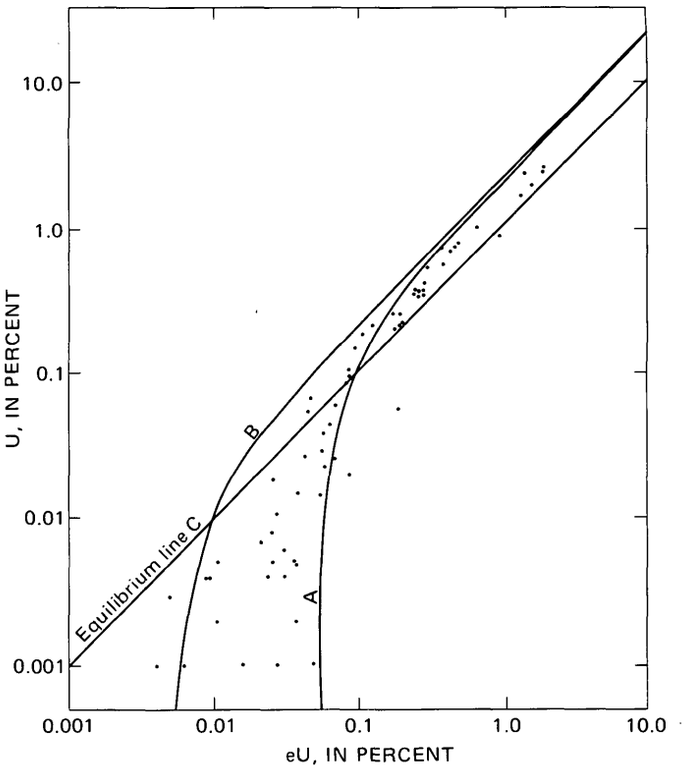

FIGURE 3.—Curves through computed values of eU for selected values of U compared to plots of U and eU analyses of samples from Ambrosia Lake, N. Mex.

Ra^{226} for the model is in essence what occurs in uranium deposits to produce the characteristic pattern of disequilibrium.

One objection to the model is an implication in the computation that an isotope is being removed and deposited simultaneously at different rates in the same volume of rock. To avoid this objection, the assumptions could be modified to the extent that no loss by redistribution would be considered to occur in low-grade material and no gain, in high-grade material. These modifications would change the values of N in the general equation but would not change the pattern of disequilibrium nor the fact that the pattern would become a system in equilibrium. These modifications, however, lead to the implication that redeposition of the mobilized Ra^{226} occurs only in low-grade rock and not in high-grade rock a few inches away. How or why this should occur cannot be adequately explained in considering the fact that some of the Ambrosia Lake deposits are above the water table.

Of the many widely scattered uranium deposits that display the characteristic pattern of disequilibrium, some are above and some are below the water table. Some contain only unoxidized rock; others contain both oxidized and unoxidized rock. The samples from

some deposits contain oxidized uranium minerals. Others contain only unoxidized uranium minerals. Changes in the environment within each deposit have no doubt occurred in the course of time, and the history of each deposit is different. It is apparent, therefore, that Ra^{226} redistribution can and does occur under a wide range of conditions. Although the rate of redistribution may conceivably change in response to changing conditions, the thrust of redistribution remains such that Ra^{226} is depleted in high-grade and enriched in low-grade rock.

An explanation for the apparent lack of a consistent pattern involving comparisons of U and the radioelements heavier than Ra may lie in their responses to changes in the environment. Unlike the redistribution of Ra^{226}, which appears to continue under a wide variety of conditions, redistribution of the heavier elements, including uranium, may change radically as the environment in a deposit changes. Thus, part of a deposit may be enriched in one element under one set of conditions, then be depleted under a slightly different set of conditions, while the thrust of Ra^{226} redistribution remains the same. The significance of the disequilibrium between U and the radioisotopes heavier than Ra^{226} in the Ambrosia Lake samples is discussed by Dooley, Granger, and Rosholt (1966).

Pairs of U and eU analyses of samples from deposits below the water table, including those from oxidized rocks, best fit the computed curves in figure 3. Pairs from unoxidized rock in deposits above the water table also fit, though less perfectly. Analyses that do not fit the curves are mostly of samples from oxidized rock above the water table and from surface exposures. Even this is not invariably true as many samples of oxidized rock above the water table in the Powder River Basin of Wyoming have U and eU values which, if plotted, would fit the curves quite well. Analyses for these samples from Wyoming are listed by Sharp, McKay, McKeown, and White (1964, p. 608–631).

Apparently oxidation, particularly within the last 1,000 yr, tends to produce changes that are sufficient, in some places, to disrupt the characteristic pattern of disequilibrium. Oxidation below the water table may have occurred 10,000 or more years ago; sufficient time has elapsed to allow the deposits containing oxidized rocks to reestablish the characteristic pattern of disequilibrium.

A clue to the distances involved in the migration of radioisotopes is provided by a comparison of the few published radiochemical analyses of mill pulp samples with those of channel-and-grab samples from the Hauber mine, Hullett Creek, Wyo. (Samples 5 through 8 in table 2 of Rosholt (1961, p. 427) are of mill pulp; samples 1 through 4 are channel-and-grab samples.) Although a considerable degree of disequilibrium is indicated for the channel-and-grab samples from that mine, samples of mill pulp are virtually in equilibrium. Apparently enough rock containing compensating quantities of various radioisotopes is mixed with ore to produce equilibrium in the rock shipped to the mill. What little low-grade rock is unavoidably mixed with ore usually constitutes a small volume immediately adjacent to ore zones. This small volume then must contain the appropriate quantities of radioisotopes to produce equilibrium in the mill pulp. The implication is that migration of radioisotopes does not extend to appreciable distances from ore.

Analyses of some samples from the Ambrosia Lake district also suggest a short distance of migration. Sample suite 9G59 (Granger, 1966, p. 34, 35) illustrates a typical situation in which a thin high-grade ore layer is bounded above and below by rock containing 0.001 percent U. The low-grade rock less than 1 ft (0.3 m) from the ore layer is greatly enriched in Pa^{231}, Ra^{226}, Rn^{222}, and Pb^{210}; $eU = 0.016$ and 0.027 above and below the ore, respectively. The quantities of these isotopes are greatly reduced 1 ft (0.3 m) or more from ore where $eU = 0.006$ and 0.004. The deficiencies of various isotopes in the ore layer are virtually compensated for by the excesses of isotopes in the 1 ft (0.3 m) of low-grade rock above and below the ore layer.

The zone containing anomalous concentrations of radiogenic isotopes is probably only slightly larger than most ore bodies themselves, and so geochemical-prospecting techniques that rely on the detection of one of these isotopes will not be successful in locating uranium deposits that have not recently been affected by oxidation or unusual geochemical processes.

CONCLUSIONS

The pattern of disequilibrium in the deposits tested, and probably in most uranium deposits, is the result of a continuous process of redistribution, mainly of Ra^{226}. Redistribution of Ra^{226} occurs under a variety of conditions normally found in water-saturated permeable sandstone and probably affects all uranium deposits from the time that they formed.

The pattern of disequilibrium described may be characteristic of most uranium deposits in sandstone, particularly those below the water table. A pattern much different from the one described could result from the redistribution of radioisotopes other than Ra^{226} and could indicate that a deposit was affected by solutions as well as by pH and Eh conditions not normally present in water-saturated sandstone.

REFERENCES CITED

Cuppels, N. P., 1962, Geologic environment of an oxidized uranium deposit in the Black Hills, South Dakota: U.S. Geol. Survey Bull. 1063–C, p. 61–83.

Dooley, J. R., Jr., Granger, H. C., and Rosholt, J. N., 1966, Uranium-234 fractionation in the sandstone-type uranium deposits of the Ambrosia Lake district, New Mexico: Econ. Geology, v. 61, no. 8, p. 1362–1382.

Finnell, T. L., Franks, P. C., and Hubbard, H. A., 1963, Geology, ore deposits, and exploratory drilling in the Deer Flat area, White Canyon district, San Juan County, Utah: U.S. Geol. Survey Bull. 1132, 114 p.

Granger, H. C., 1963, Radium migration and its effect on the apparent age of uranium deposits at Ambrosia Lake, New Mexico, *in* Short papers in geology and hydrology: U.S. Geol. Survey Prof. Paper 475–B, p. B60–B63.

—— 1966, Analytical data on samples collected at Ambrosia Lake, New Mexico—1958 through 1962: U.S. Geol. Survey open-file Rept., 485 p.

Granger, H. C., Santos, E. S., Dean, B. G., and Moore, F. B., 1961, Sandstone-type uranium deposits at Ambrosia Lake, New Mexico—An interim report: Econ. Geology, v. 56, no. 7, p. 1179–1210.

Harshman, E. N., 1972, Geology and uranium deposits, Shirley Basin area, Wyoming: U.S. Geol. Survey Prof. Paper 745, 82 p.

Robinson, C. S., and Rosholt, J. N., Jr., 1961, Uranium migration and geochemistry of uranium deposits in sandstone above, at, and below the water table—pt. 2, Relationship of uranium migration dates, geology, and chemistry of the uranium deposits: Econ. Geology, v. 56, no. 8, p. 1404–1420.

Rosholt, J. N., Jr., 1959, Natural radioactive disequilibrium of the uranium series: U.S. Geol. Survey Bull. 1084–A, 30 p.

——— 1961, Late Pleistocene and Recent accumulation of uranium in ground water saturated sandstone deposits: Econ. Geology, v. 56, no. 2, p. 423–430.

Sharp, W. N., McKay, E. J., McKeown, F. A., and White, A. M., 1964, Geology and uranium deposits of the Pumpkin Buttes area of the Powder River Basin, Wyoming: U.S. Geol. Survey Bull. 1107–H, p. 541–638.

Stephens, J. G., 1962, Geology and uranium deposits at Crooks Gap, Fremont County, Wyoming, *with a section on* Gravity and seismic studies in the Crooks Gap area, by D. L. Healey: U.S. Geol. Survey Bull. 1147–F, 82 p.

Wilmarth, V. R., 1959, Geology of the Garo uranium-vanadium-copper deposit, Park County, Colorado: U.S. Geol. Survey Bull. 1087–A, 21 p.

Jour. Research U.S. Geol. Survey
Vol. 3, No. 3, May–June 1975, p. 369–375

A COMPUTER-ASSISTED PROCEDURE FOR INFORMATION PROCESSING OF GEOLOGIC FIELD DATA

By TRAVIS HUDSON, GERALD ASKEVOLD, and GEORGE PLAFKER, Menlo Park, Calif.

Abstract.—We have examined several computer systems to see how they could aid information processing of geologic field data. The processing procedure we have chosen combines a systematic note-taking technique, a computer text-editor for creating files of data, and automated printing of selected data or of complete file copies. Traditional text notes are the foundation of each station record, and no coding of data is required. The text-editor used is an interactive computer system that allows any individual with typing skills to build and use data files. On the basis of our experience, an interactive text-editor can readily fulfill the data-handling needs of most geologic field projects and offers important advantages over other systems that were examined.

Regional field programs may involve many geologists, cover large areas, and last for several years. Such programs can quickly produce formidable quantities of new data. The value of these data depends on the effectiveness of the initial observing and recording process and on the ease with which they may be subsequently used.

This paper reports the initial results of efforts to provide a 5-yr field investigation of geologic earthquake hazards in Alaska with field-note recording procedures and computer data-handling techniques designed to facilitate successful completion of project objectives. These objectives include rapid publication of progress reports and basic field data, development of an information base that can be easily manipulated in preparation of regional syntheses, and organization of all data so that they will be readily accessible to future workers in Alaskan geology. Our principal assumptions are that the quality of the field data can be improved and that an organized file of field notes will permit the project geologists to evaluate and apply the data quickly and effectively. Some words and phrases commonly used in discussions of computer technology are explained in the glossary at the end of the paper.

Acknowledgments.—Several U.S. Geological Survey colleagues, including Warren Coonrad, Robert Detterman, Edward MacKevett, Jr., Russell Tysdal, and Gary Winkler helped design the field-note outline and participated in recording experiments. Susan Hunt provided assistance in building and using the data files.

PROBLEM ANALYSIS

Our attempt to provide the Geologic Earthquake Hazards Project with appropriate information processing began as an experiment. The first step involved an analysis of the field problems, a cataloging and organization of the anticipated data, and an appraisal of the nature of the field-observing process. This resulted in the organized format for note taking described below. In retrospect, we believe this first step contributed more to increase the effectiveness of the project than any other factor.

In the second step we examined several computer systems of potential use in our application. These included systems developed specifically for geologic applications (Hruška and Burk, 1971; Bergeron and others, 1972; Burk, 1973; and Smith and Berg, 1973), as well as those designed for general information processing (Addison and others, 1969; Vallee, 1970; SPIRES staff, 1972; Infonet, 1973). The systems used for geologic applications are typically batch processors in that the computer performs functions after being given a sequence of commands and data (usually on punch cards). On the other hand, the general information systems are mostly interactive processors that allow almost instantaneous computer response to individual commands before others need be given. In many ways, interactive text-editors such as WYLBUR (Hawker, 1972) and NLS (Irby, 1974) can be thought of as generalized information systems.

The final step was to develop a specific processing procedure for our field data that took into consideration the insights gained in step 1 and used one of the computer systems examined in step 2. On the basis of our initial work and the experience of Vallee and Askevold (1973), we decided to focus our investigation on interactive systems and finally chose to use a text-editor (WYLBUR) in our application. The following sections outline the field-note recording pro-

cedure, the way the computerized field data files are created and used, and the results of our examination of interactive computer systems.

FIELD-NOTE RECORDING PROCEDURE

In our procedure, the only requirements of the field notes are that they be legible and organized. An example of a field-notebook entry is illustrated in figure 1. The categorized data are recorded on the preprinted outline page, and traditional text information is recorded on the facing gridded page. These pages are collected and stored in surveyor's pocket-size looseleaf notebooks.

To record a station entry, the geologist fills in the blanks and circles the appropriate words or abbreviations, which is convenient because there is no special coding of the data. Text information is used for qualitative and descriptive observations, as well as for data not readily accommodated by the outline. Outlines such as this should be expected to differ depending on who creates them, the problems being studied, and where the fieldwork is being done. In order to maximize the usefulness of this approach, it is especially important that the geologists actually using the recording format be involved in its design.

This recording procedure has resulted in (1) enhanced legibility of the field notes, (2) clarification of field objectives during the design of the format, (3) use of the data outline as a checklist so that pertinent observations are not overlooked, and (4) better understanding by each geologist of field data collected by other members of the project. The procedure is of great value to the project even if the notes are not subsequently machine processed.

BUILDING COMPUTERIZED FIELD-DATA FILES

To build the files requires a typist, a computer communications terminal, and access to a time-sharing computer that supports a system similar to that described below. The typist sits at the terminal (the one we initially used resembles an IBM Selectric typewriter) and types the station data. Figure 2 is a copy of a station record that has just been typed into the machine. Each category of information in the original field notes is typed on a separate line or group of lines. The machine prompts (asks) for successive lines

STATION NO. 73 APr 47 (PAGE 1) QUAD: Anchorage D-6 AIRPHOTO: Gul 4-067
UTM: E395700 N6850500 ELEV: 3800' - 4100' DATE: June 30
TEXT TOPIC: (LITH.) (STRUCT.) (GEOMORPH.) MINERALIZ., HAZARDS, OTHER
PHOTOS: Roll 2 #'s 6, 7 Outcrop of arkose / woody frags
SKETCH: Distribution of moraine on S. side of Sheep Valley

STRUCTURE: Homoclinal section
BEDDING: 90 255 CURRENT DIR:
LINEATION: FOLIATION:
FAULT: JOINT:
LINEAMENT: FOLD:
OTHER STRUCTURE:

(SAMPLE) OR LITHOLOGY NO: 47A UNIT: Arkose Ridge Fm.
TYPE: REPRES. GRAB OR CHIP, ~~SPECIAL GRAB~~, SSS, SOIL, PAN CONC., SURFICIAL MAT.,
OTHER TYPE:
(PURPOSE:) HAND SPEC., THIN SECT., STAINED SLAB, POL. SECT., GRAIN MOUNT, MIN. SEP., MODE, CHEM., SPEC., K/AR, C-14, X-RAY, NORM, (FOSSIL DETER.)
OTHER PURPOSE:
(DESCRIPTION:)
IGNEOUS, VOLC., HYPA., PLUT., ULTRAMAF., MAFIC, INTERMED., FELSIC,
OTHER IG.:
METAMORPHIC, REGIONAL, CTCT., DYNAMIC, LOW G., MED. G., HIGH G., PELITIC,
QTZ-FELD., CALC., MAFIC, ULTRAMAF., OTHER META.:
(SEDIMENTARY) ARG., SH., MDST., SLTST. (SS.) CGL., BREC., LS., CHT., COAL, (FOSS.)
OTHER SED.:
UNCONSOL., CLY., SLT., MD., SD., GVL., CBLS., BLDRS., BLKS., ORG.,
OTHER UNCONSOL.:
OTHER DESCRIPTION:

On Eska Ridge - homoclinal section consisting mainly of coarse vy hd biot-rich arkose, orange-weath calc? arkose and carb. arkose. Carb. seams are very bright coal, plant material commonly is graphitic smear although locally some woody impressions are present.

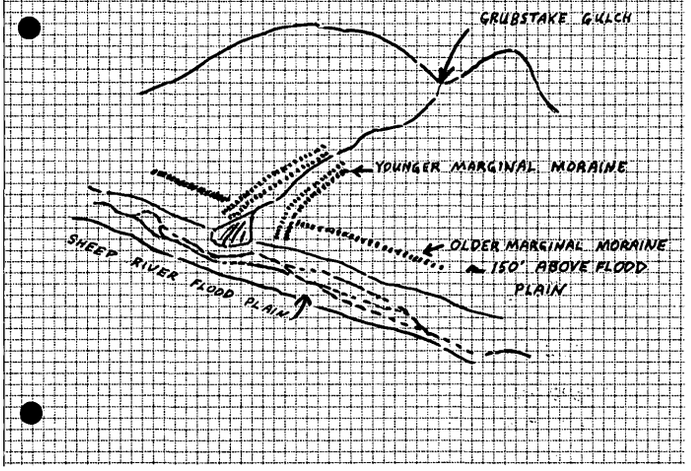

FIGURE 1.—Field-notebook entry for station 73 APr 47.

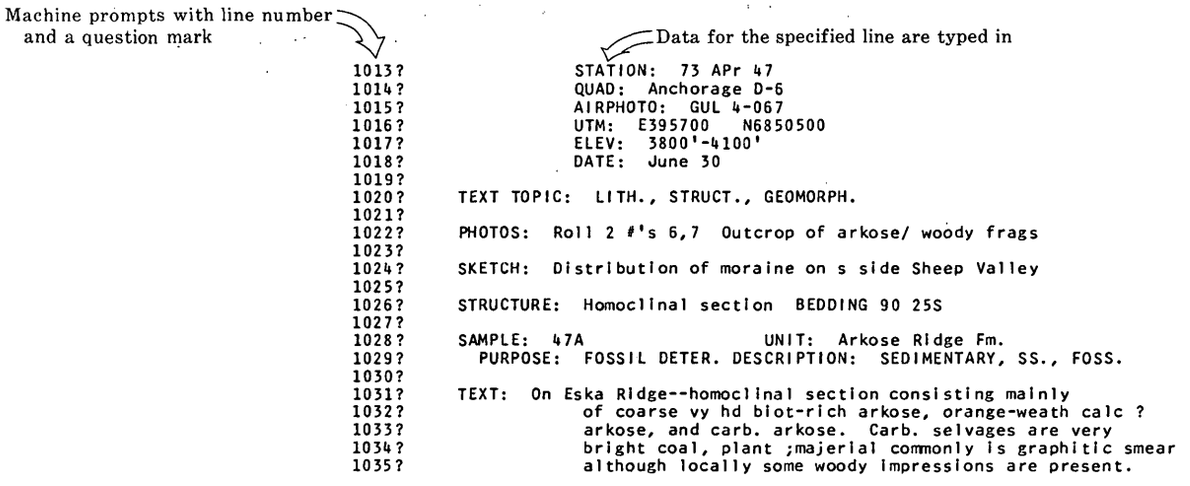

FIGURE 2.—Field notes from station 73 Apr 47 as they were originally typed into the computer (including typographical errors).

by typing a line number and question mark. The next line that will be added to the file in the example shown in figure 2 is line number 1013. This means that there are already 1012 lines of data in the file. The typist then types "STATION: 73 APR 47". When the carriage-return key is struck, this entry is immediately stored in the computer memory and a prompt for the next line is printed out; that is, "1014?". By following this procedure line after line, the complete station record can be quickly stored in the computer memory. When desired, these data can be stored on a storage device such as magnetic tape or disk. Special data entry programs that are being developed will eliminate the need for the typist to structure the file and to retype data category headings such as "STATION". This is expected to reduce the typing time needed to build the files by one-third to one-half.

CORRECTING AND UPDATING THE FILE

Information files must be easy to correct and update if they are to be useful. Correction of the typing error on line 1034 in figure 2 illustrates the ease with which we can modify our files. Figure 3 shows how we tell the computer to change the misspelled word ";majerial" to "material" in line 1034. The computer immediately prints the corrected line so that it can be checked and at the same time appropriately modifies the station record in the computer memory. We can similarly replace, delete, and insert specified text so that the file can be kept up to date. For instance, we collected the sample at station 73 APr 47 (see fig. 2) for the purpose of a fossil determination. When the determination is made, this new information can be added to the file by following the same procedure used when building the original file but collecting the new data on intermediately numbered lines (see fig. 4). The fossil data thus can be inserted immediately at the appropriate place in the original station record—in this example between lines 1030 and 1031 (fig. 5).

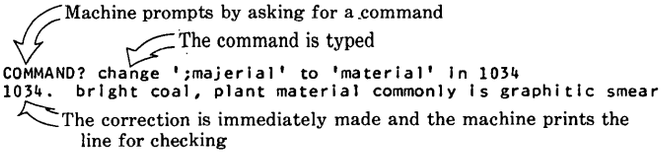

FIGURE 3.—Correction of error by use of the change command.

```
COMMAND? collect 1030.1
1030.1?    FOSSIL DETERMINATION:  The leaf impressions do not
1030.2?            show sufficient detail for specific
1030.3?            determination.  The collection probably has
1030.4?            members of the genera Populus and Salix.
1030.5?
```

FIGURE 4.—Updating the file by collecting new data on intermediately numbered lines.

USING THE FILES

So far, we have used the files to produce two products: (1) Index lists and (2) file copies of all notes for each geologist. An example of an index list is shown in figure 6. The list was printed by telling the computer to "list 'PHOTOS' ". To make such a list the computer searches the file line by line, identifies lines that contain the word "PHOTOS" (capitalized) and then prints the lines. The list is a tabulation of all the lines in the file that contain information about photographs. The procedure for obtaining this list emphasizes the connections between the recording procedure, the building of the files, and finally using the files. In our recording outline, "PHOTOS" identifies a field or a data category (fig. 1). When the files are

built, "PHOTOS" is used as a category heading in the computerized file (line 1022, fig. 2). "PHOTOS" is then used in the list request to produce the product shown in figure 6. If the list request had been for the word "photos" (written in lowercase letters), none of the lines in figure 6 would have been found because "photos" in lowercase letters does not occur in any of them. This ability to distinguish between uppercase and lowercase characters is an aid in structuring files and in permitting the use of text entries similar to those in the original field notes. We have used this procedure to produce many different index lists, including lists of sketch descriptions, samples with thin sections, and lineation measurements.

```
1013.              STATION:  73 APr 47
1014.              QUAD:  Anchorage D-6
1015.              AIRPHOTO:  GUL 4-067
1016.              UTM:  E395700   N6850500
1017.              ELEV:  3800'-4100'
1018.              DATE:  June 30
1019.
1020.    TEXT TOPIC:  LITH., STRUCT., GEOMORPH.
1021.
1022.    PHOTOS:  Roll 2 #'s 6,7  Outcrop of arkose/ woody frags
1023.
1024.    SKETCH:  Distribution of moraine on s side Sheep Valley
1025.
1026.    STRUCTURE:  Homoclinal section  BEDDING 90 25S
1027.
1028.    SAMPLE:  47A                UNIT:  Arkose Ridge Fm.
1029.      PURPOSE: FOSSIL DETER.  DESCRIPTION: SEDIMENTARY, SS., FOSS.
1030.
1030.1.  FOSSIL DETERMINATION:  The leaf impressions do not
1030.2.                show sufficient detail for specific
1030.3.                determination.  The collection probably has
1030.4.                members of the genera Populus and Salix.
1030.5.
1031.    TEXT:  On Eska Ridge--homoclinal section consisting mainly
1032.             of coarse vy hd biot-rich arkose, orange-weath calc ?
1033.             arkose, and carb. arkose.  Carb. selvages are very
1034.             bright coal, plant material commonly is graphitic smear
1035.             although locally some woody impressions are present.
```

Inserted fossil determination

FIGURE 5.—A complete and updated station record.

Indicates the line number in the text file

Abbreviated station number

Beginning of the data as stored on the specified line

```
 390.    3H241    PHOTOS:  73 AH 241  (Roll 2--photos 27-33)  Waxell Ridge scenery--elev 4250' for photos
1022.    3Pr47    PHOTOS:  Roll 2 #'s 6,7 Outcrop of arkose/ woody frags
1987.    3Pr290   PHOTOS:  73 APr 290 A-E  Kodas taken of Ragged Mtn fault trace
2014.    3Pr292   PHOTOS:  73 APr 292 A-D  Folds in slaty unit of Tos? along Stellar Gl.
2028.    3Pr293   PHOTOS:  73 APr 293 A-C  large disharmonic fold on mtn to N
2029.    3Pr293   PHOTOS:  73 APr 293 D  ridge to E (Tysdal) showing contrast in lith and topo
2435.    3Pr312   PHOTOS:  73 APr 312 A-C  ridge traverse by Tysdal showing well-bdd ss/sltst sequence and apparent thicke
2436.    3Pr312   PHOTOS:  (cont)          of rdsh-weath ss due to bending at fold axes
2450.    3Pr313   PHOTOS:  73 APr 313 A-C  9968' peak between Martin R. and Stellar Gl. to be named after Bilderbeck.
2451.    3Pr313   PHOTOS:  73 APr 313 D  9140' peak east of Mt. Hawkins to be named for Hanna or Nelson.
2490.    3Pr315   PHOTOS:  73 APr 315 A,B,C,D,E  Pan taken of mtns. to S.
2544.    3Pr318   PHOTOS:  73 APr 318 A-D  pan of mtns to south (new roll)
2659.    3Pr324   PHOTOS:  73 APr 324 A-C  McK. and Nightingale Kodas
2679.    3Pr325   PHOTOS:  73 APr 325 A-B  ctct within Strelna Gp., fault is just to N of this lineament
2783.    3Pr330   PHOTOS:  73 APr 330 AB  looking W towards altered zone north of sta 54C
2784.    3Pr330   PHOTOS:  73 APr 330 CD  helicopter and Mt St Elias
2805.    3Pr331   PHOTOS:  73 APr 331  view of Mt St. Elias
2901.    3Pr336   PHOTOS:  73 APr 336 A  Koda towards backside Mt Huxley.  Ed in foreground.
2963.    3Pr339   PHOTOS:  73 APr 339 A-C  looking W along S-flank Berkley Ridge showing fault ctct between Tk and Ts units
2977.    3Pr340   PHOTOS:  73 APr 340 AB  Kodas of ridge end
3044.    3Pr343   PHOTOS:  73 APr 343 A-H  pan Kodas from near Mt. Stellar
3058.    3Pr344   PHOTOS:  73 APr 344 AB  Kodas of Mt Stellar and Mt Miller from over Bering Glacier
3072.    3Pr345   PHOTOS:  73 APr 345 AB  Bilderbeck Peak
3130.    3Pr348   PHOTOS:  73 APr 348 AB  Bilderbeck Peak
3190.    3Pr351   PHOTOS:  73 APr 351 A-F  looking up Martin River Gl and down Miles River Gl showing fault troughs;
3191.    3Pr351   PHOTOS:  (cont)          also Koda of Mt Tom White
3225.    3Pr353   PHOTOS:  73 APr 353 A-N  Kodas taken of tillite
3260.    3Pr355   PHOTOS:  73 APr 355  4 Kodas taken of reverse fault ctct between Tv and Ts units
3320.    3Pr358   PHOTOS:  73 APr 358 A-E  pan taken from over Bering Gl looking W along Chugach-St Elias fault and N to E
3321.    3Pr358   PHOTOS:  (cont)          at Waxell Ridge
3335.    3Pr364   PHOTOS:  73 APr 364  Koda taken of ss/mdst/arg section.
3428.    3Pr368   PHOTOS:  73 APr 368 A,B  Kodas of samples 368A and 368C(?--ed.)
3502.    3Pr371   PHOTOS:  73 APr 371 A,B  Kodas taken at station and along ridge further west.
3597.    3Pr375   PHOTOS:  73 APr 375  Koda taken of unnamed glacier (Amphibolite Glacier?).
3630.    3Pr377   PHOTOS:  73 APr 377  Koda taken of metas/diorite ctct showing typical smooth weath topo.
3828.    3Pr386   PHOTOS:  73 APr 386 A-C  (no descrip.--ed)
3956.    3Pr392   PHOTOS:  73 APr 392 A-E  pan to N
```

FIGURE 6.—Results of a list request for the word "PHOTOS".

The other product is a complete copy of the entire field-note file for each of the project geologists. On high-speed printers, the computer can quickly and inexpensively print all the file data. Figure 7 is a copy of part of such a printout. Each station's record is separated from adjacent ones by a dashed line and each line at a station is indexed on the left with an abbreviated station number. Since the original notes from the stations in figure 7 contain no information concerning such subjects as photographs, structures, or samples, these categories were left out when the file was built.

COSTS

We have built three separate files of field data. These files are each 5 to 6 thousand lines long and contain data from 250 to 371 field stations. We have found empirically that the cost of building and using one of these files is roughly approximated by the following equation:

File cost = 5(CPU rate/min)
+ 55 (connect-time rate/h) + 120(personnel wage/h).

This equation is conservative and includes costs associated with becoming familiar with the system, editing of field notes and file printouts, and obtaining coordinate locations for each station. It does not include costs for storage of the data on the computer. At the rates available to us, each file has cost about $600 and was stored on the computer for 70 to 80 cents per day. The total cost of processing field notes from one season's work (954 stations) has been less than 3 percent of the field budget.

Entering the data into the computer is by far the most expensive part of the processing procedure. We are testing and developing techniques that use television screen terminals, mini-computers, local storage devices, and special data entry programs to help lower our costs in this area (Gerald Askevold, M. D. Michael, and Travis Hudson, unpub. data, 1975). The costs indicated by the above equation should be considered maximums, and future procedures could easily cut them in half.

COMPUTER TEXT-EDITORS

Our computer support system is a basic text-editor known as WYLBUR. Such systems are types of computer programs designed to aid manuscript preparation, the writing of other computer programs, and

```
  list 4139/4187
4139.     3Tz193            STATION:  73 ATz 193
4140.     3Tz193            QUAD:  Bering Glacier C-8
4141.     3Tz193            AIRPHOTO:  26-4495
4142.     3Tz193            UTM:  E337150 N6714950
4143.     3Tz193
4144.     3Tz193   SUBJECT:  LITHOLOGIC-STRUCTURAL
4145.     3Tz193
4146.     3Tz193   STRUCTURE:  Bedding  N65E 50N  top unknown--shaly arg.
4147.     3Tz193
4148.     3Tz193   TEXT:  Shaly arg and a few thin beds of (calcareous?) sltst.  Highly fractured.  A few concretions are pres
4149.     3Tz193          up the wall of the creek.  The shale just falls apart and is soft due to saturation w/ water.  Is th
4150.     3Tz193          a fault between here and the last sta?  The change from metamorphic rock to non-metamorphic rock sure
4151.     3Tz193          occurred over a short distance.
4152.     3Tz193
4153.     3Tz193----------------------------------------------------------------------------------------------------------
4154.     #
4155.     3Tz194            STATION:  73 ATz 194
4156.     3Tz194            QUAD:  Bering Glacier C-8
4157.     3Tz194            AIRPHOTO:  26-4495
4158.     3Tz194            UTM:  E337250 N6714550
4159.     3Tz194
4160.     3Tz194
4161.     3Tz194   SUBJECT:  LITHOLOGIC-STRUCTURAL
4162.     3Tz194
4163.     3Tz194   STRUCTURE:  Bedding  N85E 65N  top unknown
4164.     3Tz194
4165.     3Tz194   TEXT:  Ss--thick bdd, lt gy, f. to m.g., arkosic, containing a few dk grains--probably volcanic-rock frags.
4166.     3Tz194          There are a few thin arg interbeds present.  Top of beds is probably to the north but not sure.
4167.     3Tz194          Muscovite present at least locally.
4168.     3Tz194
4169.     3Tz194----------------------------------------------------------------------------------------------------------
4170.     #
4171.     3Tz195            STATION:  73 ATz 195
4172.     3Tz195            QUAD:  Bering Glacier C-8
4173.     3Tz195            AIRPHOTO:  26-4493
4174.     3Tz195            UTM:  E348600 N6715500
4175.     3Tz195
4176.     3Tz195   SUBJECT:  LITHOLOGIC-STRUCTURAL
4177.     3Tz195
4178.     3Tz195   SKETCH:  recumbent syncline in wall across glacier to W
4179.     3Tz195
4180.     3Tz195   STRUCTURE:  Bedding  N80E 90
4181.     3Tz195   STRUCTURE:  Other  N55E 45S  Shear plane w/ slicks
4182.     3Tz195   STRUCTURE:  Lineation  30 east  Slickensides--LL movement
4183.     3Tz195
4184.     3Tz195   TEXT:  Recumbent syncline in wall across glacier to W--vertical section.  Ss--f.g., dk gy, thick-bdd, finely
4185.     3Tz195          laminated.  Minor interbeds of arg locally.  Slickensides show LL movement.
4186.     3Tz195
4187.     3Tz195----------------------------------------------------------------------------------------------------------
```

FIGURE 7.—Machine printout of part of a field-data text file.

entering of data. Variations are abundant, but generally all are capable of storing, modifying, inserting, finding, and printing specified text. They usually accomplish this by the user making appropriate "English" commands as we have shown. Even so, few text-editors operate as simply and effectively as WYLBUR.

Text-editors like WYLBUR are generally not thought of as information storage and retrieval systems. This is because they do not use the most sophisticated search procedures. Nonetheless, the successful use of a computer text-editor in handling data of the Geologic Earthquake Hazards Project has demonstrated its effectiveness for geologic field programs. This effectiveness is a result of WYLBUR's availability (to us), low cost, simplicity of use, and flexibility. Flexibility in our computer support system was particularly important because we wanted to develop an information processing procedure that maintained the data organization defined in step 1 of the problem analysis and did not impose severe constraints on the field recording process (such as using codes and 80-column card formats).

OTHER INTERACTIVE COMPUTER SYSTEMS

Our testing of other interactive processors revealed that most of them are handicapped by one or more of the following factors: (1) Unavailability, (2) complex and alienating user procedures, (3) high costs, and (4) either an inflexible file structure or one that is complex to define. Inflexible or complexly defined file structures are the most common and significant problem with interactive general information systems. In trying to use these, the geologist must commit himself to an extended learning process about the system or he will quickly lose all but superficial contact with creation of the computerized file. This is a hazard because, in order to be most useful, the computerized file must conform to the user's concept of his data base; that is, the inherent order (or lack of it) and logical structure the user perceives in his data. If file definition becomes the responsibility of someone other than the geologist, the likelihood of discrepancies between the user's perceptions (and expectations) and the resulting computerized file are seriously increased.

CONCLUSIONS AND SUMMARY

We offer the following suggestions to individuals contemplating applying information technology to their own research problems.

1. In building a computerized data file, try to use terms you have always understood and used in connection with the data. Codes and computer jargon can be a severe handicap to the usefulness of the file.
2. Be directly involved in creating the file and develop a good understanding of the file structure and organization. This should conform as much as possible to your "precomputer" conceptual understanding of your data.
3. Your application of information technology should be viewed as an evolving project. It should be simple at first, have clear short-range goals, and be based on the understanding that changes in the application and use of the tools are expected. Time should be allowed for experimentation and redesign by using small test files of dummy or real data.
4. Because information technology is evolving very rapidly, commitment to a rigid system about which you have significant reservations should be avoided.

Interactive computer systems that combine simplicity of operation with flexible and easily defined file structures are most useful and appropriate for handling geologic field data. Using such a system we have developed an effective processing procedure for geologic field notes. The procedure involves an integrated system of field-note recording, building of text files with computer text-editors, searching these files to produce index lists, and finally, printing complete file copies for the geologists' use. Our work is in many ways a first step. We think it has important implications concerning concepts of data bases, the nature of geologic field data, the effects of expanded computer use in geology, and future communications procedures within the scientific community.

GLOSSARY

Central processing unit (CPU). The part of the computer that controls the interpretation and execution of instructions, the arithmetic functions and the input/output (I/O) channels, which are computer components that transfer input and output between *memory* devices.

Computer communications terminal. A device through which a user can remotely communicate with a computer, usually by typing commands that are transmitted over telephone lines.

Connect time. The duration of time a user actually occupies a connecting line (port) to a *time-sharing* computer.

Data base. A term that may have different meanings for different people; as it is used in the context of this paper, it comprises all the data a user depends on in his work.

Disk. A flat circular metal disk upon which a machine can store data by selectively magnetizing different areas. One of the main advantages of a disk is that it may be searched randomly rather than just serially or sequentially as in searches of *magnetic tape.*

Local storage device. A device that usually employs *magnetic tape* or *disk* to store machine-readable data remotely from the main computer.

Magnetic tape. A medium upon which a machine can store data in the form of a sequence of magnetically polarized spots; this medium is similar to that used in home tape recorders.

Memory. The part of a computer that stores programs and data so that they are readily accessible to the *CPU*.

Mini-computer. A small computer that may perform many of the functions of a larger computer but that generally is used for specialized tasks, such as data communication, data entry, or process control (programable terminals are included in our use of the term mini-computer).

Program. A sequence of instructions that tells the computer what series of operations to perform for a particular application.

Record. A group of related facts or fields of information treated as a unit within a computerized file; that is, in a field-data file, all the information obtained from or related to a particular field station.

Time sharing. A method of operation in which a computer is shared by several users for different purposes at apparently the same time; although the computer actually serves each user in sequence, the high speed of the computer makes it appear that the users are all handled simultaneously.

REFERENCES CITED

Addison, C. R., Coney, M. D., Jones, M. A., Shields, R. W., and Sweeney, J. W., 1969, GIPSY—General information processing system application description: Norman, Oklahoma Univ. Inf. Science Ser., Mon. no. 4, 129 p.

Bergeron, Robert, Burk, C. F. Jr., and Robinson, S. C., conveners, 1972, Computer-based storage, retrieval, and processing of geological information—geological field data systems: Internat. Geol. Cong., Montreal, Proc., sec. 16, p. 3–46.

Burk, C. F., Jr., 1973, Computer-based storage and retrieval of geoscience information: Bibliography 1970–72: Canada Geol. Survey Paper 73–14, 38 p.

Hawker, Eileen, ed., 1972, WYLBUR reference manual [4th ed.]: Stanford, Calif., Stanford Univ., Stanford Center for Inf. Processing, 76 p.

Hruška, J., and Burk, C. F., Jr., 1971, Computer-based storage and retrieval of geoscience information: Bibliography 1946–49: Canada Geol. Survey Paper 71–40, 52 p.

Infonet, 1973, Data management language reference and users guide: Los Angeles, Calif., Computer Sci. Corp., 249 p.

Irby, C. H., 1974, Display techniques for interactive text manipulation: Am. Federation Inf. Processing Soc. Conf., Natl. Computer Conf. and Exposition, Chicago, Proc., p. 247–255.

Smith, J. G., and Berg, H. C., 1973, Use of machine-processable field notes in a wilderness mapping project (Granite Fiords area), southeastern Alaska: U.S. Geol. Survey Jour. Research, v. 1, no. 5, p. 579–585.

SPIRES staff, 1972, SPIRES users manual: Stanford, Calif., Stanford Univ., Stanford Center for Inf. Processing, pts. 1–3, 63 p.

Vallee, J. F., 1970, DIRAC: an interactive retrieval language with computational interface: Jour. Inf. Storage Retrieval [Oxford], v. 6, no. 5, p. 387–399.

Vallee, J. F., and Askevold, Gerald, 1973, Information organization for interactive use: Design implications in data base systems: Jour. Am. Soc. Inf. Sci., v. 24, no. 4, p. 287–299.

Jour. Research U.S. Geol. Survey
Vol. 3, No. 3, May–June 1975, p. 377–378

A PROCEDURE, USING HYDROFLUORIC ACID, FOR QUANTITATIVE MINERAL SEPARATIONS FROM SILICATE ROCKS

By GEORGE J. NEUERBURG, Denver, Colo.

Abstract.—Some minerals of silicate rocks can be quantitatively recovered from rock fragments by prolonged digestion in cold, concentrated hydrofluoric acid. The procedure yields clean, physically unharmed crystals, mostly of minerals that occur largely or only in trace amounts.

The use of hydrofluoric acid in separating minerals from silicate rocks (Neuerburg, 1961; Whitney, 1972) has been refined and simplified into an efficient and versatile tool. Many of the HF-insoluble minerals (table 1) occur as minor constituents of rocks, and some are the sole compounds of their elements in the host rock. Recognition of minor accessory minerals is facilitated by separating and concentrating them; for example, the new mineral galkhaite (Botinelly and others, 1973) was first found in a hydrofluoric acid separate. The method provides exceptionally clean and physically unharmed mineral grains for precise measurements and description. Quantitative modal analyses of minerals occurring in trace amounts are possible, and this type of data can be related to specific geologic processes or events, such as the migration of ore fluids (Neuerburg, 1971) or the shock of meteorite impact (Fahey, 1971). The sensitivity and precision of chemical analyses can be greatly increased by concentrating an element of interest from much larger samples rather than by relying on the rather small samples required for the total sample dissolutions of the usual analytical schemes. For example, the molybdenum contents of some granitic rocks, for which little or no molybdenum was reported by chemical and spectrographic analyses, have been estimated by concentrating with hydrofluoric acid the few, unevenly distributed molybdenite crystals of 100-g samples (Neuerburg and others, 1974, p. 13).

PROCEDURE

The separation of a 100-g sample with hydrofluoric acid requires 3 to 4 weeks. Total operator time for separation of, for example, 48 samples is less than 8 h over the 4-week period; hence it is more efficient to do several samples at a time. Separation of one 100-g sample requires an average of 1,135 g of 52-percent technical-grade hydrofluoric acid, 113.5 g of reagent-grade dibasic ammonium citrate ($(NH_4)_2C_6H_5O_7$), 113.5 g of U.S.P.-grade aluminum chloride ($AlCl_3 \cdot 6H_2O$), and 60 ml of 99.5-percent pure acetone. Specified reagent grades are those readily available. No contamination of ore metals has been traced to these reagents. Note: The sample must not be crushed. Caution! All work with hydrofluoric acid must be done under a hood with a good draft.

The sample, generally a single 100-g piece, is placed in a 400-ml polyethylene beaker. Hydrofluoric acid is added to the sample to make a total volume of 250–300 ml. The sample is allowed to digest, undisturbed, at room temperature for 1 week. The mixture of sample, solid reaction products, and mostly spent acid is

TABLE 1.—*Minerals routinely recovered by digestion of silicate rocks and vein fragments in cold hydrofluoric acid*

Acanthite
Aikinite
Allanite (nonmetamict)
Anatase
Andalusite
Anhydrite
Arsenopyrite

Barite
Bismuthinite
Bornite
Boulangerite
Brookite

Carbon
Cassiterite
Celestite
Chalcocite
Corundum
Covellite
Cryptomelane

Diaspore
Digenite

Enargite

Fluorite (etched by $AlCl_3$)

Galkhaite
Garnet, some varieties
Gold
Graphite

Loellingite

Marcasite
Matildite
Melonite
Molybdenite

Orpiment

Pentlandite
Proustite
Pyrargyrite
Pyrite
Pyrolusite
Pyrophyllite

Realgar
Rutile

Sillimanite
Sphalerite, many varieties
Spinels, aluminum
Spinels, iron, some varieties
Stibnite
Sulfur

Talc
Tennantite-tetrahedrite
Topaz
Tourmaline, some varieties

Wolframite
Wurtzite

Xenotime

Zircon

slurried with cold water, allowed to stand for a moment, and decanted. Acid is again added and the sample digested another week. These steps are repeated until no obvious rock fragments remain. At this point, the residue that remains after decanting is digested in 300 ml of 2 *M* (454 g/l) dibasic ammonium citrate for 4–6 h., with occasional stirring. The digestion with ammonium citrate effectively removes those water-insoluble fluorides that would tend to form gels with aluminum chloride in the next digestion. The liquid is decanted off the solid residue, 100 ml of hydrofluoric acid added to the residue, and the whole allowed to stand overnight. The whole is then slurried with cold water and decanted. Three hundred millilitres of about 1 *M* (226 g/l) aluminum chloride is added and the mixture is allowed to stand with occasional stirring for 4–6 h. Addition of hydrofluoric acid and digestion in aluminum chloride are repeated at least once, more often if the insoluble residue adheres to the beaker or if white fluorides persist. The residue from the final aluminum chloride digestion is rinsed once with water and twice with acetone and is washed onto a Whatman No. 50—or equivalent—filter paper with a stream of acetone. This is the final separate, for weighing and study.

DISCUSSION

The minerals recovered as insoluble residues (table 1) show no evidence of reaction with cold hydrofluoric acid, such as etching or tarnishing. Some of the listed minerals dissolve in or react with hot hydrofluoric acid and most, if not all, of them dissolve in hot hydrofluoric acid under pressure (Langmyhr, 1968). Some minerals dissolve very slowly, at the cost of excessive amounts of hydrofluoric acid; these include many carbonates, some garnets, hematite, and epidote.

Failure to carry the procedure to the prescribed end results in recovery of corroded remnants of many HF-soluble minerals, such as galena, magnetite, muscovite, and even amphiboles and pyroxenes. Shortening the specified digestion periods for ammonium citrate and aluminum chloride favors retention of artificially formed "minerals," most commonly elpasolite (K_2NaAlF_6), ill-crystallized fluorite, and hieratite (K_2SiF_6).

This procedure has evolved during separations of about 4,000 samples and is very simple and trouble free. Modifications of the procedure will usually be detrimental or dangerous. Many obvious changes, such as heating digestions and varying reagent concentrations, regress to more complicated and troublesome procedures. Progress of the separation is not visually obvious and the tendency to try to push the separation is compelling: Don't! The water-insoluble products formed on reaction with hydrofluoric acid differ greatly from rock to rock in appearance, degree of adhesion to rock fragment, abundance, and behavior on dissolution in aluminum chloride. These differences are of no concern. Centrifuging before decanting is necessary for quantitative recovery of HF-insoluble minerals of low specific gravity or of extremely small grain size. The spontaneous floating of sulfides on acid or water is a problem in some samples, but most of the floating grains can be sunk by an acetone spray. Aluminum chloride must be rinsed from the final concentrate with water before washing with acetone to avoid the formation of a water-soluble gummy precipitate. An acetone wash allows the use of a hardened fine filter paper that does not significantly ensnare mineral grains or yield loose fibers; an acetone wash also prevents oxidation-tarnishing of sulfide grains, which may result if the grains are dried from a water-wet state.

REFERENCES CITED

Botinelly, Theodore, Neuerburg, G. J., and Conklin, N. M., 1973, Galkhaite, (Hg,Cu,Tl,Zn) (As,Sb)S_2, from the Getchell mine, Humboldt County, Nevada: U.S. Geol. Survey Jour. Research, v. 1, no. 5, p. 515–517.

Fahey, J. J., 1971, The removal of potassium silicofluoride formed in the determination of coesite and stishovite: Am. Mineralogist, v. 56, no. 11–12, p. 2145–2146.

Langmyhr, F. J., 1968, Recent development in the use of hydrofluoric acid as decomposing agent for inorganic materials: Acta Geol. Geog. Univ. Comenianae, Geol. no. 15, p. 23–33.

Neuerburg, G. J., 1961, A method of mineral separation using hydrofluoric acid: Am. Mineralogist, v. 46, no. 11–12, p. 1498–1501.

——— 1971, Maps showing distribution of selected accessory minerals in the Montezuma stock, Summit County, Colorado: U.S. Geol. Survey Misc. Geol. Inv. Map I–608.

Neuerburg, G. J., Botinelly, Theodore, and Watterson, J. R., 1974, Molybdenite in the Montezuma district of central Colorado: U.S. Geol. Survey Circ. 704, 21 p.

Whitney, P. R., 1972, Spinel inclusions in plagioclase of metagabbros from the Adirondack highlands: Am. Mineralogist, v. 57, no. 9–10, p. 1429–1436.

☆U.S. Government Printing Office: 1975-585-406/5

RECENT PUBLICATIONS OF THE U.S. GEOLOGICAL SURVEY

(The following books may be ordered from the U.S. Geological Survey, 1200 South Eads Street, Arlington, VA 22202 (an authorized agent of the Superintendent of Documents, Government Printing Office). Prepayment is required. Remittances should be sent by check or money order payable to U.S. Geological Survey. Gives series designation and number, such as Bulletin 1368–A, and the full title. Prices of Government publications are subject to change. Increases in costs make it necessary for the Superintendent of Documents to increase the selling prices of many publications offered. As it is not feasible for the Superintendent of Documents to correct the prices manually in all the publications stocked, the prices charged on your order may differ from the prices printed in the publications and in this list)

Professional Papers

491–E. Water use by saltcedar as measured by the water budget method, by T. E. A. van Hylckama. 1974. p. E1–E30. $1.30.

716–D. Stratigraphy of the Kohat quadrangle, Pakistan, by C. R. Meissner, J. M. Master, M. A. Rashid, and Muzaffar Hussain. 1974. p. D1–D30; plates in pocket. $2.40.

751–C. Geohydrology of the artificial-recharge site at Bay Park, Long Island, N.Y., by John Vecchioli, G. D. Bennett, F. J. Pearson, Jr., and L. A. Cerrillo. 1974. p. C1–C29; plates in pocket. 95¢.

786. Pleistocene geology of the northeast Adirondack region, New York, by C. S. Denny. 1974. 50 p.; plates in pocket. $1.45.

813–A. Summary appraisals of the Nation's ground-water resources—Ohio Region, by R. M. Bloyd, Jr. 1974. p. A1–A41. $1.75.

813–C. Summary appraisals of the Nation's ground-water resources—Upper Colorado Region, by Don Price and Ted Arnow. 1974. p. C1–C40; plates in pocket. $3.15.

821. Some upper Miocene and Pliocene(?) Ostracoda of Atlantic coastal region for use in hydrogeologic studies, by F. M. Swain. 1974. 50 p.; 13 plates showing fossils. $1.85.

898. Slump blocks in the Atlantic Highlands of New Jersey, by J. P. Minard. 1974. 24 p. 95¢.

901. Explanatory text to accompany the geologic map of the United States, by P. B. King and H. M. Beikman. 1974. 40 p. $1.25.

921. Earth science in the public service, by U.S. Geological Survey. 1974. 73 p. $2.15.

Bulletins

1306. Bibliography and index of geology and hydrology, Front Range Urban Corridor, Colo., by Felicie Chronic and John Chronic. 1974. 102 p. $1.15.

1313–D. Use of Dar Zarrouk curves in the interpretation of vertical electrical sounding data, by A. A. R. Zohdy. 1974. p. D1–D41; plate in pocket. $1.45.

1326. Pumice and other pyroclastic deposits in Mount Rainier National Park, Wash., by D. R. Mullineaux. 1974. $1.35.

1330. Geochemistry of gold in the weathering cycle, by H. W. Lakin, G. C. Curtin, and A. E. Hubert, with chapters by H. T. Shacklette and K. G. Doxtader. 1974. 80 p. $1.15.

1373. Geology of Gravina Island, Alaska, by H. C. Berg. 1973 (1974). 41 p.; plate in pocket. $1.70.

1385–B. Mineral resources of the Scapegoat Wilderness, Powell and Lewis and Clark Counties, Mont., by M. R. Mudge, R. L. Earhart, K. C. Watts, Jr., E. T. Tuchek, and W. L. Rice, *with a section on* Geophysical surveys, by D. L. Peterson. 1974. p. B1–B82; plates in pocket. $2.75.

1395–C. Stratigraphic nomenclature of the Thirtynine Mile volcanic field, central Colorado, by R. C. Epis and C. E. Chapin. 1974. p. C1–C23. 50¢.

1395–D. The Iyanbito Member (a new stratigraphic unit) of the Jurassic Entrada Sandstone, Gallup-Grants area. New Mexico, by M. W. Green. 1974. p. D1–D12. 45¢

Water-Supply Papers

2007. Geologic and hydrologic features of Indian Wells Valley, Calif., by L. C. Dutcher and W. R. Moyle, Jr. 1973 (1974). 30 p.; plates in pocket. $3.75.

2152. Quality of surface waters of the United States, 1970—Part 2, South Atlantic slope and eastern Gulf of Mexico basins. 1974. 668 p. $5.45.

U.S. GOVERNMENT
PRINTING OFFICE
PUBLIC DOCUMENTS DEPARTMENT
WASHINGTON, D.C. 20402